

FACILITY FORM 502

N 66 - 16 525	
(ACCESSION NUMBER)	(THRU)
316	1
(PAGES)	(CODE)
CR 70013	29
(NASA CR OR TMX OR AD NUMBER)	(CATEGORY)

FEASIBILITY STUDY OF
DIRECT FLOW GASEOUS CORE REACTOR SYSTEM

4393-6003-R0-000

31 January 1966

Prepared for
NASA Headquarters
Under Contract NASw-1166

GPO PRICE \$ _____
CFSTI PRICE(S) \$ _____
Hard copy (HC) 7.00
Microfiche (MF) 1.75

ff 653 July 65

TRW SYSTEMS

FEASIBILITY STUDY OF
DIRECT FLOW GAS CORE REACTOR SYSTEM

Contract NASw-1166

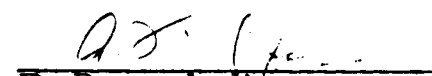
31 January 1966

for

NASA Headquarters
Code BCA, Washington, D. C.

NI, 625 R Bldg


Henry M. Hunter
Study Director


P. Degarabedian
Director, Systems Research
and Engineering Laboratory

TRW Systems
Redondo Beach, California

ACKNOWLEDGEMENTS

The following people have contributed to this study.

E. S. Diamant
L. A. Gore
A. G. Hammitt
H. M. Hunter
J. R. McDougall
R. K. Plebuch
R. B. Spencer
K. L. So

ABSTRACT

16525

The purpose of this study is to investigate the feasibility of a direct-flow gas-core propulsion reactor concept employing a single axial gaseous fuel jet surrounded by a coaxial stream of gaseous hydrogen propellant. The proposed concept avoids the problems of fuel retention associated with more complex flow fields by collecting the single fuel stream in a scoop located at the discharge end of the reactor where it is cooled, condensed to the liquid phase, and recirculated.

The study is primarily concerned with the feasibility of the scoop that collects the hot gaseous fuel at the reactor discharge and, consequently, operates in a severe thermal environment. NASA Lewis computer programs were used to determine the heat loads and mixing between fuel and propellant streams. Various advanced cooling techniques were used to determine the feasibility of cooling the fuel scoop.

The propulsion system was analyzed in sufficient depth to uncover critical problem areas and to establish reasonable design and performance conditions for evaluation of system feasibility.

Aator.

CONTENTS

<u>Section</u>	<u>Page</u>
1. INTRODUCTION	1-1
1.1 CONCEPT AND PROBLEM AREAS	1-1
1.2 STUDY OUTLINE	1-4
1.3 STUDY APPROACH	1-4
2. REACTOR HEAT TRANSFER AND FLUID FLOW STUDY	2-1
2.1 THERMAL RADIATION ANALYSIS	2-1
2.1.1 Analytical Methods	2-1
2.1.2 Schedule of Calculations	2-6
2.1.3 Results and Discussion	2-6
2.2 FLUID FLOW AND MIXING ANALYSIS	2-25
2.2.1 Analytical Methods	2-25
2.2.2 Schedule of Calculations	2-30
2.2.3 Results and Discussion	2-31
3. ADVANCED COOLING STUDIES	3-1
3.1 TRANSPIRATION COOLING TECHNIQUES	3-1
3.1.1 Model Description	3-1
3.1.2 Temperature Distribution (Infinite Heat Transfer Coefficient)	3-2
3.1.3 Pressure Drop	3-7
3.1.4 Temperature Distribution (Finite Heat Transfer Coefficient)	3-22
3.1.5 Conclusions	3-33
3.2 CONVECTIVE COOLING TECHNIQUES	3-33
3.2.1 Gas-Side Convective Heat Transfer	3-34
3.2.2 Gas-Side Heat Transfer with Boundary Layer Injection	3-34
3.2.3 Coolant Side Heat Transfer	3-35
3.2.4 Scoop Coolant Pressure Drop	3-36
3.2.5 Conclusions	3-45
3.3 SEEDING TECHNIQUES	3-45

CONTENTS (continued)

<u>Section</u>	<u>Page</u>
4. SCOOP COOLING FEASIBILITY ANALYSIS	4-1
4.1 SCOOP DESCRIPTION	4-1
4.2 SCOOP DESIGN CONSIDERATION	4-1
4.2.1 Scoop Fuel Loss and System Cost-Effectiveness	4-1
4.2.2 Cycle Thermodynamic Efficiency	4-3
4.2.3 Heat Flux and Coolant Requirements	4-3
4.2.4 Thermo Structural Considerations	4-12
4.2.5 Stress Analysis	4-14
4.2.6 Material Strength	4-18
4.2.7 Conclusions	4-21
5. ENGINE PRELIMINARY DESIGN	5-1
5.1 NUCLEONICS	5-3
5.1.1 Criticality	5-3
5.1.2 Power Distribution	5-13
5.2 ENGINE COOLING CONSIDERATIONS	5-15
5.2.1 Nozzle Convective Cooling	5-15
5.2.2 Reflector Cooling	5-38
5.2.3 Uranium Condensation	5-55
5.3 ENGINE COMPONENT WEIGHTS	5-75
5.3.1 Total Uranium Inventory	5-75
5.3.2 Reflector Weight	5-76
5.3.3 Pressure Vessel	5-80
5.3.4 Radiation Shield Weight	5-83
5.3.5 Nozzle Weight	5-86
5.3.6 Turbopump Weight	5-94
5.3.7 Propellant and Uranium Line Weights	5-97
5.3.8 Thrust Structure Weight	5-104
5.3.9 Scoop Weight	5-107
5.3.10 Separator Weight	5-111
5.3.11 Auxiliary Component Weights	5-113

<u>Section</u>	CONTENTS (continued)	<u>Page</u>
5.4	ENGINE TEMPERATURES, PRESSURE, AND MASS FLOW RATES	5-117
5.4.1	Cycle Description	5-117
5.4.2	Pressure Drops	5-119
5.4.3	Jet Pump	5-121
5.4.4	Hydrogen Return Line	5-121
5.4.5	Pressure and Temperature Decrease through the Turbine	5-122
5.4.6	Summary	5-124
5.5	TOTAL ENGINE WEIGHT	5-127
5.5.1	Total Engine Weight	5-127
6.	ENGINE PERFORMANCE ANALYSIS	6-1
6.1	URANIUM LOSSES	
6.2	TRANSPIRATION COOL HYDROGEN ADDITION	6-2
6.3	COOL HYDROGEN ADDITION WITH SEEDING	6-5
6.4	SPECIFIC IMPULSE DEGRADATION	6-7
6.5	TOTAL THRUST AND MASS FLOW RATE	6-8
6.6	ENGINE PERFORMANCE AS A FUNCTION OF POWER	6-8
7.	SUMMARY AND RECOMMENDATIONS	7-1
7.1	SCOOP EVALUATION	7-1
7.2	HEAT TRANSFER	7-2
7.3	COAXIAL MIXING OF THE STREAMS	7-3
7.4	ENGINE PERFORMANCE	7-4
7.5	NUC LEONICS	7-6
7.6	RECOMMENDED STUDIES	7-8
	APPENDIX A	A-1
	APPENDIX B	B-1

1. INTRODUCTION

The study is primarily concerned with the technical feasibility of a coaxial stream gaseous-core reactor in which the fuel at the reactor discharge is collected and recirculated. The major area requiring a detailed analysis is the survivability of the exit scoop under severe thermal environment. The heat transfer, stream mixing, and cycle analysis are mainly used in support of this effort.

1.1 CONCEPT AND PROBLEM AREAS

The TRW gaseous-core concept shown in Figure 1-1 consists of a parallel coaxial stream of propellant and gaseous fuel flowing through the central cavity of the reactor. In this configuration, the cavity is surrounded by a composite moderating reflector consisting of an inner region of graphite and an outer region of beryllium oxide. The fuel circulates in a closed loop. At the reactor discharge, the central hot gaseous fuel is collected by the scoop, mixed with cold propellant, condensed, and subsequently separated from the propellant by exploiting the liquid/gas phase difference and finally returned to the reactor inlet.

The propellant from the tanks is pumped to the required pressure and used to cool two prime areas; the uranium in the scoop and the surrounding reactor structures such as reflector walls and nozzles.

This concept characteristically shares with the other gaseous-core concepts the problems of fluid mixing, heat transfer, nuclear critical mass requirements, and structural containment under severe heat loads. In place of difficult vortex fluid dynamic problems are the difficult engineering problems associated with recirculating the fuel. This concept hopes to show a higher degree of fuel retention, such as a fuel loss to propellant mass flow ratio of about 10^{-4} . This is because the local velocity of the uranium core can be matched exactly at the interface with the outer hydrogen flow and the resulting shear mixing associated with a bulk velocity difference between the streams can be eliminated.

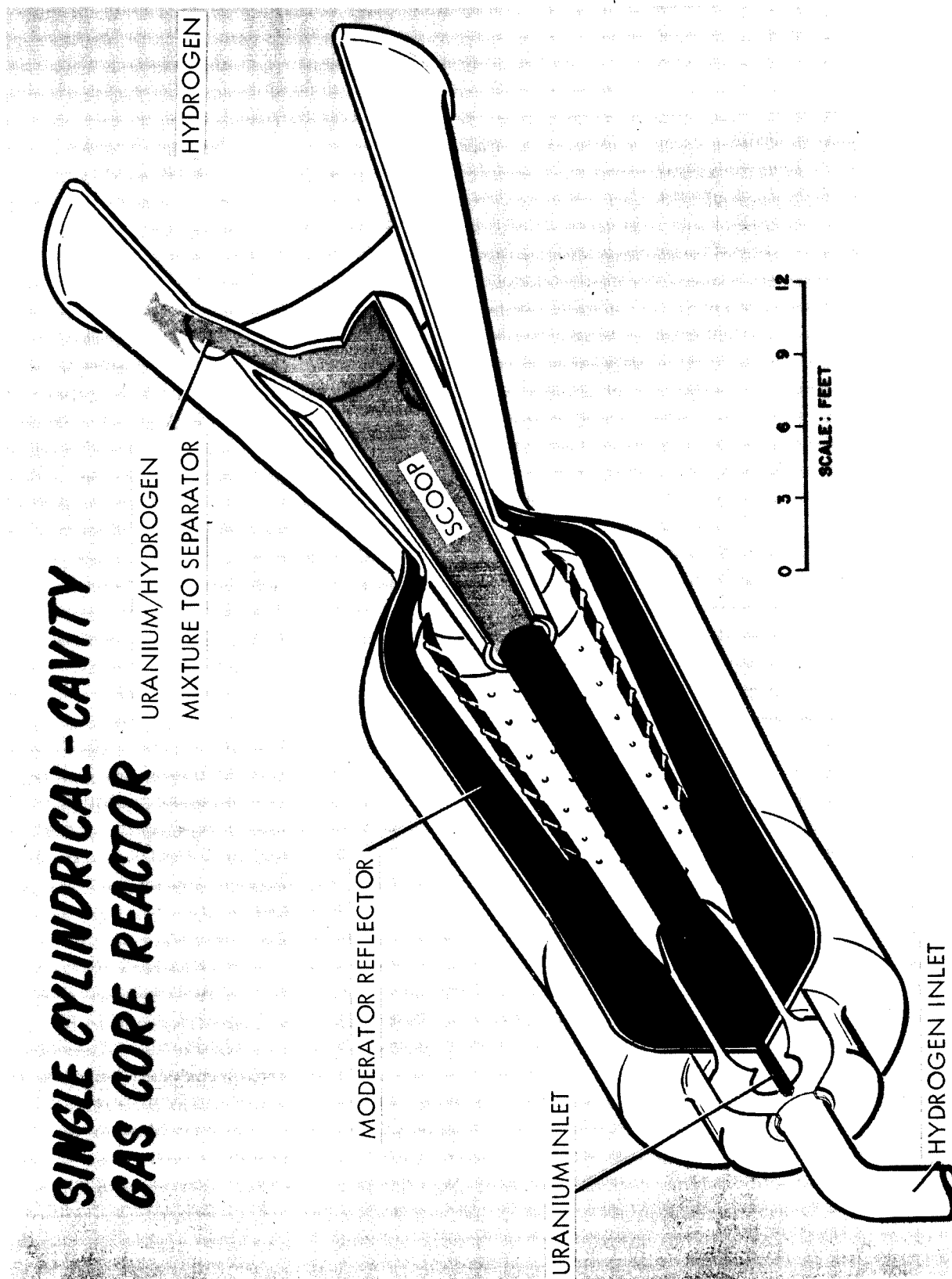


Figure 1-1 Direct Flow Gaseous-Core Reactor

The next problem is one transferring the heat from the fissioning inner core to the outer stream of propellant without transferring significant quantities of heat to the reactor walls. Thermal radiation is the principal heat transfer agent. However, the hydrogen propellant at the lower temperature is transparent to radiation and seeding with small particles of carbon, refractory of alkali metals, is mandatory if satisfactory opacities are to be achieved. The central issue is one of making the propellant sufficiently opaque that minimum heat passes through to the surrounding walls and, at the same time, transparent enough that the propellant is heated to a sufficient depth that acceptable heat energy per unit volume of propellant is achieved. The gaseous fuel column has a steep fuel temperature gradient because of the high opacity of the fuel. This means the average fuel temperature required in the gaseous core is sufficiently large that extremely high pressures are necessary to produce a critical fuel density. Therefore, means must be found to reduce the critical mass or to obtain more efficient heat transfer from the fuel column to the propellant.

The structural vulnerability of the scoop exposed to the severe heat environment has been singled out as the major task of this study since heat fluxes of as much as 500 Btu/sec-in^2 are incident on the leading edge of the scoop. Again, radiation rather than convection is the principal mechanism of heat transfer which means that existing solutions and techniques developed for cooling chemical and nuclear rocket nozzles are not directly applicable. Fortunately, seeding a film-cooled boundary between the hot gas and wall offers, in principle, sufficient thermal resistance that advanced cooling techniques as transpiration or film cooling appear to offer practical solutions. This study examines seeded film cooling and transpiration cooling in detail.

The performance potential of gaseous-core reactor propulsion systems for future space exploration is great, but the various schemes under study contain many critical problems which are so interconnected that it is difficult to isolate and examine each problem area separately. At present, many of the proposed schemes have not been investigated sufficiently to make a fair appraisal of the system feasibility. As with gas-core concepts, the TRW gaseous-core concept has its share of critical problem areas. These problems are not thought to be insurmountable, but will require

additional analysis before a semblance of practicality can be proven. Such items as the injection of propellant and fuel into the reactor cavity, nuclear control, start-up and shut-down, liquid/gas phase separation efficiency, materials compatibility are some of the major areas requiring further investigation before the promise offered by this gaseous-core reactor can be materialized.

In this present study, we are directed to examine one of the most crucial items in the concept, i.e., scoop survivability under its extreme heat environment. If it passes this test we feel hopeful that there is justification for additional investigations.

1.2 STUDY OUTLINE

The tasks as outlined in Article 1 of the NASA negotiated Contract NASw-1166 dated 1 March 1965 are as follows :

- o A feasibility analysis of the scoop survivability under its severe thermal environment.
- o Analysis of the core heat transfer and fluid flow to support engine thermodynamic analysis and scoop analysis.
- o A thermodynamic cycle analysis appraising in a parameter form the specific impulse and propulsion system weight of the gas core reactor concept.

1.3 STUDY APPROACH

The main areas of study have been investigated in a preliminary manner by TRW prior to this contract, establishing the range of the values of the major parameters. Next the computer programs on thermal radiation and fluid flow which existed in the Nuclear Reactor Division of the Lewis Research Center were modified by TRW to meet the requirements of the TRW reactor concept and to provide the information on the heat distribution in the reactor and the mass transfer between the streams. This was to be the main input to the scoop cooling and cycle analysis. TRW would then investigate advanced cooling techniques to insure the scoop structural integrity under the ultra-high heat fluxes. Finally, a parametric cycle analysis would be performed to insure the design conditions taken for the scoop represented a reasonable engine specific impulse and weight. This analysis was also to aid in uncovering other problem areas which could critically affect the performance of the system.

2. REACTOR HEAT TRANSFER AND FLUID FLOW STUDY

2.1 THERMAL RADIATION ANALYSIS

The gaseous core nuclear rocket concept studied herein consists of a hot core of fissioning gaseous uranium surrounded by an annulus of propellant. The gaseous uranium is recovered in a scoop and the hot propellant discharges through a nozzle. To evaluate the heat transfer to the scoop, it is necessary to define the environment surrounding the scoop. Since the temperature level of the gaseous uranium is very high, radiation is the principal mode of heat transfer. It is also desirable to minimize mixing of the uranium core and the propellant, as convective heat transfer and mixing are similar processes, the success of the concept requires that radiation be the predominant heat transfer mechanism.

The fluid flow equations with the radiant heat transfer term have not been solved in the general case. The assumption of a radiantly transparent or opaque gas can lead to a substantial simplification. Neither of these limiting conditions, however, is really appropriate for the present problem. The propellant gas must be sufficiently opaque so that the radiation does not pass directly through to the wall. The propellant gas therefore must be sufficiently transparent so that most of the propellant gas can be heated by the hot gaseous fuel core.

The radiation problem is treated in this analysis by two methods. The method of Einstein⁽¹⁾, a numerical integration of the radiation equation will be used for certain restricted geometries and absorptivities. The Rosseland approximation for an optical dense gas will be used where it appears to be a better approximation than the Einstein method.

2.1.1 Analytical Methods

2.1.1.1 Einstein Method

The radiant heat transfer prediction in the reactor chamber is based on the work by Einstein⁽¹⁾. This method assumes a gray gas of uniform absorptivity flowing in a cylindrical pipe of finite length. The gas and the interior surface of the pipe are heated by radiation from energy sources distributed in an inner concentric core of the gas. The assumptions made in the analysis are as follows:

1. Conditions in the pipe are axisymmetric.
2. Conditions at the ends of the pipe are represented by porous black surfaces.
3. This gas is gray and the absorptivity is uniform in the entire cylinder.
4. The interior cylindrical surface is black.
5. The axial component of conduction is neglected.
6. The product of absorptivity and cylinder diameter must be less than 20.

These assumptions result in a gross approximation to the actual problem being considered. Since the absorptivity in the uranium core is much greater than in the hydrogen propellant, the uniform gray gas assumption makes it impossible to treat both regions with accuracy. Furthermore, the cylinder must be completely filled with gas and it is impossible to treat the problem of radiation to the scoop from the outer flow annulus with the existing program. However, at present this method is the best available. After a short description of the method, the results and their use will be discussed.

A heat balance on an infinitesimal volume dV , located at position \vec{S}_0 inside the pipe, gives an energy equation in the following form:

$$4k\sigma T^4(\vec{S}_0) + \rho u C_p \left[\frac{\partial T(\vec{S})}{\partial Z} \right] \vec{S}_0 - \frac{\lambda}{r} \frac{\partial}{\partial r} \left[r \frac{\partial T(\vec{S})}{\partial r} \right] \vec{S}_0$$

$$= k \iiint \sigma T^4(\vec{S}) f(\vec{S} - \vec{S}_0) dV + k \iint \sigma T_S^4(\vec{S}) g(\vec{S} - \vec{S}_0) dA + \dot{q}'''(\vec{S}_0)$$

- a) The first term on the left hand side represents the radiant energy emitted per unit volume at \vec{S}_0 .
- b) The second term is the rate of enthalpy increase of the flowing gas at \vec{S}_0 .
- c) The last term on the left is the radial conduction per unit volume at \vec{S}_0 .
- d) The first term on the right hand side is the radiation absorbed per unit volume at \vec{S}_0 from emission given off by the rest of the gas in the pipe.
- e) The second term represents the radiation absorbed per unit volume at \vec{S}_0 from emission of pipe wall and end surfaces.
- f) The last term in the equation is the energy source per unit volume At \vec{S}_0 .

This integro-differential equation is extremely difficult to solve. Einstein divided the gas volume in the pipe into 50 gas-ring zones of equal cross-section, 10 zones axially and 5 zones radially. Similarly, the surfaces are divided into surface zones whose boundaries correspond with those of the adjoining gas zones. Thus, the solution of the above equation may be approximated by writing heat balance equations on infinitesimal volumes located at the centers of the cross-sections of each of the 50 gas zones. Furthermore, the temperature of each surface zone is assumed to be uniform over that zone, but may vary from one surface zone to the next. A similar assumption is made for the distribution of energy sources in the gas. However, the temperature of the gas in each zone is assumed to vary as a two-dimensional linear function of the temperatures of the centers of the gas zones. With these assumptions, the temperature terms in the above equation can be taken outside of the volume and the surface integrals which then become merely geometry-dependent. Finally, by approximating the derivatives in the above equation with algebraic difference quotients in terms of the gas-zone-center temperatures and the integrals in terms of finite sums that are algebraic functions of the gas-zone-center temperatures, the above equation can be replaced by a system of 50 algebraic equations with the 50 gas-zone-center temperatures as unknowns. By solving the simultaneous equations on a digital computer, the temperature distribution in the gas and heat flux to the surface can be determined for a given surface temperature distribution and for a given distribution of energy sources in the gas.

2.1.1.2 Rosseland's Diffusion Approximation

The previous method for making the radiation heat transfer calculations has several limitations and requires supplementary calculations in the region of the optical dense uranium core. For an optically dense gas, the radiation can be adequately determined by Rosseland's diffusion approximation⁽⁷⁾ with a discontinuous temperature boundary condition. This reduces the problem to one of solving a heat conduction equation.

For an energy balance the general differential energy equation can be written as

$$\rho C_p \frac{DT}{Dt} = w_i - \text{div } \vec{q} + T \alpha \frac{Dp}{Dt} + u \cdot \nabla \quad (1)$$

where D/DT is a substantial derivative. For the case of constant pressure in the reactor, the work of compression Dp/Dt is zero. In the problem considered here, the viscous dissipation is negligible and can be assumed equal to zero. Therefore, the rate of change of enthalpy within a unit volume $\rho C_p DT/Dt$ can be equated to the heat source within the volume w_i minus the net rate of heat flow out of the volume $\nabla \cdot \vec{q}$

$$\rho C_p \frac{DT}{Dt} = w_i - \nabla \cdot \vec{q} \quad (2)$$

For steady-state conditions and velocities in the axial direction only, the substantial derivative on the left hand side of Equation (2) becomes $U \frac{\partial T}{\partial Z}$

$$\therefore \rho U C_p \frac{\partial T}{\partial Z} = w_i - \nabla \cdot \vec{q} \quad (3)$$

The Rosseland's diffusion approximation gives

$$\vec{q} = -k_R \text{ grad } T \quad (4)$$

where

$$k_R = \frac{16}{3} \sigma T^3 \quad (5)$$

The term $-\text{div } \vec{q}$ becomes

$$-\text{div } \vec{q} = \text{div } [k_R \nabla T]$$

If the heat transfer in the direction of motion is neglected, as is usually true for heat conduction in moving fluids, and in a cylindrical coordinate system, the net rate of heat flow becomes

$$-\text{div } \vec{q} = \frac{1}{r} \frac{\partial}{\partial r} \left[r k_R \frac{\partial T}{\partial r} \right]$$

Hence, the heat balance equation, Equation (1), becomes

$$\rho U C_p \frac{\partial T}{\partial Z} = \frac{1}{r} \frac{\partial}{\partial r} \left[r k_R \frac{\partial T}{\partial r} \right] + w_i \quad (6)$$

For the case of no internal heat sources, this equation is reduced to

$$\rho U C_p \frac{\partial T}{\partial Z} = \frac{1}{r} \frac{\partial}{\partial r} \left[r k_R \frac{\partial T}{\partial r} \right] \quad (7)$$

This equation can be solved in conjunction with the temperature jump boundary condition suggested by Hammitt (8),

$$\begin{aligned} T_W^4 - T^4 &= C l \frac{\partial T^4}{\partial r} \\ &= 4 C l T^3 \frac{\partial T}{\partial r} \end{aligned} \quad (8)$$

where C is a constant which can be evaluated from the black body radiation limit. This temperature jump boundary condition extends the usefulness of the Rosseland's approximation to lower optical densities. In the black body radiation, the heat flux q can be written as

$$q = \sigma (T^4 - T_W^4) = -4 \sigma C l T^3 \frac{\partial T}{\partial r}$$

and from Rosseland's diffusion approximation, the heat flux is given by Equation (4)

$$q = -\frac{16}{3} \sigma l T^3 \frac{\partial T}{\partial r}$$

A comparison of these two heat flux expression reveals that $C = 4/3$. Hence, the jump boundary condition for the black body radiation becomes

$$T_W^4 - T^4 = 4/3 l \frac{\partial T^4}{\partial r} \quad (9)$$

Equation (6) or (7) can be solved numerically by a standard method of solving the heat conduction equation with the aid of a digital computer (9). The numerical methods used in resolving Equation (7) are detailed in Appendix II. In determining the uranium temperature in the scoop, the actual core temperature distribution in the reactor must first be obtained for optically dense uranium. This can be done by using Equation (6) with the assumption that the uranium temperature just before entering the scoop is independent of the axial distance. This assumption is justified by the fact that the uranium temperature in the reactor reaches a steady-state condition near the exit, as is shown by the results of the earlier radiation analysis in the reactor. With this assumption the left hand side of Equation (6) vanishes, and the right hand side can be used to solve for the inlet uranium temperature.

2.1.2 Schedule of Calculations

The calculations were made for a general parametric study and for detailed specific engine cases.

In the parametric study, the factors considered include the variations in velocity, heat source, absorption coefficient and size of uranium core. The ranges of those factors are:

Propellant velocity	5 - 250 fps
Fuel velocity	25 - 250 fps
Total heat source	2×10^6 - 30×10^6 Btu/sec
Absorption coefficient	1 - 5 ft^{-1}
Fuel core diameter	2 and 3 ft.

For the specific engine cases, the inputs are shown in Table 2-1. Case 1 conditions were initially thought to be most representative of an acceptable propulsion system, but subsequently, the higher powers appeared to offer substantially improved performance.

In all cases considered in this report, the reactor has cylindrical geometry (five feet in diameter and ten feet in length) and the following parameters remained constant

Reactor outer wall temperature	3000°R
Average specific heat	5 Btu/lb - °R
Average thermal conductivity	2.5×10^{-4} Btu/ft - sec - °R
Average absorption coefficient	3 ft^{-1}
Uranium density	1.55 lb/ft ³

2.1.3 Results and Discussion

The results of the heat transport analysis are discussed under the parametric study and the heat transfer to the scoop.

The general results of the heat transfer analysis for the parametric study are subdivided and discussed as follows:

Table 2-1

SPECIFIC ENGINE CONDITIONS

Reactor pressure-atmos.	100	100	100	100	1000	1000	1000
Total thermal heat - Btu/sec	6×10^6	1.8×10^7	3×10^7	6×10^6	1.8×10^7	3×10^7	1.84×10^6
Hydrogen flow - lb/sec	81.6	244.8	408	81.6	244.8	408	1.84x10 ⁶
Uranium flow - lb/sec	54.8	54.8	54.8	27.4	27.4	27.4	1.84x10 ⁶
Average exit propellant Temperature °R	13,300	14,000	14,300	15,100	16,600	16,900	1.84x10 ⁶
<u>Average exit propellant temp.</u> <u>Fuel average temp.</u>	0.6	0.486	0.444	0.673	0.570	0.519	1.84x10 ⁶
Heat incident on reactor wall Btu/sec	5.44×10^5	9.83×10^5	1.37×10^6	0.24×10^4	1.39×10^6	1.84×10^6	1.84x10 ⁶

Case 1 is represented by the first column conditions

2.1.3.1 Heat Transport in Streams

Figures 2-1 and 2-2 show the effect of inlet velocity ratios of propellant to fuel of one and two, respectively. The ordinate axis represents that portion of the total heat which is gained by the propellant flow and the abscissa the fraction of total heat absorbed by the uranium fuel. Since a heat balance on the reactor reveals that the balance of the total heat is transferred to the wall surface, the inclined lines on the figure represent a measure of the heat flux to the wall surface. However, the computer program has some inherent error in the heat balance and these lines can only be used for qualitative comparisons.

The most desirable situation is when the propellant receives the highest fraction of the total thermal heat generated. A comparison of the results in Figure 2-1 reveals that a reduction in the velocity of both fuel and propellant improves the heat transfer to the propellant. An equally desirable result can be realized by lowering the fuel velocity, as is shown in Figure 2-2. Physically, this can be explained by the fact that a lower flow rate of the fuel will yield a higher core temperature at the same heat generation rate and consequently more heat is delivered to the propellant. A lower fuel velocity is also desirable from the overall systems viewpoint since a lower fuel velocity means less fuel must be handled by the pumping system and scoop.

Furthermore, Figures 2-1 and 2-2 show two general conclusions. The first is that an absorption coefficient of 2 or 3 ft^{-1} is best for radiation heat transfer, and the second is that the heat transfer for a fuel core diameter of 2 feet is generally better than for a 3 foot diameter core.

2.1.3.2 Temperature Distribution in Streams

A typical temperature distribution obtained from the same parametric study is shown in Figure 2-3. In this figure, the dimensionless temperature T_{po}/T_f is plotted against the heat generation with absorption coefficient and core size as parameters. This temperature ratio T_{po}/T_f is a measure of I_{sp} in the system, and both T_{po} and T_f are average values weighted by the corresponding mass flow rate. From the results of the parametric study, a reduction in propellant velocity has greatly increased the temperature ratio while a change in fuel velocity does not indicate any significant variation in the temperature ratio results. The effect of absorption coefficient on temperature is the same as that on heat transport; i.e., the best results are obtained

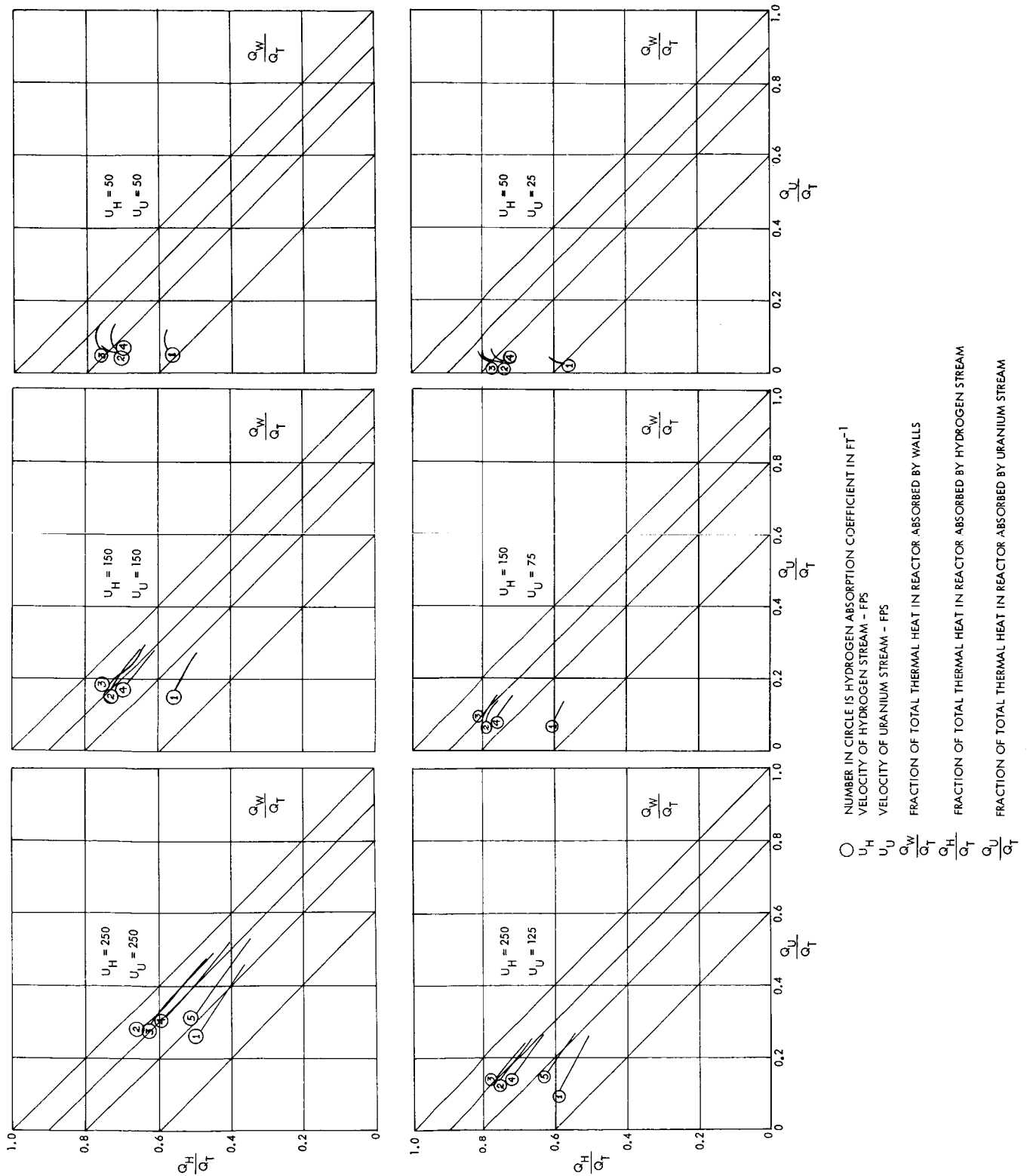
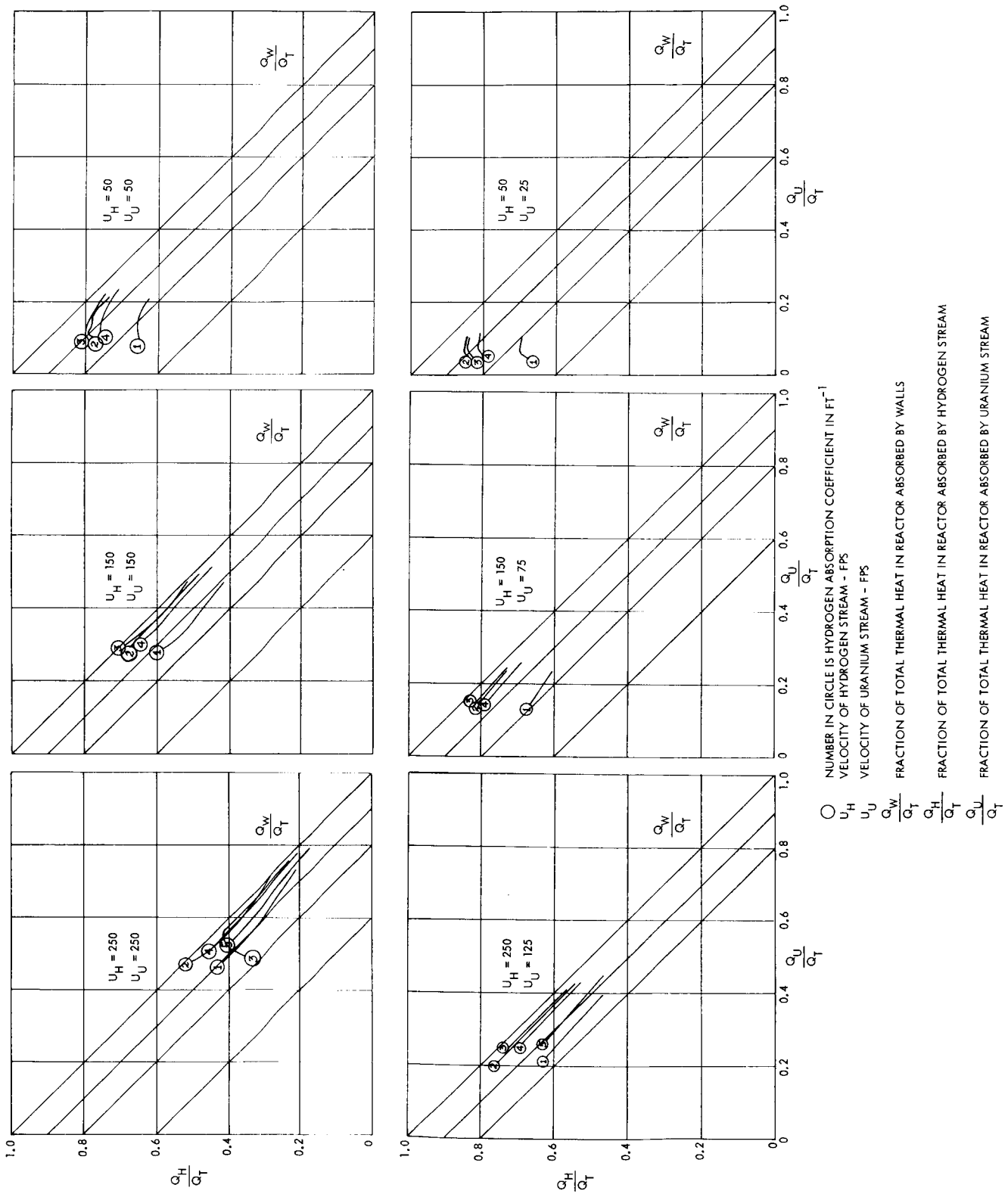


Figure 2-1 Reactor Cavity Heat Transfer (at $\frac{\text{core rad.}}{\text{cavity rad.}} = 0.6$)



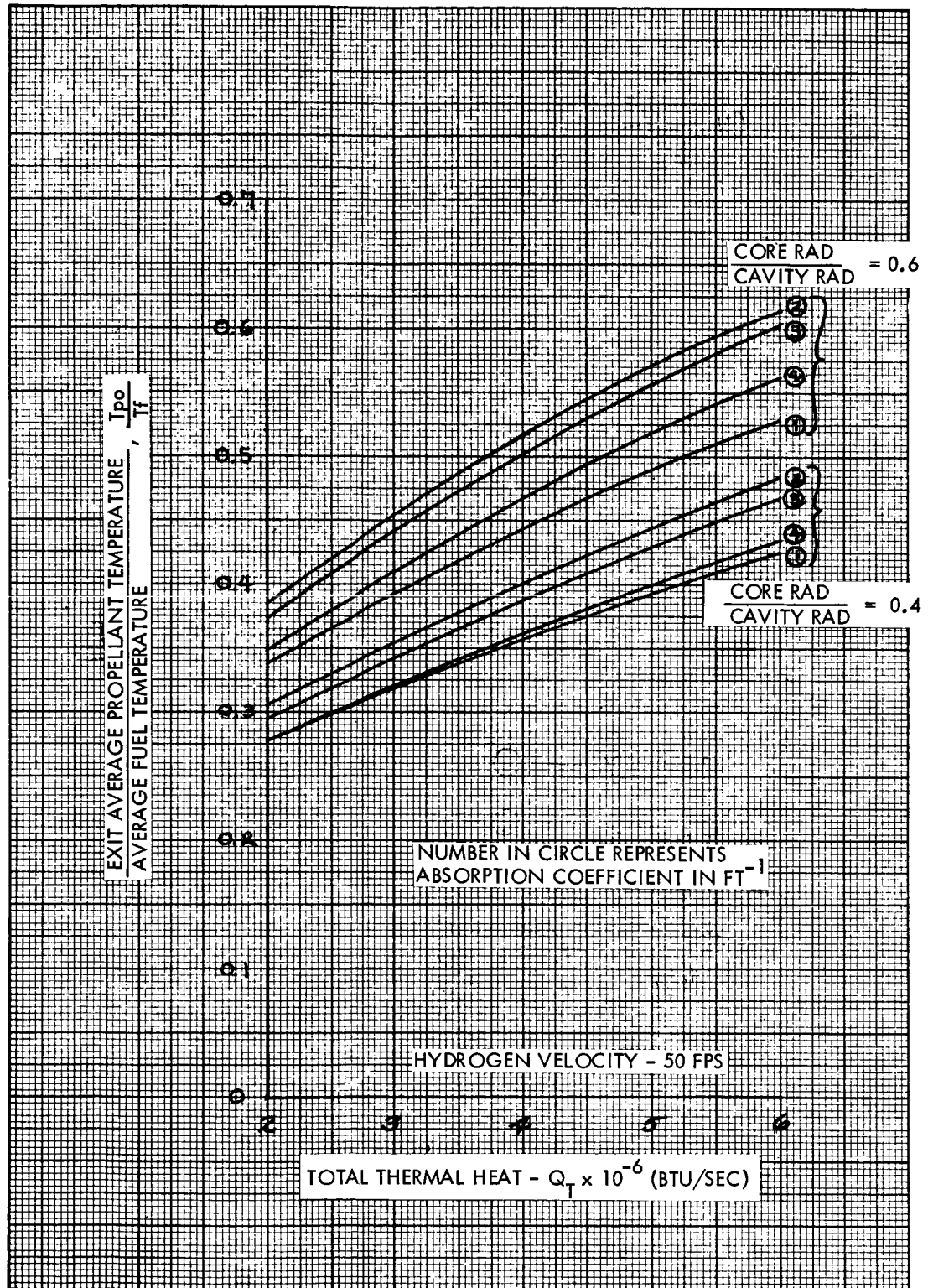


Figure 2-3 Reactor Exit Average Propellant Temperature/
Average Fuel Temperature vs Total Reactor
Thermal Heat 2-11

with absorption coefficient equal to 2 or 3 ft⁻¹. Generally, the temperature ratio is increased with the heat source, and the cases with a core size equal to 3 feet give higher temperature ratios than those with a smaller core size. The reason for having a reverse effect of core size in the case of heat consideration (figures 2-1 and 2-2) is due to the fact that (for the core size equal to 2 feet) the increase in the propellant mass flow rate exceeds the reduction in the average propellant temperature.

One very important point about the uranium core temperature must be mentioned here. The temperature results obtained with the analysis using Einstein's method⁽¹⁾ are based on the extremely low and uniform absorption coefficient. In reality, the absorption coefficient of uranium is a function of temperature, and at the temperature considered here it has a very high value⁽²⁾. As is shown later in this report, the correct uranium core temperature is much higher and so is the correct average uranium core temperature. Therefore, the dimensionless temperatures, shown in Figure 2-3, are too high and it is believed that the correct temperature ratios should have values reduced by a factor of 2.5 to 3.

2.1.3.3 Heat Flux to Wall

In designing a nuclear-reactor powered rocket, it is most important to know the heat transfer to the reactor wall. The values of this heat transfer are typically shown in figure 2-4. From the results of the parametric study, the conclusion can be made that the amount of heat transferred to the wall is reduced with increases in absorption coefficient and propellant velocity. Changes in fuel velocity and the total heat generation considered do not show any significant effect on the heat ratio, but a core size of 2 feet generally gives a lower heat flux to the wall than that of 3 feet.

Figure 2-5 shows a typical axial distribution of heat flux to the reactor wall. The results are obtained from Case 1, which will be discussed in the section 3. The results beyond the end of the reactor are obtained by overlapping two computer runs. This technique was used to obtain results for more than ten stations. The first run is made for the reactor and the second run starts at a section three feet down-stream from the first one. The curve shown in Figure 2-5 resulted from these two runs when the gas temperatures and the

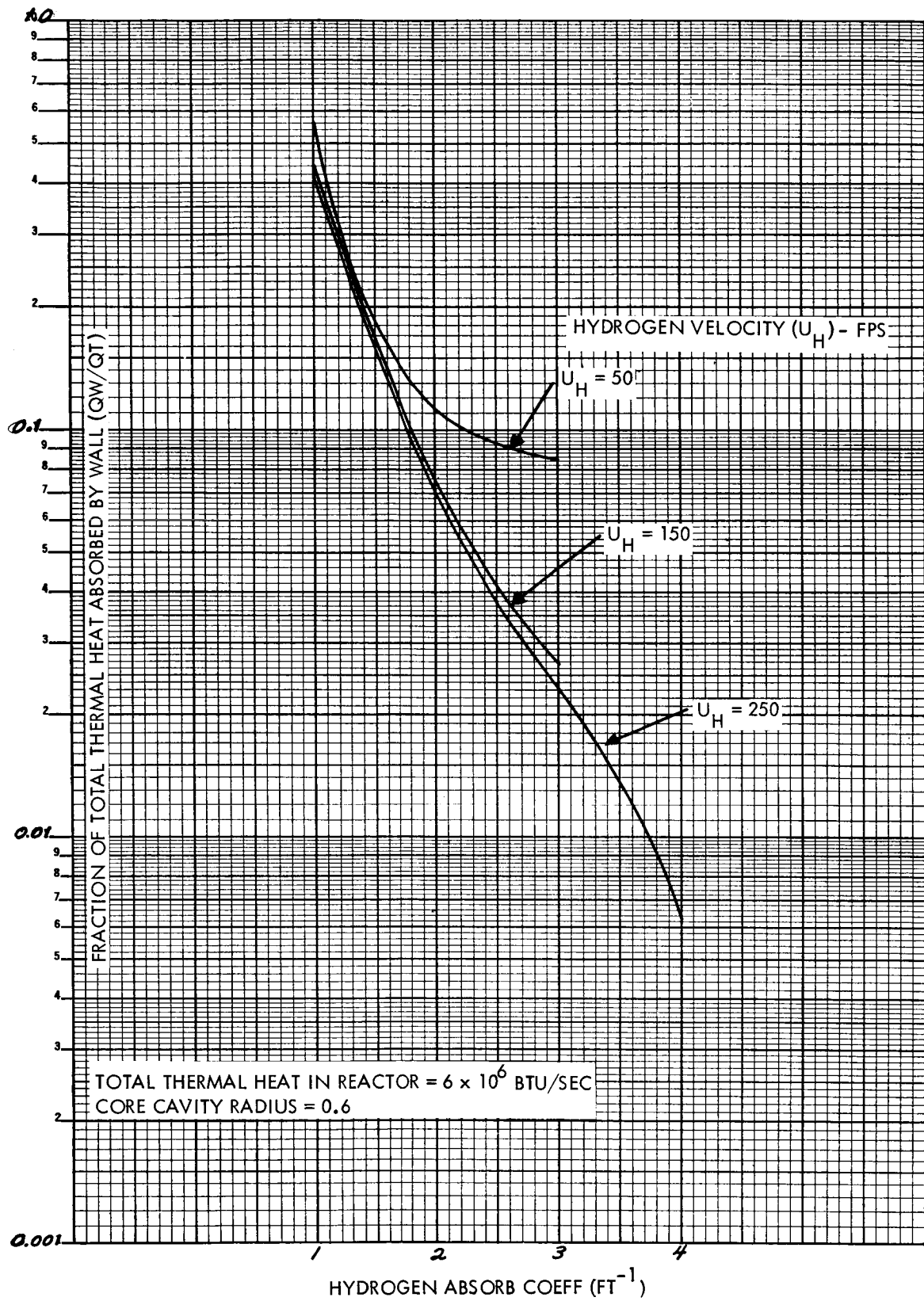


Figure 2-4 Heat Absorbed by Wall as a Function of Hydrogen Absorptivity and Velocity

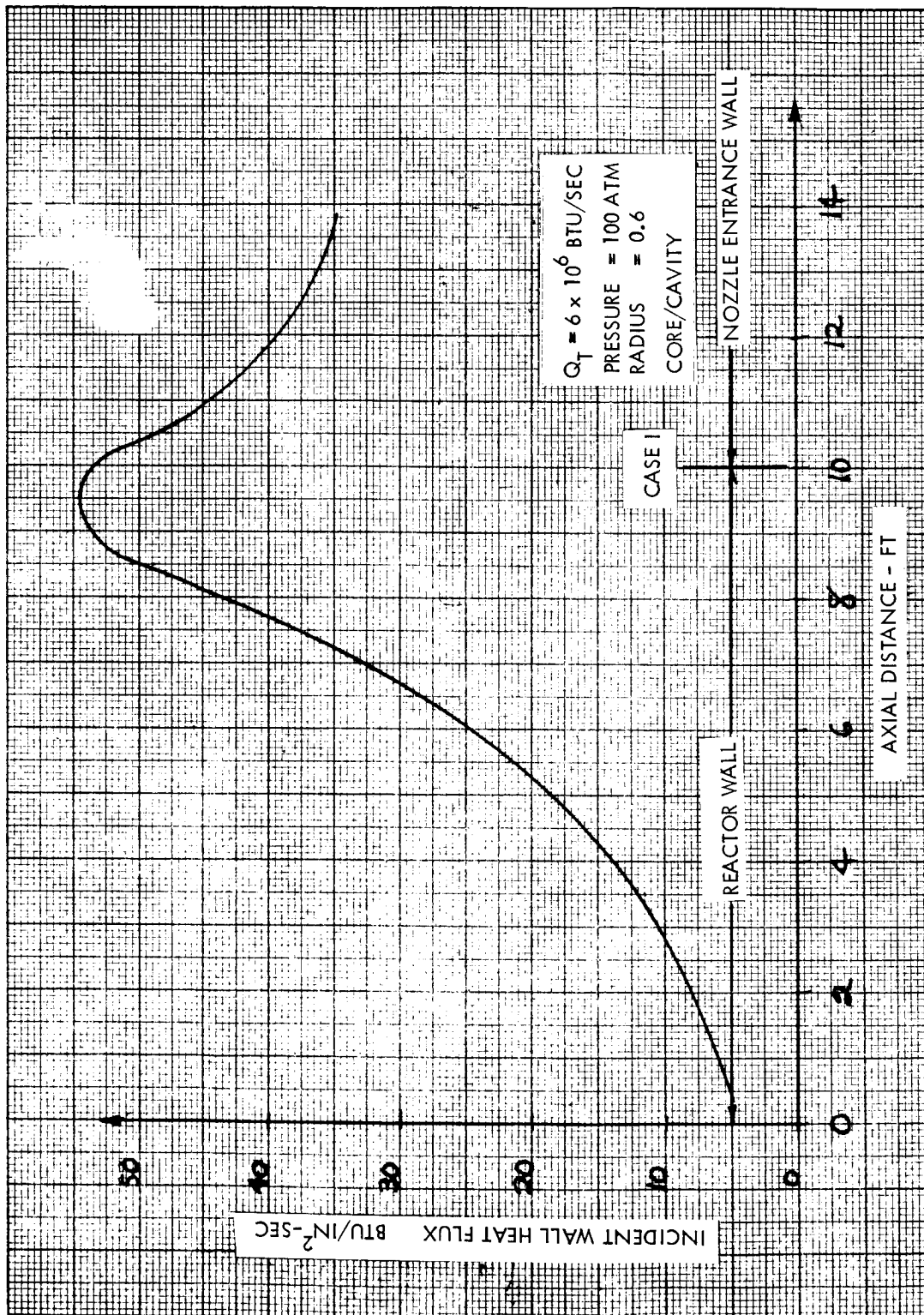


Figure 2-5 Axial Distribution of Heat Flux to the Reactor Wall

wall heat fluxes of the runs are matched in the overlapping region. The matching is done by adjusting the heat sources in the uranium column. Figure 2-5 shows a decline in heat flux after the reactor exit is reached. This decline is caused by the fact that the hot uranium column is swallowed by the scoop at this point. The wall in this section receives heat mainly from the propellant and the fissioning core inside the reactor. Thus, as the wall is further away from the core, less heat will be received by the wall and the heat flux to the wall is decreasing.

Several important assumptions of the radiation analysis should be discussed. First, the assumption that the gas in the reactor has a uniform absorption coefficient is a gross approximation. For the propellant, it is possible to obtain the assumed absorption coefficient. This can be accomplished by seeding the propellant flow with a heat-absorbing material such as carbon particles. Seeding is required since the propellant (hydrogen) has a very low absorptivity (10^{-5} ft^{-1} to 10^{-2} ft^{-1}) in the temperature range considered. The uranium in the core, however, has a very high absorption coefficient, and it does not seem possible to reduce this value to the value assumed for the propellant by any known method. Since the difference between these two values can go as high as a factor of 2000, it is doubtful that the temperature distribution of uranium in the core, as calculated by the Einstein method, would come close to the actual distribution. The inaccuracies in the uranium temperature will also affect the propellant temperature distribution, but it is believed that the effect is small and the amount of heat transferred to the propellant from the heat-generating core remains about the same.

An examination of the inputs to the radiation computer program indicates that the analysis used here takes average values of specific heat and thermal conductivity. In reality, these physical properties vary by two-orders-of-magnitude between the fuel and the propellant, so the average values can only give an approximate solution. In the case of specific heat, the average value for the propellant has been used as an input. This value is incorrect for the uranium, but the error can be compensated by changing the mass velocity (ρu) of the uranium. This adjustment can be made because ρu and C_p always appear together as a quantity in the analysis. Thus, it is only important to have this correct $\rho u C_p$. As a result, both the fuel and the propellant have their correct average value of $\rho u C_p$. In the case of thermal conductivity, it is unfortunate that a similar method cannot be applied. Therefore, an average value for both gases still has to be used in the input, but this effect is not very important because of the predominance of the radiation transfer mechanism.

2.1.3.4 Temperature Distribution in the Uranium Core

The temperature distribution in the core developed under Einstein's method is unrealistic since it does not, in its programmed form, allow the use of the high optical density of the uranium gas. To supplement this method, the Rosseland diffusion approximation with a temperature jump boundary condition was programmed on a computer. For different total heat generation rate the radial temperature distribution in the core is shown in figure 2-6. The temperature distributions are parabolic in shape and the temperature at the axis is three times as large as that obtained from Einstein's radiation analysis. The gas in the center of the core cannot see the lower temperature propellant and must radiate to the neighboring high temperature uranium with the result that the center of the core must become very hot to dispose of the heat generated. By calculating the heat transfer in the core by this method, using Rosseland's approximation, to give the same heat flux crossing the core's boundary as in Einstein's method, the results of the external propellant flow should be about the same. A reasonable approximation for the complete temperature radiant flux field has been obtained by combining these two methods. In this manner, the real properties of the gases can be considered. This means that C_p and k_R in Equation (7) are functions of temperature and pressure. They are fed into the digital computer in tabulated forms. The results obtained by this combined analysis are believed to be more accurate than the results obtained by Einstein's method above. To compare the uranium core result of this analysis with that of the radiation analysis discussed in the previous section, the absorption coefficient has been taken as a constant in the evaluation of radiation conductivity k_R in Equation (7). By reducing the constant absorption coefficient, the uranium core temperature in the reactor is consequently decreased, as is shown in figure 2-7. When the absorption coefficient in k_R is approaching that used in the Einstein radiation analysis, the temperature profile is also similar to the uranium core temperature of that radiation analysis. This shows that the radiation analysis with Rosseland's diffusion approximation reduces to that analysis made by the Einstein method when constant physical properties of the gas are used.

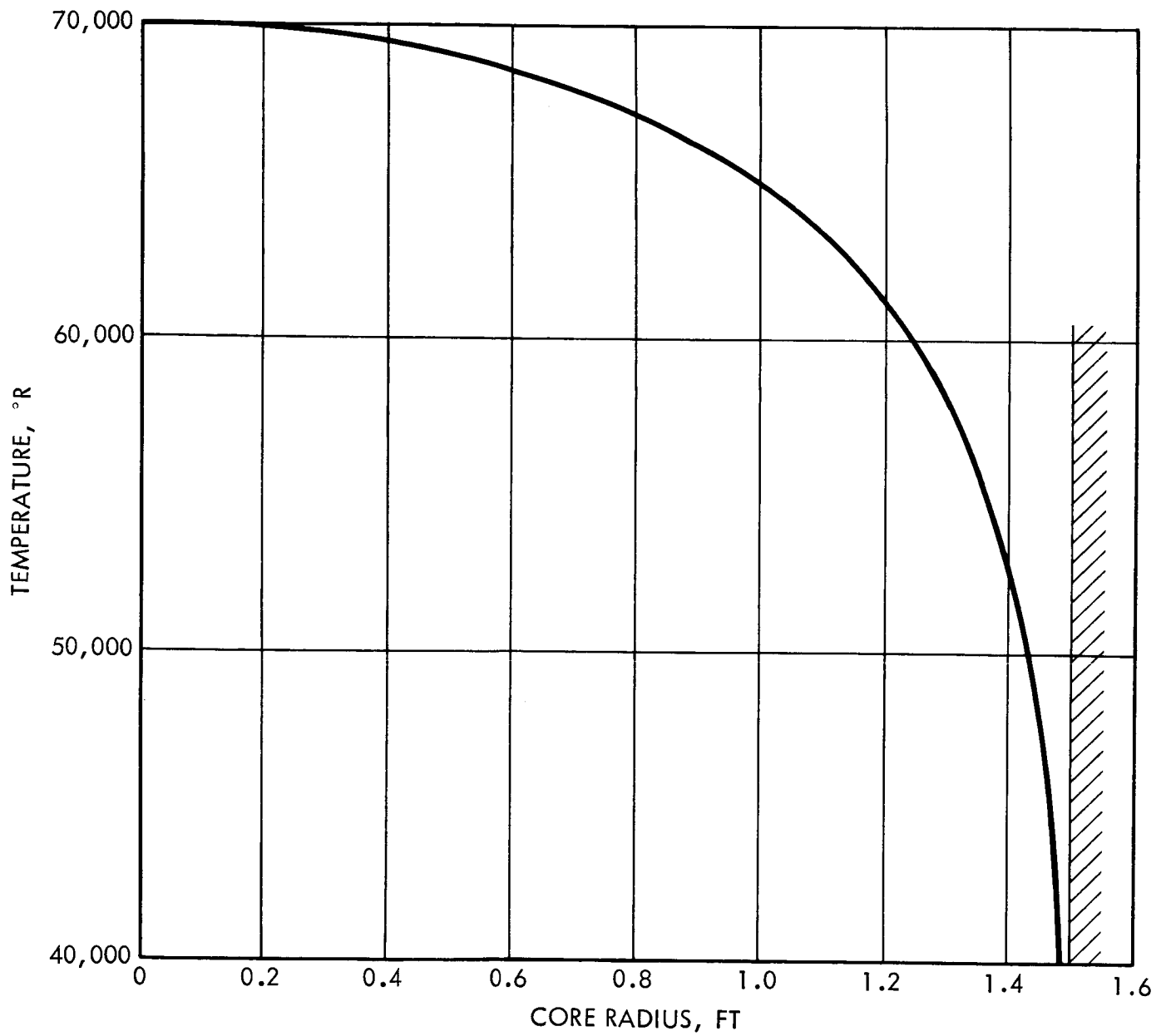


Figure 2-6 Fuel Core Temperature Distribution by
Rosseland's Diffusion Method - Case 1

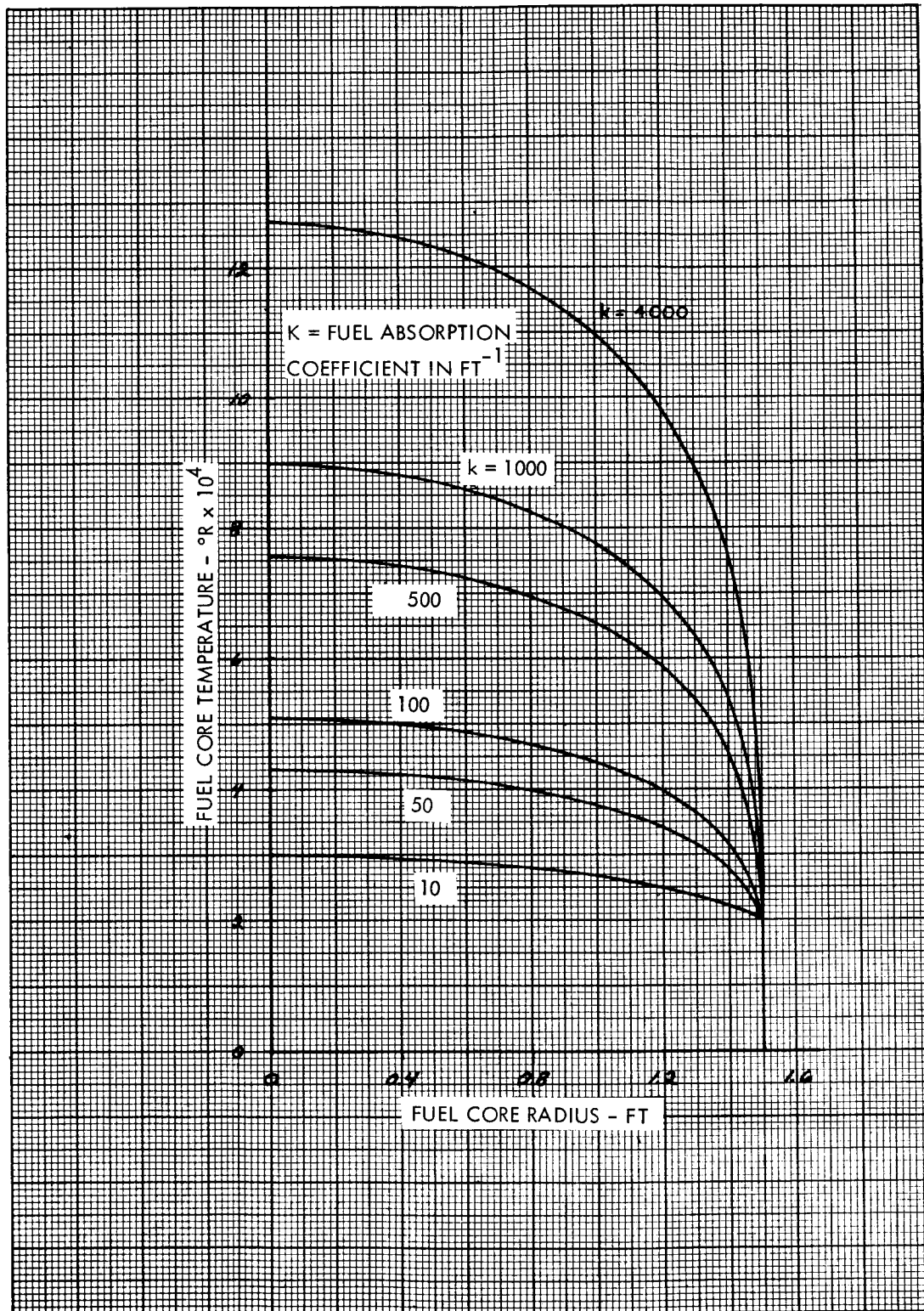


Figure 2-7 Variation of Fuel Core Radial Temperature
Distribution with Fuel Absorptivity
2-18

2.1.3.5 Heat Transfer to Scoop

The principal reason for the heat transfer analysis was to obtain the incident heat flux on the interior and exterior surface of the scoop. In this section, the results pertain to a specific scoop design under the engine design condition (Case 1).

Since the gas temperature around the scoop is very high, the radiative heat flux to the scoop will be very important. The convective mode of heat transfer is of less importance, but is also considered. The gamma heating has been neglected in this analysis. In the case of a flowing gas, the radiative heat transfer depends on the temperature and the mass flow rate, the specific heat, and the distribution of gas spectral absorptivity for radiation, which, in turn, depends on the temperature and pressure distribution in the flow field. The convective energy transfer is affected by the variations in Prandtl number, Reynolds number, specific heat, mass flow rate and surface temperature. Recently, Howell and Strite (8) (9) concluded that the radiative and convective modes of heat transfer in rocket nozzles do not interact with each other. Since the problem of heat transfer in the scoop is similar to that in a rocket nozzle, considerations of the radiative and convective heat transfer of the scoop can be made separate.

The radiative heat transfer to the surface of the scoop includes the one to the interior surface from the extremely hot uranium fuel and the one to the exterior surface from the outgoing propellant.

The gaseous uranium core has a very high optical absorptivity so that the method based on Rosseland's approximation is the best method for calculating the energy radiated to the scoop. In the study of scoop cooling, it has been assumed that the object was cooling the scoop to maintain its structural integrity. The uranium fuel which enters the scoop is to be cooled and condensed by the introduction of cold hydrogen. The cold hydrogen injected into the scoop will considerably reduce the internal scoop cooling problem. The present analysis, therefore, may be considered conservative in that it neglects this additional cooling effect. By using the inlet temperature for $w_i = 2.645 \times 10^8$ Btu/hr-ft³ and the jump boundary condition shown in Equation (9), Equation (7) is used to determine the uranium temperature in the scoop. In this calculation, the wall temperature T_w is assumed constant and equal to 3000°R, and the mass velocity ρu is also assumed constant and equal to 7.75 lbs/sec-ft², which are

the conditions used in Case 1 as mentioned in the earlier sections. The results of this computation are shown in figure 2-8. It shows that in a distance of 2 feet, the axis temperature has dropped to about two-thirds of its initial value. This is because of the inherent property of low specific heat for the uranium. The heat flux to the scoop wall is determined by the expression

$$q = \sigma (T^4 - T_W^4) \quad (10)$$

where T is the gas temperature at the wall. This is the wall heat transfer rate based on the temperature jump boundary condition. Using this relationship, the axial distribution of heat flux to the scoop surface is shown in figure 2-9. The curve decays exponentially with the axial distance from a high of 500 Btu/in² sec at the leading edge.

In determining the propellant temperature outside the scoop, the reactor exit temperature of propellant, as obtained in Case 1, is used as the inlet temperature distribution. This is shown in figure 2-10. Once again, Equation (7) is used to determine the propellant temperature outside the scoop with the given initial temperature condition and slip boundary conditions. The wall temperatures are assumed to be the same, and the mass velocity ρu is assumed uniform and equal to 6.5 lbs/sec-ft² (same as Case 1). The absorption coefficient has been set equal to 10 ft⁻¹. With these inputs, the propellant temperature distributions are determined and shown in figure 2-10. The corresponding axial distribution of heat flux to the scoop wall is obtained by using Equation (10) and shown in figure 2-11.

Since the photon mean free path of uranium is extremely small, the heat content in the middle part of the core cannot be rapidly dissipated by radiation. Thus the heat flux to the scoop, as shown in figure 2-9 is rather low. In contrast, the propellant has a comparatively high photon mean free path, so that more heat can be radiated to the outer surface of the scoop. For this reason the propellant has a very high heat flux to the scoop as shown in figure 2-11. Since the propellant is more optically transparent, it has a greater tendency to reduce its temperature variation. As a result, the temperature of hot gas near the scoop drops while the cold gas near the reflector is heated up, as is shown in figure 2-10.

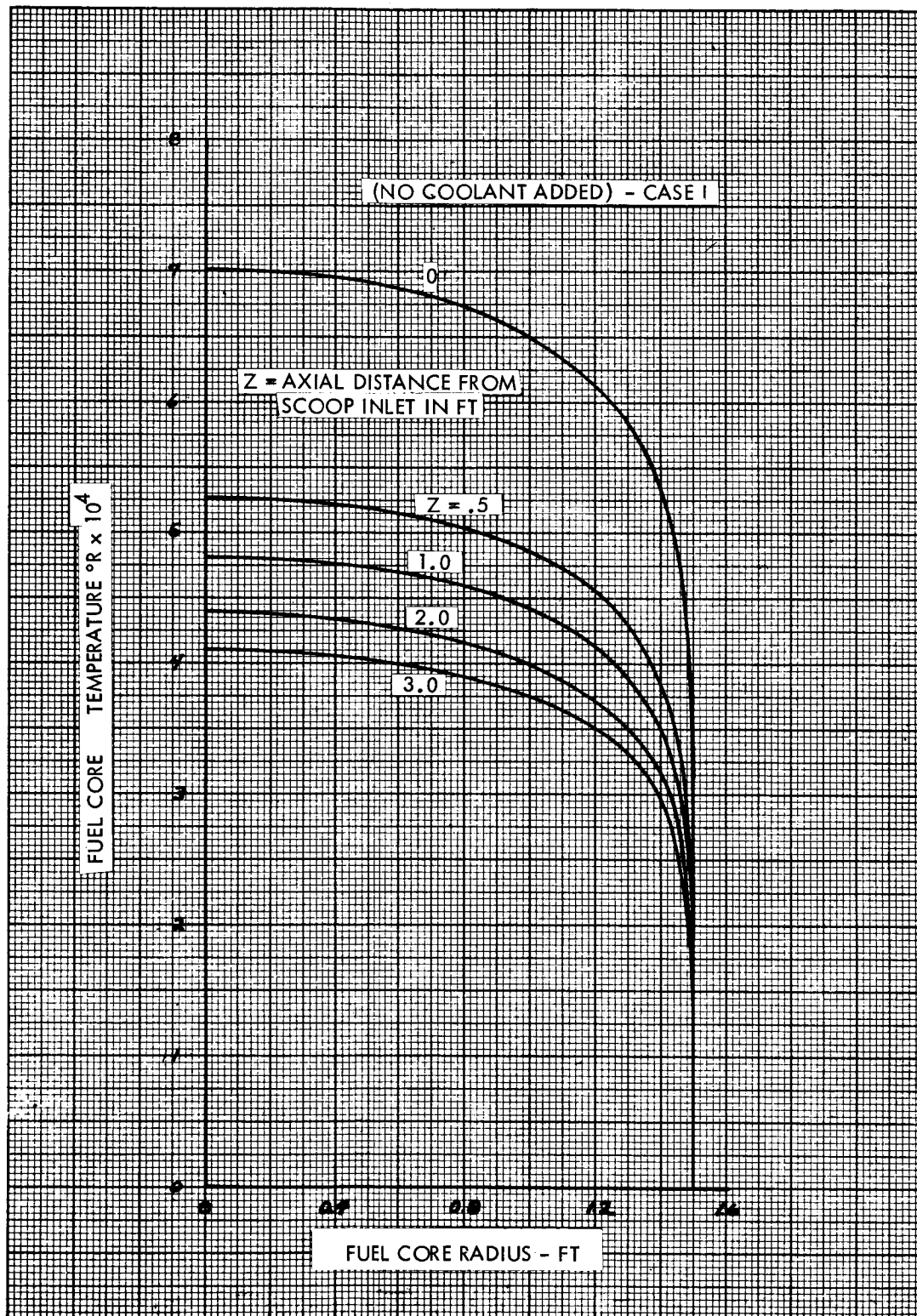


Figure 2-8 Temperature Distributions of Uranium Inside
the Scoop
2-21

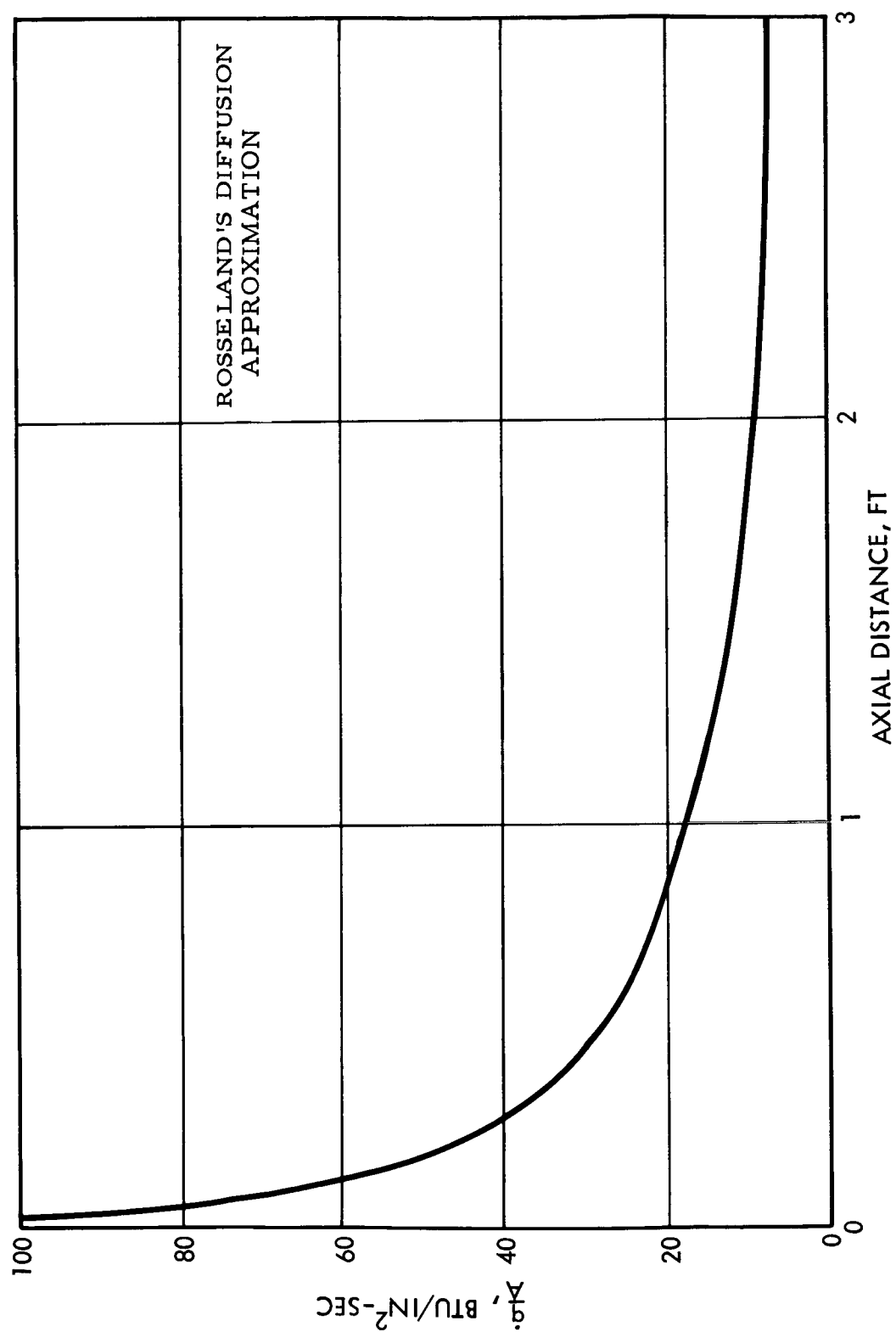


Figure 2-9 Heat Flux to the Interior Wall of the Scoop (Case 1)
(From Uranium)

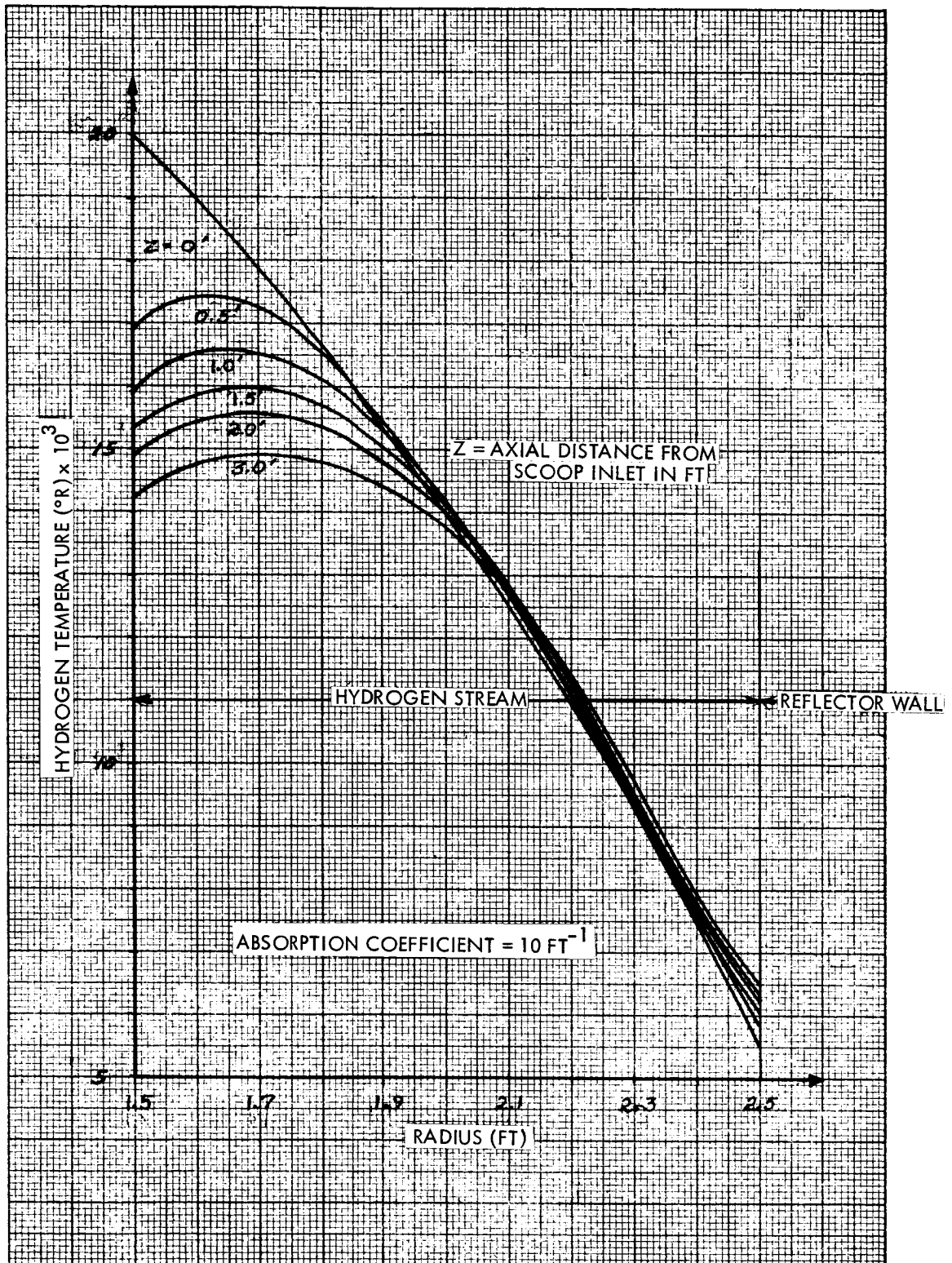


Figure 2-10 Temperature Distributions of Hydrogen
Outside the Scoop (Case 1)
2-23

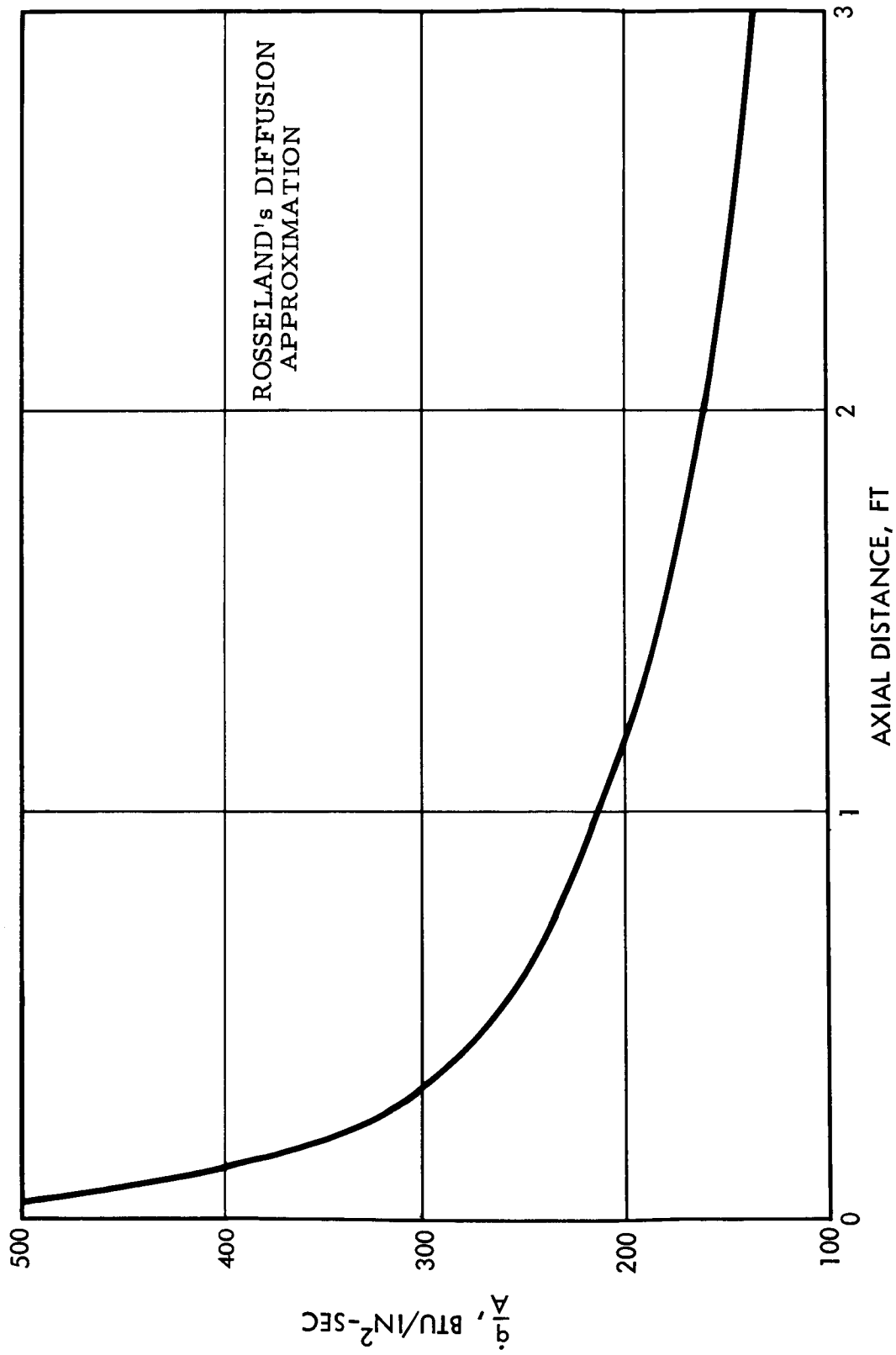


Figure 2-11 Heat Flux to the Exterior Surface of the Scoop (Case 1)

2.2 FLUID FLOW AND MIXING ANALYSIS

2.2.1 Analytical Methods

As mentioned earlier in this report, the problem of fluid flow is to determine the mass and momentum diffusion of coaxial parallel flows of two different fluids. Due to the similarity in the flow models between the model initially derived for the purposes of this study and the one considered by Weinstein and Todd⁽³⁾, the latter method of analysis for the mixing of coaxial streams of dissimilar fluids has been adopted with slight modifications. A brief discussion of this analysis is presented in the following paragraphs.

The flow model considered a heavy inner fluid in a circular cross section surrounded by a light annular stream infinite in extent. The flow may be laminar or turbulent in nature and have distributed heat sources throughout the flow field as a prescribed function of geometric location and concentration of the inner stream fluid.

The assumptions made in this analysis are listed below:

1. The flow in the system is steady and axisymmetric.
2. The entire flow field is at a constant pressure with the static and total temperatures considered equal.
3. The fluids mix ideally; there is no pressure, temperature or volume change on mixing.
4. The thermal conductivity, heat capacity, viscosity, and diffusivity are assumed to be independent of temperature.
5. The eddy diffusivities of heat, mass, and momentum are equal.
6. The normal boundary-layer assumptions are used; that is, $\partial u / \partial r \gg \partial u / \partial Z$, $u \gg v$, $\partial C / \partial r \gg \partial C / \partial Z$, $\partial T / \partial r \gg \partial T / \partial Z$, etc.

The set of equations which describe the flow system includes the following continuity, momentum, diffusion, and energy equations.

$$\frac{\partial}{\partial r} (\rho v r) + \frac{\partial}{\partial Z} (\rho u r) = 0 \quad (1)$$

$$v \frac{\partial u}{\partial r} + u \frac{\partial u}{\partial Z} = \frac{1}{\rho r} \frac{\partial}{\partial r} (r \mu \frac{\partial u}{\partial r}) \quad (2)$$

$$v \frac{\partial w}{\partial r} + u \frac{\partial w}{\partial Z} = \frac{1}{\rho r} \frac{\partial}{\partial r} (r \rho D_{12} \frac{\partial w}{\partial r}) \quad (3)$$

$$v \frac{\partial h}{\partial r} + u \frac{\partial h}{\partial Z} = \frac{1}{\rho r} \frac{\partial}{\partial r} (r k \frac{\partial T}{\partial r}) + G \quad (4)$$

In the process of synthesis, these equations are first normalized by the initial conditions of the inner flow. Then, a transformation of coordinates from $\bar{Z} - \bar{r}$ plane into a $\bar{Z} - \psi$ plane is made with the additional assumption that $\partial \psi / \partial r \gg \partial \psi / \partial Z$. The mass fraction w is substituted in terms of the mole fraction C

$$w = \frac{m_1}{m_2} \left(\frac{C}{\beta C + 1} \right), \quad (5)$$

The enthalpy term h in the energy equation is expressed by

$$h = \int_{T_o}^T C_p(C) dT^*, \quad (6)$$

and the normalized heat-generation term G is defined as

$$G = u \frac{(\beta C + 1) C_p}{T} \left[V_1 + V_2 \frac{C}{T} + V_3 r^2 + \frac{V_4}{0.1 + Z} \right] \quad (7)$$

The dimensionless transport properties, such as viscosity and conductivity, are evaluated from the following elementary mixing equation

$$x = \frac{M}{\frac{C m_1}{x_{1,0}} + \frac{(1-C) m_2}{x_{2,0}}} \quad (8)$$

and the dimensionless diffusivity is calculated from the Gilliland's empirical equation

$$\bar{D} = \frac{D_{1,2}}{D_{1,1}} = \frac{\left(2 v_1^{1/3} \right)^2}{\left(v_1^{1/3} + v_2^{1/3} \right)^2} \sqrt{\frac{m_1}{2} \left(\frac{1}{m_1} + \frac{1}{m_2} \right)} \quad (9)$$

The turbulent effect is also included in the analysis by defining that

$$\mu_t = \mu \left(1 + \frac{\rho \epsilon}{\mu} \right) \quad (10)$$

$$D_t = D \left(1 + \frac{\epsilon}{D} \right) \quad (11)$$

$$k_t = k \left(1 + \frac{C_p \rho \epsilon}{k} \right) \quad (12)$$

where the eddy diffusivity ϵ is evaluated from the expression

$$\frac{\rho \epsilon}{\mu} = A + B \bar{Z}^C \quad (13)$$

An important additional term is now added to the momentum equation so that $\rho \bar{u} = \text{const.}$ along any stream line. This term involves the heat generation term G and results in an increase in velocity along stream lines to which heat is added. This term is added to prevent the stream lines from diverging as would otherwise occur if the pressure were constant and heat were added. Actually if heat is added to a subsonic stream and the stream tube area held constant, the flow will accelerate and the pressure will fall. However, if the heat added to each stream line is different and the density of the flow along each stream line is also different, then different accelerations will occur and a different pressure drop if the flow cross section along each stream tube remains the same. Since the pressure at each axial station should be roughly constant as a function of radius, the pressure drop along each stream line should be approximately the same and accelerations will be roughly inversely proportionate to the density.

Therefore, the method of Weinstein and Todd does not satisfy the correct momentum equation. The added term could be considered a pressure gradient term but, if this is done, would result in radial pressure gradients. Therefore the velocity distributions found by this method must be considered questionable. The solutions for concentrations, however, are not closely coupled with the velocity solutions, so the fact that the momentum equation is not satisfied may not result in important errors in the concentration profiles.

With this additional term in the momentum equation and appropriate manipulations, Equations (1) through (4) become (in dimensionless form)

$$r^2 = 2 \int_0^{\psi} \frac{T d\psi'}{u (\beta C + 1)} \quad (14)$$

$$\frac{\partial u}{\partial Z} = \frac{\beta + 1}{\text{Re}} \frac{\partial}{\partial \psi} \left[r^2 \mu u \frac{\beta C + 1}{T} \frac{\partial u}{\partial \psi} \right] + \frac{a G}{C_p (\beta C + 1)} \quad (15)$$

$$\frac{\partial C}{\partial Z} = \frac{(\beta C+1)^2}{Re Sc} \frac{\partial}{\partial \psi} \left[\frac{Dr^2 u}{T} \frac{\partial C}{\partial \psi} \right] \quad (16)$$

$$(1 - C_{p2}) \Delta T \frac{\partial C}{\partial Z} + C_p \frac{\partial T}{\partial Z} = \frac{\beta+1}{Re Pr} \frac{\partial}{\partial \psi} \left[kr^2 u \frac{\beta C+1}{T} \frac{\partial T}{\partial \psi} \right] \quad (17)$$

$$+ \frac{TG}{u(\beta C+1)}$$

and the transport property equations become

$$\mu = \frac{(\beta C+1)}{\frac{(\beta+1)C}{1+F_1} + \frac{(1-C)}{\mu_2(1+F_1)}} \quad (18)$$

$$D = \frac{(\beta C+1)}{\frac{(\beta+1)C}{D_1+F_1 Sc} + \frac{(1-C)}{D_1+F_1 \mu_2 Sc (\beta+1)}} \quad (19)$$

$$k = \frac{(\beta C+1)}{\frac{(\beta+1)C}{1+Pr F_1} + \left(\frac{(1-C)}{Pr \mu_2 C_{p2} F_1} \right) k_2} \quad (20)$$

where

$$G \equiv u \frac{\beta C+1}{T} C_p \left[V_1 + V_2 \frac{C}{T} + V_3 r^2 + \frac{V_4}{0.1+Z} \right]$$

$$D_1 \equiv \frac{2\sqrt{2(\beta+2)}}{\left(1 + \bar{V}_2^{1/3} \right)^2}$$

The above final equations, Equations (14) through (20), contain seven unknowns; r , u , T , C , V , D , and k . These equations are linear in form and can be solved numerically with proper boundary conditions to determine the mass diffusion and momentum transport for a certain distribution of energy generation in the flow field.

2.2.1.1 Computer Considerations

The computation steps used in solving Equations (14) through (20) have been programmed into an IBM 7094 digital computer by Lewis Research Center. The input to this program consists mainly of the inlet conditions and physical properties of the fluids, the turbulence parameters, the coefficients of the heat generation expression, and the step sizes of the numerical iteration. The sources of information for the physical properties of the fluids have been obtained from References (2), (4), (33), and (36). These references represent the up-to-date knowledge on the propellant and the fuel. The flow has been assumed turbulent, and the turbulence parameters, A, B, and C in Equation (13), are taken to be ten, zero, and one respectively, so that $\rho \epsilon / \mu$ has a constant number of ten. This means that the turbulent transport properties are eleven times larger than the laminar values. The choice of such a turbulent level is completely arbitrary. However, it is believed that the selection is suitable for the low-velocity cases considered here.

In using the computer program, the method is to match the temperature profiles obtained by this program with those obtained by the aforementioned radiation program. Once the matching is accomplished, the inlet and boundary conditions of these two programs should be identical. The method of varying the temperature in the fluid flow program is to adjust the values of the coefficients of the heat-generation expression shown in Equation (7). Unfortunately no close matching of the temperature profiles was obtained after a series of trials had been made with Equation (7). A new heat-generation expression was then formulated. Instead of adding the effects of each term as shown in Equation (7), the new expression uses the product of several of these terms. With this new expression, the temperature matching was improved and is expressed.

$$G' = \frac{u(3C+1)C_p}{T} \left[(V_1 + V_2 r^{2.5}) (1 + V_3 \frac{\sqrt{C}}{T}) \left(\frac{V_4}{V_4 + Z} \right) \right] \quad (21)$$

The level of heat input throughout the flow field is essentially provided by the V_1 term, and the radial variation in heat generation is contained in the V_2 term. It was determined that a power of 2.5 for r would produce better results than 2. The V_3 term provides for heat generation in the inner stream; the power of C is reduced to 0.5 to increase its significance in the outer stream. The effect of local density variation is combined into the V_3 term by the factor $1/T$. The V_4 term gives the axial variation of the heat input. 2-29

Most of the input parameters are dimensionless. In evaluating the ratios of viscosities, thermal conductivities, and specific heats, the values of these physical properties are based on the average temperatures of the fuel and the propellant. The average temperature of the fuel column has been taken equal to 21000°R and 7000°R for the propellant flow. The Reynolds number, the Schmidt number, and the Prandtl number are all evaluated with the inlet fuel conditions. The temperature of the fuel at the inlet is taken to be 20000°R , the \bar{v}_2 in the D_1 expression, Equation (20), is 0.225, and β is 117.

2.2.2 Schedule of Calculations

Since the temperature matching mentioned above involves tedious trial and errors, no attempt was made to perform a parametric study. Only two specific examples are considered, having flow conditions identical to Cases 1 and 2 in the radiation problem previously discussed. The input values are listed as follows:

	<u>Case 1</u>	<u>Case 2</u>
Reynolds number	5.81×10^5	2.905×10^4
Schmidt number	1.29	34.9
Prandtl number	0.916	0.597
μ_2/μ_1 $\frac{\text{Hydrogen viscosity (avg)}}{\text{uranium viscosity (avg)}}$	0.398	0.229
k_2/k_1 $\frac{\text{Hydrogen thermal conductivity (avg)}}{\text{uranium thermal conductivity (avg)}}$	94.1	93.2
$\frac{C_{p2}}{C_{p1}}$ $\frac{\text{H}_2 \text{ specific heat (avg)}}{\text{v}_{235} \text{ sp. heat (avg)}}$	118	150
u_2/u_1 $\frac{\text{Inlet H}_2 \text{ velocity}}{\text{Inlet v}_{235} \text{ velocity}}$	10	2
T_2/T_1 $\frac{\text{Inlet H}_2 \text{ temperature}}{\text{Inlet v}_{235} \text{ temperature}}$	1	1
IMAX Computer input	425	425

Here IMAX represents the number of intervals in the ψ direction that the computer can take. This number has been modified so that a maximum number of 425 can be used in the program. This means that more stream lines can be computed by the machine.

2.2.3 Results and Discussion

With the above fixed inputs, attempts were made to match the temperature profiles by varying the value of V 's in Equation (21) and of $\Delta\psi$ which is the mesh size of the stream function. For Case 1, it was found that with $V_1 = 15$, $V_2 = -2.64$, $V_3 = 2$, $V_4 = 0.1$, and $\Delta\psi = 0.155$, the temperature profiles calculated by the fluid flow program matched quite closely those obtained from the radiation program, especially at the interface of the gases. For Case 2, a good match can be obtained with the same values of V 's, but $\Delta\psi$ must be changed to 0.143. Figure 2-12 shows the temperature results of Case 1 from the fluid flow program. A comparison of the results of figure 2-12 with the results of figure 2-13 indicates that the matching is poor near the wall. Fortunately, this is not critical since the interface between the fuel and propellant is mainly the region of interest and the temperature distribution near a boundary for the radiation program is not exact.

The velocity distributions of Case 1 are plotted in figure 2-14. Due to the heat generation term added to the momentum equation, the velocity of the fuel in the core has jumped about eleven to twelve times in the axial direction. Generally, the velocity near the axis is slightly higher than that near the interface because of the higher temperature near the center. In the outer stream, the energy transferred from the central core causes the velocity of the much lighter propellant to increase approximately six times. The closer the propellant gets to the hot fuel, the higher the velocity. For the reasons previously given, these velocity results must be considered very questionable but are reported here since they do represent the result of this method of computation.

The main purpose of running the fluid flow program is to determine the mixing of gases near the interface so that the amount of fuel escaped from the scoop and that of propellant diffused into fuel can be determined for the cycle and engine analyses. The method of determining the diffusion rates is illustrated in Appendix I. The results of diffusion for both Case 1 and 2 are shown in figures 2-15 through 2-18. Figure 2-15 shows the fraction of uranium which is retained in a certain size of scoop placed at some axial distance in the reactor. For example, if a scoop of 3.03 feet in diameter is placed at the exit

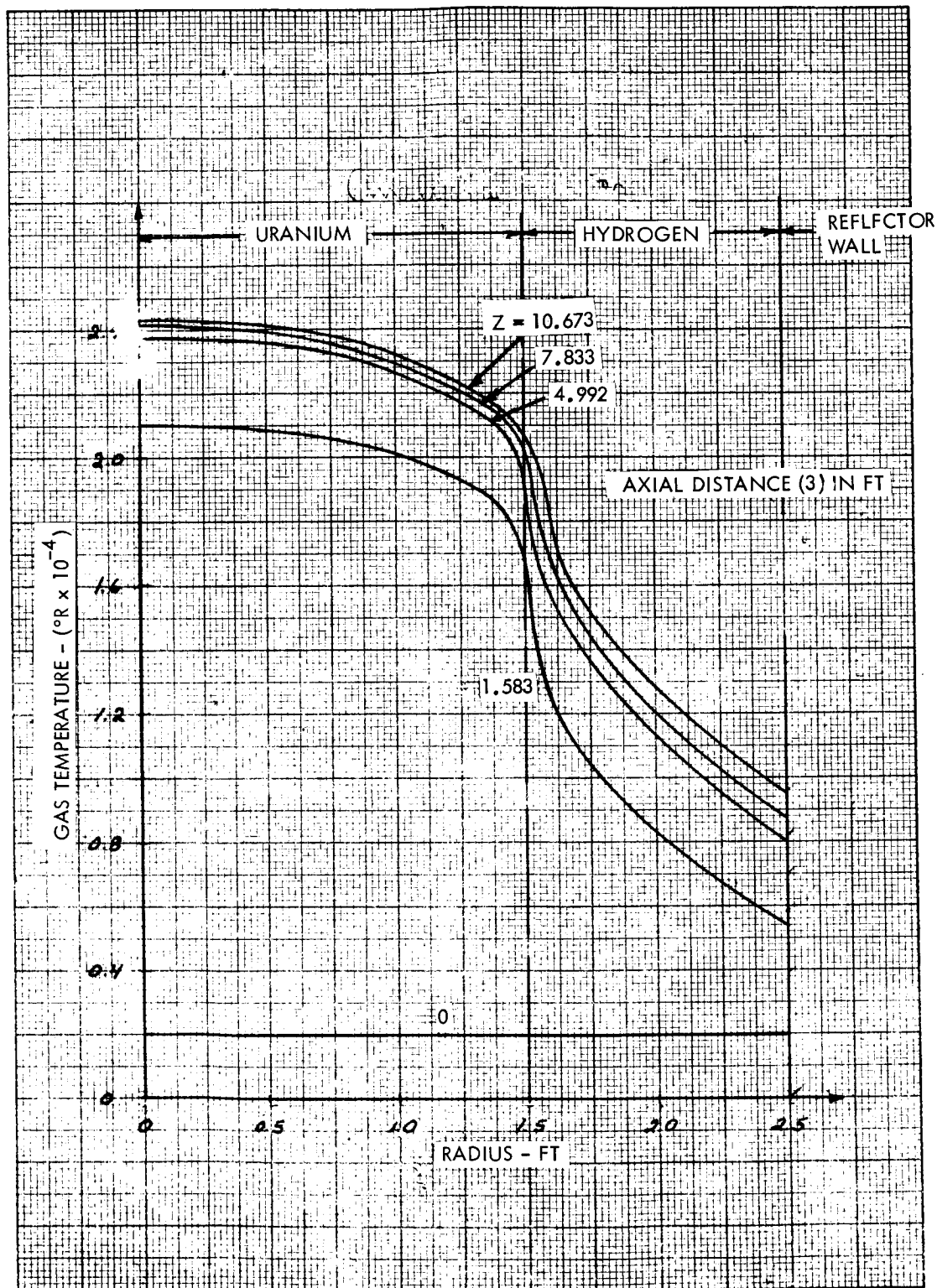


Figure 2-12 Temperature Distributions in the Reactor
From Fluid Flow

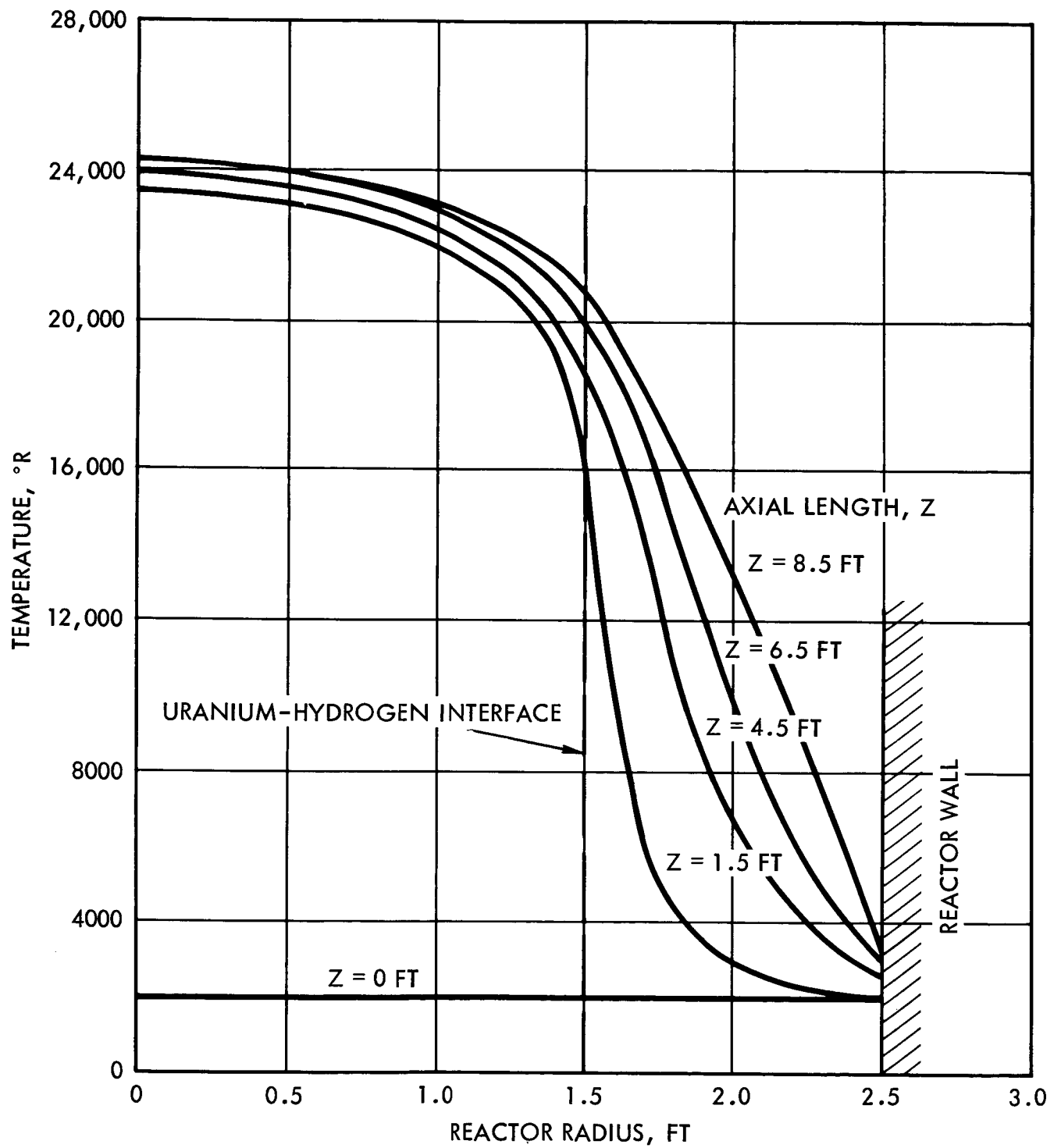


Figure 2-13 Temperature Distribution in the Reactor Based on Einstein Radiation Analysis

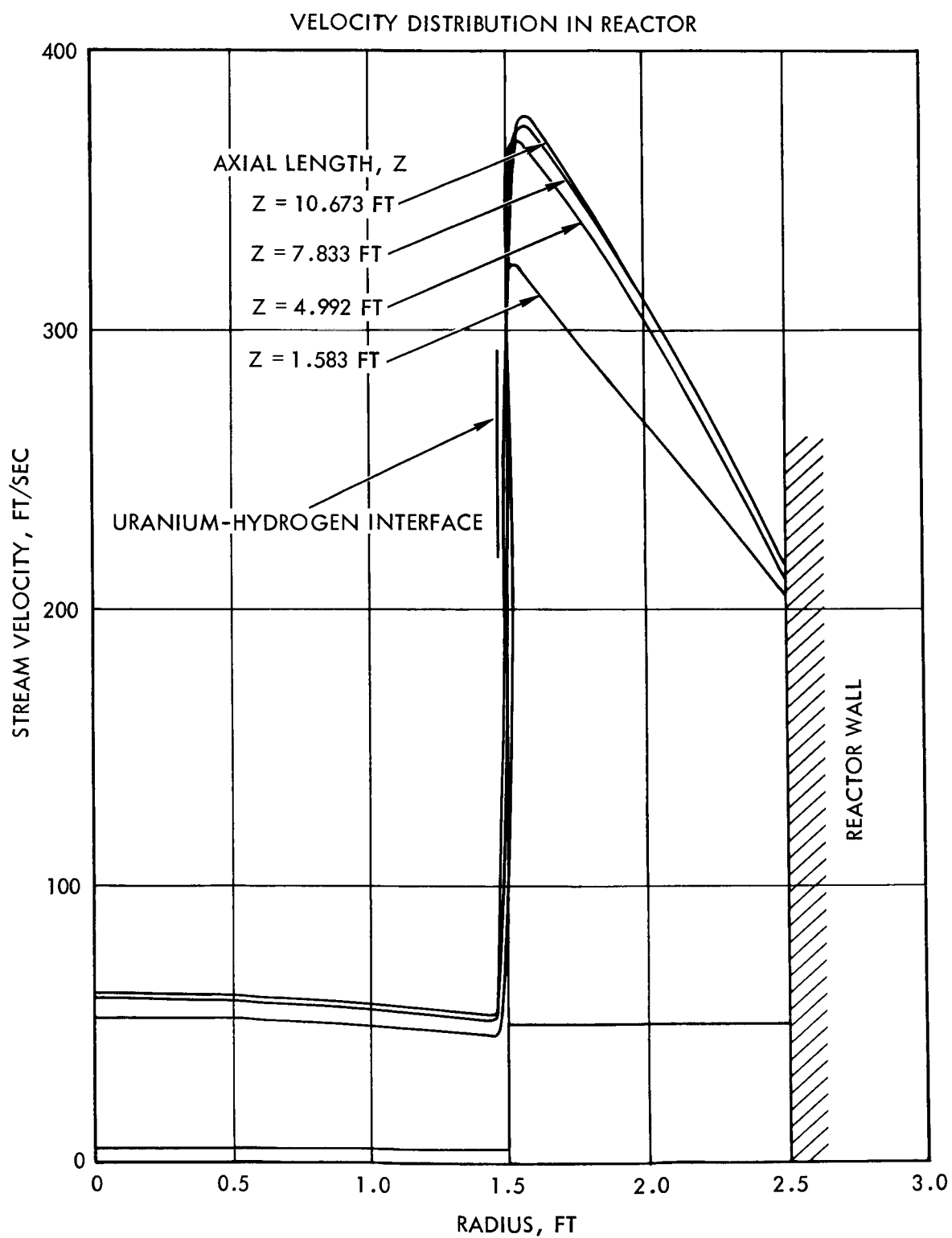


Figure 2-14 Velocity Distribution in Reactor From
Fluid Flow Computer Program (Case 1)

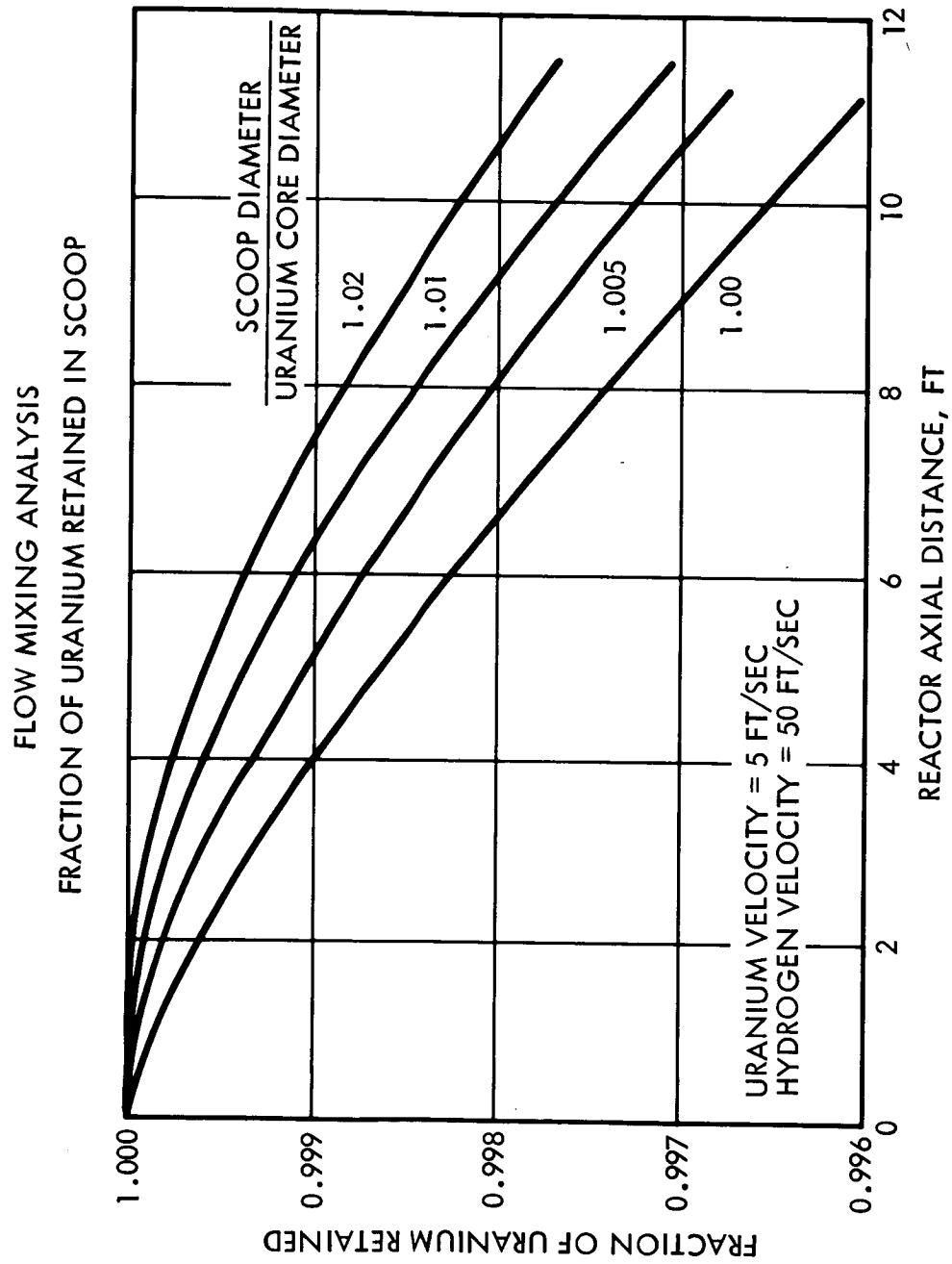


Figure 2-15 Uranium Mass Diffusion From Fluid Flow Computer Program (Case 1)

of the reactor, the amount of uranium collected by this scoop is equal to 99.77% of the inlet uranium. At the same time, the amount of propellant diffused into this scoop is only 0.45% of the inlet propellant flow rate. This result is shown in figure 2-16, which relates the propellant diffusion rate to the scoop size.

The results of mass diffusion for Case 2 are shown in figures 2-17 and 2-18. Generally, the diffusion rate of Case 2 is higher than that of Case 1. If the same scoop is considered, the corresponding values for uranium and hydrogen are 99.0% and 2.35% respectively. It is seen that Case 2 has a diffusion rate approximately four times larger than Case 1. From the momentum consideration, the mass diffusion is proportional to $1/\sqrt{R_e}$. The effect of pressure on diffusivity has been omitted here since the diffusion coefficients, as calculated by Equation (9) are based only on the molecular volumes and the molecular weights which have been assumed constant in this analysis.

The analysis of fluid flow in a reactor by Weinstein and Todd is questionable for the reasons stated previously; however, it is a workable means of computation. From the computer outputs, it is seen that the addition of an extra term into the momentum equation has made all the streamlines parallel to the axis. Thus, the simulation of a channel flow by a coaxial flow model with an annular stream infinite in extent is realized. The other assumptions made in this analysis are generally acceptable with the exception of temperature independence of the physical properties. As mentioned earlier in this section, the values of thermal conductivity, viscosity, diffusivity, etc., used in the calculations, are obtained with the average temperatures of the fuel and the propellant. Since the inlet and the outlet temperature can be differed by a factor of six or seven, it is evident that using the average values of physical properties can only result in an approximate solution. Moreover, it is noted that the parameter β has been assumed constant in the whole computation. As the gas temperature is increased, the dissociation or ionization of the gas will occur, and the molecular weight of the gas will change accordingly. It is difficult to visualize then how the parameter β can be kept constant.

The computer programs, as obtained from NASA Lewis Research Center, exhibit certain deficiencies in putting the programs to effective use. The primary deficiency was the lack of program documentation. This lack causes an undue amount of time to be spent whenever it is necessary to modify the program. Also, the programs themselves are not written so that they are very flexible. This, in itself, makes modification more difficult. Therefore, for further use of these programs in the future, it is recommended that attempts should first be made to remedy these deficiencies. 2-36

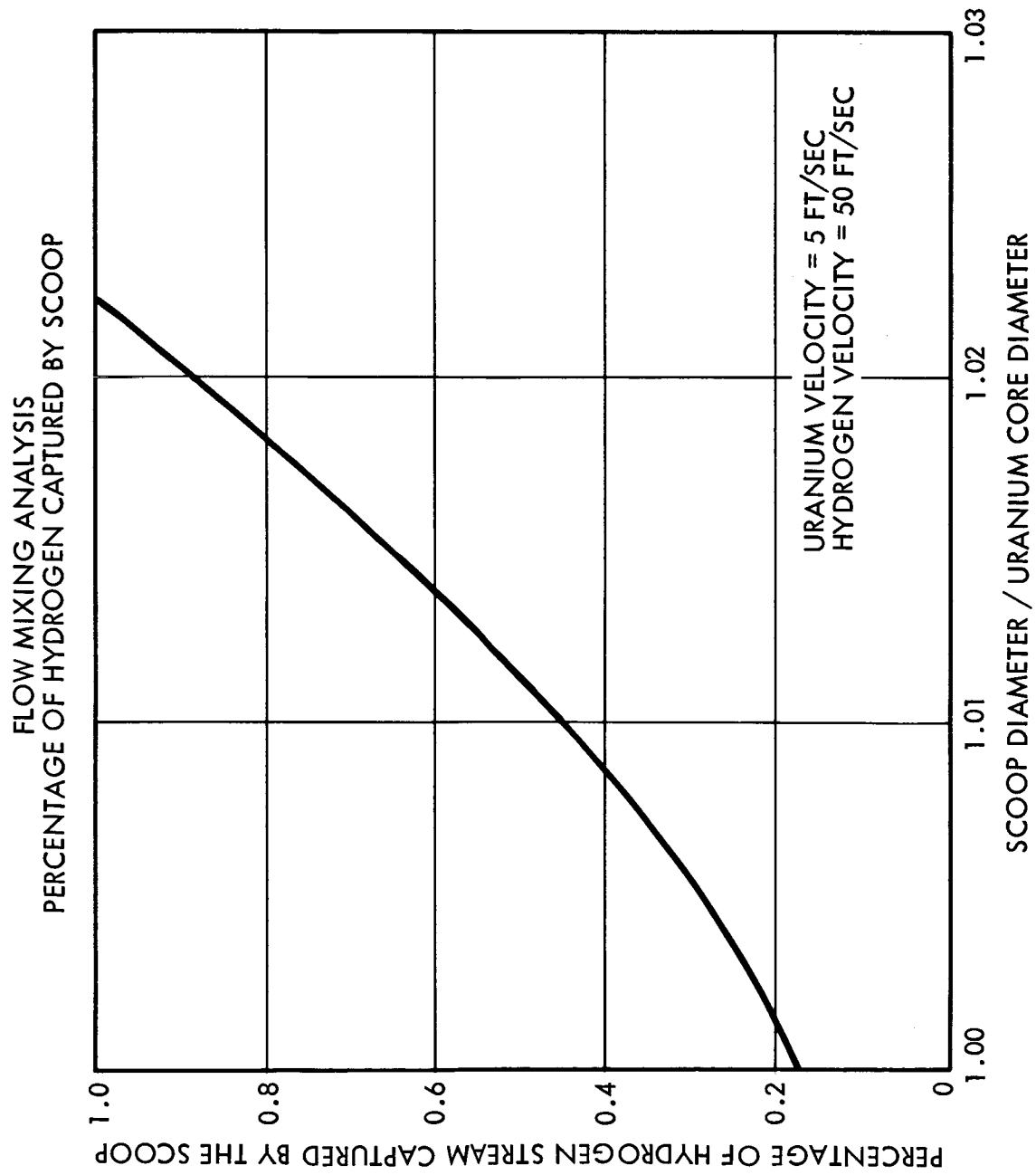


Figure 2-16 Hydrogen Mass Diffusion at Scoop Entrance from Fluid Flow Computer Program

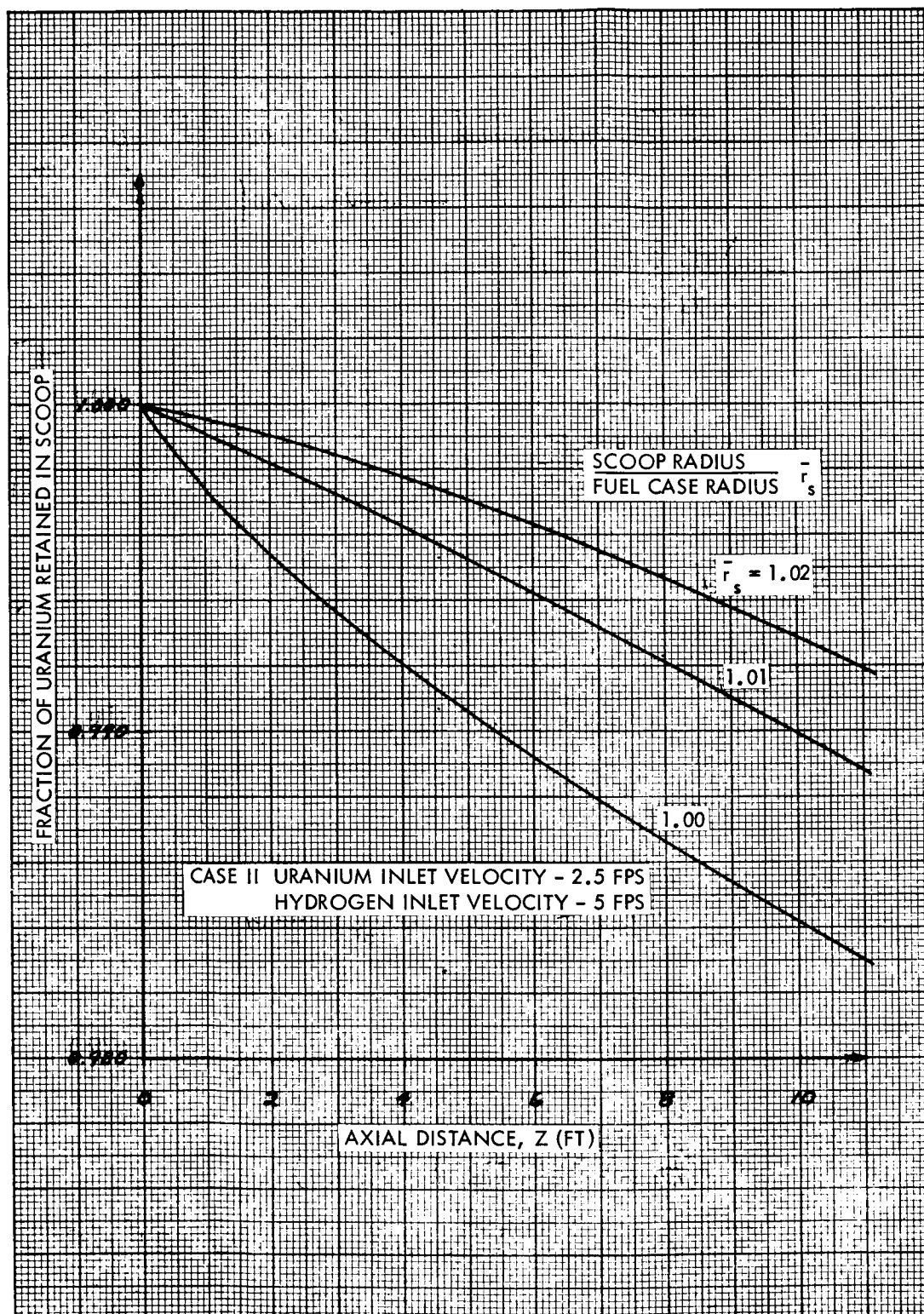


Figure 2-17 Uranium Mass Diffusion from Fluid Flow
Computer Program

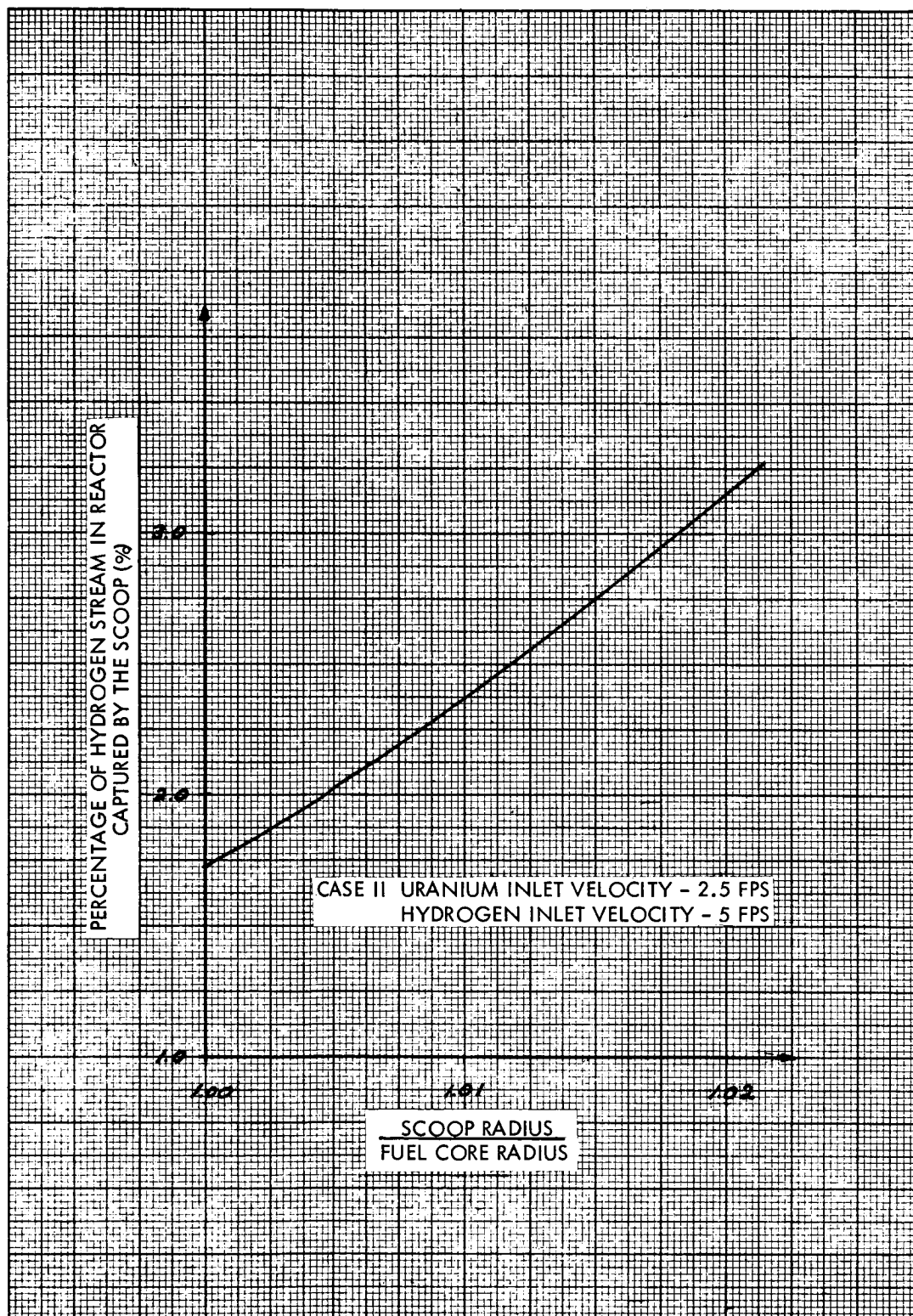


Figure 2-18 Hydrogen Mass Diffusion at Scoop Entrance
from Fluid Flow Computer Program

3. ADVANCED COOLING STUDIES

3.1 TRANSPIRATION COOLING TECHNIQUES

The realization of high performance rocket propulsion systems depends on the achievement of high temperatures. However, sustained operation at high temperature requires the development of methods capable of cooling components exposed to high heat fluxes. In gas core reactors, the ultimate performance of the system depends on the effectiveness with which material surfaces can be cooled. Techniques must, therefore, be developed so that materials can withstand the high heat fluxes produced in the nozzle and reactor cavity.

Regenerative cooled components which rely on purely convective cooling techniques can be applied to surfaces with maximum heat fluxes in the vicinity of 15 to 20 Btu/in²-sec. Regeneratively-cooled nozzles with heat fluxes of this magnitude at the throat have been developed and successfully tested on solid core nuclear reactors. In gas-core rockets, materials are subjected to heat fluxes at an order of magnitude greater than experienced in solid-core rockets. These materials must be capable of withstanding high heat fluxes if the gas core reactor ever is to become a feasible space propulsion system. For heat fluxes significantly greater than 20 Btu/in²-sec, regenerative cooling is inadequate. Gas core reactor components must, therefore, utilize more advanced cooling techniques such as film or transpiration cooling, which require the injection of coolant through a porous wall. The principal advantages of transpiration cooling over convective cooling are two-fold. First, the coolant passing through the wall efficiently removes heat from the wall materials since the porous wall provides a large surface area for heat transfer. The second advantage of transpiration cooling is the injection of mass into the boundary layer which decreases the local convective heat flux to the material wall.

3.1.1 Model Description

For study purposes, a segment of a transpiration-cooled wall, shown schematically in figure 3-1 will be analyzed. The porous wall has a coolant that is injected through the porous wall and forms a boundary layer on the surface of the wall. Heat is transferred to the wall by simultaneous convection

and radiation. The heat actually reaching the wall surface can be conducted from the wall material to either the coolant injected through the wall or can be transferred to the coolant flowing along the inside of the wall.

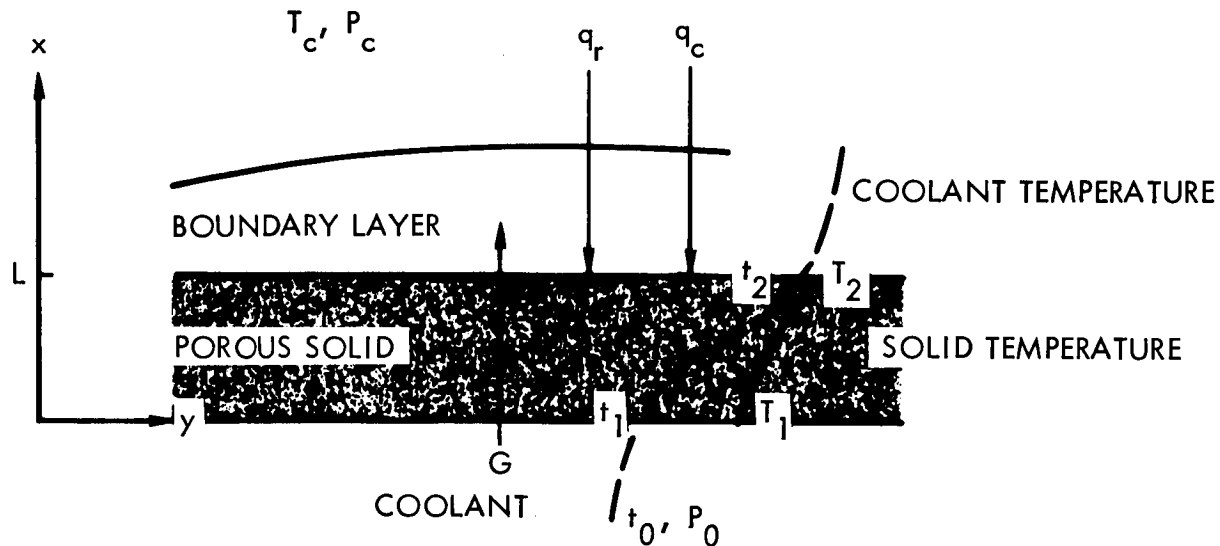


Figure 3-1 Schematic of Transpiration-Cooled Wall

The analysis in this transpiration study is only concerned with the coolant passing through the porous walls and the attendant wall temperature distribution and pressure drop. The additional effect of mass injection into the gas-side boundary layer and the consequent blockage if the heat transfer mechanism is convective is treated under convective cooling techniques.

3.1.2 Temperature Distribution (Infinite Heat Transfer Coefficient)

Before studying more complex models of transpiration cooling, much can be learned by investigating the limiting case of heat removal from a porous wall by gaseous coolant*. In this model, the surface per unit volume of porous structure is assumed high enough that the temperature of the fluid at each location in the solid is equal to that of the adjacent solid. In other words, this model assumes that the heat transfer coefficient between the solid and coolant is infinite.

* The gas and adjacent wall temperatures are equal in the porous wall (the convective heat transfer coefficient is infinite). 3-2

A schematic of a porous wall through which gas is flowing is shown in figure 3-2. For purposes of this derivation, the temperature distribution of the gas flowing through a porous wall is evaluated based on the following assumptions:

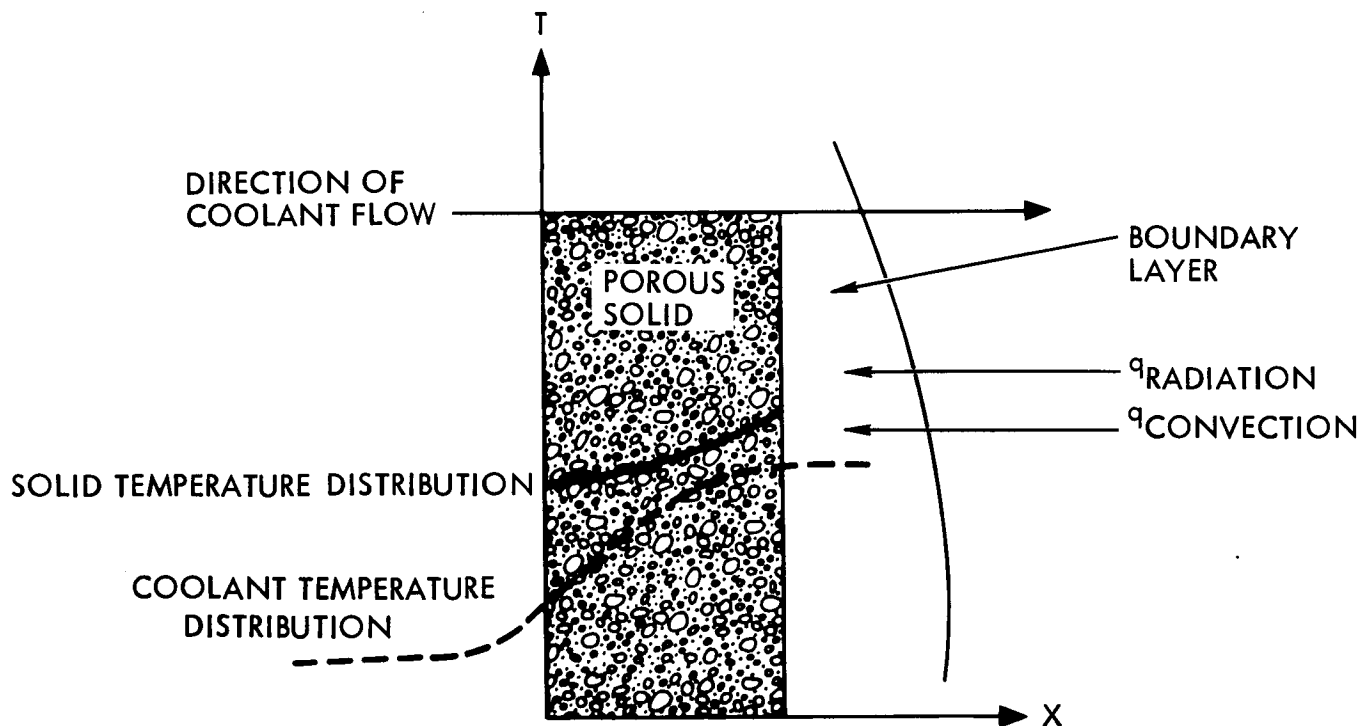


Figure 3-2 Temperature Distribution of Gas Flowing Through a Porous Wall

1. The gas and adjacent wall temperatures are equal in the porous wall (the convective heat transfer coefficient is infinite).
2. Heat and mass flow is one-dimensional.
3. Heat conduction through the coolant is negligible compared to through the solid material.
4. The thermal conductivities of the solid and gas and the specific heat of the gas are constant.

A heat balance on an element of volume in the porous wall which has a uniform rate of heat generation is illustrated in the following schematic:

$$\dot{m} C_p T - k_s A_s \frac{dT}{dx} \left(\overset{\text{A}}{\underbrace{Q_o A_s dx}} \right) \rightarrow \dot{m} C_p \left(T + \frac{dT}{dx} dx \right) - k_s A_s \left(\frac{dT}{dx} + \frac{d^2 T}{dx^2} dx \right)$$

where

\dot{m} = weight flow rate of coolant

C_p = specific heat of gas

T = solid wall temperature

t = gas temperature

x = length

k_s = thermal conductivity of solid

Q_o = solid volumetric heat generation rate

P = open porosity = $\frac{\text{effective flow area}}{\text{total area}}$

A = total cross sectional area

$A_s = (1 - P) A$ = solid cross sectional area

$G = \frac{(1 - P)}{P} \left(\frac{\dot{m}}{A_s} \right) = \frac{\dot{m}}{PA}$ = weight flow rate per unit flow area

The heat balance leads to the following second order differential equation for the temperature distribution in the wall.

$$\text{Wall: } \frac{d^2 T}{dx^2} - \frac{GPC_p}{(1-P)k_s} \frac{dT}{dx} + \frac{Q_o}{k_s} = 0$$

A similar balance on an element of gas results in a similar equation

$$\text{Gas: } \frac{d^2 T}{dx^2} - \frac{GPC_p}{k_g} \frac{dT}{dx} = 0$$

The boundary conditions which must be satisfied when a heat flux of q/A is incident on the transpiration-cooled wall are as follows:

$$1. \text{ At } x = 0, T = T_1$$

$$t = T_o$$

$$\text{and } k_g \left(\frac{dt}{dx} \right)_{\text{gas}} = k_s (1 - P) \left(\frac{dT}{dx} \right)_{\text{solid}}$$

$$2. \text{ At } x = -\infty, t = t_o$$

$$3. \text{ At } x = L, \frac{q}{A} = k_s (1 - P) \left(\frac{dT}{dx} \right)_{\text{solid}}$$

The solutions of the differential equations are

$$\begin{aligned} \text{Wall: } T - t_o = & \left(\frac{q}{A} - \frac{Q_o k_s (1-P)^2}{G P C_p} \right) \frac{1}{G P C_p} \exp \frac{G P C_p L}{k_s (1-P)} \left(1 - \frac{x}{L} \right) \\ & + \frac{Q_o L (1-P)}{G P C_p} \left(\frac{x}{L} \right) + \frac{Q_o k_s (1-P)^2}{(G P C_p)^2}, \quad (0 \leq x \leq L) \end{aligned}$$

where q/A = heat flux per unit of surface area

$$\begin{aligned} \text{Gas: } t - t_o = & \left[\left(\frac{q}{A} - \frac{Q_o k_s (1-P)^2}{G P C_p} \right) \frac{1}{G P C_p} \exp \frac{G P C_p L}{k_s (1-P)} + \frac{Q_o k_s (1-P)^2}{(G P C_p)^2} \right] \\ & \exp \frac{G P C_p L}{k_g} \left(\frac{x}{L} \right), \quad (-\infty \leq x \leq 0) \end{aligned}$$

If there is no internal heat generation (i.e., $Q_o = 0$), the equations for the temperature distribution in the gas and solid reduce to

$$\begin{aligned} \text{Wall: } \frac{T - t_o}{\frac{q}{A G P C_p}} = & \exp - \frac{G P C_p L}{k_s (1-P)} \left(1 - \frac{x}{L} \right) \\ \text{Gas: } \frac{t - t_o}{\frac{q}{A G P C_p}} = & \exp - \frac{G P C_p L}{k_s (1-P)} \exp \frac{G P C_p L}{k_g} \frac{x}{L} \end{aligned}$$

Figure 3-3 shows curves of the dimensionless temperature distribution in the wall with no internal heat generation as a function of the parameter

$$\frac{G P C_p L}{k_s (1-P)} \quad \text{where } \eta = \frac{x}{L}$$

For $x = L$, the wall temperature distribution with no internal heat generation reduces to a simple heat balance between the fluid and solid. For a specific maximum allowable wall temperature T_w^{\max} , the maximum heat flux that can be removed is given by the relationship

$$(q/A)_{\max} = G P C_p (T_w^{\max} - t_o)$$

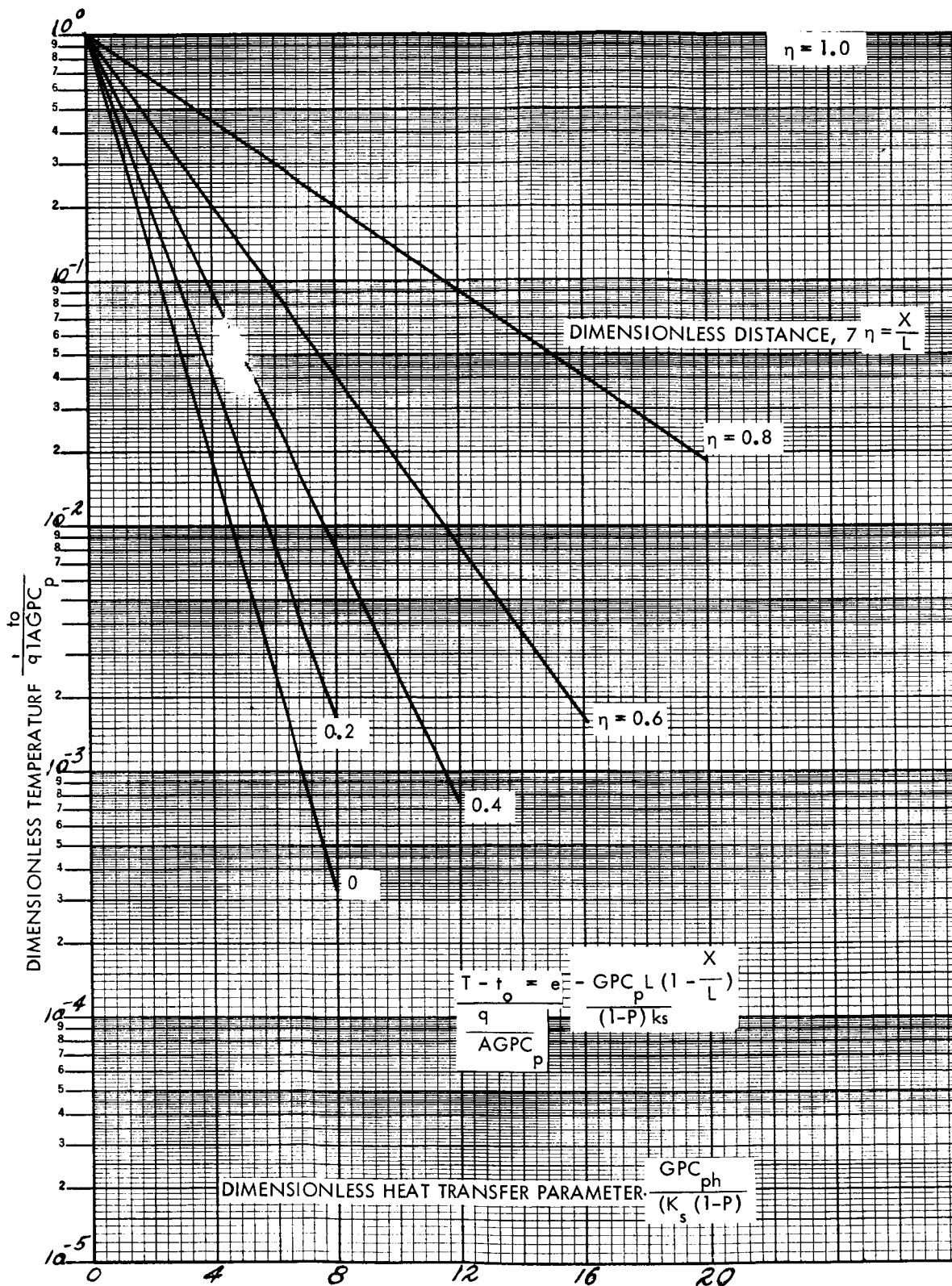


Figure 3-3 Transpiration Cooled Wall Temperature Distribution (Infinite Heat Transfer Coefficient)

The variation of the maximum heat flux as a function of weight flow rate per unit of flow area G and the maximum allowable wall temperature T_w^{\max} is shown in Figure 3-4. For a maximum wall temperature of 3000°R , the maximum heat flux which can be removed as a function of weight flow rate per unit area and porosity is shown in Figure 3-5. The results presented in Figures 3-4 and 3-5 show that if high heat transfer rates can be maintained between the coolant and porous matrix material, surface heat fluxes as high as $200 \text{ Btu/in}^2\text{-sec}$ can theoretically be removed with reasonable values of wall temperature and coolant weight flow rates.

3.1.3 Pressure Drop

The heat flux which can theoretically be removed from a transpiration-cooled surface is very dependent on the flow rate per unit area of coolant passing through the wall. The pressure drop of a fluid flowing through a porous wall will be due to friction and momentum losses. The frictional pressure drop is due to shear stress and for laminar flow may be considered linear with the flow velocity. The momentum losses are proportional to the dynamic pressure of the flow and result from the expansions and contractions of the flow passage. Hence the total pressure drop can be considered to be proportional to the sum of the frictional and momentum losses, i.e.,

$$-\frac{dp}{dx} = \frac{\alpha\mu v}{g_c} + \beta\rho \frac{v^2}{g_c}$$

where α and β are constants of proportionality

$$\begin{aligned}\mu &= \text{fluid viscosity} \\ \rho &= \text{fluid density} \\ v &= \text{fluid velocity} \\ g_c &= \text{universal gravitational constant}\end{aligned}$$

For an isothermal flow of a compressible fluid, the preceding equation may be rewritten in terms of weight flow rate per unit of flow area,

$$-\rho \frac{dp}{dx} = \frac{\alpha\mu G}{g_c} + \frac{\beta G^2}{g_c}$$

where $G = \rho v =$ weight flow rate per unit of flow area. Assuming a perfect gas ρ can be replaced by $\frac{P}{RT}$ so that

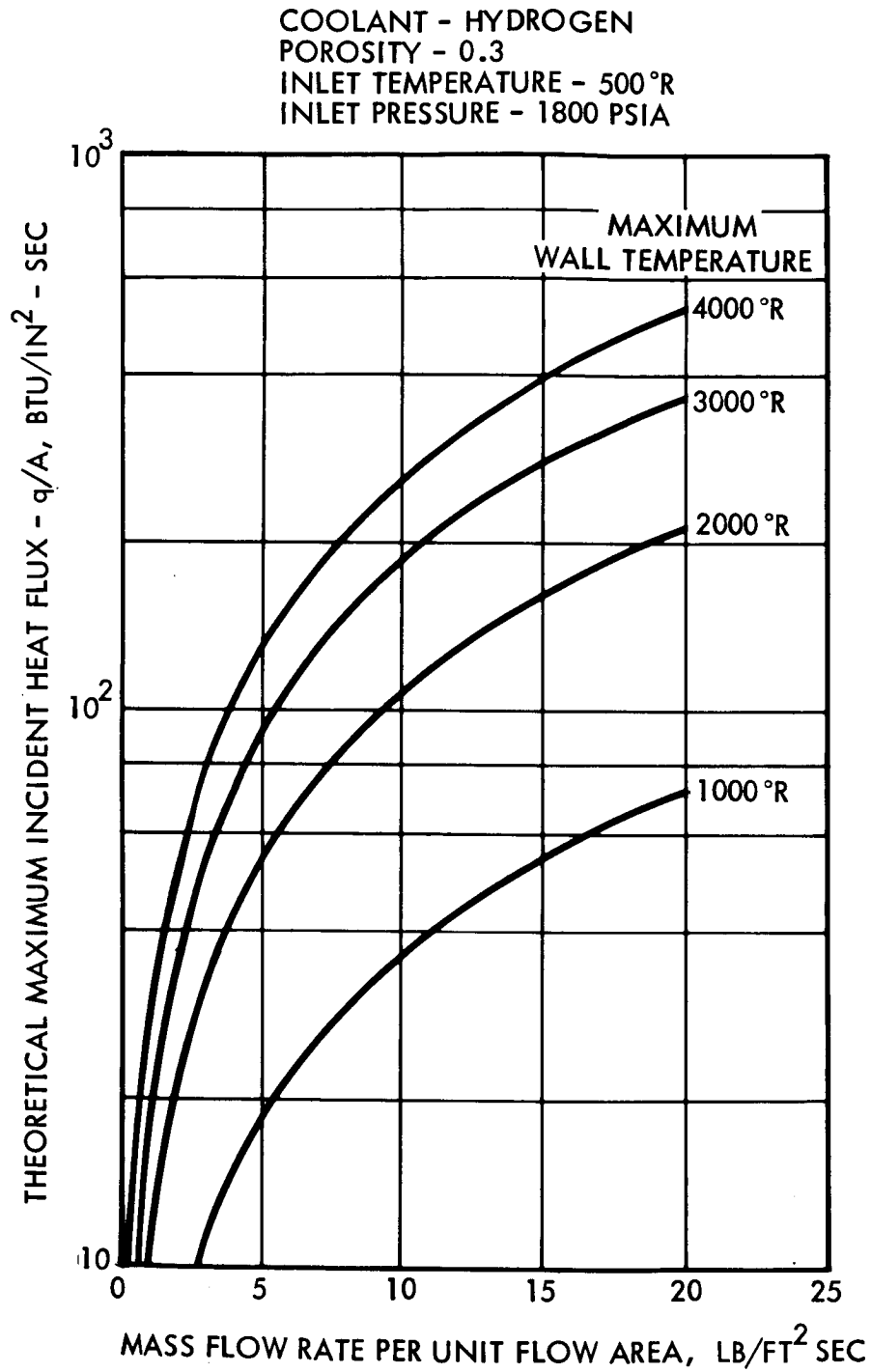


Figure 3-4 Transpiration Cooling Maximum Scoop Wall Heat Flux
(Infinite Heat Transfer Coefficient)

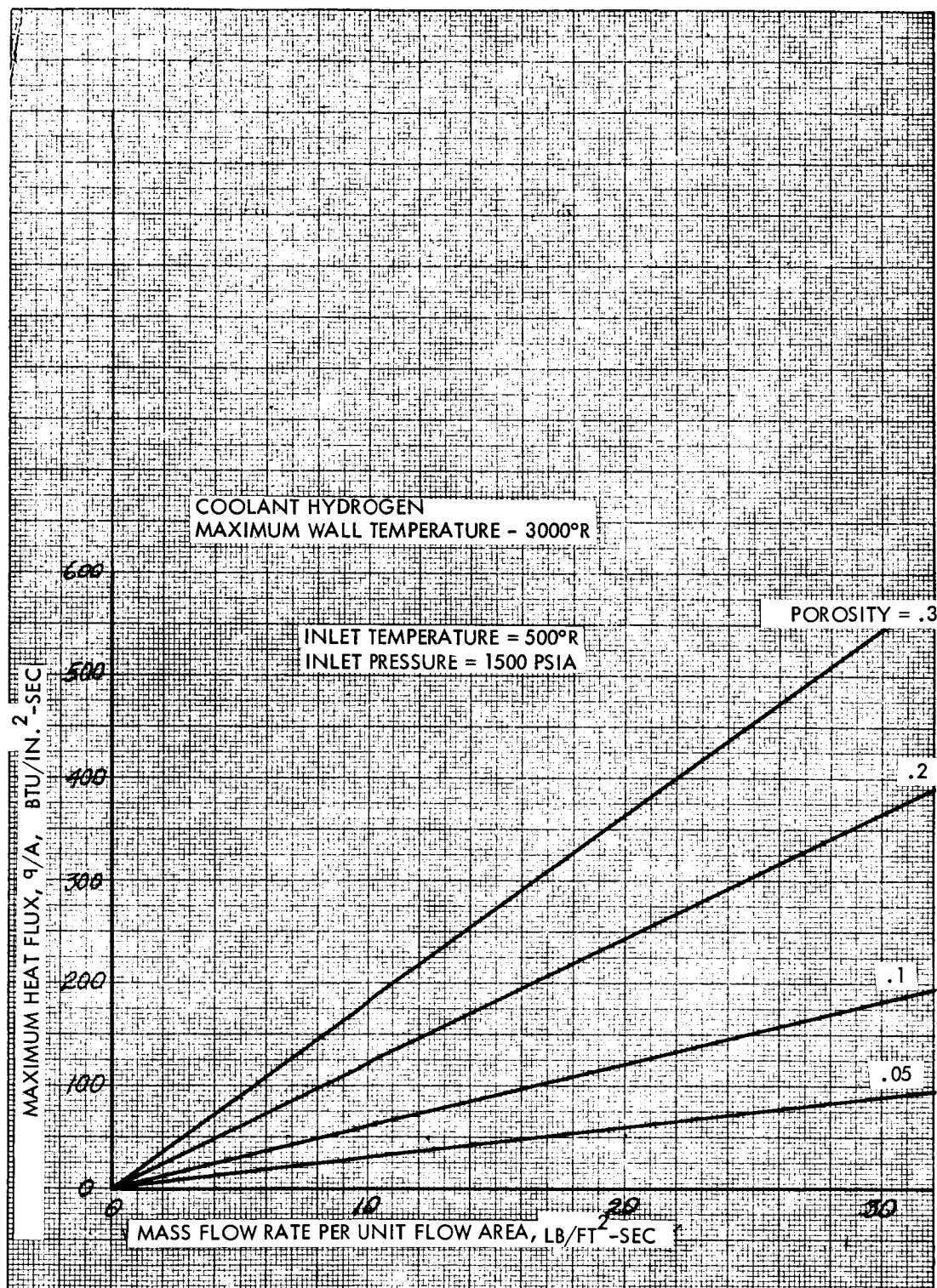


Figure 3-5 Transpiration Cooling Maximum Wall Heat Flux
(Infinite Heat Transfer Coefficient)

$$-\frac{d(p^2)}{dx} = \alpha \left(\frac{2RT\mu}{g_c} \right) G + \beta \left(\frac{2RT}{g_c} \right) G^2$$

where

$$R = \frac{R_u}{M} = \text{specific gas constant}$$

$$P = \text{pressure}$$

Experiments with porous metals² have verified that the pressure gradient in a perfect gas in steady, isothermal flow through a moderately fine-grained porous medium can be presented by the preceding quadratic pressure-drop equation. The proportionality constants α and β are length parameters characteristic of the structure of the porous material and are called the viscous and internal-resistance coefficients of the material, respectively. The viscous coefficient, α , with dimensions, L^{-2} , characterizes the flow resistance of the material in the regime of "creeping" flow, where inertia forces are negligible. The inertial coefficient, β , of dimensions, L^{-1} , provides a measure of the additional resistance due to microscopic accelerations of the fluid within the interstices of the material. Figure 3-6 gives values of α and β for various material porosities.

A rigorous solution of the pressure-drop through the wall would require the integration of the pressure-drop equation across the thickness of wall, substituting at each point, the proper temperature and corresponding viscosity of the coolant gas. For the purpose of this derivation, the coefficients α and β were assumed to be independent of temperature since experimental data indicates that such an assumption is justified. For simplicity, an average viscosity will be assumed initially since a linear temperature dependence of viscosity results in a cumbersome solution which will be presented later. Substituting the temperature distribution with no internal heat source into the pressure drop equation and integrating the equation, we obtain

$$p_o^2 - p^2(x) = \left[\frac{2\alpha R\mu G}{g_c} + \frac{2\beta R G^2}{g_c} \right] \left[t_o x + \frac{q k_s (1-P)}{A(G P C_p)^2} \right. \\ \left. \exp \frac{G P C_p L}{k_s (1-P)} \exp \left(\frac{G P C_p L}{k_s (1-P)} \frac{x}{L} - 1 \right) \right]$$

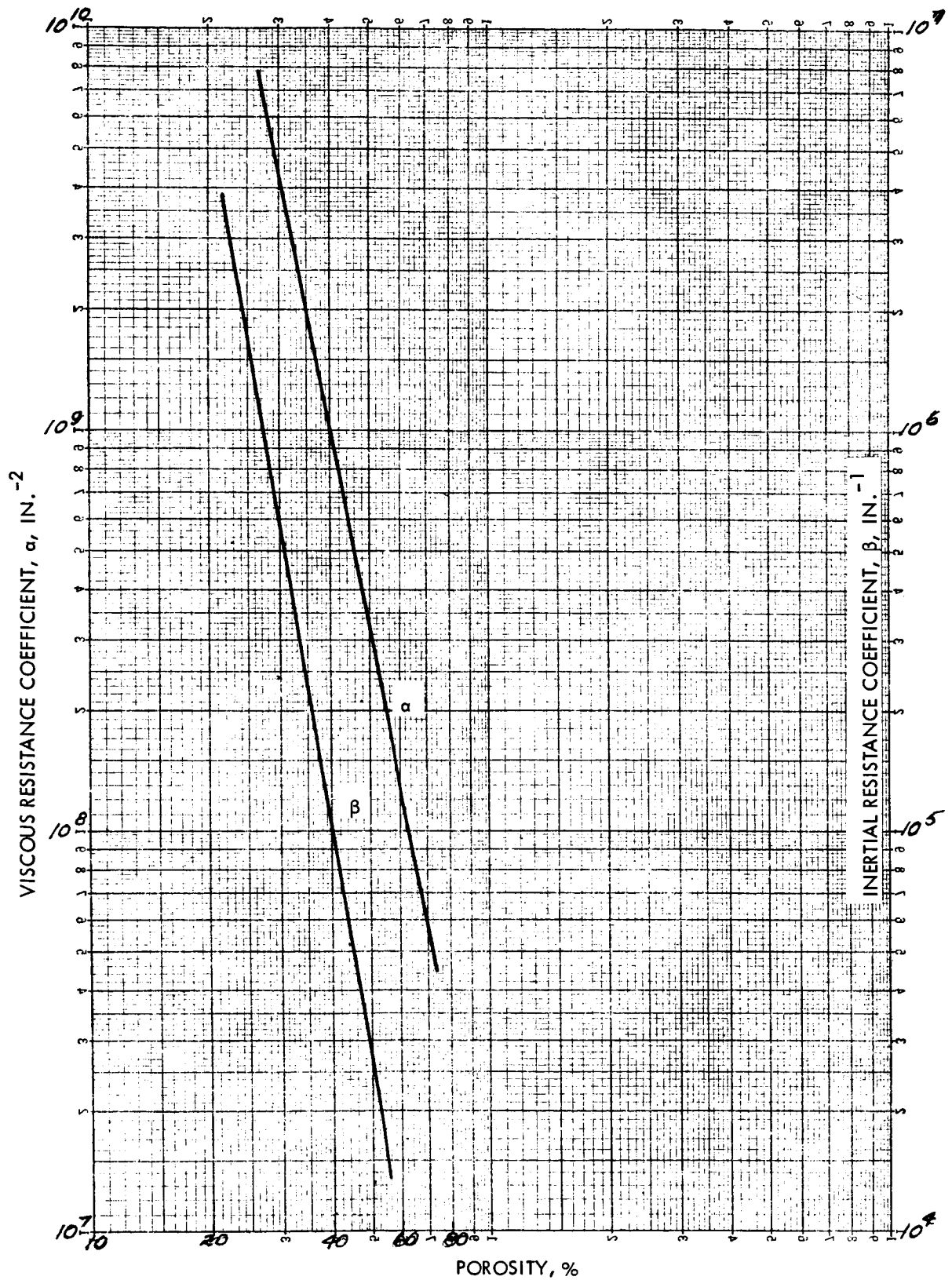


Figure 3-6 Viscous and Inertial Coefficients
3-11

For $x = L$, the equation for the pressure drop across a porous wall reduces to

$$p_o^2 - p_2^2 = \left[\frac{2 \alpha R \mu G}{g_c} + \frac{2 \beta R G^2}{g_c} \right] \left[t_o L + \frac{q k_s (1-P)}{A(GPC_p)^2} \left(1 - \exp - \frac{GPC_p L}{k_x (1-P)} \right) \right]$$

A typical variation of pressure drop with weight flow rate and surface heat flux is shown in figure 3-7 for a 10-mil wall and in figure 3-8 for a 20-mil wall. The possible combinations of surface heat flux, porosity, and weight flow rate per unit flow area resulting in a given pressure drop for a 10-mil wall are shown in figures 3-9 and 3-10 for pressure differentials of 500 and 1000 psi, respectively. These results show that for 10 and 20-mil walls with a 30 per cent porosity, weight flow rates of from 1.5 to 10 lb/ft²-sec can be achieved with a pressure drop of 500 psi. In actual practice, a system would be designed to operate at a given wall temperature and with a specified pressure drop across the porous wall. By combining the results shown in figures 3-5 and 3-9, we can determine as shown on figure 3-11, the maximum heat flux that can be removed from a surface with a specified wall temperature and pressure drop. The maximum heat fluxes that can be removed from a 10-mil porous wall with a maximum wall temperature of 3000°R are shown as a function of porosity in figures 3-12 and 3-13 for wall pressure drops of 500 and 1000 psi, respectively. These curves show that surface heat fluxes as high as 150 Btu/in²-sec can be removed from a 30% porous wall with a 500 psi pressure drop.

If the viscosity is assumed to vary linearly with temperature (i.e., $\mu = \gamma T + \delta$), the pressure drop across a wall of thickness L is given by

$$p_o^2 - p_2^2 = 2 R G t_o L \left(\frac{\alpha \gamma t_o + \alpha \delta + \beta G}{g_c} \right) + \frac{2 R q k_2 (1-P)}{G A (PC_p)^2} \left(\frac{2 \alpha t_o + \alpha \delta + \beta G}{g_c} \right) \\ \left[1 - e \left(- \frac{GPC_p L}{k_s (1-P)} \right) \right] + \frac{\alpha R \gamma q^2 k_s (1-P)}{g_c G^2 (PC_p)^3 A^2} \left[1 - e \left(\frac{2 GPC_p L}{k_s (1-P)} \right) \right]$$

A comparison of the pressure drop as a function of coolant weight flow rate for surface heat fluxes of 50 and 100 Btu/in²-sec are shown in figure 3-14 for an average viscosity and for a linear variation of viscosity with temperature.

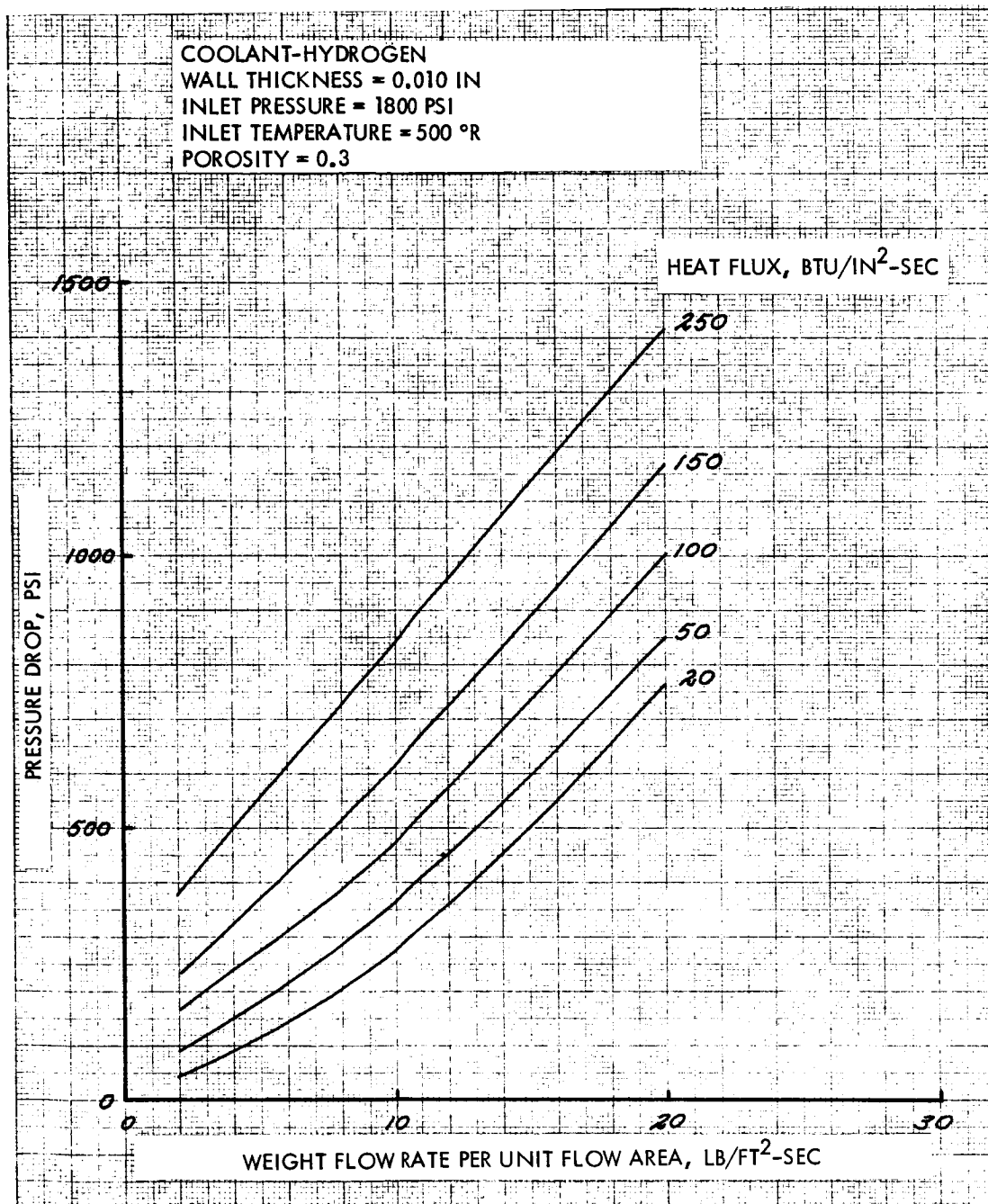


Figure 3-7 Porous Wall Pressure Drop (Infinite Heat Transfer Coefficient)

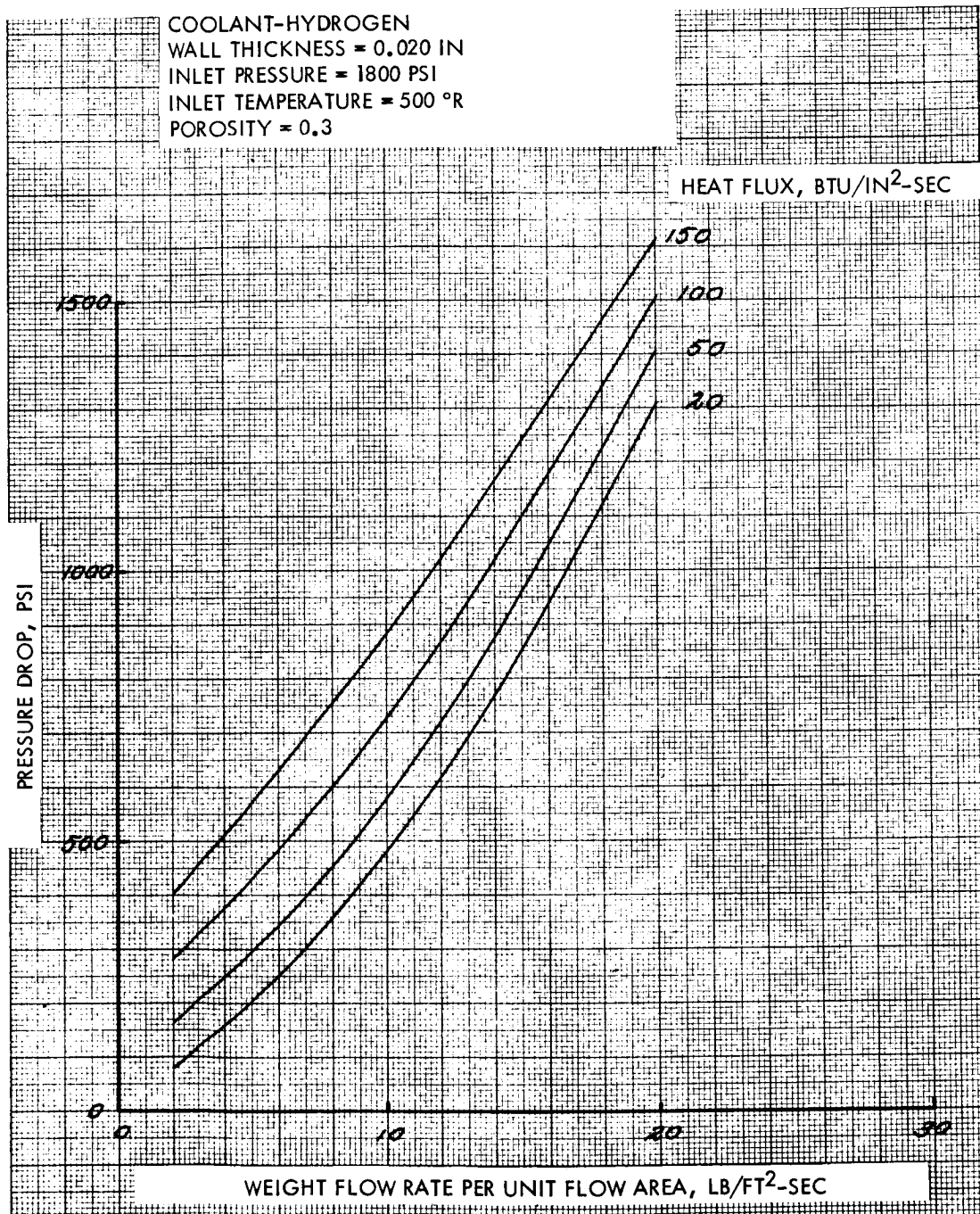


Figure 3-8 Porous Wall Pressure Drop (Infinite Heat Transfer Coefficient)
3-14

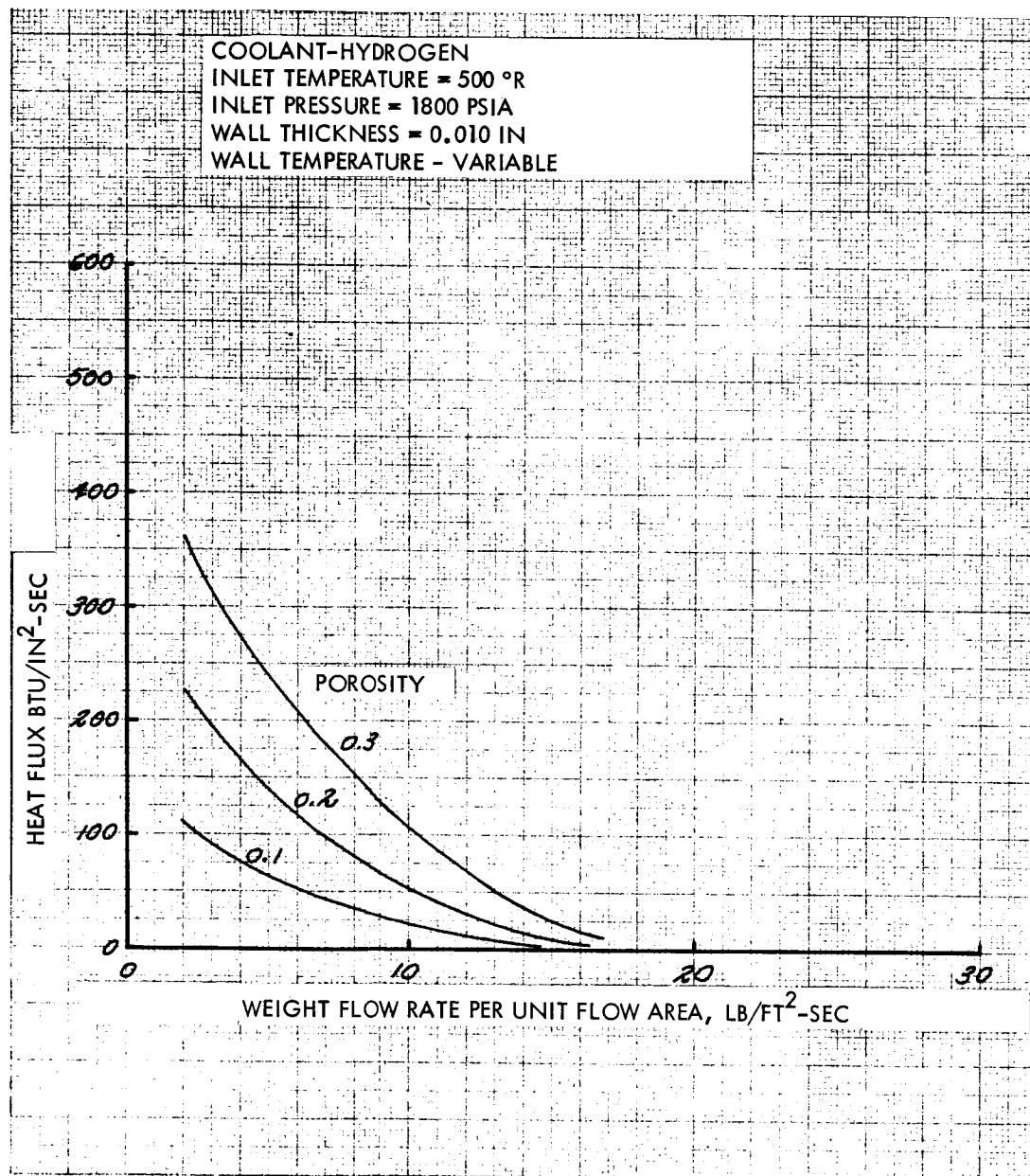


Figure 3-9 Compatible Heat Flux and Weight Flow Rate
Yielding a 500 PSI Pressure Drop (Infinite Heat
Transfer Coefficient)

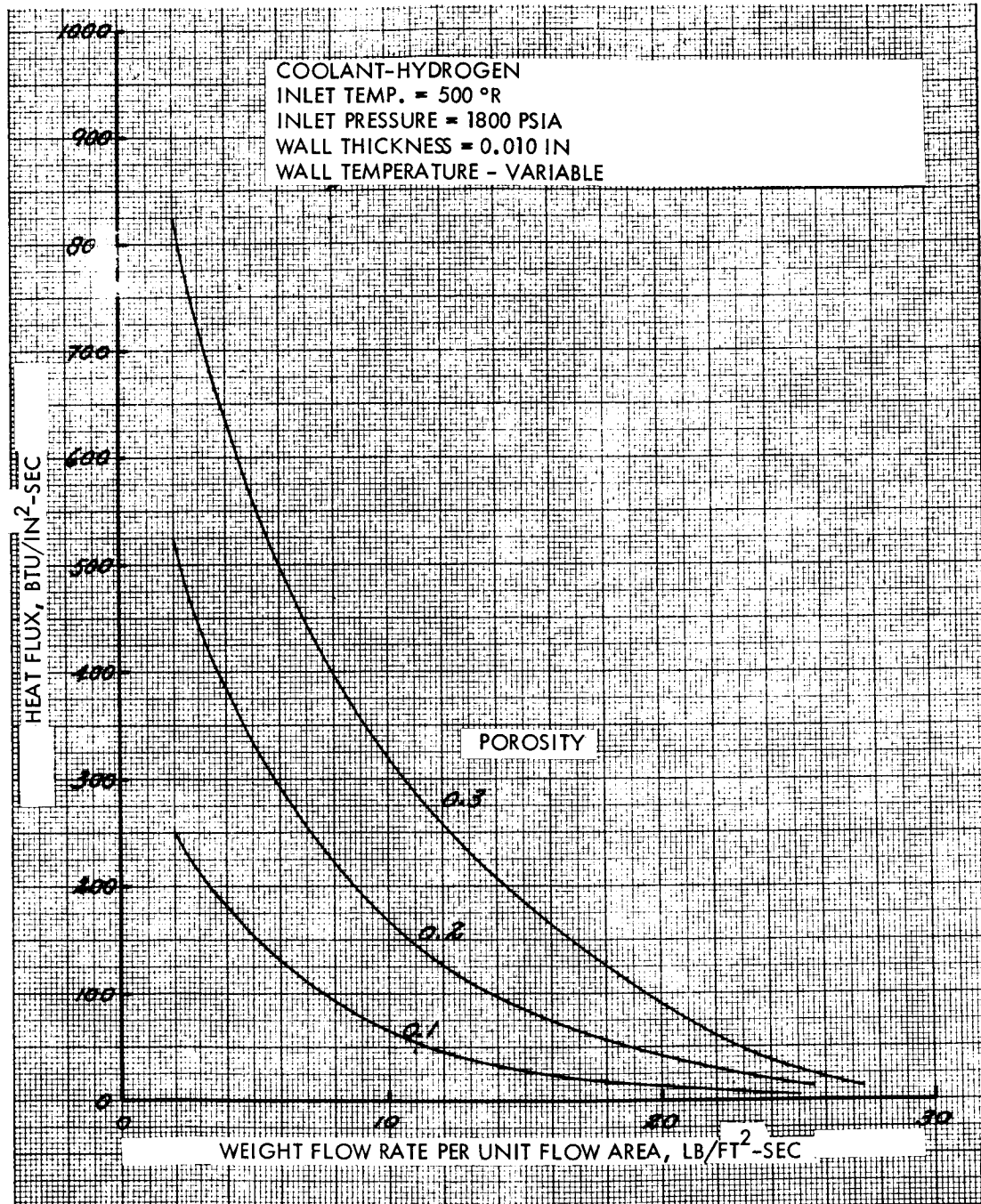


Figure 3-10 Compatible Heat Flux and Weight Flow Rate Yielding a 1000 PSI Pressure Drop (Infinite Heat Transfer Coefficient)

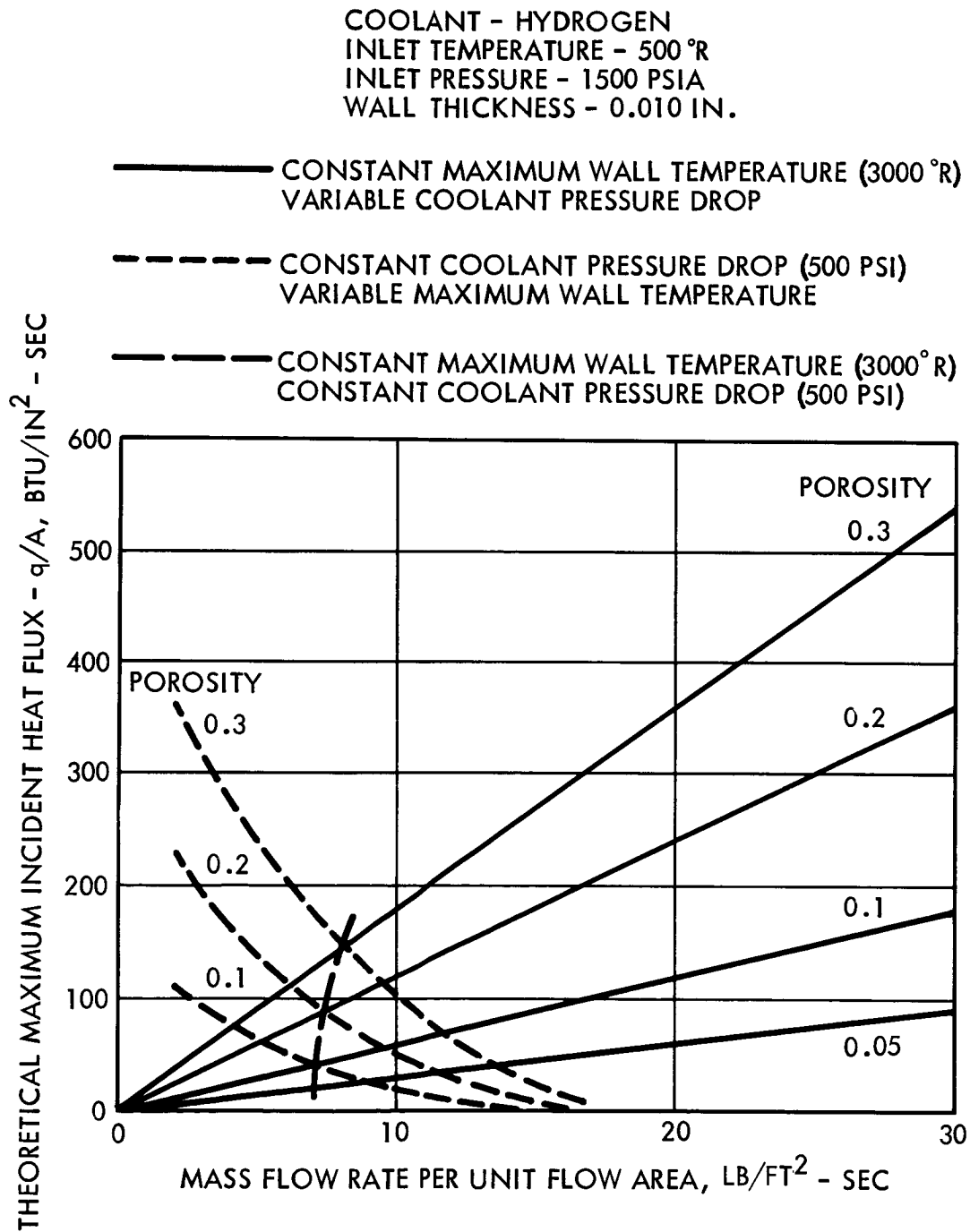


Figure 3-11 Transpiration Cooling Maximum Scoop Wall Heat Flux
(Infinite Heat Transfer Coefficient)

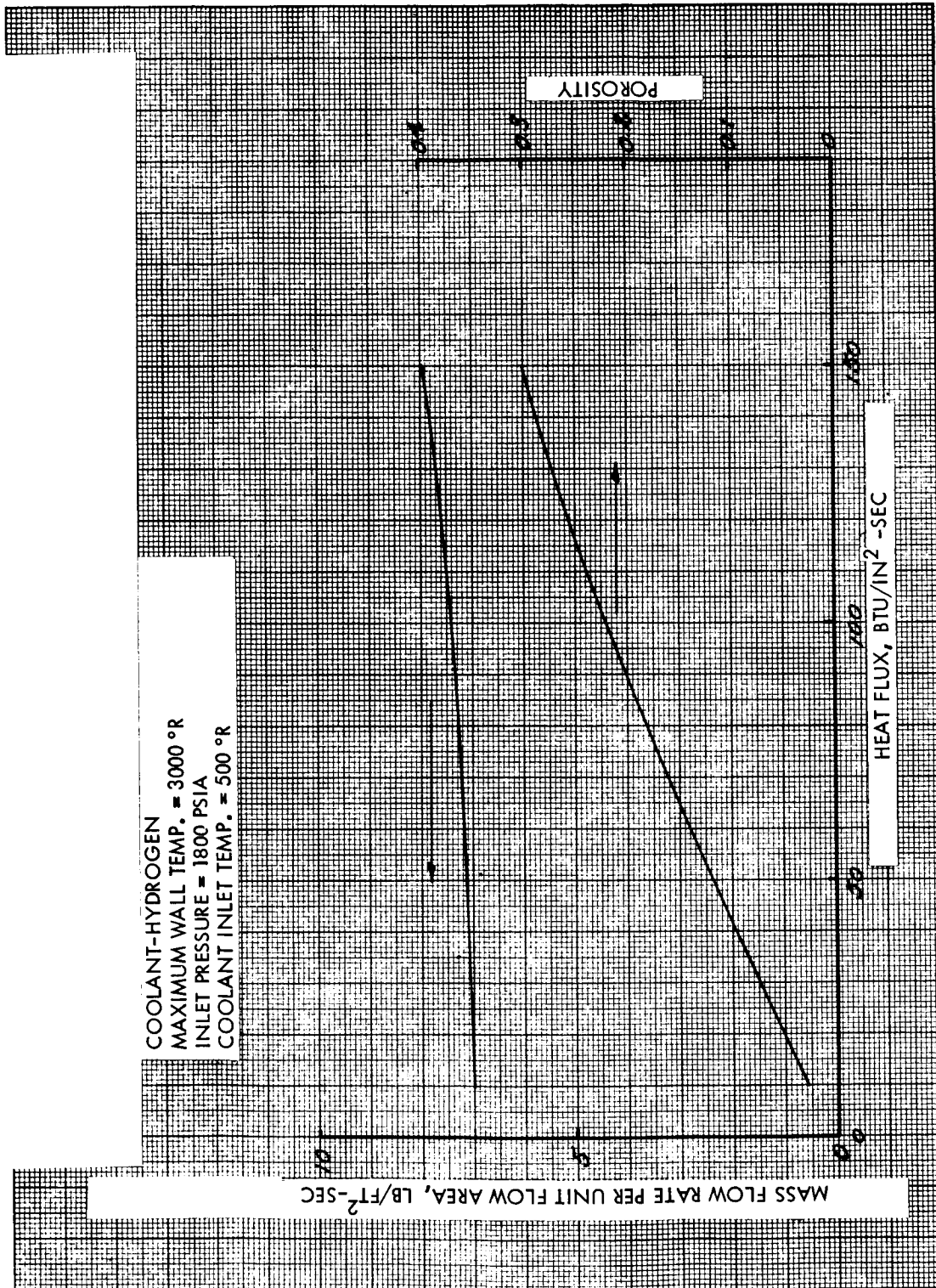


Figure 3-12 Maximum Surface Heat Flux for a 500 PSI Pressure Drop
 (Infinite Heat Transfer Coefficient)

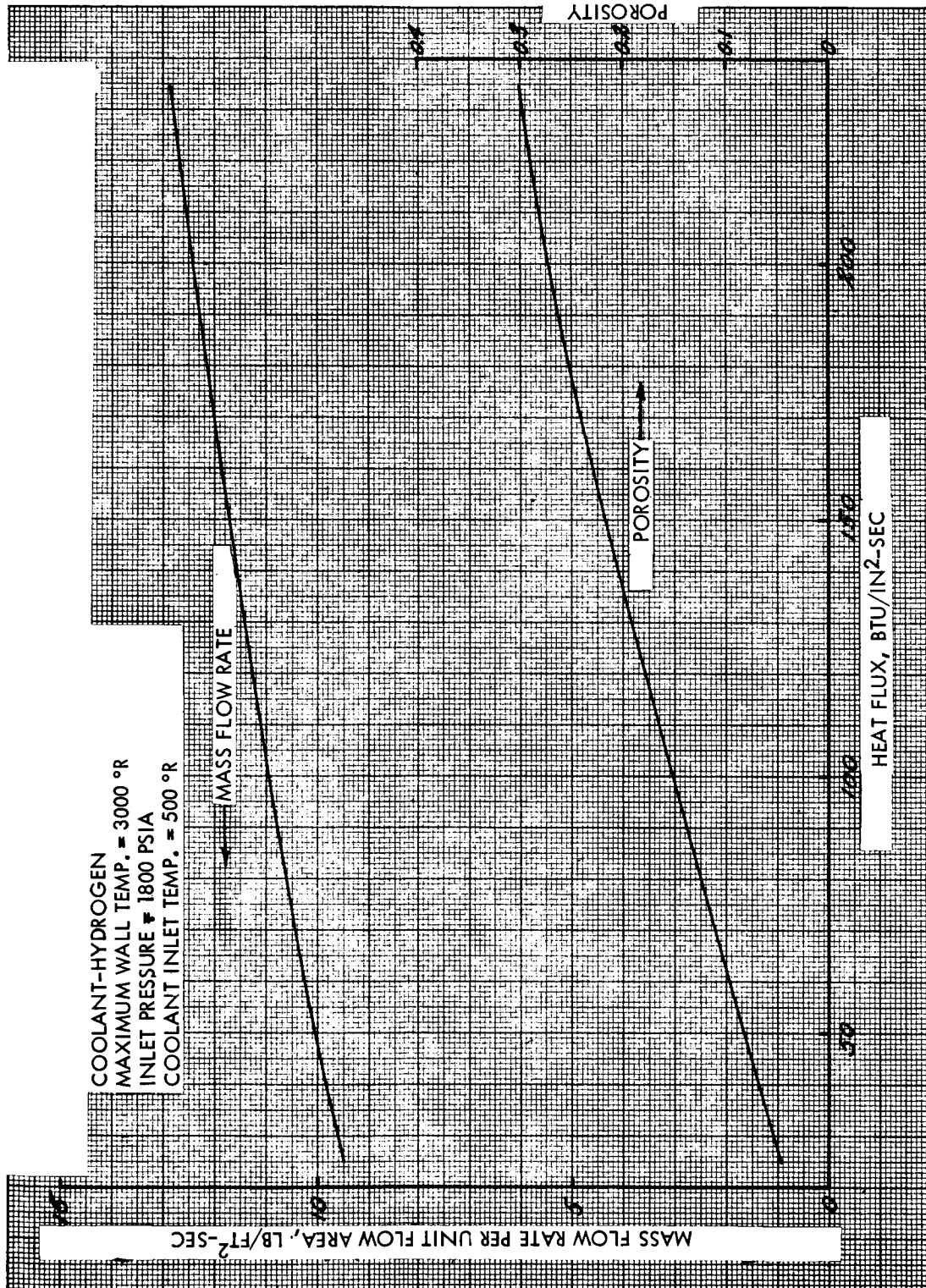


Figure 3-13 Maximum Surface Heat Flux for a 1000 PSI Pressure Drop
 (Infinite Heat Transfer Coefficient)

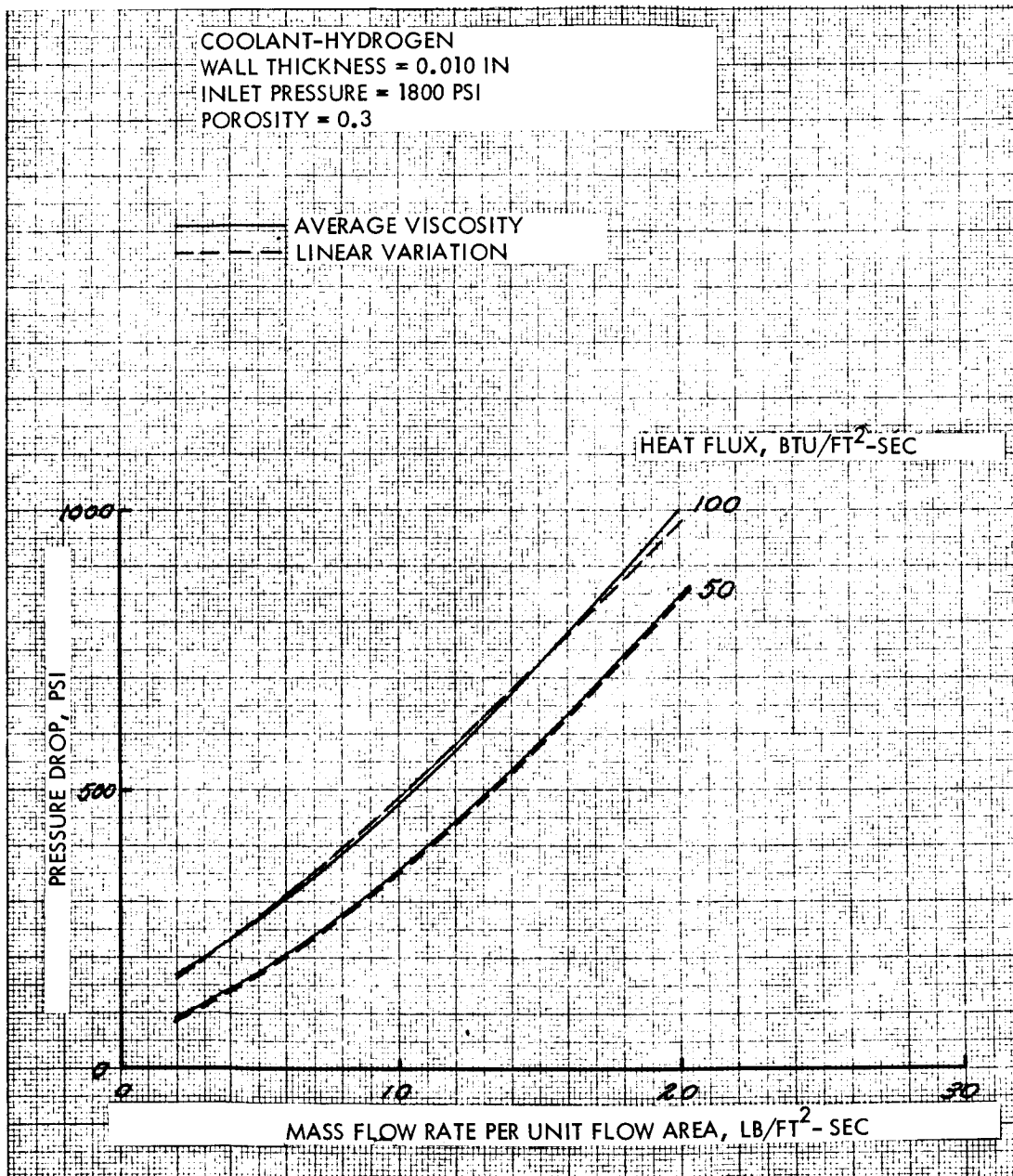


Figure 3-14 Comparison of Average Viscosity Pressure Drop Model and Linear Variation of Viscosity Model

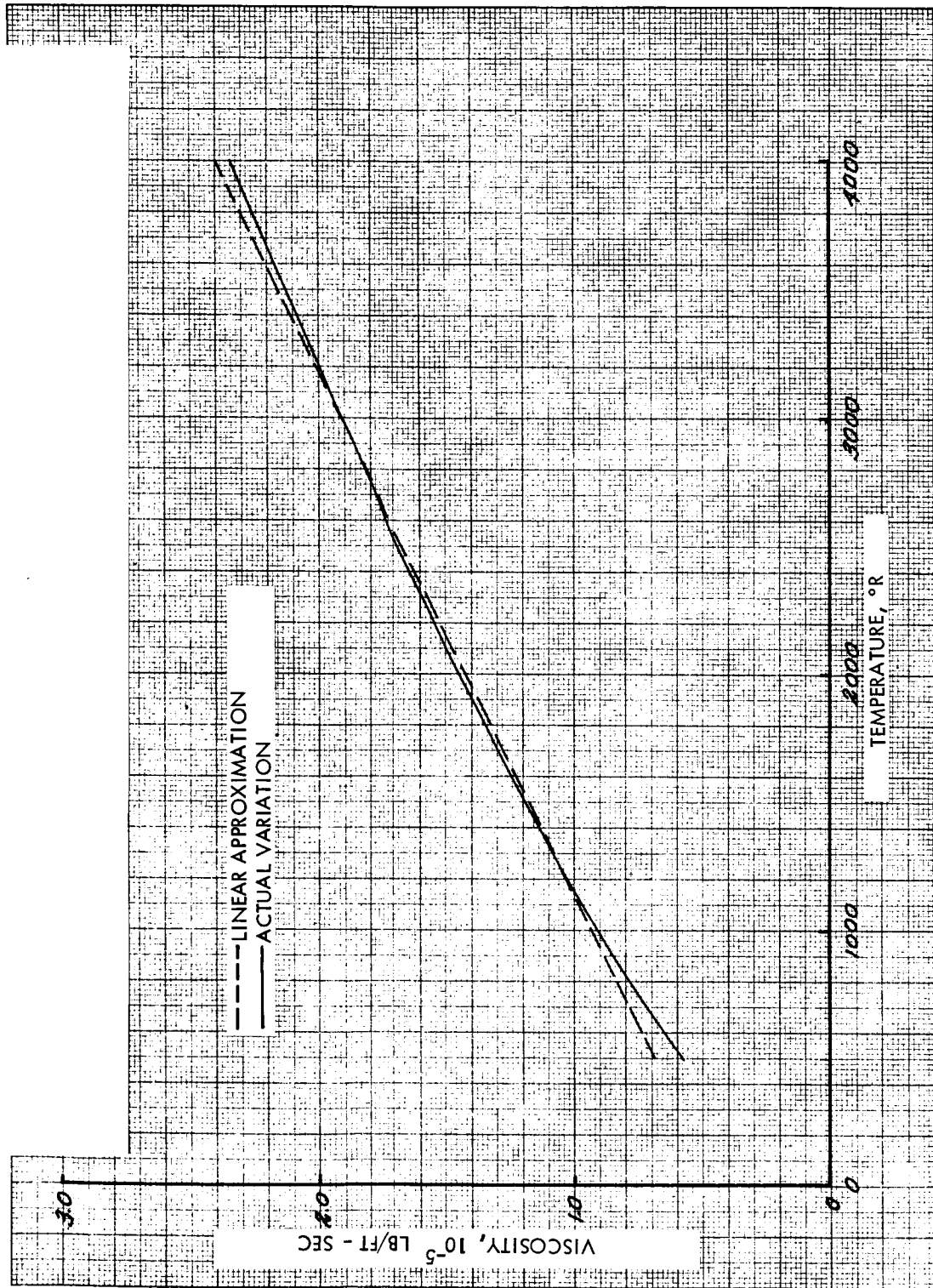


Figure 3-15 Variation of Viscosity with Temperature for a Pressure of 1500 PSIA

The actual variation of viscosity with temperature is plotted in figure 3-15 with the linear approximation also plotted for comparison purposes. The comparison shows that in the range of interest, there is essentially no difference between the model using an average viscosity and the model assuming a linear variation of viscosity.

3.1.4 Temperature Distribution (Finite Heat Transfer Coefficient)

Since the coolant passages in a porous media are composed of randomly dispersed non-uniform capillaries, a rigorous solution of the temperature distribution is difficult to analyze. Following the model suggested by Weinbaum and Wheeler, ⁽²⁰⁾ Bernicker ⁽¹⁹⁾ has evaluated the wall and coolant temperature distribution in a porous wall by assuming that the random passages can be equated to a uniform network of identical parallel cylindrical passages piercing the material. Based on this model, both analytical and numerical solutions of the temperature distribution will be investigated.

3.1.4.1 Numerical Solution

A two-dimensional heat transfer analysis of a segment of transpiration-cooled wall surrounding a single pore was performed using the TRW Thermal Analyzer Computer Program. A schematic of the segment of wall which was analyzed is shown in figure 3-16. The 7094 digital computer program analytically simulates the heat transfer characteristics of the system by means of an electrical analog network. The program simultaneously evaluates the conductive, radiative, and convective heat transfer rates and provides a complete temperature description of the system. A typical network used in this study is shown in figure 3-17. The resulting resistances and temperature distribution for a specific case using this network are presented in table 3-1. The program evaluates both transient and steady state systems but for this study only steady state problems were considered.

Using the heat transfer coefficient presented by Bernicker:

$$h = 0.0019 \frac{kc}{d} \left[P_r R_e \right]^{0.9} \left[\frac{P}{1-P} \right]^{-0.9}$$

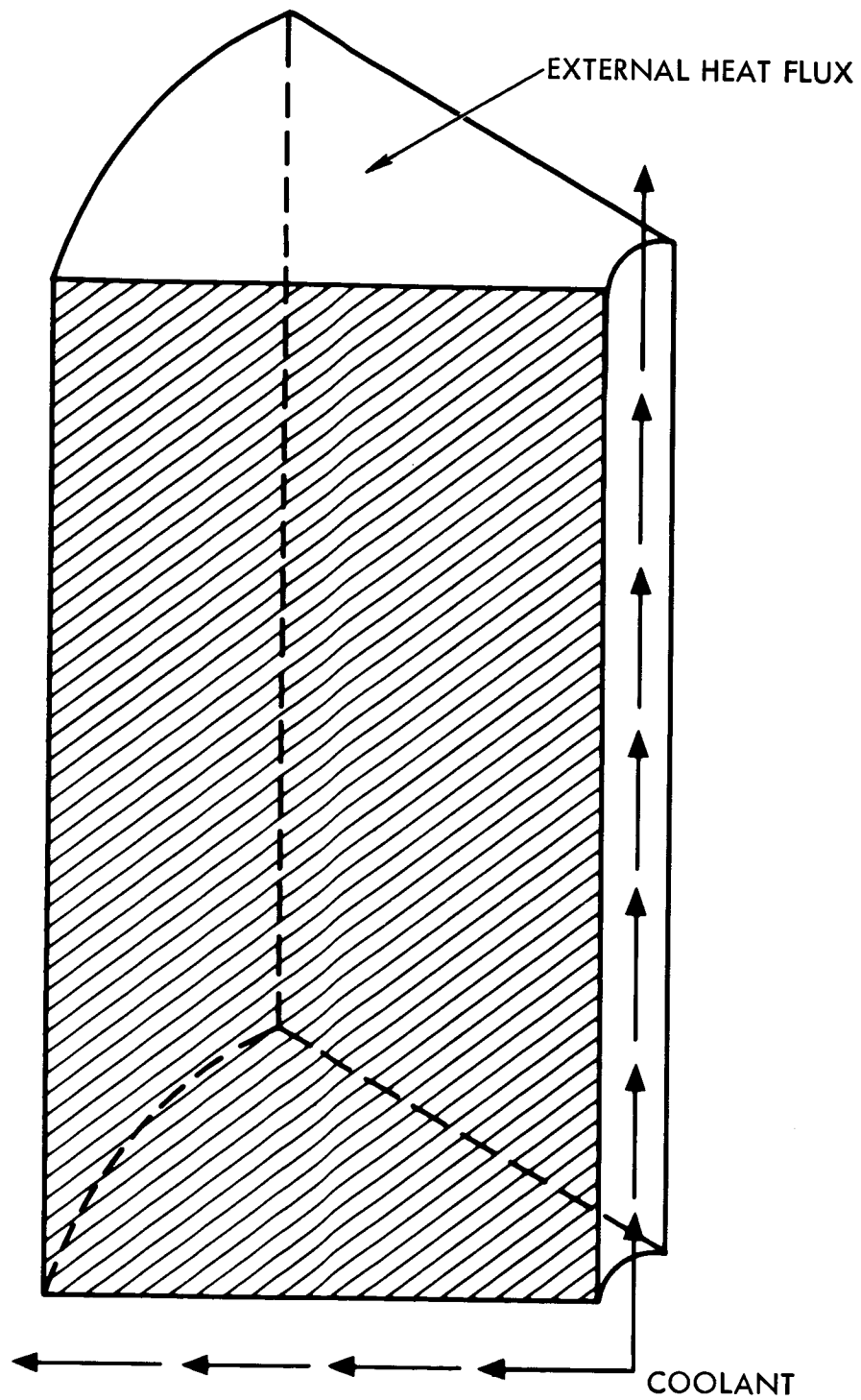


Figure 3-16 Schematic of Idealized Single Pore

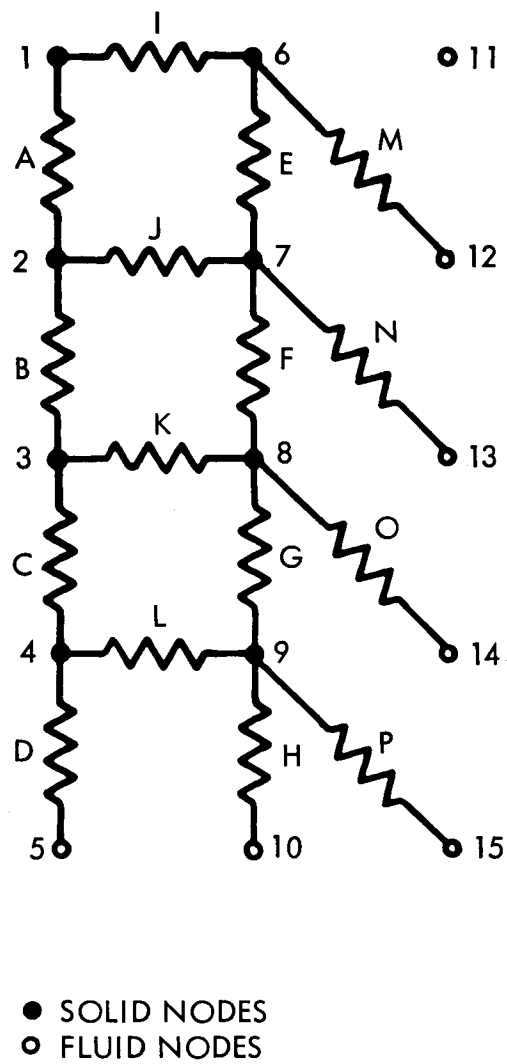


Figure 3-17 Thermal Resistance Network

Table 3-1

TABLE OF RESISTANCE AND TEMPERATURE DATA

Weight flow rate per unit flow area
 $= 10 \text{ lb/ft}^2\text{-sec}$

Pore diameter = .0004 in.

Surface area $= 4.67 \times 10^{-8} \text{ in}^2$

Heat flux incident on solid area
 $= 210 \text{ Btu/in}^2\text{-sec}$

Wall thickness = .010 in.

Porosity = .3

Resistance No.	Resistance
A	1.867×10^8
B	1.867×10^8
C	1.867×10^8
D	6.161×10^9
E	1.867×10^8
F	1.867×10^8
G	1.867×10^8
H	6.161×10^9
I	3.148×10^5
J	3.148×10^5
K	3.148×10^5
L	3.148×10^5
M	2.452×10^8
N	2.587×10^8
O	2.731×10^8
P	2.731×10^8
Mode No.	Temperature, °R
1	3499
2	2597
3	1972
4	1574
5	500
6	3499
7	2597
8	1972
9	1574
10	500
11	3237
12	2409
13	1817
14	1315
15	500

where:

- h = heat transfer coefficient
- k_c = conductivity of the coolant
- d = equivalent pore diameter
- P_r = Prandtl number, $\frac{\mu C_p}{k_c}$
- R_e = Reynolds number, $\frac{Ga}{\mu P}$
- P = porosity
- μ = coolant viscosity
- G = weight flow rate per unit surface area
- a = wall thickness
- C_p = coolant specific heat

Temperature distribution as a function of weight flow rate per unit flow area and equivalent pore diameter were investigated for weight flow rates of 5 and 15 lb/ft²-sec and pore diameters between 10⁻² inches and 10⁻⁴ inches. Curves showing the maximum wall temperature as a function of incident heat flux and pore diameter are shown in figures 3-18, 3-19 and 3-20. Figure 3-21 shows the heat flux, pore diameter and weight flow rate per unit area which yield a maximum wall temperature of 3000°R. Figures 3-18, 3-19 and 3-20 and 3-21 show that heat fluxes approaching the values for an infinite heat transfer coefficient can be realized by going to equivalent pore diameters of the order of 10⁻⁴ inches.

Several typical wall temperature distributions are presented in figures 3-22 and 3-23. These results show that the wall temperature has an exponential distribution which can be closely approximated by the relation

$$T = T_c \left(\frac{T_H}{T_c} \right)^{\frac{x}{L}}$$

where

- T = temperature at point x , within the wall where $x = 0$ on the coolant side and $x = L$ on the hot side
- T_H = hot side wall temperature
- T_c = coolant side wall temperature
- L = wall thickness

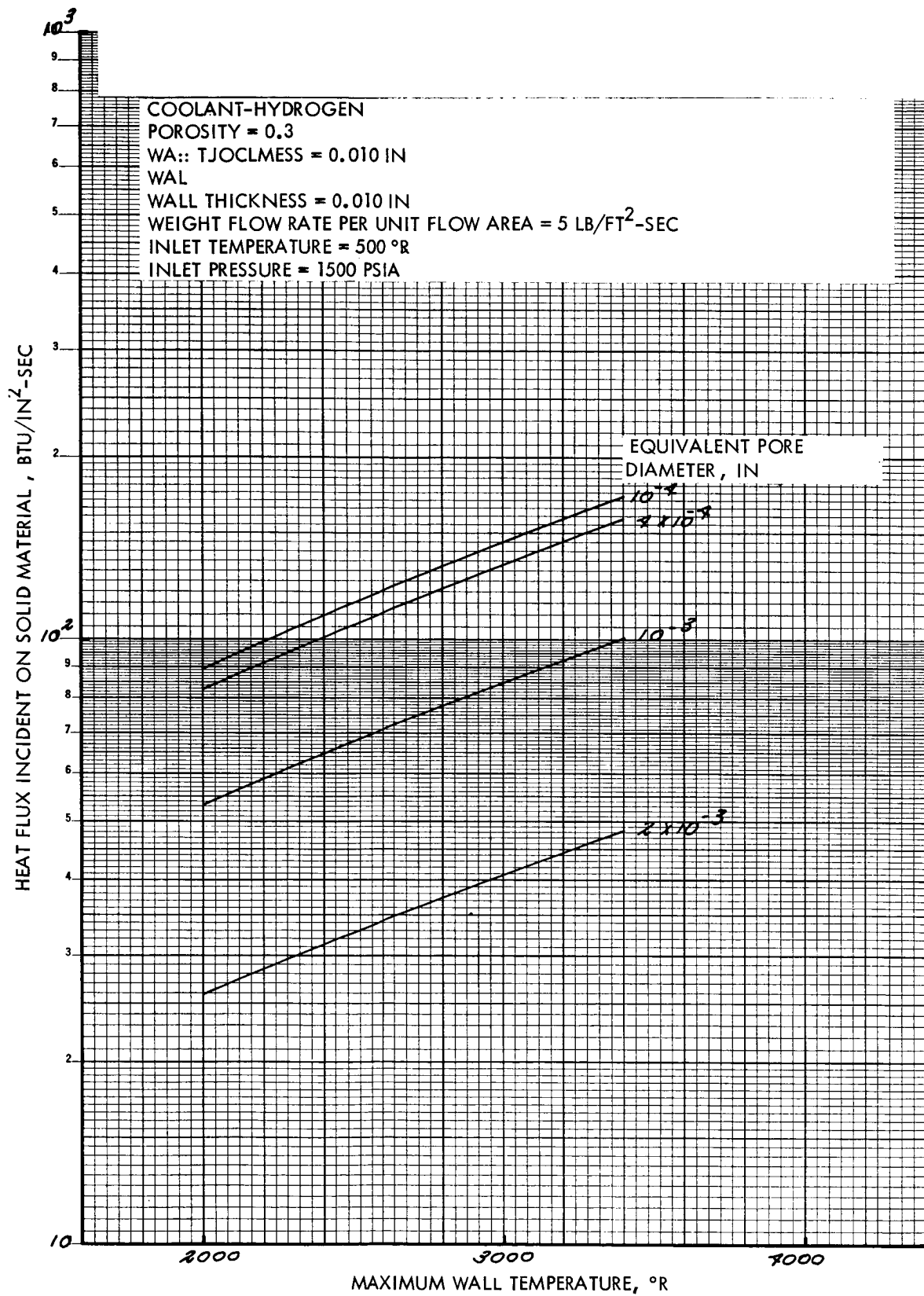


Figure 3-18 Maximum Wall Temperature Variation With Incident Heat Flux

COOLANT - HYDROGEN
 INLET TEMPERATURE - 500° R
 INLET PRESSURE - 1500 PSIA
 MASS FLOW RATE PER UNIT AREA - 10 LB/FT²- SEC
 WALL THICKNESS - 0.010 IN.
 POROSITY - 0.3

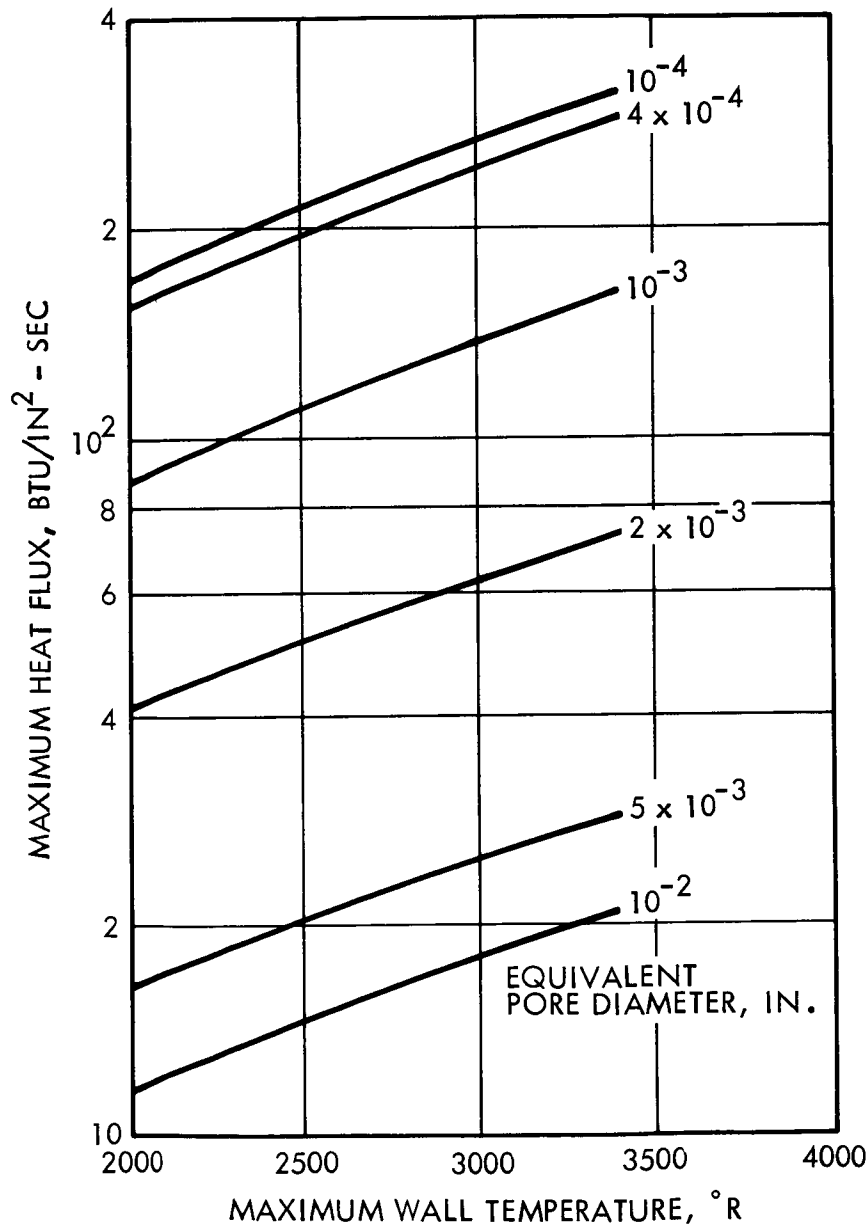


Figure 3-19 Maximum Wall Temperature Influence on
 Transpiration Cooling Maximum Scoop Wall
 Heat Flux
 3-28

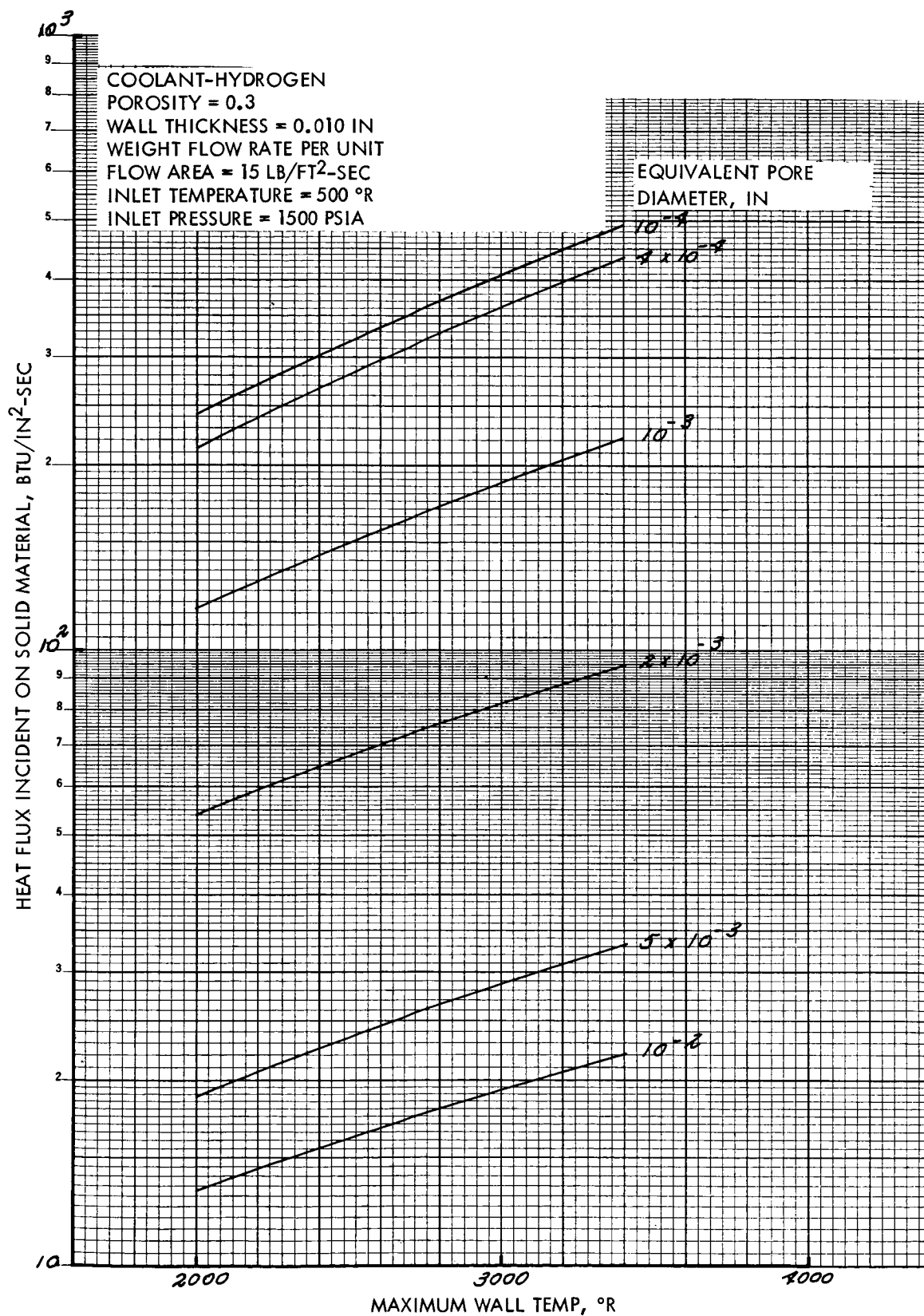


Figure 3-20 Maximum Wall Temperature Variation With
 Incident Heat Flux

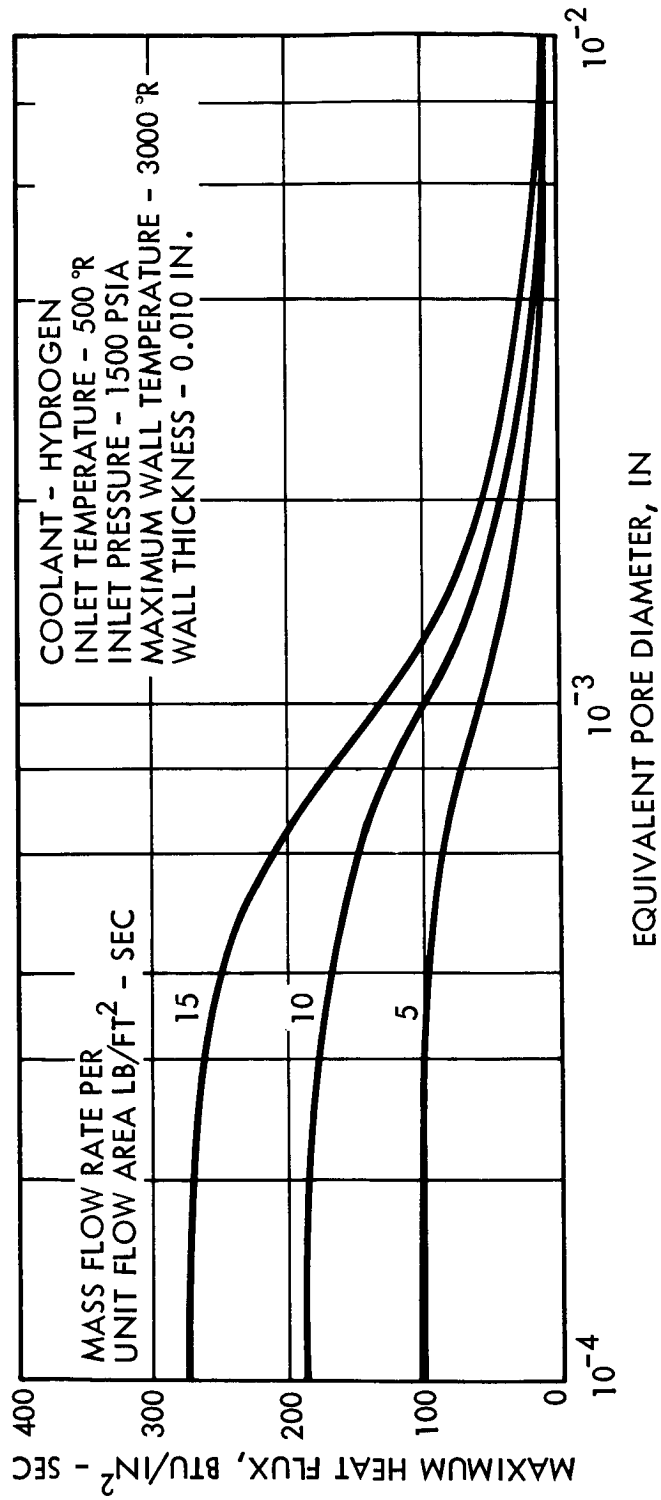


Figure 3-21 Pore Size Influence on Transpiration Cooling Maximum Scoop
 Wall Heat Flux (Finite Heat Transfer Coefficient)

COOLANT - HYDROGEN
 INLET TEMPERATURE - 500°R
 INLET PRESSURE - 1500 PSIA
 INCIDENT HEAT FLUX - $140 \text{ BTU}/\text{IN}^2 - \text{SEC}$
 WALL THICKNESS - 0.010 IN.
 POROSITY - 0.3
 PORE DIAMETER - $4 \times 10^{-4} \text{ IN.}$

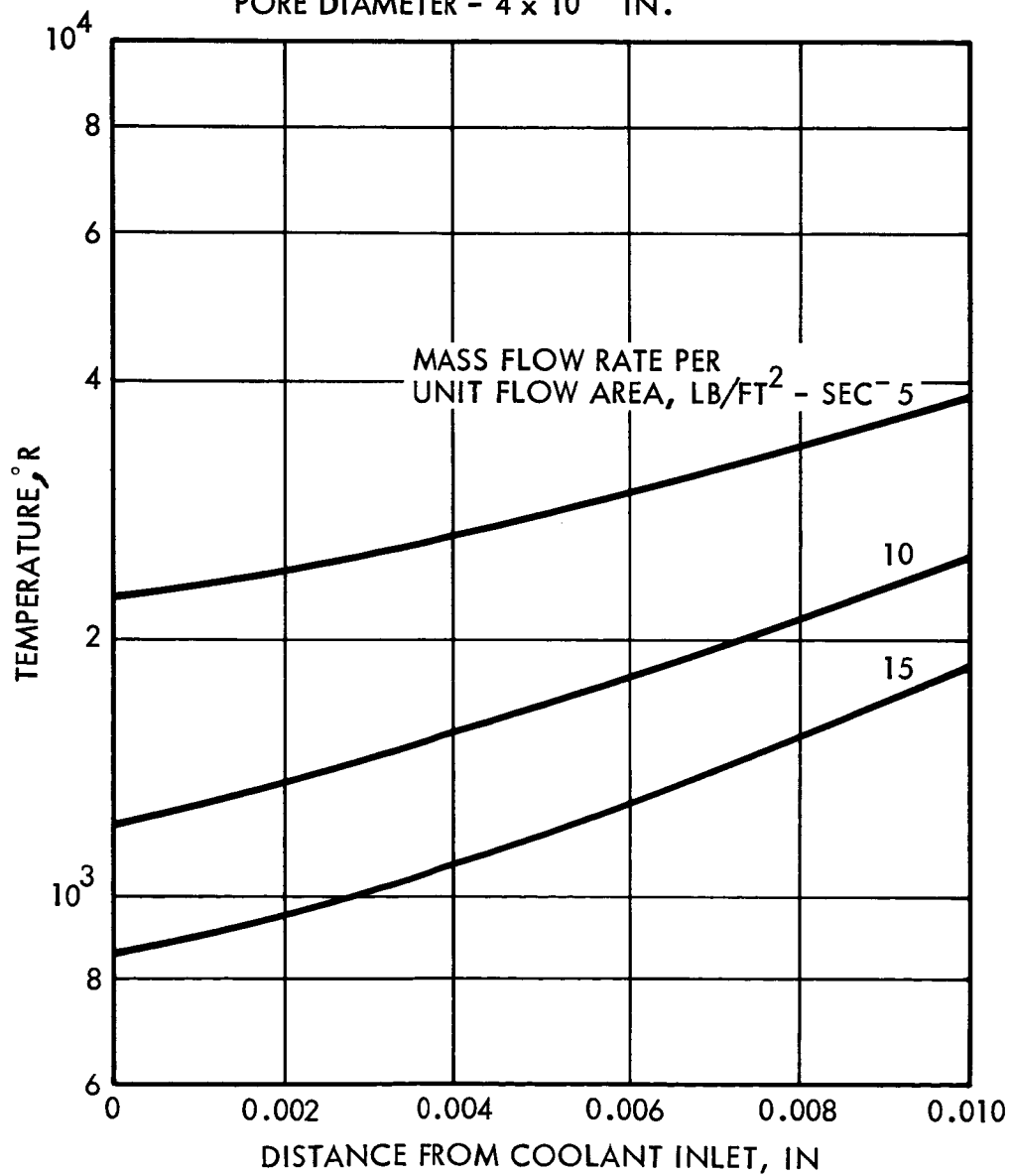


Figure 3.22 Transpiration Cooled Wall Temperature Distribution

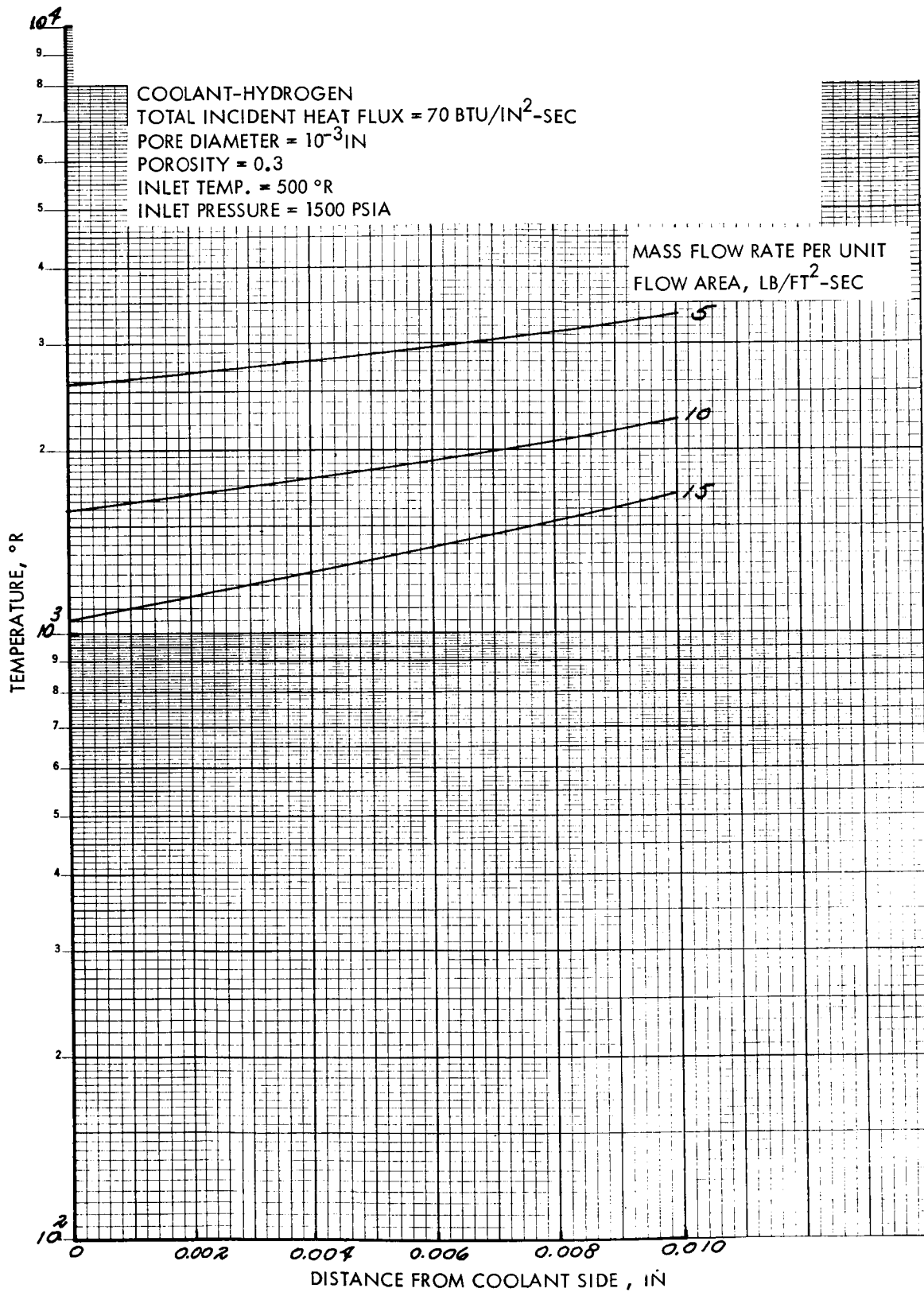


Figure 3-23 Transpiration Cooled Wall Temperature Distribution

3.1.5 Conclusions

From the results presented herein, it appears feasible to transpiration cool walls with heat fluxes as high as $150 \text{ Btu/in}^2\text{-sec}$. Surface heat fluxes of this magnitude require pressure drops of 500 psi to cool a wall with a thirty percent porosity. The limiting pressure drop must, however, be determined from thermal and pressure stress limitations. The results indicate that the effectiveness of transpiration cooling is very dependent upon the pore size. For transpiration cooling to be effective, pore sizes of 5×10^{-4} inches, or less, are necessary in a 30 percent porous wall. If equivalent pore diameters of 2×10^{-3} inches, or larger, are used, transpiration cooling is not effective for the particular wall studied. At the larger pore sizes, the majority of the heat is removed by the coolant flow along the inside wall and very little is transferred to the coolant injected through the wall. Another consideration which must be investigated when evaluating the feasibility of transpiration cooling is the thermal stresses present in the wall material. If the temperature gradients are large and if the pressure drops required for cooling are also large, the allowable stresses in structural materials may be exceeded. If this occurs, the structural materials may well limit the heat fluxes which can be removed by transpiration cooling to much lower values. The analysis of thermal and pressure stresses present in transpiration cooled surfaces have been analyzed in a later section.

3.2 CONVECTIVE COOLING TECHNIQUES

There are two principal reasons for the need to examine convective cooling. The first is the significant attenuation in convective heat transfer if a cold mass is injected into the boundary layer. The second is the need to subsequently analyze the high convective flux in the nozzle throat. In the vicinity of the scoop, radiation heat transfer is by far the most severe. Since the hydrogen propellant is transparent to radiation, mass injection as such will not reduce the incident flux to the wall. However, seeded hydrogen can be made sufficiently opaque that the residual flux can be further reduced by cold mass injection or by conventional solid wall convective cooling (regenerative cooling).

3.2.1 Gas-Side Convective Heat Transfer

If the curvature of the surface is neglected and the model is a flat plate with a parallel stream passing over it, the classical solution for a turbulent free stream analog of Colburn⁽³⁹⁾ can be applied. The local heat transfer coefficient (h_g) can be approximated by⁽¹⁰⁾

$$\frac{h_g x}{K} = .0296 (Re)^{0.8} Pr^{0.33}$$

where

- h_g = local heat transfer coefficient at distance x
- x = distance from leading edge
- K = conductivity of the gas
- Re = Reynolds number
- Pr = Prandtl number

3.2.2 Gas-Side Heat Transfer with Boundary Layer Injection

Boundary layer injection cooling provides the most significant attenuation in convective heat transfer. Rubesin and Pappas^{(11), (12)} have theoretically studied the injection of a gaseous species into a turbulent boundary layer. They used the standard turbulent boundary layer techniques and neglected the streamwise variations in the differentiation of terms to obtain a set of laminar sublayer conservation equations and a set of corresponding fluctuation equations. The results of their analyses were then correlated to minimize the effects of Mach number, Reynolds number, and wall temperature. Extrapolation based on Rubesin's theoretical results indicates that the heat transfer can be represented by the simple formula

$$\left(\frac{St}{St_o} \right)_x = 1 - \frac{1}{3} \left(\frac{F}{St_o} \right)_x$$

where St refers to Stanton number and F is the injection flow parameter defined by

$$F = \frac{\rho_w V_w}{\rho_\infty u_\infty}$$

and the subscript o refers to the case with no boundary layer injection and the subscript x indicates local values. However, further correlation of the results⁽⁴⁰⁾ is necessary for the effects of different gaseous injection species. Stewart suggested that the heat transfer coefficient with different injection species can be approximated by

$$\left(\frac{St}{St_o} \right)_x = 1 - (0.3) \frac{(F_x) (\bar{C}_p)^{0.6}}{(St_o)_x}$$

where \bar{C}_p is the specific heat ratio, injected species over free-stream value. This correlation shows reasonable agreements with the limited experimental results of Rubesin et al⁽¹³⁾ and Leadon and Scott⁽¹⁴⁾ on the turbulent boundary layer case.

3.2.3 Coolant Side Heat Transfer

The maximum heat flux that can be removed by the coolant flow and its attendant pressure drop. The coolant temperature rise allows the specification of the scoop transpiration cooling requirements and also sets the limit on convective cooling methods.

Calculation of the convective coolant heat flux requires that the coolant flow channel geometry be specified because the heat flux is dependent upon the channel hydraulic diameter. The scoop flow channel geometry was approximated by an annular region of thickness, t_s . Although the actual scoop coolant channel geometry is somewhat different than the geometry assumed for the following calculations, the heat transfer results based upon the above geometry should closely approximate the results for the actual geometry.

The coolant flow area is given by:

$$A_f = \pi t_s (2 r_s + t_s)$$

where

$$A_f = \text{coolant flow area, in}^2$$

$$t_s = \text{coolant channel width, in}$$

$$r_s = \text{scoop inside radius, in}$$

Incorporating the above coolant flow area equation into the basic Wolf-McCarthy heat transfer correlation, assuming a coolant wall temperature of 2500°R , and assuming an average bulk coolant temperature of 500°R , the heat flux equation becomes:

$$q/A = 630 \frac{\phi_b}{t_s} \left[\frac{\dot{m}}{2 r_s + t_s} \right]^{0.8}$$

where

$$\begin{aligned} q/A &= \text{heat flux, Btu/in}^2\text{-sec} \\ \phi_b &= \text{heat transfer parameter} = \frac{k_b (P_r)^{0.4}}{T_b^{0.8} \mu_b^{0.8}} \\ &\quad \text{Btu}/[(\text{ft-sec})^{0.2} (\text{lbm})^{0.8} (^{\circ}\text{R})^{1.8}] \\ \dot{m} &= \text{coolant mass flow rate, lbm/sec} \\ r_s &= \text{scoop radius} = 18 \text{ in} \\ t_s &= \text{scoop coolant channel width, in} \end{aligned}$$

The above heat flux equation was evaluated for bulk coolant pressures of 5500 psi and 2000 psi which correspond to chamber pressures of about 5000 psi and 1000 psi. The heat flux which may be removed by the scoop coolant is shown in figures 3-24 and 3-25 as a function of mass flow rate with coolant channel thickness and chamber pressure as parameters.

The enthalpy rise of the coolant may be obtained by multiplying the heat flux by the heat transfer area, thus:

$$H = \frac{(q/A) 2\pi (2 r_s + t_s)}{\dot{m}}$$

The temperature rise was obtained from the calculated enthalpy rise for chamber pressures of 5000 psi and 1000 psi. Results are shown in figures 3-26 and 3-27 as a function of mass flow rate with coolant channel width as a parameter.

3.2.4 Scoop Coolant Pressure Drop

The scoop coolant pressure drop was evaluated using an integrated form of the general pressure drop equation.

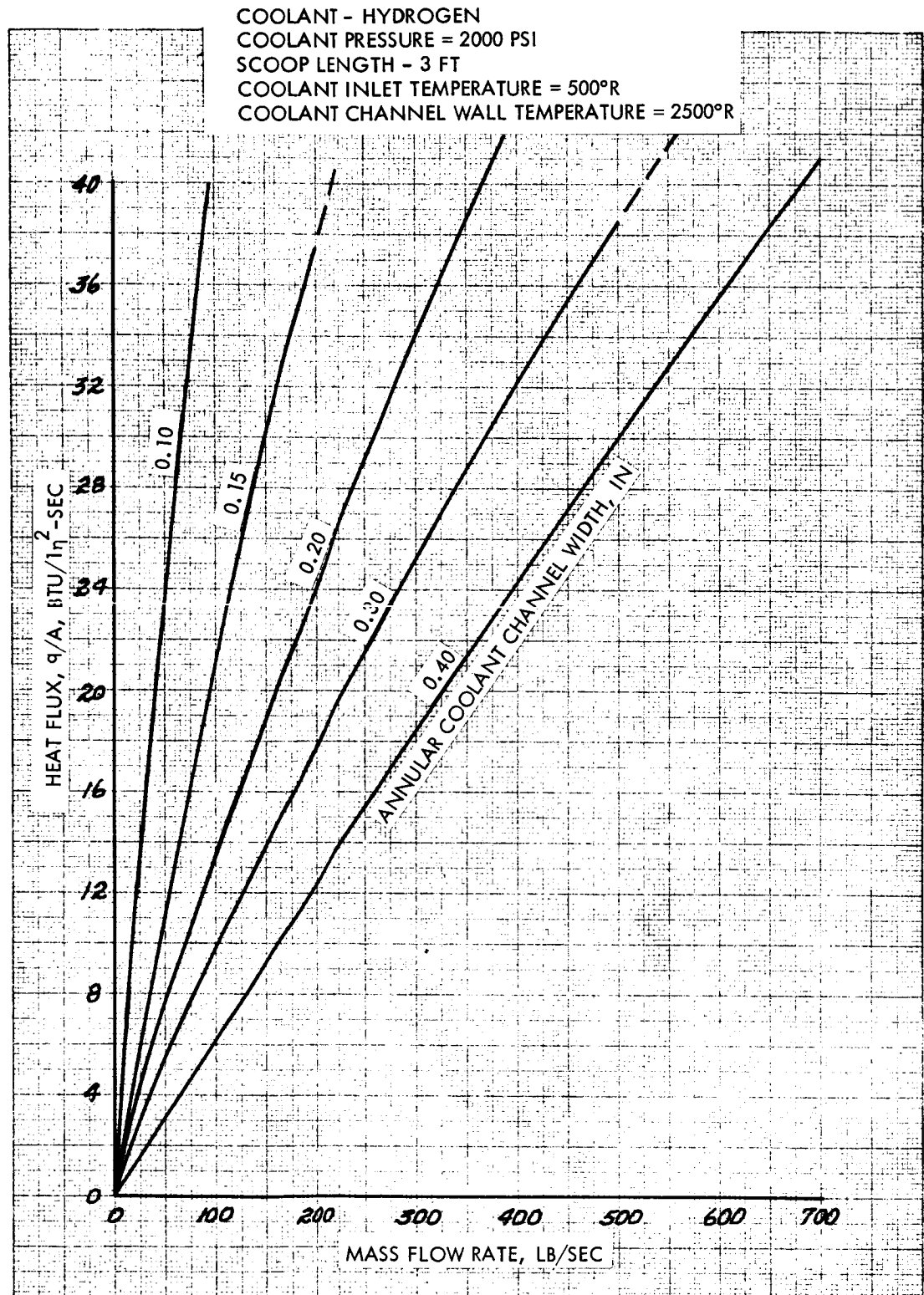


Figure 3-24 Scoop Coolant Heat Flux
 3-37

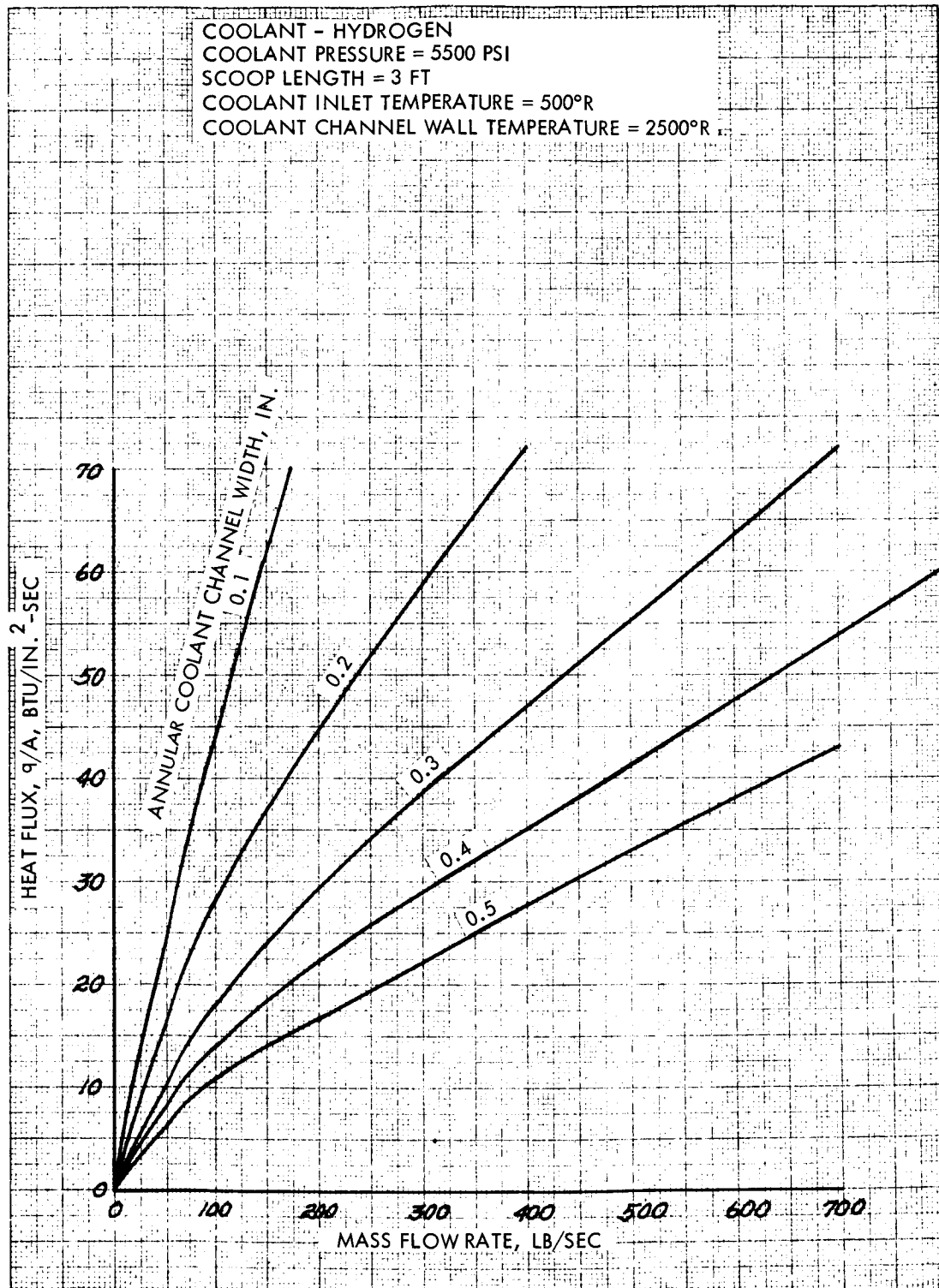


Figure 3-25 Scoop Coolant Heat Flux
3-38

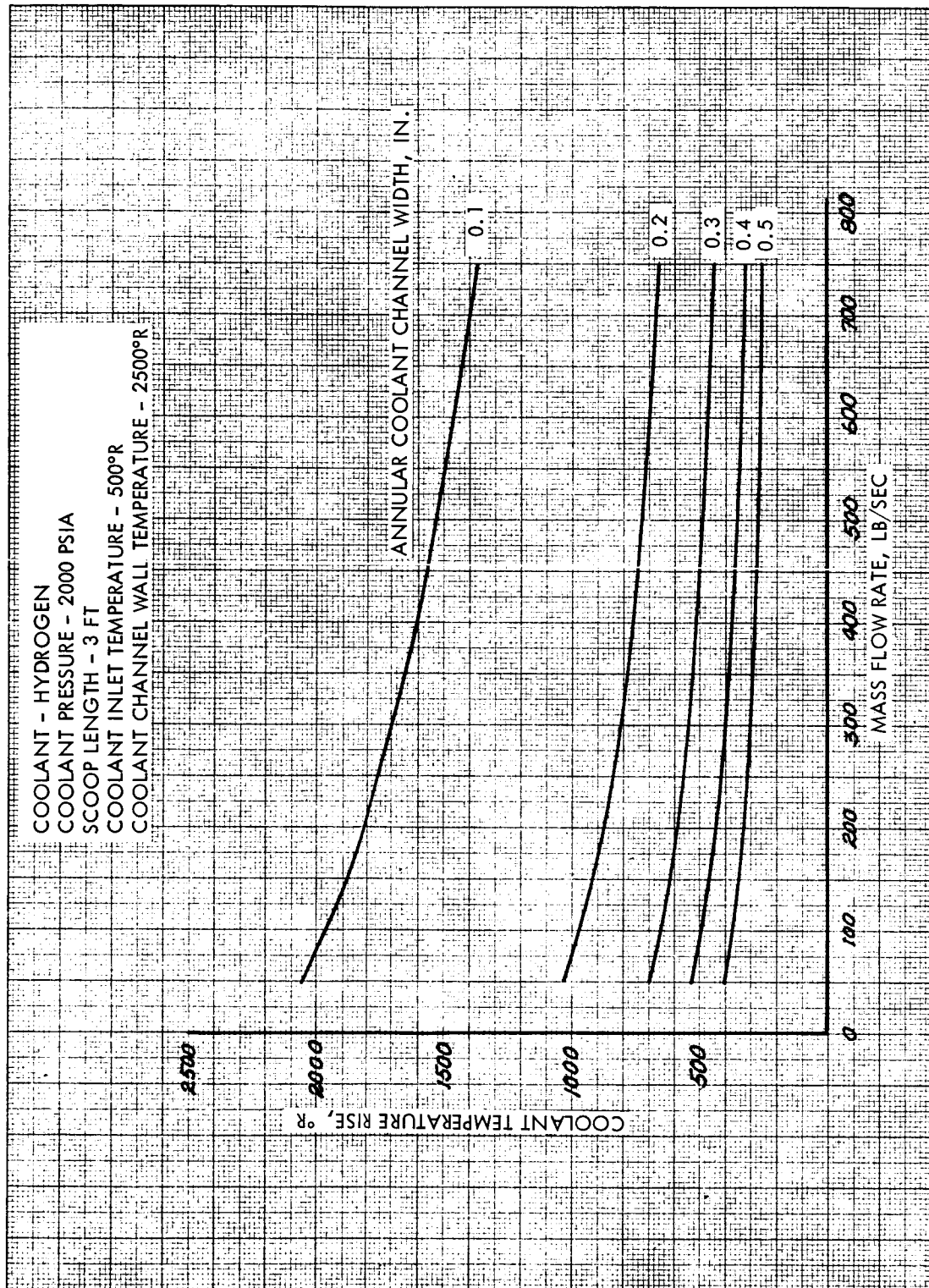


Figure 3-26 Scoop Coolant Temperature Rise

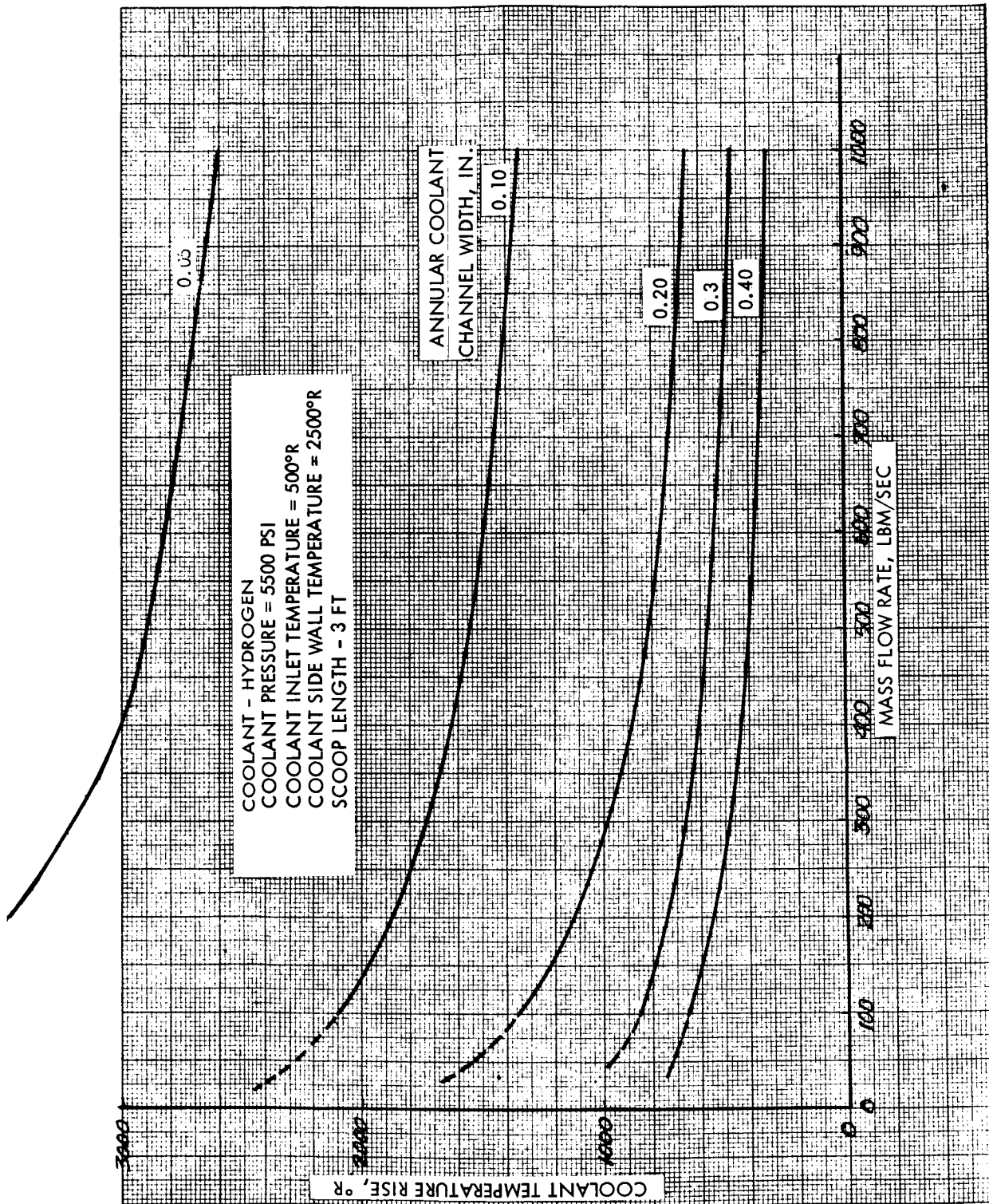


Figure 3-27 Scoop Coolant Temperature Rise

$$P_2^2 = P_1^2 + \frac{R_u}{M} \left\{ \left(\frac{\dot{m}}{A_f} \right)^2 \left[(T_1 + T_2) \ln P_2/P_1 - 2 (T_2 - T_1) \right] \right. \\ \left. - 0.0669 \left(\frac{\dot{m}}{A_f} \right)^{1.8} \frac{1}{D_c^{1.2}} (T_1 \mu_1^{0.2}) (X_2 - X_1) \right\}$$

where

- P_1 = coolant inlet pressure, psia
 P_2 = coolant exit pressure, psia
 R_u = universal gas constant = 1545 $\frac{\text{ft} \cdot \text{lbf}}{\text{mole} \cdot ^\circ\text{R}}$
 M = hydrogen molecular weight, 2.016 lbm/mole
 \dot{m} = coolant mass flow rate, lbm/sec
 A_f = coolant flow area = $\pi t_s (2 r_s + t_s)$, in²
 T_1 = coolant inlet temperature = 500 °R
 T_2 = coolant exit temperature, °R
 D_c = coolant flow channel hydraulic diameter, in.
 μ = fluid viscosity, lbm/ft-sec
 $X_2 - X_1$ = coolant channel length, in.

After substituting the flow area relationship into the pressure drop equation, the result is:

$$P_2^2 = P_1^2 + 2.41 \left\{ \frac{\dot{m}^2}{[t_s (2 r_s + t_s)]^2} \left[(T_1 + T_2) \ln P_2/P_1 - 2 (T_2 - T_1) \right] \right. \\ \left. - 0.0365 \frac{\dot{m}^{1.8}}{t_s^3 (2 r_s + t_s)^{1.8}} \left[T_1 \mu_1^{0.2} + T_2 \mu_2^{0.2} \right] (X_2 - X_1) \right\}$$

Various scoop coolant channel widths were selected and pressure drop calculations were made using the above equation. Composite curves showing the coolant heat removal capability as a function of pressure drop and mass flow rate are shown in figures 3-28 and 3-29. Figure 3-30 shows the effect of scoop length on the convective coolant capability.

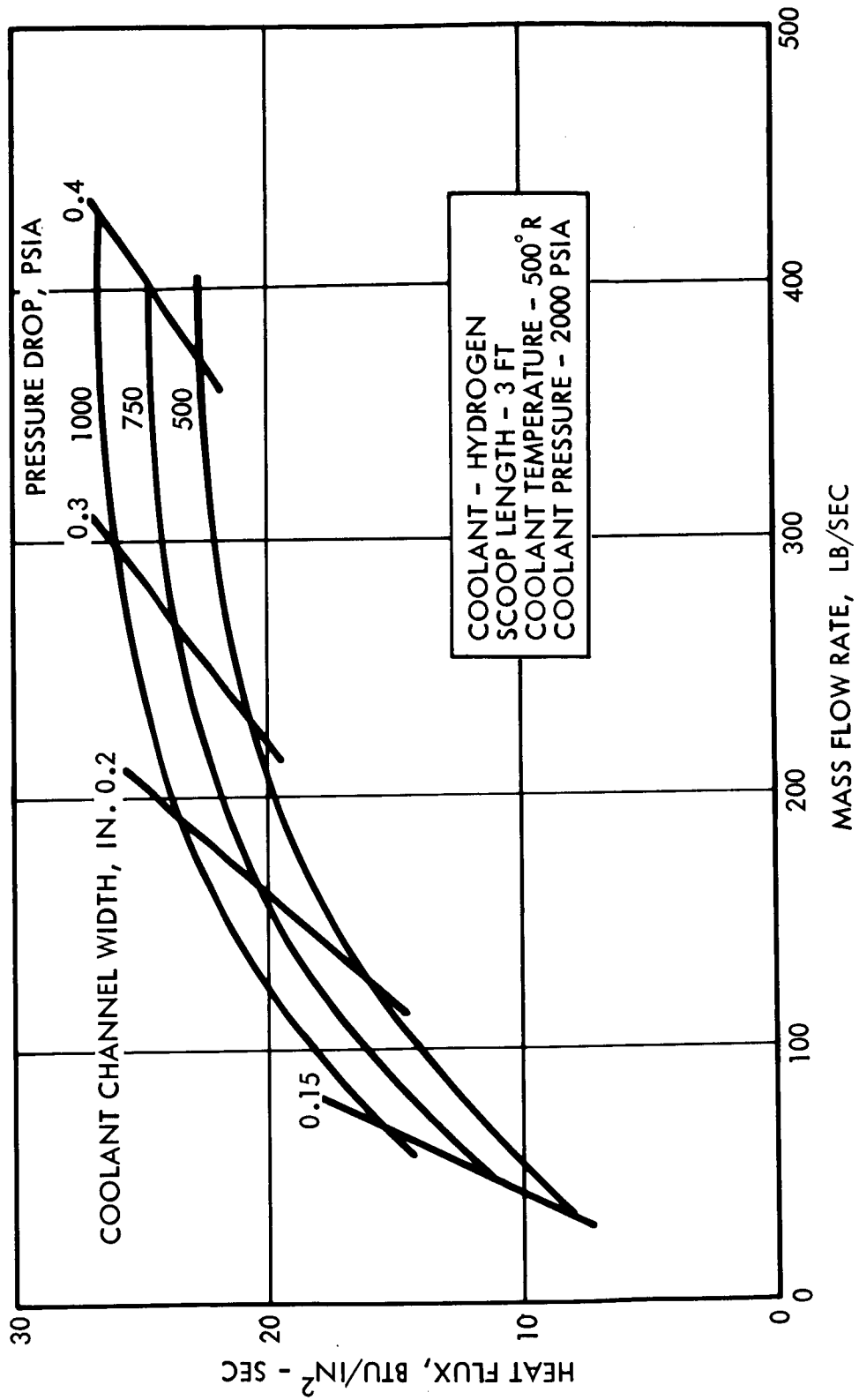


Figure 3-28 Convective Cooling Maximum Scoop Wall Heat Flux

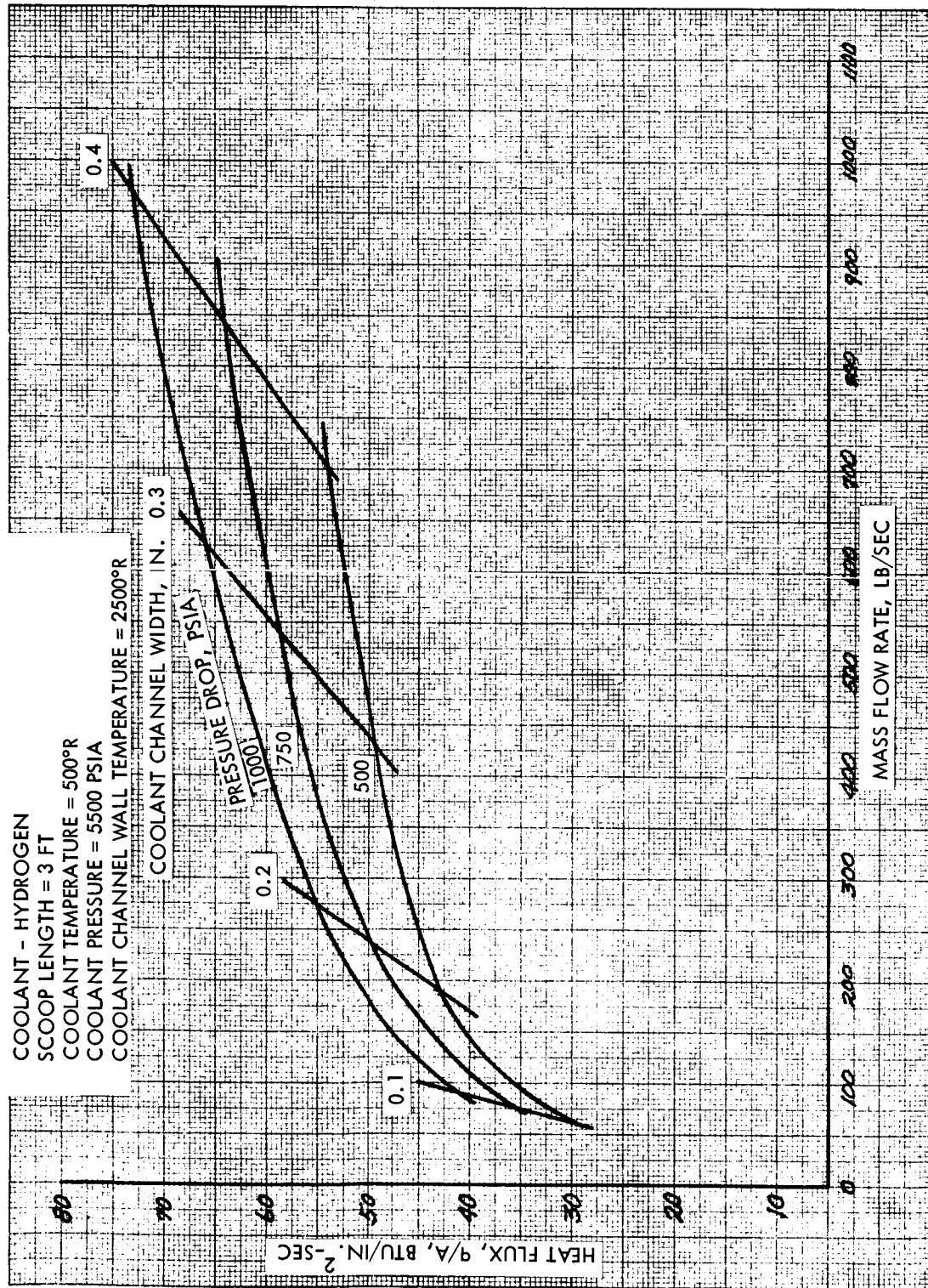


Figure 3-29 Scoop Convective Heat Flux Removal Capability

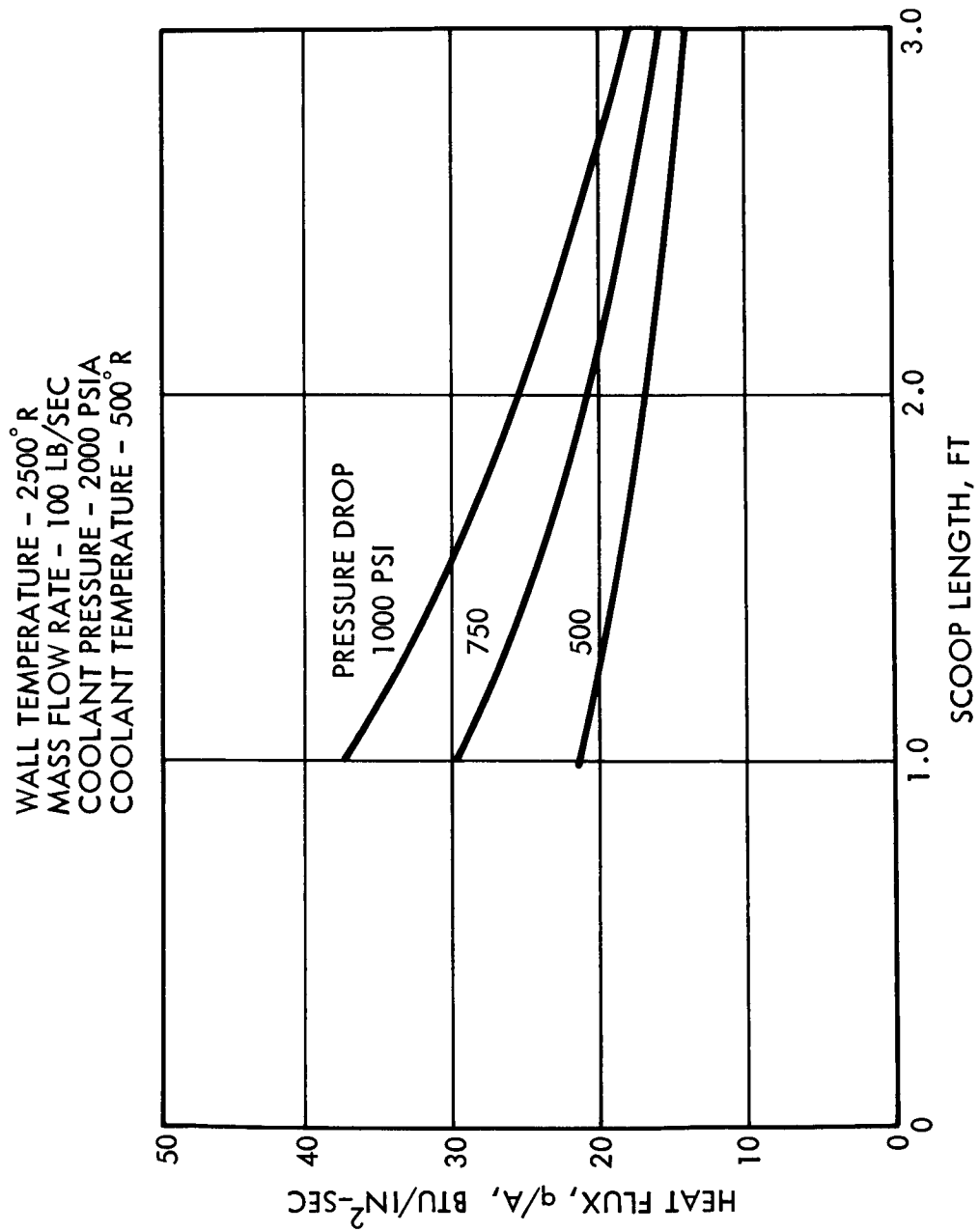


Figure 3-30 Convective Cooling Maximum Scoop Wall Heat Flux

3.2.5 Conclusions

The curves presented in this section may be used to produce a scoop convective cooling design. For example, selecting an allowable coolant pressure drop of about 500 psi and a mass flow rate of 235 lbm/sec, figure 3-28 shows that a coolant channel width of about 0.30 in. is required for a chamber pressure of 1000 psi. For these values of mass flow rate and channel width, figure 3-24 shows that about 20 Btu/in²-sec may be removed convectively and figure 3-26 shows that the temperature rise is about 440°R. If the scoop length is reduced from 3 feet down to 1 foot, a heat flux of 38 Btu/in²-sec could be removed with a 1000 psi pressure drop.

3.3 SEEDING TECHNIQUES

From the results of boundary layer injection cooling, it is evident that further protection of the scoop from the extreme influx of heat is needed. In this section, a simple but effective method of attenuating the radiative heat flux is examined. This method involves the injection of a high opacity material, such as fine carbon particles, into a boundary layer. By so doing, a large portion of the heat flux is absorbed or blocked away by this layer of optically dense gas so that the heat flux to the surface is reduced. The degree of attenuation depends on the absorbing material, the density of this material, and the thickness of the seeded layer.

(15)

Lanzo and Ragsdale have experimentally determined the effect of seeding particle size on the parameter ϵ/N , the extinction coefficient per particle, for a few seeding materials. From their results, the percent by weight of the seeding material required for a given absorption coefficient can be calculated. In turn, by applying Beer's law

$$\frac{I}{I_0} = e^{-kl}$$

the radiation transmissivity can be determined. In other words, to attenuate a given radiant energy to a certain percent of its initial intensity in a certain path length, the percent by weight of the seeding particles required in the seeded layer can be calculated. Such calculations have been performed for carbon particles and tungsten particles. The results are shown in figures 3-31 and 3-32.

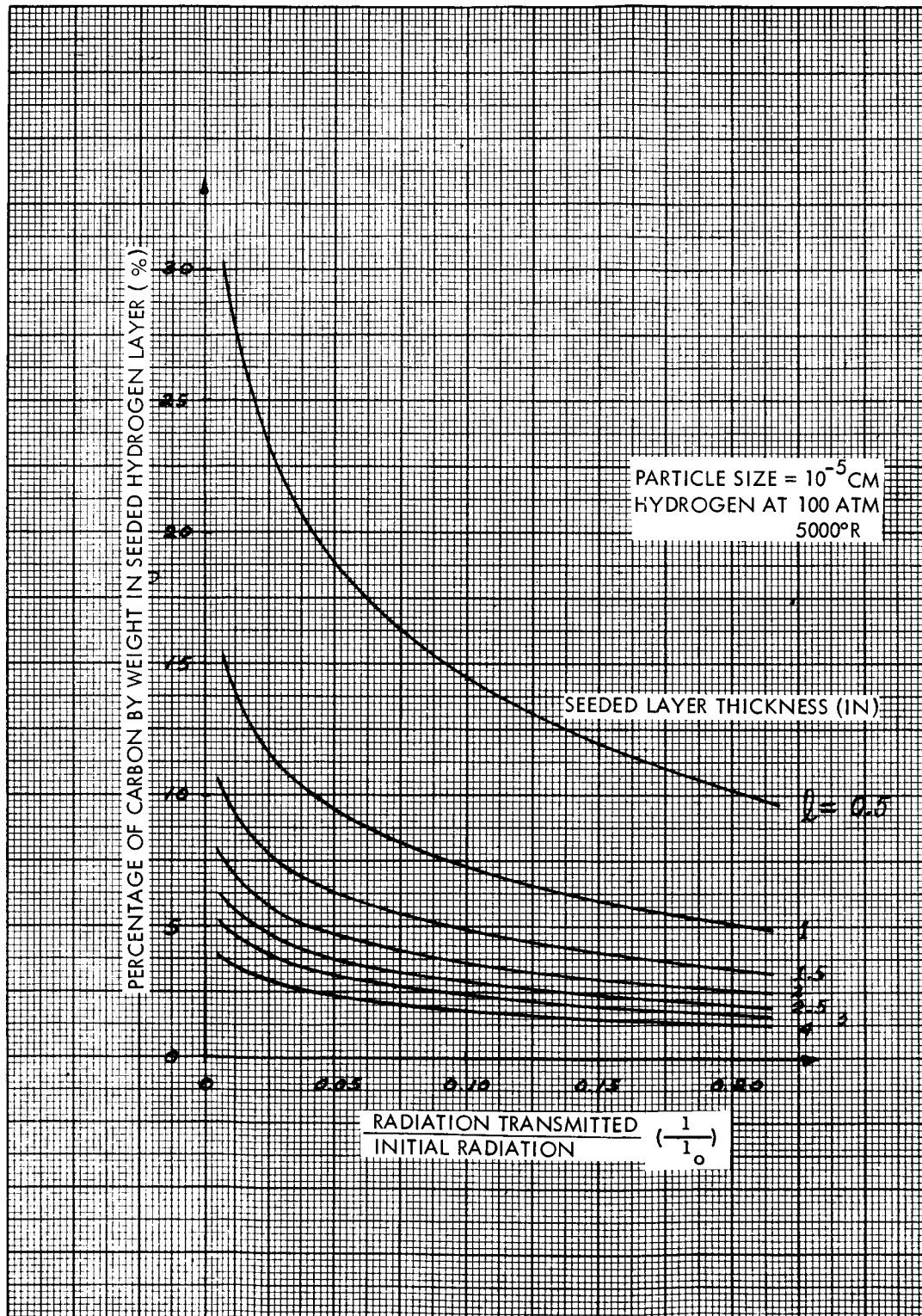


Figure 3-31 Effect of Seeding Hydrogen with Carbon
3-46

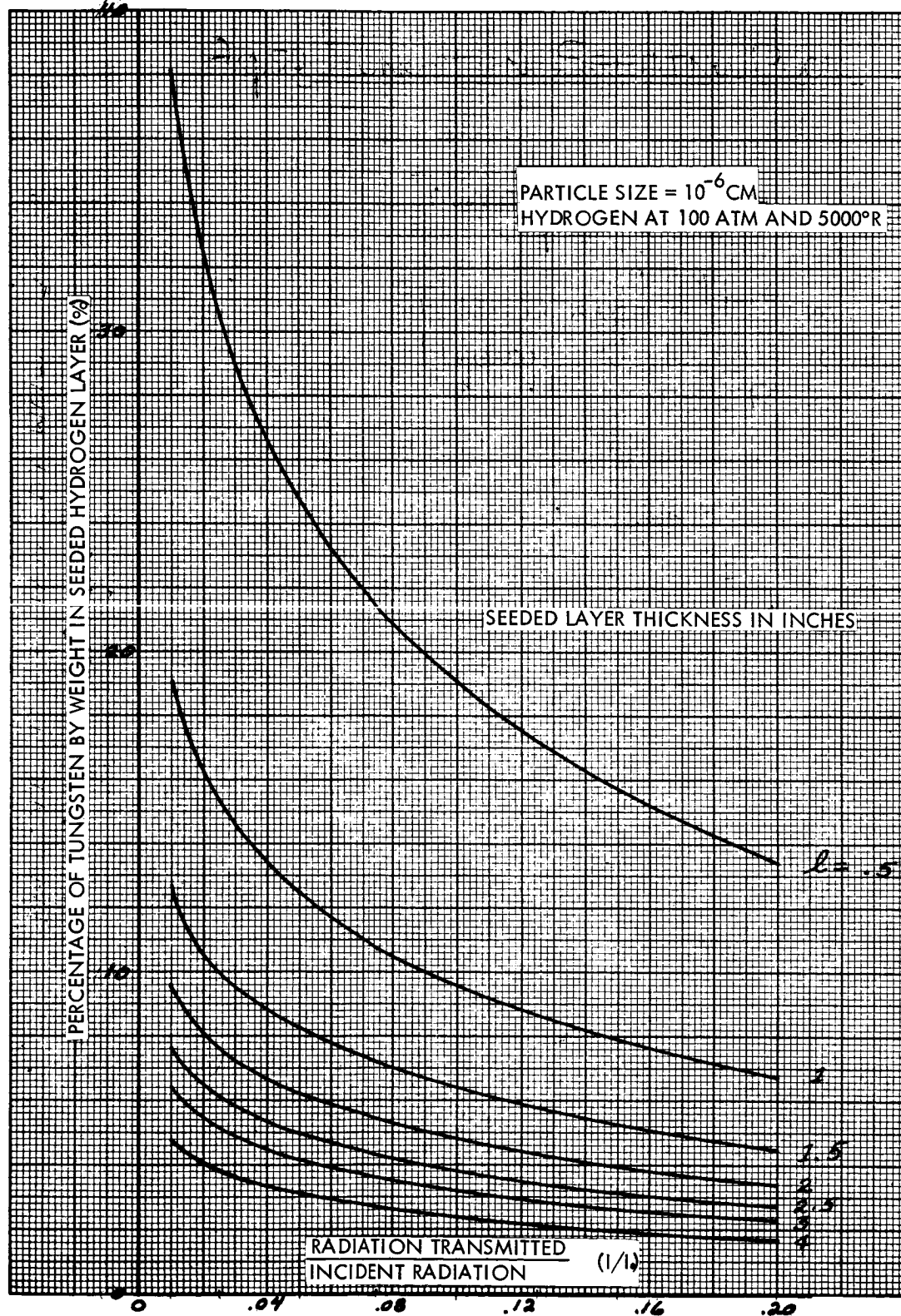


Figure 3-32 Effect of Seeding Hydrogen with Tungsten
3-47

In these calculations, it was assumed that the seeded layer is homogeneous in composition and the presence of seeding material does not affect the physical properties of seeded layer except its density and absorption coefficient. An average layer temperature of 5000°R is also assumed in the calculations. By introducing approximately 7% by weight of carbon particles of 0.1 microns in size into a one-inch layer of hydrogen, the predicted thermal radiative flux can be reduced by one order of magnitude. This amount of seeding becomes negligible in weight when the total mass flow rate of propellant is considered. Therefore, such an addition should have little effect on the specific impulse or overall performance of the system.

A comparison of figures 3-31 and 3-32 indicates that carbon particles have a better effective heat shielding. The tungsten material requires a higher weight ratio for the same heat flux attenuation.

The assumption of temperature uniformity in the seeded layer is rather crude. In reality, the outer portion of the layer will have a higher temperature than the portion near the surface. Since the seeding material will have to be injected through the wall surface, the density of seeding material in the region near the surface will also have a higher value. The effect of a lower temperature and higher seeding density near the surface will undoubtedly give a better radiation attenuation. This means that the radiation attenuation is a function of gas temperature. Further studies on this effect are deemed necessary. While the thermal and diffusion problem of this seeded layer is still not fully understood, the assumption that the temperature of the gas in the layer is uniform should be considered as a reasonable one.

As mentioned earlier in this report, the propellant at the temperature level considered here has too low an absorption coefficient for heat retention purposes, so seeding must be applied to the propellant. The method of calculating the seeding is similar to that for the boundary layer seeding. The assumptions made here include:

1. The propellant is originally transparent.
2. The temperature effect on seeding is neglected.

By making use of the experimental results of Lanzo and Ragsdale, it is possible to calculate the amount of carbon particles required by a certain volume flow rate of propellant for a prescribed absorptivity. For the case of fuel core size of 3 feet and carbon particle size of 0.1 microns, a computation has been made and the results are shown in figure 3-33. The relationship between the amount of seeding and the absorptivity is linear, and at low propellant velocity, the required amount of seeding is very small. For a constant absorptivity, the amount of seeding is directly proportional to the propellant velocity. With these results, it is possible then, to compute the amount of seeding required by the propellant both in the reactor and outside the scoop for obtaining specified levels of absorptivity.

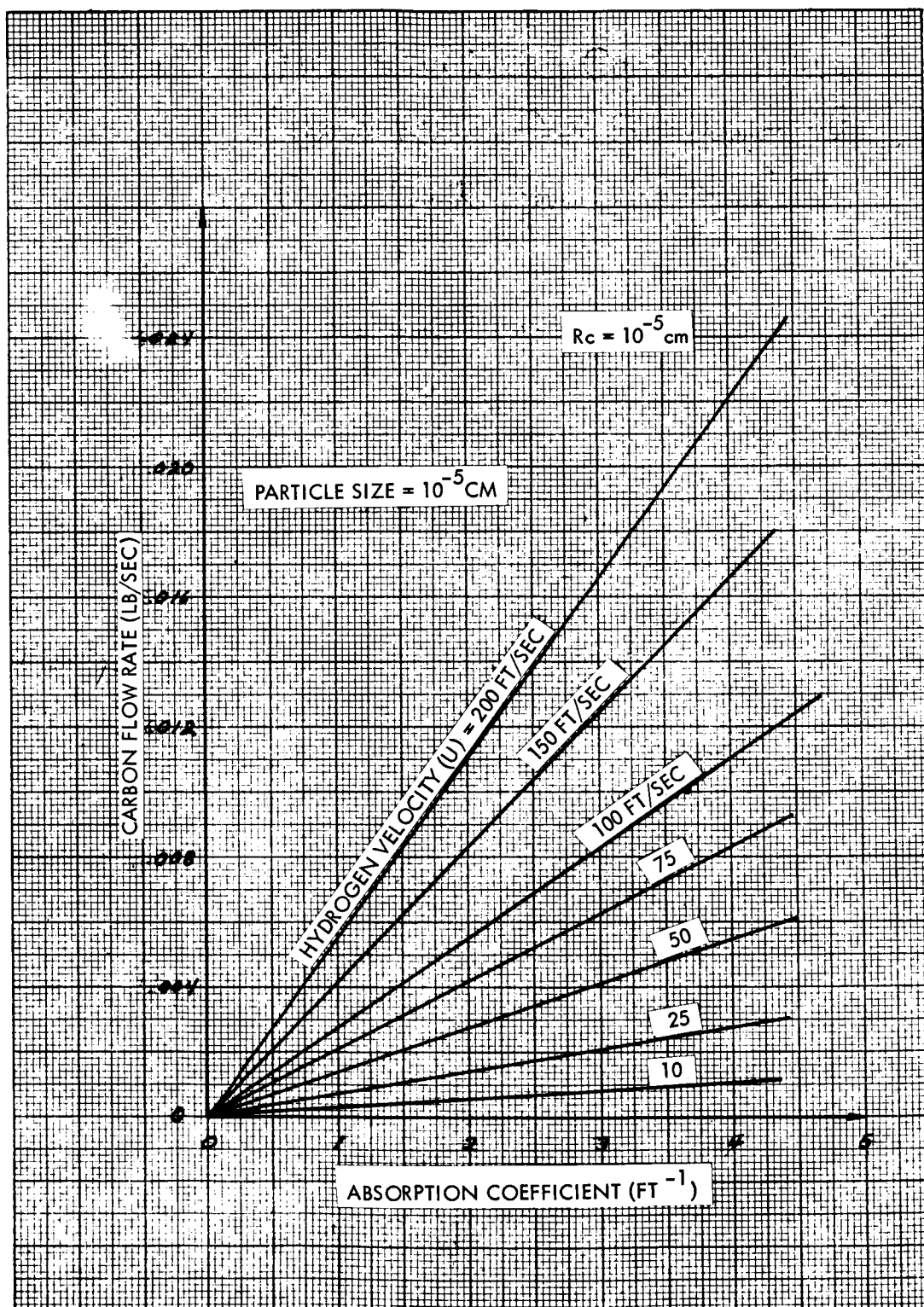


Figure 3-33 Carbon Mass Flow Rate Required for Attaining Hydrogen Absorptivity in Reactor Cavity (Case 1)

4. SCOOP COOLING FEASIBILITY ANALYSIS

4.1 SCOOP DESCRIPTION

The scoop is a cylindrical structure with primary function to capture the central stream of gaseous uranium at reactor exit and separate it from the outer propellant stream. ^{The URANIUM} collected in the scoop is simultaneously cooled by cold propellant to near wall material temperature, condensed as a consequence, and subsequently separated by exploiting the liquid/gas phase of the mixture. The uranium is then recirculated in the reactor. The propellant from the separator and the additional propellant needed to regeneratively cool the structure is passed through the reactor and out through the nozzle.

The scoop is a cylindrical structure 3 feet in diameter made up of a multiple circular array of tubes as shown in figure 4-1. The outer and inner array of tubes are of porous material and are primarily used for transpiration cooling required to maintain a cool stable film layer between the hot gases and wall. Internal to these tubes is an array of solid wall tubes that contain the respective seeded materials in separate streams of cold hydrogen ejected through the leading edge of the scoop such that, in effect, an aerodynamic leading edge is formed. A stream of carbon seeded hydrogen passes in front of and over the outer surface of the scoop while a stream of hydrogen seeded with uranium passes in front of and over the internal surface of the scoop. The respective seeded films of hydrogen forms the major thermal resistance to the incident heat flux and the residual heat flux is handled by conventional transpiration cooling methods.

4.2 SCOOP DESIGN CONSIDERATION

The major considerations affecting the design of the scoop are as follows:

4.2.1 Scoop Fuel Loss and System Cost-Effectiveness

The loss of uranium into the main propellant stream is a function of stream mixing in the reactor and the geometry of the scoop at reactor exit. If the scoop diameter is greater than the diameter of the uranium stream by 1 percent the uranium loss rate/total hydrogen flow rate can be kept within 1/1000 and this introduces sizable economy into the overall system cost-effectiveness.

SCOOP COOLING REQUIREMENTS

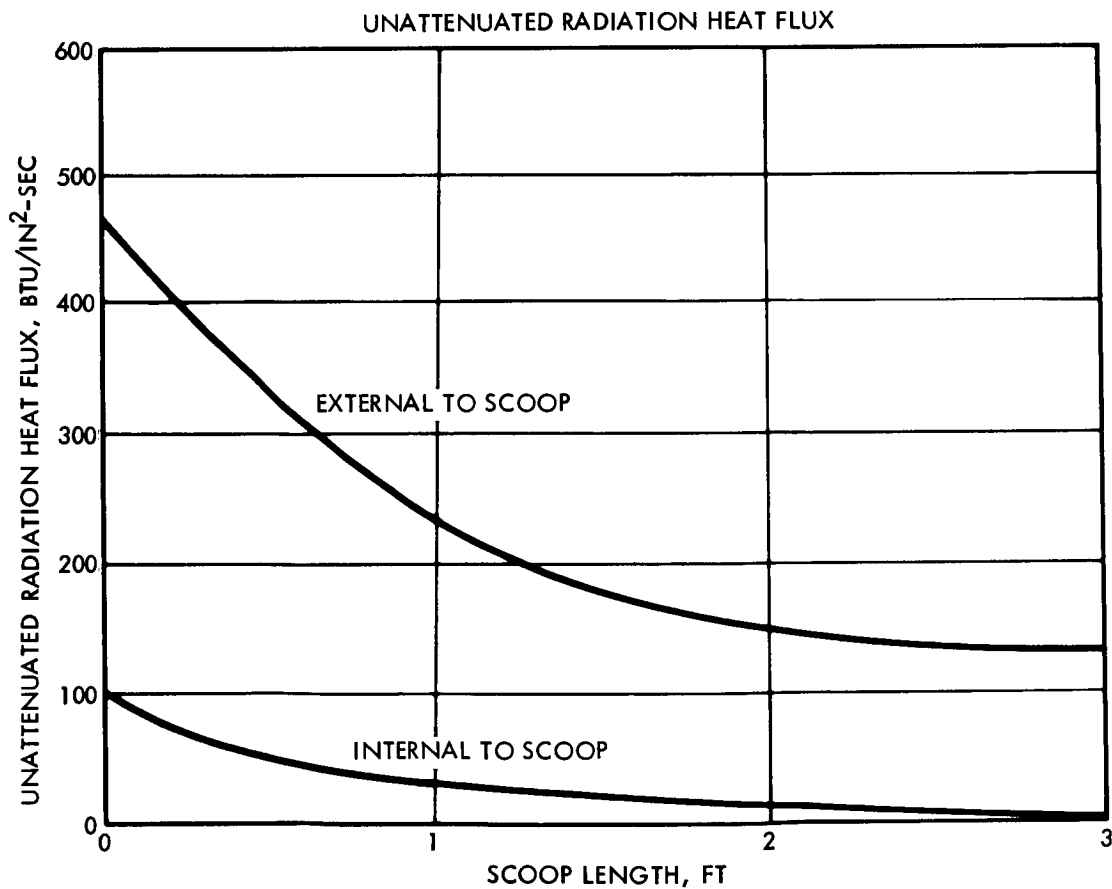
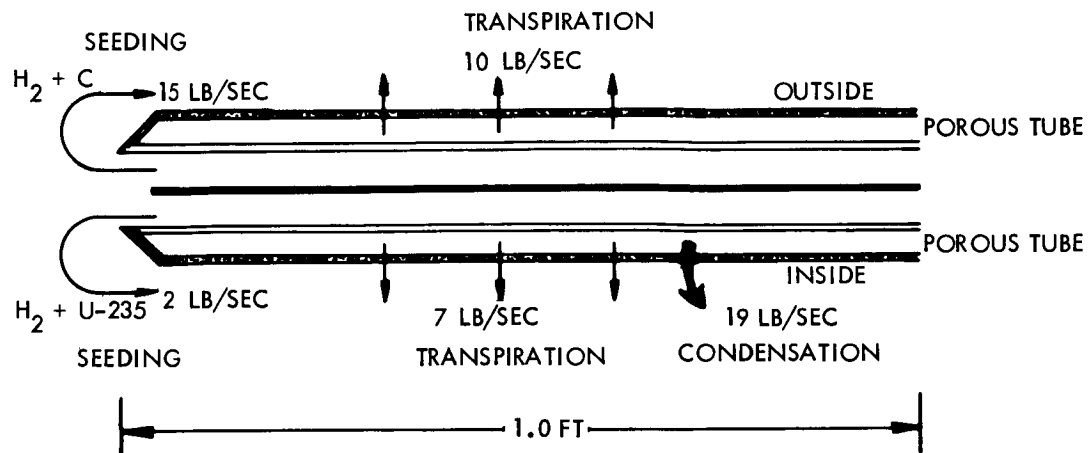


Figure 4-1 Scoop Configuration, Coolant Requirements and Unattenuated Radiation Heat Flux on Scoop

4.2.2 Cycle Thermodynamic Efficiency

The enthalpy of the hot hydrogen stream adjacent to the uranium stream is sufficiently high that the small amount entrained in the scoop (1/2 percent of the hydrogen flowing through the reactor) substantially raises the regenerative cooling load of the engine system. Similarly, the heat transferred from the outer surface of the scoop to the interior uranium stream can increase this regenerative cooling load. The regenerative cooling load is made up of the total heat absorbed by the incoming hydrogen before it enters the reactor and this is made up of the heat in the uranium stream at reactor exit and the heat absorbed by the structure. The engine specific impulse is a function of this regenerative cooling load as follows:

$$(\text{Specific Impulse})^2 \propto \text{reactor inlet temperature} / \text{fraction of } \frac{\text{regenerative}}{\text{total heat}}$$

This effect is minimized by keeping the scoop surface area to a minimum by bringing the throat to within a foot of the scoop's leading edge and by keeping the heat from entering the scoop by interposing a cold seeded boundary layer.

4.2.3 Heat Flux and Coolant Requirements

4.2.3.1 Unattenuated Heat Flux

The heat input to the scoop consists of both radiative and convective heat input. The radiation is by far the most serious, since it is of a higher rate and more difficult to block with film cooling techniques. The scoop must be protected from both the external and internal heat loads. The unattenuated radiation heat flux on both the external and internal surface of the scoop is shown in figure 4-1, as a function of scoop length for a typical engine design conditions (Case 1).

At the scoop leading edge, the incident radiative heat flux is 500 Btu/sec-in² on the outer and inner surface. This is an order of magnitude larger than any advanced heat engine presently in development. On the inner surface the heat flux falls off sharply with axial length because the photon mean free path of uranium is extremely small and the heat in the middle of the uranium core can hardly escape. On the external surface, the hydrogen has a relatively high photon mean free path and has a larger tendency to even up its radial temperature distribution as it axially flows along. This helps in reducing the hydrogen temperature at the scoop boundary and the attendant heat flux.

In all cases, it has been assumed that the fissioning can be substantially reduced once the uranium stream has entered the scoop and no additional fission heating has been included in this analysis.

4.2.3.2 Wall Heat Flux and Resulting Coolant Requirements

The heat transfer processes and coolant requirements are designed to attenuate the severe incident heat fluxes such that less than 20 Btu/sec-in² reaches the wall surface from both the radiative and convective processes. The basic cooling model and unattenuated radiation heat fluxes are shown in figure 4-1. It is assumed that 96 percent of the radiative flux is blocked on the external surface of the scoop and 99 percent on the interior surface and the seeded coolant flows are sized for these conditions. The convective component of wall heat fluxes are shown in figure 4-2, and is negligible at the leading edge because the coolant flow ejected from the leading edge is initially at 1000°R and as it flows along the length of the scoop it is continually fed with transpiration coolant at 3000°R such that the mixed temperature of the seeded film boundary never exceeds 6500°R. The convective heat is thus greatly reduced by the low temperature difference between the coolant bulk temperature and wall temperature 3000°R. In the vicinity of the nozzle throat at a scoop length of 0.6 to 1.0 ft, additional convective coolant must be added and this is treated separately under nozzle coolant requirements in a following section. In summary, it can be said that at the proximity of the scoop leading edge the total heat reaching the wall never exceeds 20 Btu/sec-in².

In the following discussion the heat protection schemes and coolant requirements to protect the scoop leading edge, internal and external surfaces are described in more detail.

4.2.3.3 Leading Edge Protection

It is planned to protect the leading edge of the scoop by injecting coolant directly out of the leading edge as shown in figure 4-3. Part of the coolant flow will then enter the scoop and part will pass down the outside of the scoop. Analytically, it is rather difficult to predict which will be the dividing stream line between the inner and outer flows, but this stream line does exit and can be determined by experiment. If the standoff distance caused by this leading edge blowing becomes too large, instabilities may exist. An experimental investigation of these problems would seem to be necessary to answer such questions.

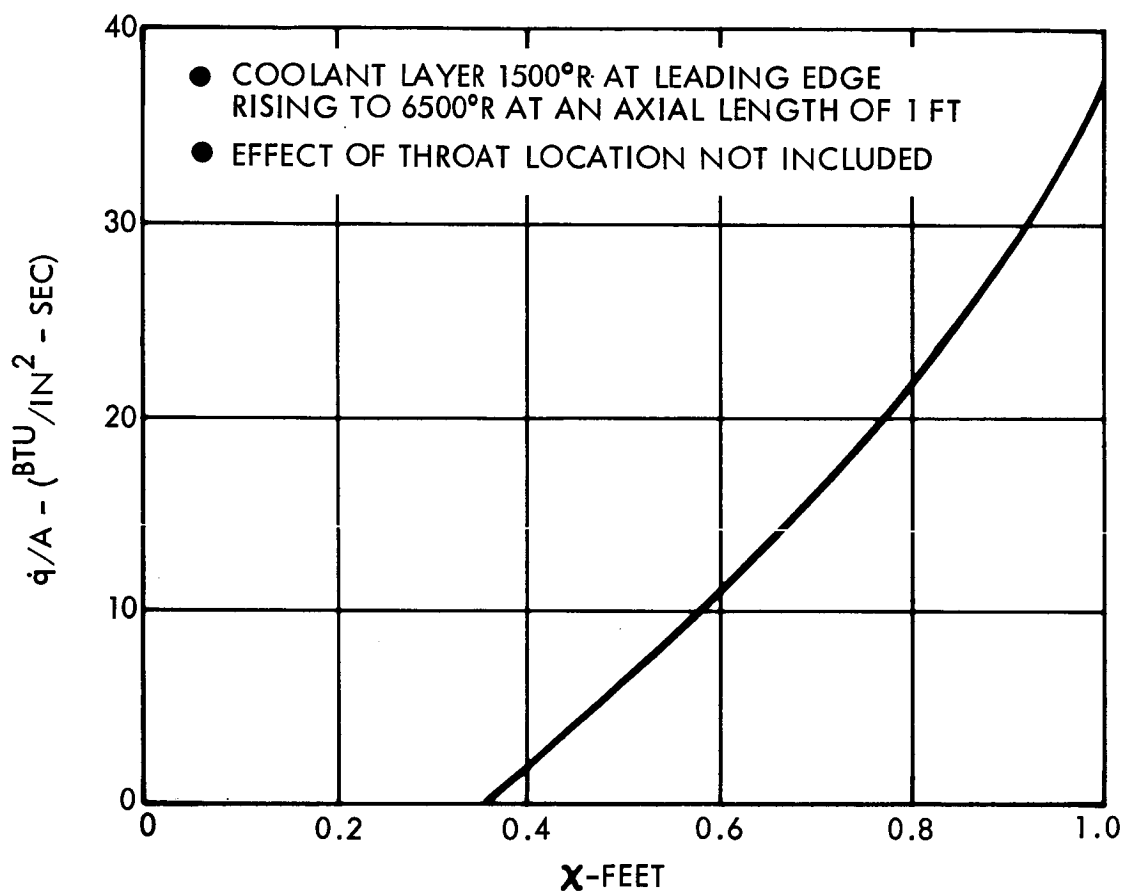


Figure 4-2 Convective Heat Flux on Scoop Surface

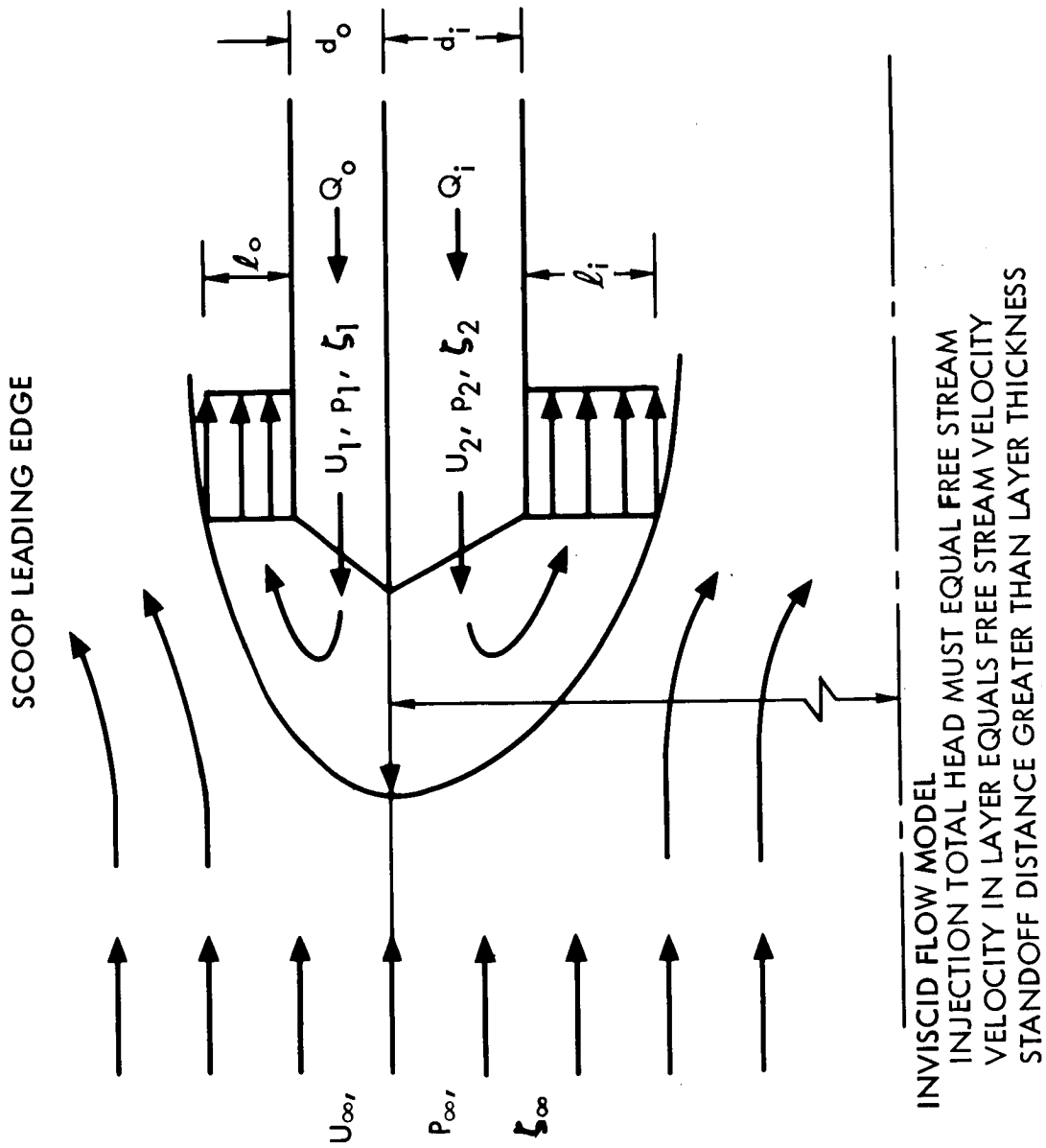


Figure 4-3 Flow Model for Scoop Leading Edge

4.2.3.4 Internal Surface Protection

The internal problem is somewhat less critical in that it is desired to add sufficient coolant to the internal flow to condense the uranium and lower its temperature to less than the permissible wall temperature. There is plenty of coolant available for internal use and it is only necessary to determine how to inject this coolant so that the initial part of the scoop is protected.

To prevent the radiated heat flux from the hot core from reaching the scoop walls, the cool injected film will have to be seeded so that this cool layer is opaque to the radiative flux and the radiated heat will be absorbed by the cool layer. Seeding the layer with solid or liquid particles has been demonstrated to be an effective technique for doing this (reference 15). Since it is not desirable to introduce solid foreign material within the scoop which will be collected within the condensed liquid uranium, it was decided to use uranium itself as the seeding material. On a weight basis, uranium is a rather inefficient seeding material. Since uranium may be taken from the separator, either before or after separation, and simply recirculated, the amount required is not important. In fact the cool boundary layer injected into the scoop will seed itself naturally to some degree from the gaseous uranium that will condense when it enters this cool layer. At high temperatures, the gaseous uranium is quite opaque but data at temperatures much below $15,000^{\circ}\text{R}$ are not available and it is difficult to determine how much to count on the gaseous uranium as a seeding material before it is condensed to the liquid phase. A disadvantage in respect to using the uranium in the hot core to furnish the seeding material is that the layer of fluid at the outer edge of the core has mixed with hydrogen during its passage through the chamber, so the outer edge of the core flow only contains a low uranium concentration. The added uranium may in future nuclear studies be found to greatly complicate the attenuation of the fissioning process at the scoop inlet and in this case the use of seeded material like carbon will be acceptable.

4.2.3.5 External Surface Protection

The external side of the scoop must be protected from the hot hydrogen propellant flow. A cool opaque film must be provided to absorb the incident radiation and block the heat transfer. A minimum amount of injected hydrogen is desired and a minimum amount of seeding since these both decrease the performance of the rocket. Carbon has been selected for this external seeding material since it appears to be the most efficient one available. (Reference 15)

4.2.3.6 Coolant Requirements

The means used to predict the coolant and seeding flows are described as follows. The coolant flow in the neighborhood of the leading edge can be crudely described by an inviscid flow model (figure 4-3). Along the dividing stream line, the coolant flow and the oncoming core flow both stagnate, which requires that they have equal stagnation pressures. Both flows now divide and pass along either side of the scoop. The static pressure along the straight sides of the scoop will be of the order of free stream static pressure, so the velocity head of the coolant will be about the same as of the core flow along the dividing stream line. The thickness of the cooling layers on both the internal and external sides of the scoop as a function of leading edge coolant flow is shown in figure 4-4. The leading edge standoff distance would be expected to be greater than the layer thickness because of the lower velocity in this region.

The total amount of coolant flow to absorb the total heat input to either side of the scoop as a function of distance behind the leading edge is shown by the dotted lines in figures 4-5 and 4-6 as a function of seeding ratio. Since the seeding material only absorbs a small amount of heat compared with the hydrogen, these curves are relatively flat. Solid lines designate the amount of seeding material as a function of coolant flow to block the radiated heat flux. Carbon is used for the seeding for the external coolant and uranium for the internal coolant. For the external coolant, a blocking factor of 0.9 and 0.99 is shown. To demonstrate the use of these curves, consider the case in which it is desired to block 0.99 of the heat flux for a distance of one foot along the scoop (figure 4-6). Enough seeding is available for any point to the right of the 0.99 solid curve and enough cooling at any point above the one foot dotted curve. Since the carbon required is the same for any point along the 0.99 solid curve and the hydrogen flow along the one foot dotted curve is relatively constant, the intersection of these two curves at a hydrogen flow rate of about 15 lbs/sec and a carbon-hydrogen flow ratio of 0.055 would appear to be the best design condition.

For the internal flow, the same curves have been drawn for different particle sizes. Unless the particle size can be kept to values of about 10^{-5} cm radius, the ratio of uranium mass flow to hydrogen mass flow becomes quite large. This conclusion is for the minimum hydrogen flow required to perform the cooling. It should be noted that the ratio can always be lowered by injecting more hydrogen up to the 28 lbs/sec required to condense the uranium flow.

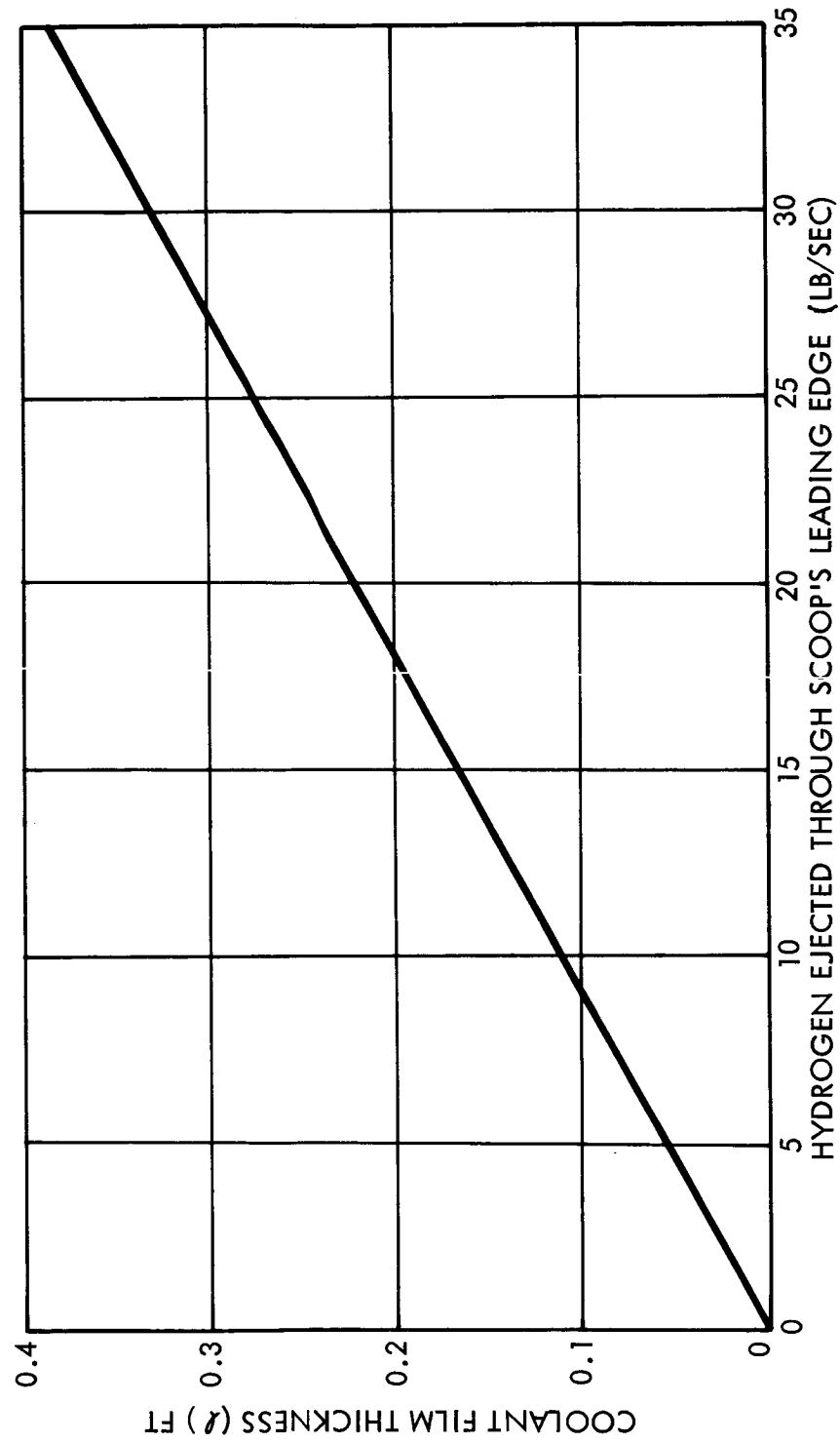


Figure 4-4 Thickness of Coolant Film on Scoop of Surface Resulting from Ejecting
Coolant Through Leading Edge of Scoop

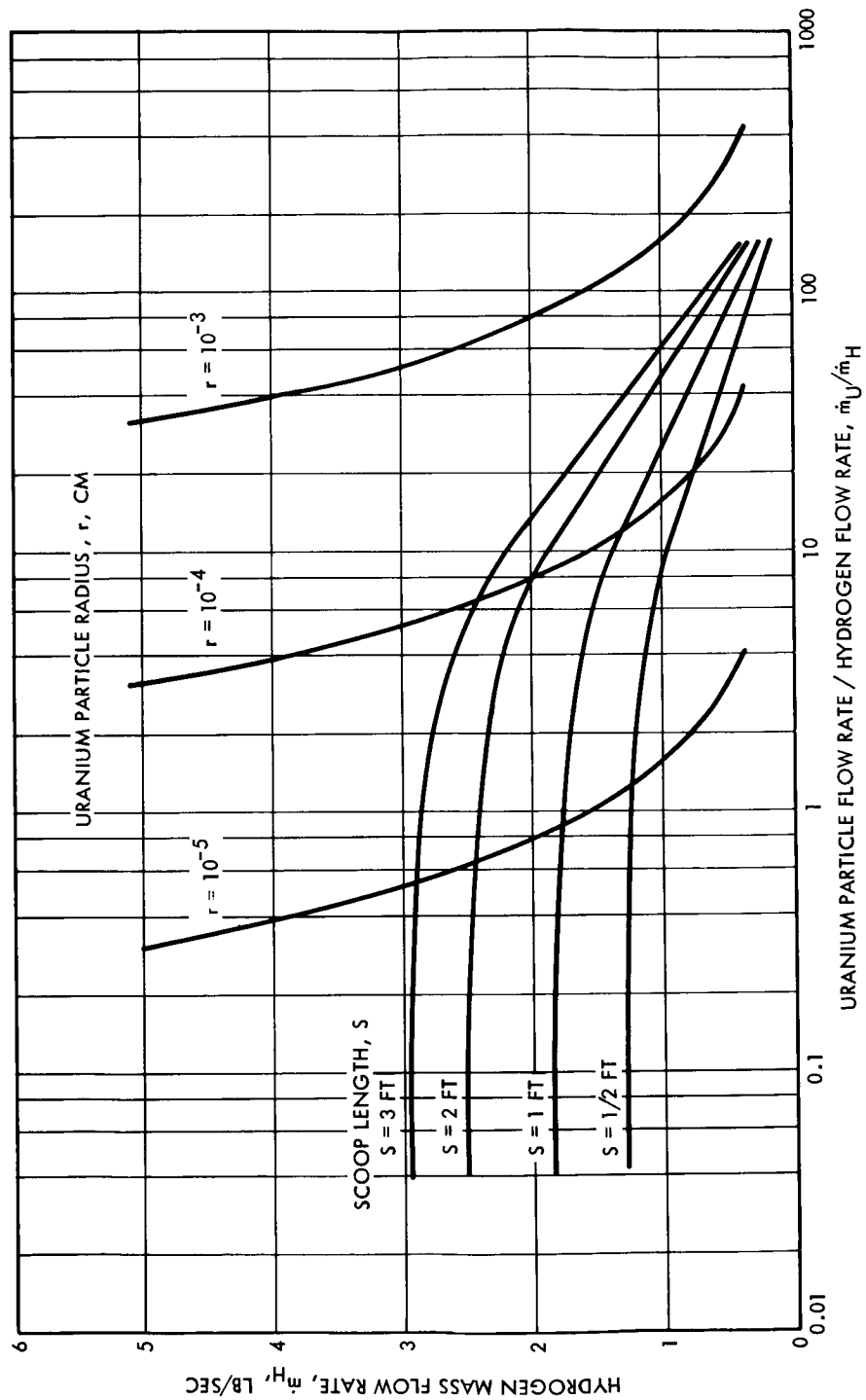


Figure 4-5 Radiation Blocking (99% Attenuation) by Uranium Particles Near the Scoop Inlet (Interior)

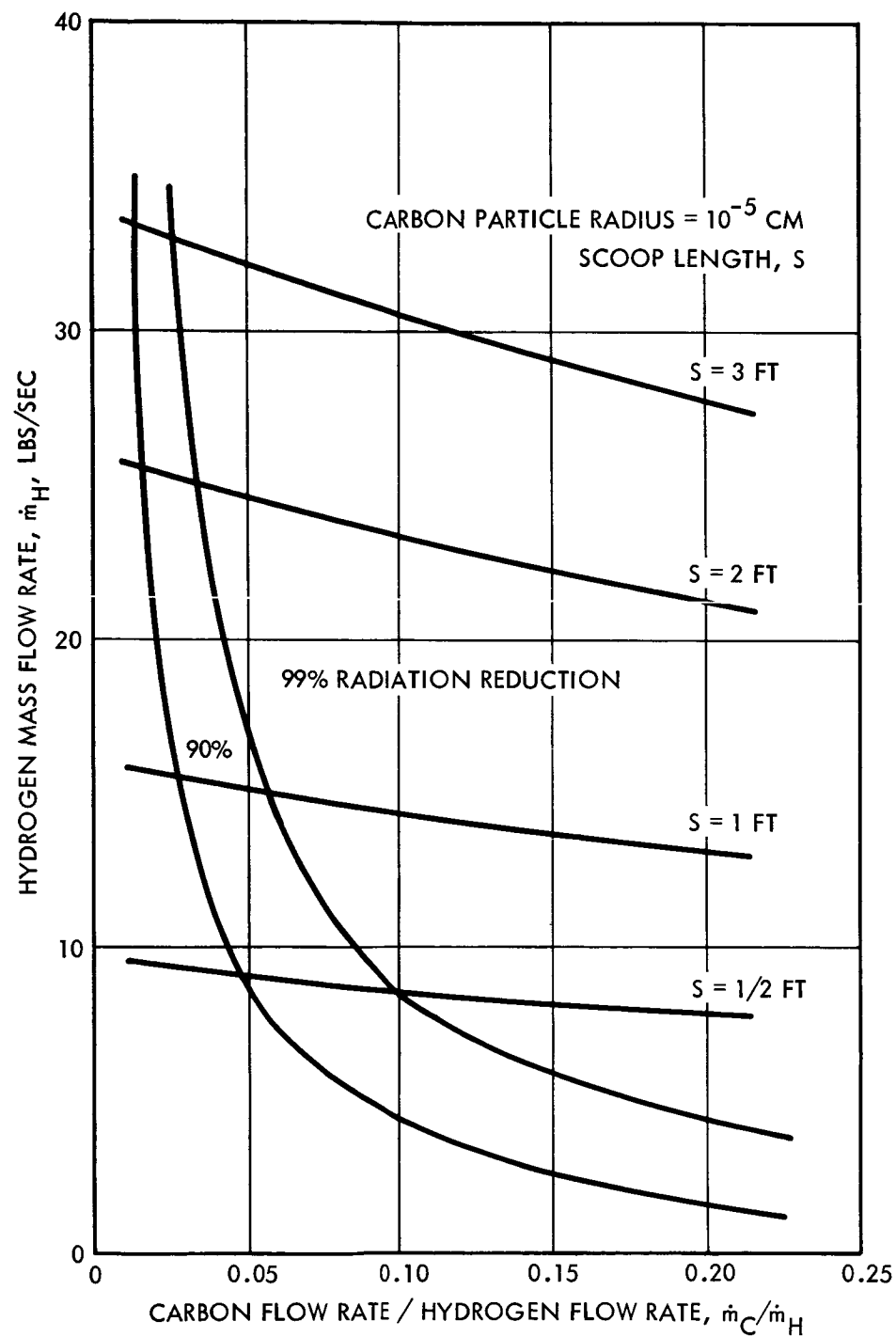


Figure 4-6 Radiation Blocking by Carbon Particles Near the Scoop Inlet (Exterior)

4.2.4 Thermo Structural Considerations

The foremost thermo-structural problem of the scoop is the design and fabrication of a structure which will maintain its integrity during the engine's duty cycle in the presence of extremely high heat fluxes. A secondary problem is the overall structural integrity of this component when subjected to launch dynamic loads and, during engine operation, to the engine vibration environment. In this study, the analysis was confined to the thermo structural problems encountered during engine operation. The secondary structural problems of the scoop can be dealt with best in the context of an overall system design study. This is due to the fact that the response of the structure to the applied loads will depend greatly on interaction with adjacent engine and spacecraft components which are not well defined at this time.

A basic scoop structural model was chosen satisfying the cooling requirements necessary to maintain the material within reasonable temperature, and, at the same time, retains the desired geometrical configuration. This model consists of a circular array of tubes (in a cylindrical or conical arrangement) through which coolant is passed (figure 4-7). Both transpiration, as well as regenerative cooling schemes were considered. In the first case, the tube material must be porous and the analysis was concerned with the ability of porous materials to withstand the thermostructural loads. In the second case, the tube material is a refractory metal in the tungsten alloy family. Current emphasis on the tungsten 25 rhenium alloy as a promising structural material for high temperature applications led to its selection for the regenerative cooling application.

In all cases considered, the blocking of the intense gaseous radiation with carbon particles requires that seeded coolant be dumped into the flow field surrounding the scoop. This is accomplished by carrying hydrogen to the forward end of the scoop (and, for that matter, to any other intermediate point along the axis of the scoop) in separate tubes. In the structural model chosen for study, these are carried in tubes housed within the basic scoop structure. The separation of wall cooling hydrogen from the seeded gas reduces the possibility of chemically contaminating the hot tube material and blocking of coolant exit passages.

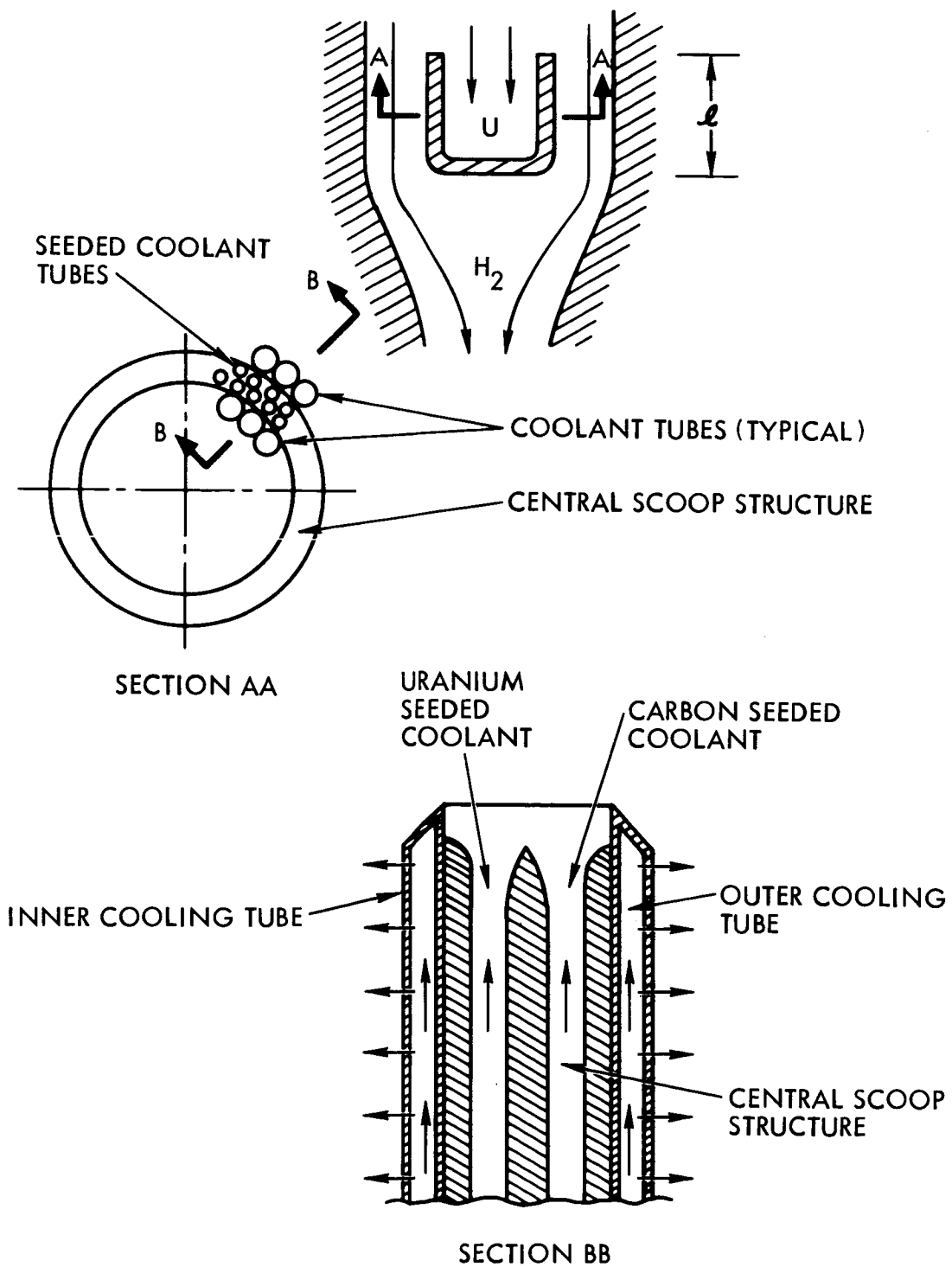


Figure 4-7 Study Configuration of Scoop

4.2.5 Stress Analysis

4.2.5.1 Thermal Stresses

The primary load on the tube wall is due to the temperature gradient established between the 3000°R gas side surface and the inside of the tube. In the model selected for study, the tubes are not heated uniformly around the circumference since they are exposed only partially to fluxes from the propellant and the gaseous uranium; the segments of circumference in the weld area are only heated by conduction. The net result is that in addition to the radial thermal gradient, some circumferential thermal gradient is also established. The circumferential variations in temperature will depend on the radius and thickness of the tube and its thermal properties, the temperature distribution in the central scoop structure, and the heat transfer through the tube scoop structure joint. It is assumed, in this study, that these circumferential effects are small and that the significant gradient is the radial one. The extent to which the assumption is valid can be determined with additional analysis and experimental work.

It is also assumed that transient effects can be eliminated or reduced so that the problem of thermal shock does not arise. This can be achieved by gradually preheating the tubes or else by appropriate reactor starting procedures. In any event, the extent to which thermal transients could contribute to the state of stress in the tube can not be fully assessed without a complete system analysis which includes the reactor starting procedures.

It follows that the significant temperature profiles, for purposes of this study, are the steady state circumferentially uniform distributions. These have been obtained, numerically, for walls of the required thickness and porosity. The analysis was restricted to 0.5-in diameter tubes with 0.10 inch walls. The analysis considered both regenerative and transpiration cooling. The flux-pressure drop relations for regenerative cooling are dependent on the length of the scoop and are shown in figure 4-8. These results were obtained for an inside wall temperature of 2500°R . The temperature profile in the wall is assumed to be linear and the temperature drop from the outside to the inside surface of the tube is given by

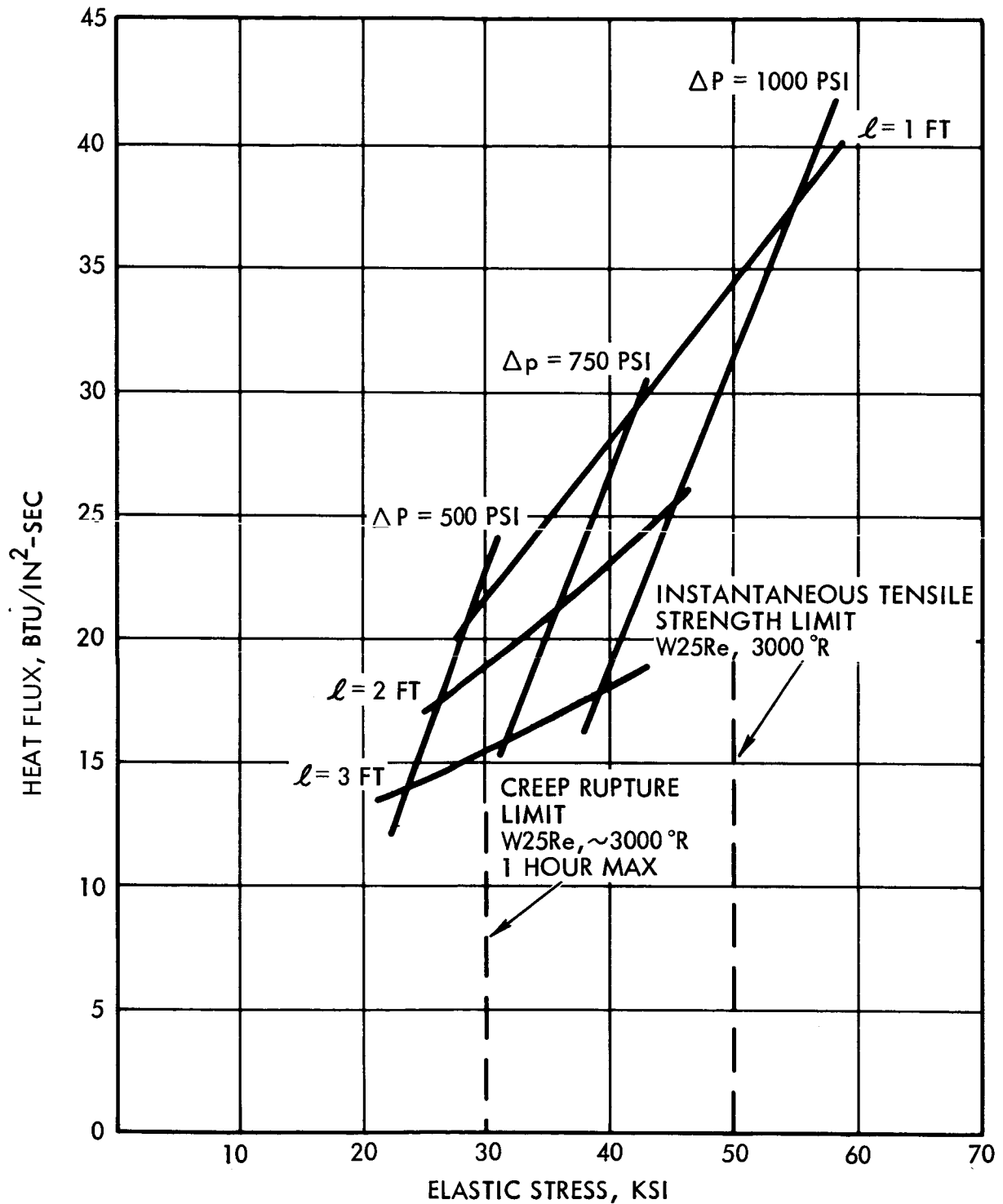


Figure 4-8 Total Stress in Convectively Cooled Tubes
as a Function of Scoop Length ℓ
4-1 5

$$\Delta T = (7.64 \times 10^4)^{-1} \frac{\dot{q}}{A} t \quad (22)$$

where

$\frac{\dot{q}}{A}$ = the flux shown in figure 4-6

t = the wall thickness (in)

and the thermal conductivity of tungsten was used

For transpiration cooling, the fluxes chosen for analysis, the associated maximum temperature differences, ΔT , across the wall thickness and corresponding fluid pressures, p , necessary to circulate or inject the coolant through the wall as shown in table 4-1. In all cases, the outer wall is kept at 3000°R. The computed temperature distributions can be correlated by the equation

$$T(r) = T_i \left(\frac{T_o}{T_i} \right)^{\frac{r-a}{b-a}} \quad (23)$$

where

$T(r)$ = temperature at any point, r in the wall of the tube

T_i = inside face temperature

T_o = outside face temperature

a = interior radius of the tube

b = exterior radius of the tube

In the table 4-1 below

$$T = 3000 - T_i$$

Table 4-1

Case	\dot{q}/A Btu/in ² -sec	ΔT °R	p psi
1	5	200	50
2	10	250	100
3	20	300	110
4	50	400	190
5	100	600	280

In the regenerative cooling case, the linear temperature profiles produce thermal stresses given by the thin wall formula. The maximum elastic stresses on the inner wall are given by

$$\sigma_T = \frac{E \alpha \Delta T}{2(1-\kappa)} \quad (24)$$

where

E is the modulus of elasticity

α is the coefficient of thermal expansion

κ is Poisson's ratio

Using available data in reference 21 for the W25Re alloy

$$E = 30 \times 10^6 \text{ psi}$$

$$\alpha = 2.8 \times 10^{-6} \text{ in/in-}^\circ\text{R}$$

and assuming

$$\kappa = .3$$

equation (23) becomes

$$\sigma_T = 60 \Delta T \text{ psi}$$

In the porous material tubes, the temperature profiles are nonlinear. However, the departure from linearity is sufficiently small in these thin walls to justify stress calculations based on the linear temperature formula (24) rather than on thick tube equations. These calculations were restricted to elastic behavior only and may, therefore, predict higher stresses than those which would result in an elastoplastic material. Since porous refractory materials display only minimum plasticity at fracture (reference 22), it seems reasonable to restrict the calculations at this time to the more conservative elastic case. However, this may be removed later through analytic and experimental work aimed at a better definition of the mechanical behavior of porous materials and structures.

Using data from reference 23 for typical porous materials it was shown that in this case also, the hoop stress is given by Equation (24).

4.2.5.2 Pressure Stresses

The tube geometry used in the study makes it possible to use the thin wall formula for hoop stresses in pressure vessels.

$$\sigma_p = p \frac{r}{t} \quad (25)$$

where

t = tube thickness, i.e., $t = b - a$

The pressure stresses are relatively low in the porous tubes contributing up to a maximum of less than 20 percent of the total stress.

4.2.5.3 Total Stresses

The thermal and pressure stresses are additive on the inside face of the tube. Hence, the maximum elastic stresses experienced in the tube can be obtained by evaluating Equations (24) and (25) and adding the results. The resulting maximum stresses are plotted in figures 4-8 and 4-9 as a function of the flux for the transpiration and the regenerative cooling case, respectively. The stresses in the regenerative cooled tubes are shown as a function of scoop length and pressure drop. The pressure parameter is important in this case, since the scoop cooling must be integrated within the complete engine assembly and must, therefore, reflect overall system requirements. The transpiration cooling curve is independent of scoop length since the pressure drop is determined only by the mass flow rates through the chosen wall and the applied fluxes.

4.2.6 Material Strength

4.2.6.1 Convective Cooling

The short time tensile strength of W25Re at 3000°R is given in reference 21. Applying a reduction factor to account for the usual scatter in strength data of refractory metals the instantaneous tensile strength can be taken at 50 ksi. Figure 4-8 shows that this stress level is adequate for a maximum heating rate of 38 Btu/in²-sec at 1000 psi pressure differential in a 1-ft scoop and lower pressure differentials for longer scoops. However, for sustained high temperature service, the creep rupture allowable of a metal is a more meaningful criterion of strength than the instantaneous value. Creep rupture data for W25Re compiled from a number of sources, is summarized in figure 4-10. This plot shows that for operating times up to 1 hour, the rupture strength varies from 60 to 30 ksi for temperatures of 3000°R and 3360°R, respectively. Accounting again for the usual scatter, an allowable of 30 ksi is suggested. When this allowable is superimposed on the plot in figure 4-8, it limits the allowable fluxes to a range of 21 to 15 Btu/in²-sec for scoop lengths ranging from 1 to 3

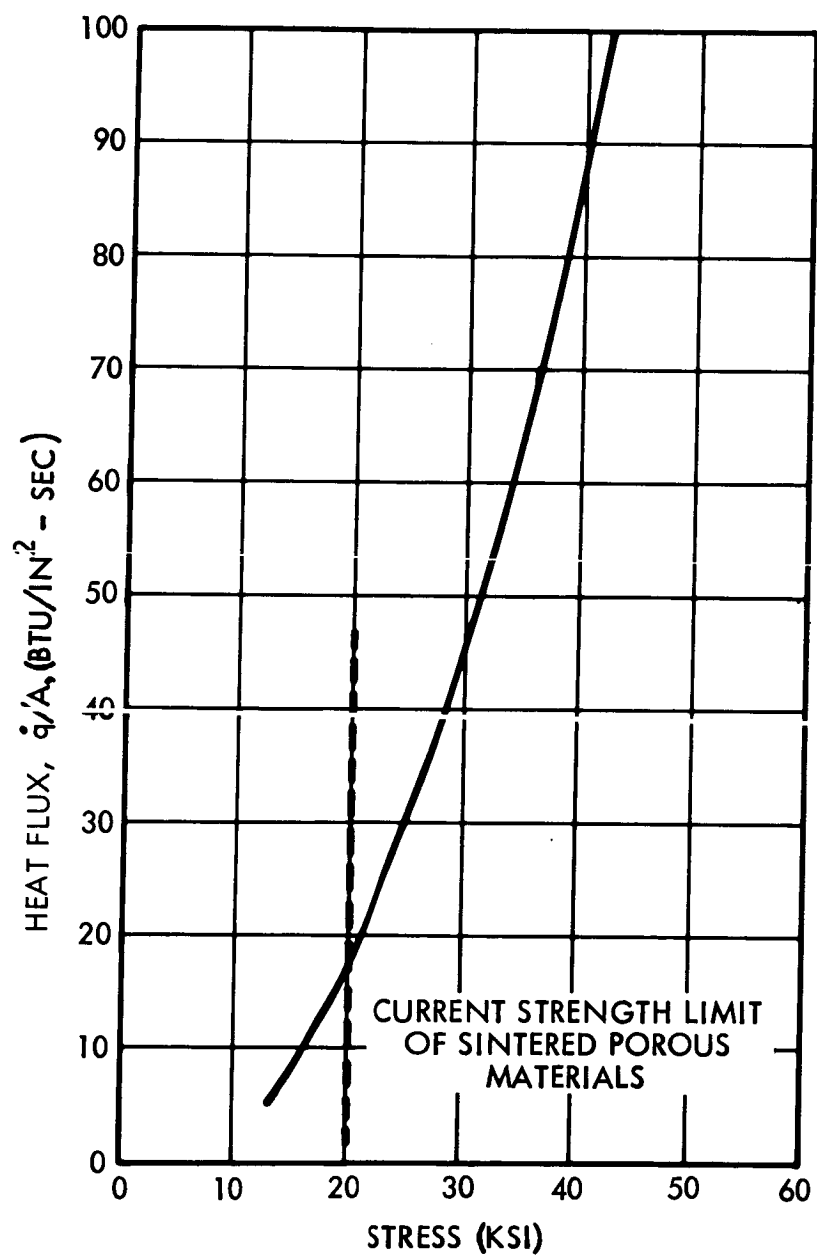


Figure 4-9 Total Stress in Transpiration Cooled Tubes

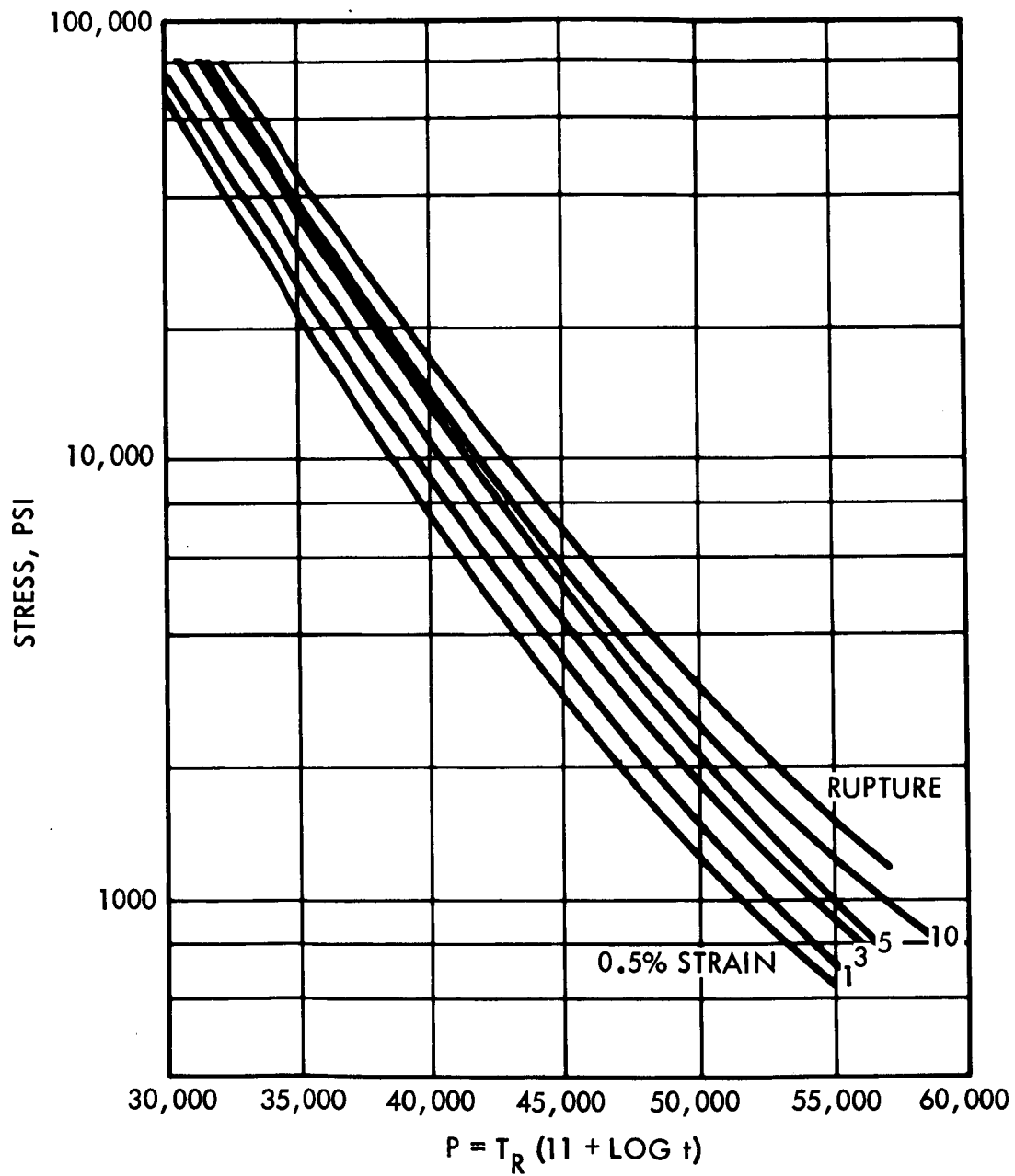


Figure 4-10 Creep and Creep Rupture of W25Re Alloy
Larson Miller Parameter
4-20

feet. However, the state of stress in the tube also changes as a function of time due to creep action. The thermal stresses tend to relax while the pressure stresses alter somewhat due to the high sensitivity of the creep parameters to temperature (reference 24). It follows, therefore, that the feasible range of 15 to 21 Btu/in²-sec heating rates is conservative. The exact degree of conservatism cannot be estimated without more elaborate creep data and considerable analysis.

4.2.6.2 Transpiration Cooling

The efficiency of the transpiration cooling concept depends in great measure on the size of the pores. Calculations show that, for porosities of the order of 0.3, pore sizes must be fairly small, of the order of 10^{-3} to 10^{-4} inch diameter, to remove fluxes in the range 5 to 20 Btu/in²-sec. The enormous hole density needed to meet this requirement precludes, on practical grounds, the consideration of refractory metal tubes with porosities induced mechanically, i.e., by machine, electron beam, laser, or other drilling procedures. The transpiration tubes must, therefore, be made from porous, sintered refractory materials by powder metallurgy techniques. The tensile strengths of these materials generally exhibit large scatter attributable to the many variables associated with their fabrication. Figure 4-11 is a composite of reported bend strength of porous tungsten (20 to 30 percent porosity) as a function of test temperature. From this plot it appears that 20 ksi is a reasonable upper limit of available strengths based on current powder metallurgy techniques. When this value is superimposed on figure 4-9, it is seen that porous tubes may be used for transpiration cooling up to 20 Btu/in²-sec fluxes. Of course, advances in powder metallurgy techniques will, in time, increase the available strength and thus make possible cooling to even higher fluxes.

4.2.7 Conclusions

This study indicates that a scoop design appears feasible for duty cycles of the order of 1/2 to 1 hour at temperatures in the 3000°R range. The design is predicated on reduction of wall heating rates into the 15 to 20 Btu/in²-sec range by seeding the gas streams. For a chosen coolant tube geometry of 0.5 inch diameter and 0.010 inch wall thickness, the study indicates that regenerative cooling could be utilized conservatively in the 15 to 21 Btu/in²-sec range with W25Re tubing. However, regenerative cooling of the scoop imposes severe thermodynamic penalties on the overall system which would tend to limit its growth potential. Therefore, this concept is placed in a secondary position with respect to the alternate approach of transpiration cooling.

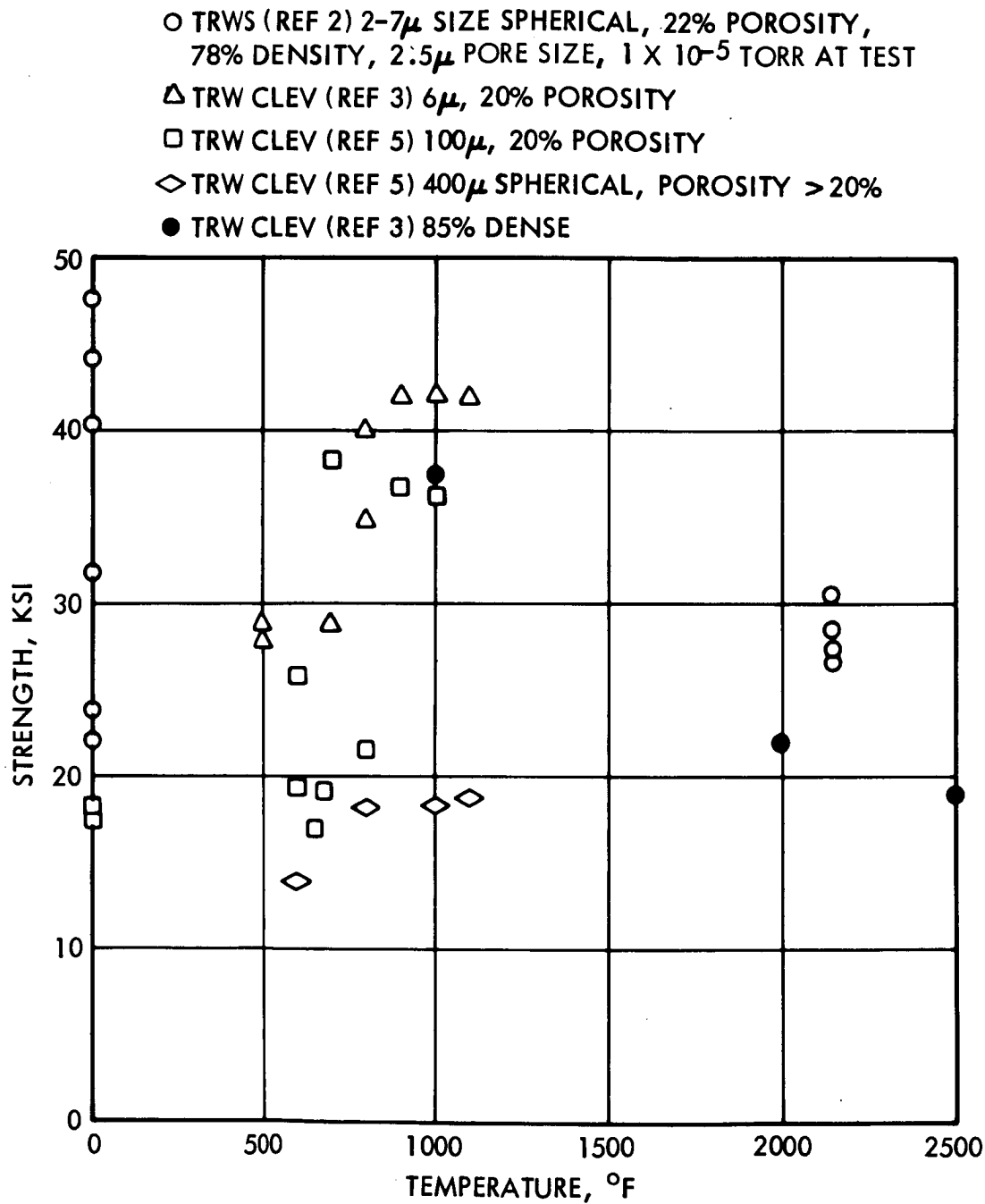


Figure 4-11 Bend Strength of Porous Tungsten

The study further indicates that a transpiration cooled scoop can be designed with current porous materials to absorb heating rates of the order of 20 Btu/in²-sec for the required duty cycles. Unlike the regenerative cooling concept, transpiration cooling is not system growth limiting; indeed, reasonable advances in the technology of porous materials could substantially increase the upper limit of the wall fluxes and thus reduce the demands on the gas seeding system.

These conclusions were reached on the basis of a broad spectrum of assumptions concerning modes of heating, heat transfer effects, and mechanical behavior of the materials considered. These assumptions must be reinforced by additional study and research.

5. ENGINE PRELIMINARY DESIGN

The purpose of the engine preliminary design is to establish a consistent engine design and determine the major characteristics, dimensions, and weights of the various components constituting the gas core nuclear rocket engine. Figure 5-1 shows the general features of the gas core nuclear rocket engine and the major engine components comprising the overall engine system. The direct flow, externally separated gas core reactor utilizes a parallel coaxial stream of propellant and fissioning fuel, with the hydrogen propellant surrounding the uranium fuel. At reactor discharge, the fuel is collected and cooled to a temperature below the boiling point of the uranium by mixing the fuel with incoming cold propellant. The resulting mixture is an aerosol of condensed uranium liquid droplets in a gas mixture. The mixture is then separated outside the reactor core, exploiting the liquid-gas phase difference to achieve nearly complete retention of the fuel. Once separated, the uranium fuel is recycled through the reactor.

The propellant contained in the propellant tank is pumped to a high pressure by the turbopump. The high pressure propellant is then used to cool the major reactor components: a portion regeneratively absorbs the heat of the fissioning reactor that is deposited in the nozzle and reflector, another portion is used to pressurize the uranium stream and to condense the uranium fuel, the remainder is used to transpiration cool and film cool the structural surfaces subjected to high heat fluxes.

The determination of the temperatures, pressures, and mass flow rates throughout the gas core system requires a knowledge of the pressure necessary to achieve criticality, the heat loads incident on the major subsystem components, and the cooling requirements of each component. The criticality analysis determines the critical mass of uranium fuel required for criticality, and more important, critical density and thus the pressure required to sustain a controlled nuclear chain reaction in the temperature environment of the gaseous core. To establish the overall engine performance, an estimation of the various component weights is required. The total engine weight can then be estimated and the thrust-to-weight ratio of the gas core nuclear rocket engine determined.

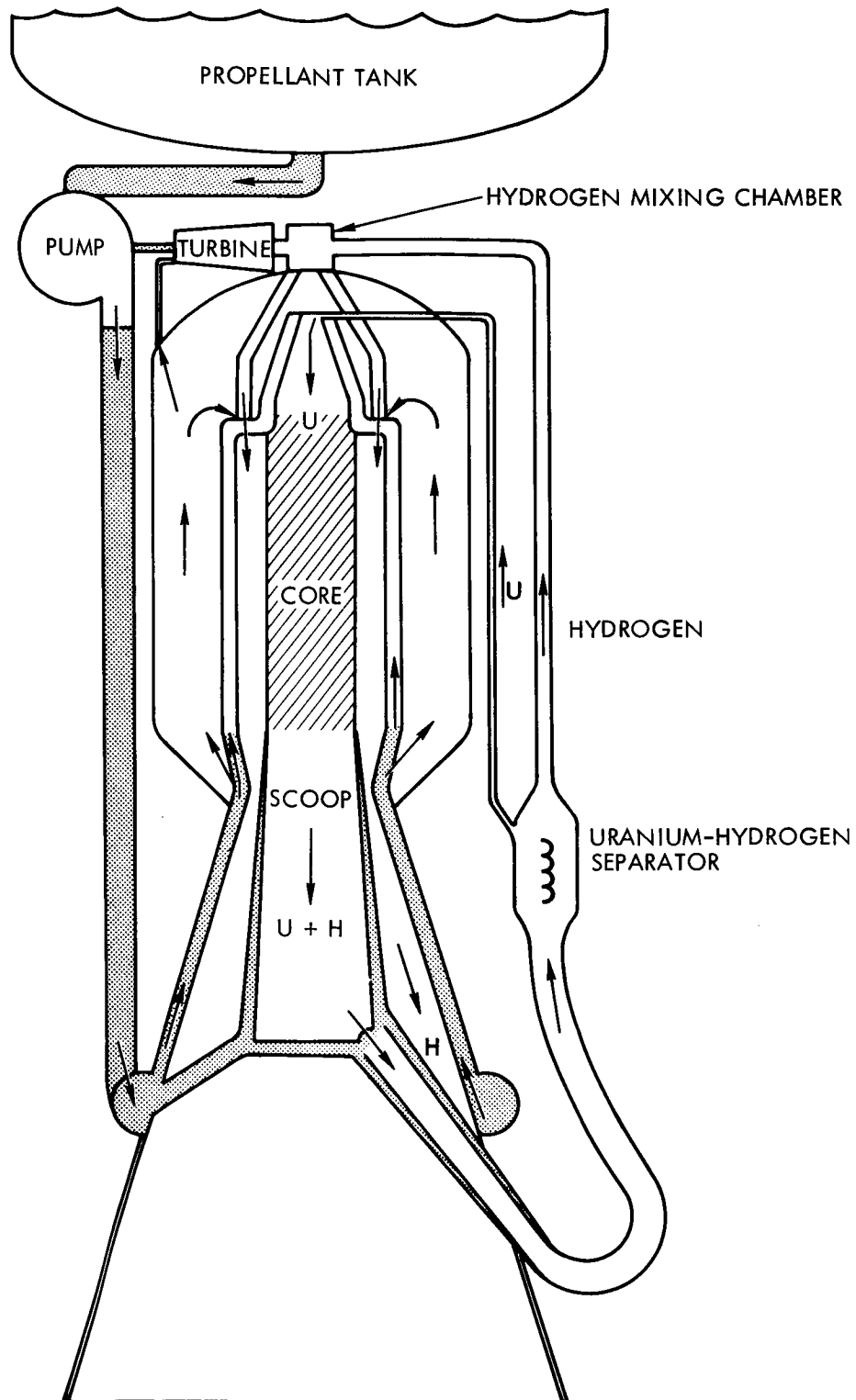


Figure 5-1 Gas Core Nuclear Rocket Engine Schematic
(Externally Separated Uranium Cycle)

5.1 NUCLEONICS

5.1.1 Criticality

A knowledge of the conditions required for criticality is fundamental to the analysis of the gas core reactor. Criticality in a gas core reactor, as in other reactors, is dependent upon the size, geometry, composition, and temperature of the fuel, moderator and structural materials comprising the reactor. To achieve criticality, the fuel atom density in the fissioning fuel column must be high enough to produce a critical mass in the reactor geometry of interest. The attainment of high propellant exit gas temperatures requires the achievement of high temperatures in the central fissioning column to transfer heat by radiation from the fuel to the propellant. Since the operating pressure and temperature in a gas core reactor are directly coupled through the perfect gas law, $P = nRT$, the critical mass and fuel atom density required for criticality has a significant influence on the system operating conditions and, ultimately, on the systems overall performance. The direct dependence of operating pressure on operating temperature and critical mass provides great incentive to attain the lowest possible critical mass since higher propellant temperatures can be generated for the same operating pressures.

The desirability of low critical masses and the incentive for low gaseous fuel densities tends to restrict the gas core system to operation in the thermal neutron regime. In the gas core reactor, the fast neutrons released by the fission process occurring in the central fissioning column are thermalized in a moderating reflector surrounding the gas core.

Several nuclear fuels which can potentially be utilized in a gas core reactor include uranium -233, uranium-235, and plutonium-239. Preliminary calculations indicate that U-233 and Pu-239 are capable of achieving criticality at considerably lower critical masses than U-235. However, multigroup calculations show that high purity plutonium produced in a reactor contains sufficient Pu-240 to increase the critical mass to more than that of U-235. Figure 5-2 compares the critical mass of U-233, U-235, and Pu-239 in a spherical gaseous core surrounded by 100 cm of graphite at 7110°R. A single point is also presented for Pu-239 containing 8.2 percent Pu-240 and 0.5 percent Pu-241. These results show that higher quality plutonium would be

SPHERICAL CRITICAL MASSES FOR U-233, U-235, PU-239

REFLECTOR MATERIAL - GRAPHITE
REFLECTOR THICKNESS - 100 CM
REFLECTOR TEMPERATURE - 7170° R

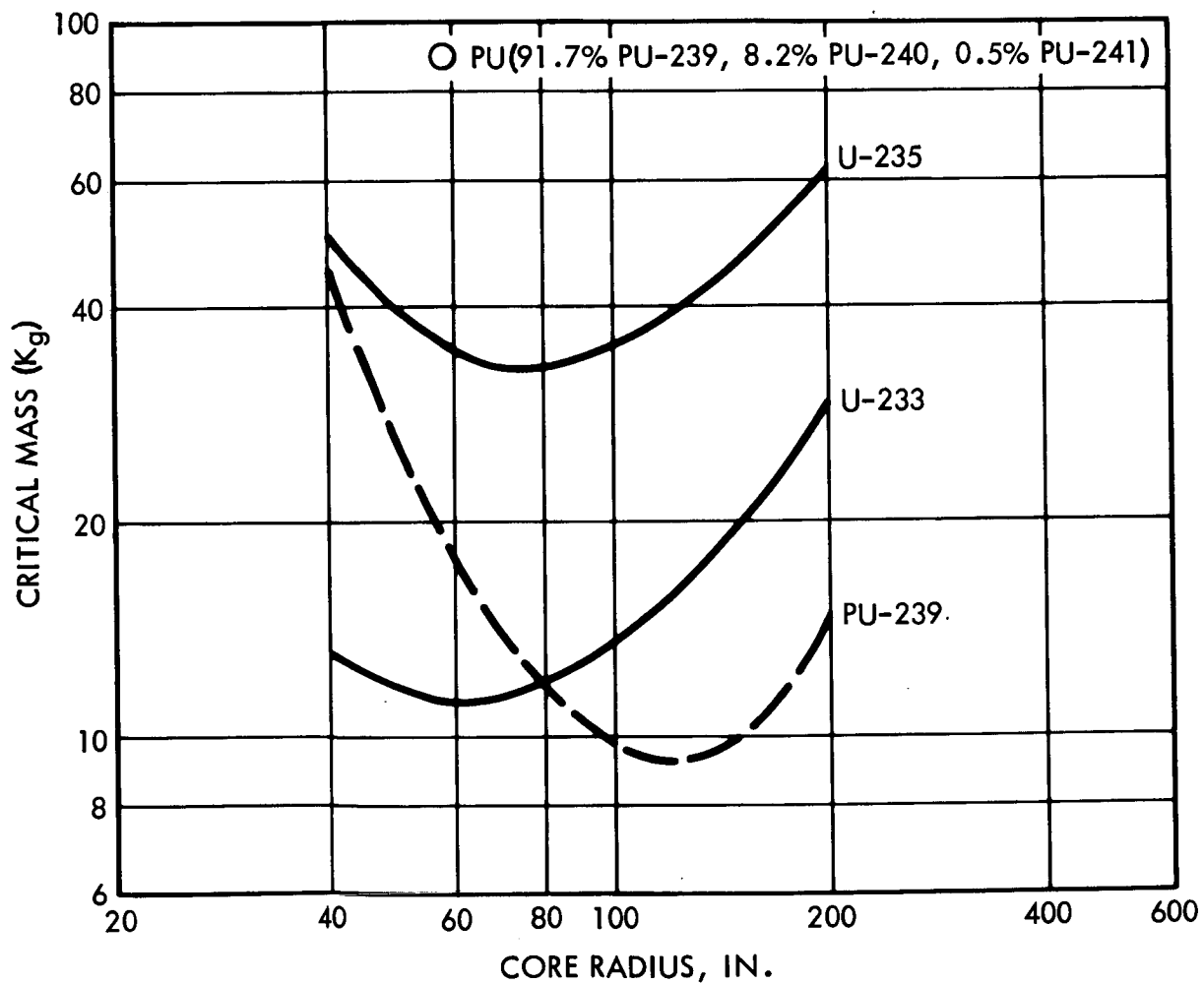


Figure 5-2 Spherical Critical Masses for U-233, U-235, Pu-239

required if plutonium is to be attractive for gas core reactors. The prohibitively high cost of high purity Pu-239 and the present cost and availability of U-233 tend to rule out these fuel materials at present. If the cost and availability of U-233 improved significantly in the future, it would most likely be the most desirable fuel. For purpose of this analysis, U-235 is considered to be the most practical choice.

The selection of the reflector material can have a significant influence on the criticality of a gas core reactor. The variation of critical mass as a function of cavity radius and reflector thickness is shown in figure 5-3 for U-235 spherical cavities surrounded by 100 cm thicknesses of graphite, beryllium, beryllium-oxide, and deuterium-oxide. These results are presented for the case where the fuel uniformly fills the reactor cavity. The moderating effect of heavy water is by far superior to beryllium-oxide or beryllium which, in turn, is superior to graphite. Unfortunately, the moderator-reflector surrounding the cavity is subjected to high thermal heat fluxes in addition to high gamma and neutron radiation heating. Thus, a high temperature material such as graphite is necessary for the inner portion of the moderator reflector. To reduce the critical mass, it may be desirable to use other reflector materials such as beryllium, beryllium oxide, or deuterium oxide for the outer portion of the reflector.

For the gas core reactor concept under investigation, a composite reflector was chosen consisting of an inner liner of 15 cm of graphite surrounded by 70 cm of beryllia. The graphite was placed between the fuel and the beryllium oxide as the high melting point graphite allows the wall to be operated at a higher temperature leading to less severe cooling problems. The composite reflector of graphite and beryllium oxide requires nearly the same critical mass as a pure beryllium oxide reflector of the same total thickness.

Since in the gas core reactor, nearly all the neutron thermalization occurs in the reflector, the reflector temperature can affect the system's criticality. The rapid increase of critical mass with increasing reflector temperature is shown in figure 5-4 for various fuels. These results show the importance of operating at reflector temperatures below 5400°R for U-235 fueled graphite reflected cavity reactors. If high reflector temperatures are required to be able to cool the reflector and still achieve reasonable performance,

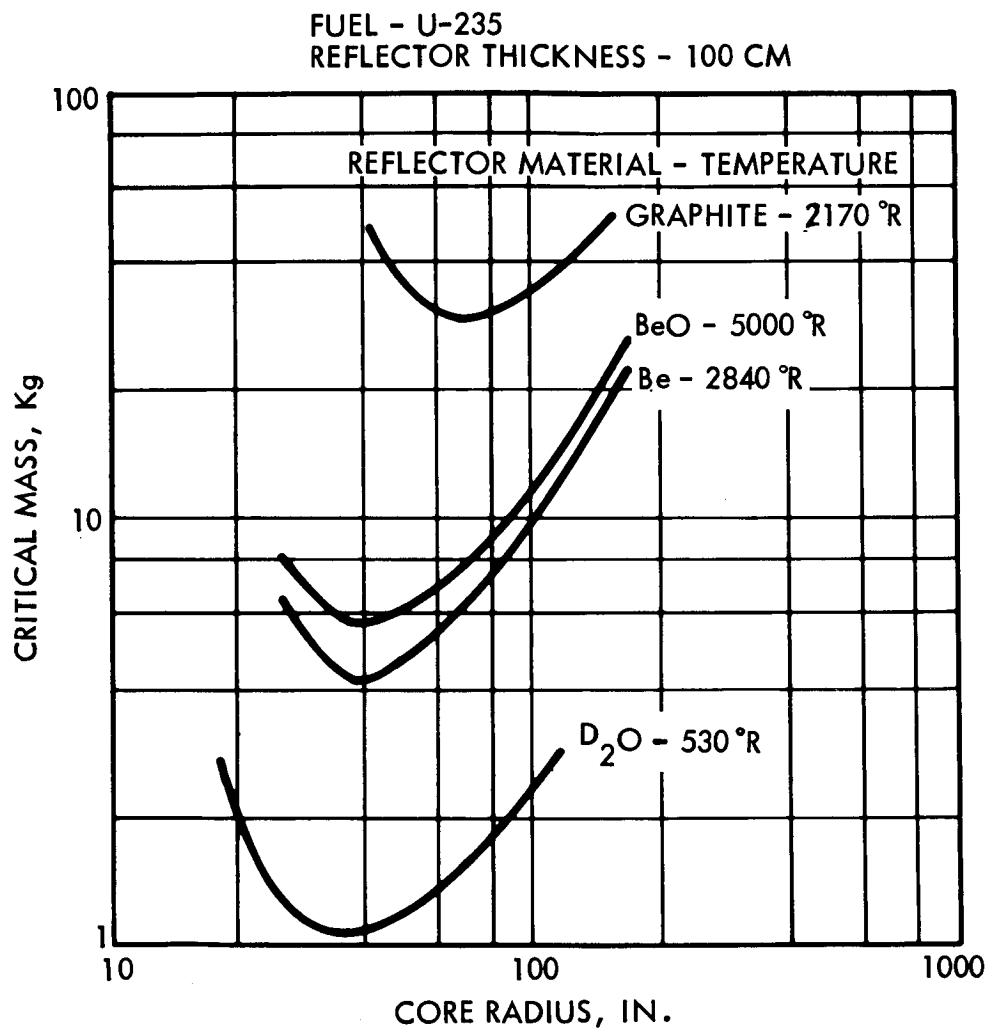


Figure 5-3 Spherical Critical Masses of Reflected Systems

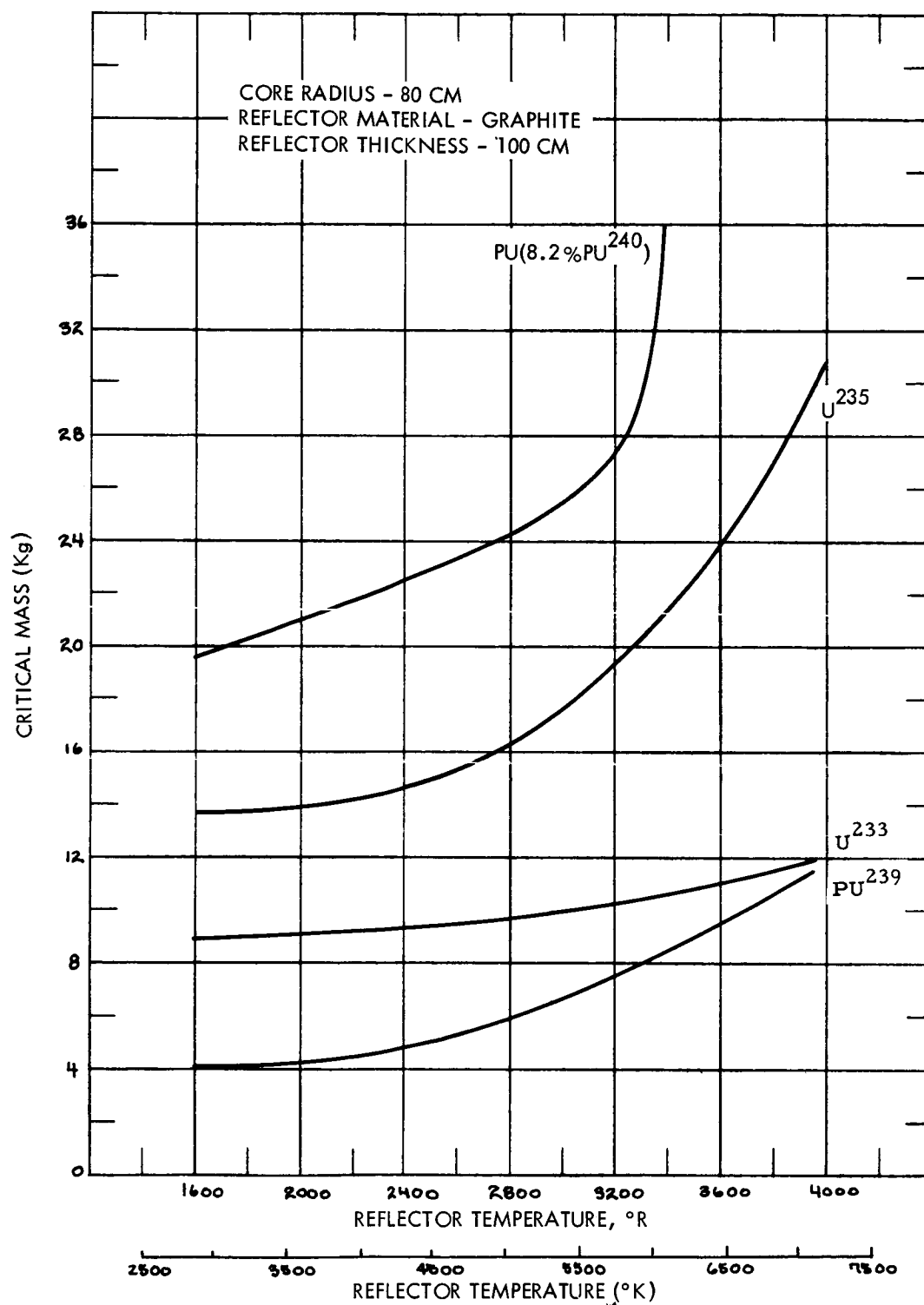


Figure 5-4 Spherical Critical Mass for Different Fuels and Reflector Temperatures
5-7

then U-233 would be a very desirable fuel since it is less sensitive to reflector temperature. For the reference system, the graphite inner reflector was assumed to operate at 5400°R while the beryllium-oxide reflector was considered to operate at 3500°R .

Another parameter influencing the criticality and performance of the coaxial flow gas core reactor is the cavity radius and the central fuel zone radius. As the fuel column radius is reduced, the critical mass increases. This variation of critical mass with the ratio of fuel radius to cavity radius is shown in figure 5-5 for an infinite cylinder, and a sphere. These curves show a rapid increase in critical mass for fuel radius to cavity radius ratios less than 0.5. The significant increase in critical mass for smaller radius ratios probably restricts operation to fuel-to-cavity ratios between 0.5 and 1.0. The effect of hydrogen in the annular region surrounding the fuel column has been found to be almost negligible.

The values of the principle design parameters of a gas core reactor yielding the lowest critical mass consistent with a realistic design are tabulated in table 5-1. This basic geometry was selected to determine the performance characteristics of a gas core reactor which collects, condenses, and recycles the nuclear fuel. The cylindrical reactor cavity with a length to diameter ratio of 2 will be investigated. A cavity radius of 2.5 feet and length of 10 feet was considered to be a reasonable compromise capable of delivering meaningful thrust levels. For these cavity dimensions and a composite reflector, the mass of uranium-235 required for criticality varies from 50 to 76 kg depending on the ratio of fuel to cavity radius. The critical mass of uranium for fuel to cavity radius ratios of 0.4, 0.5, and 0.6, are also presented in table 5-1. These results have accounted for the neutron leakage through an exhaust nozzle with a throat radius of 6 inches. The operating pressure required to achieve criticality in the reference system is shown in figure 5-6 as a function of fuel temperature and fuel radius to cavity radius. These curves account for the ionization of uranium as a function of temperature.

Heat transfer analyses as shown in figure 5-7, on the fuel column indicate that the average fuel column temperature to propellant temperature must be approximately 5.0 to transfer the heat by radiation from the fuel to the propellant. This means that to achieve exit gas temperatures greater than $10,000^{\circ}\text{R}$,

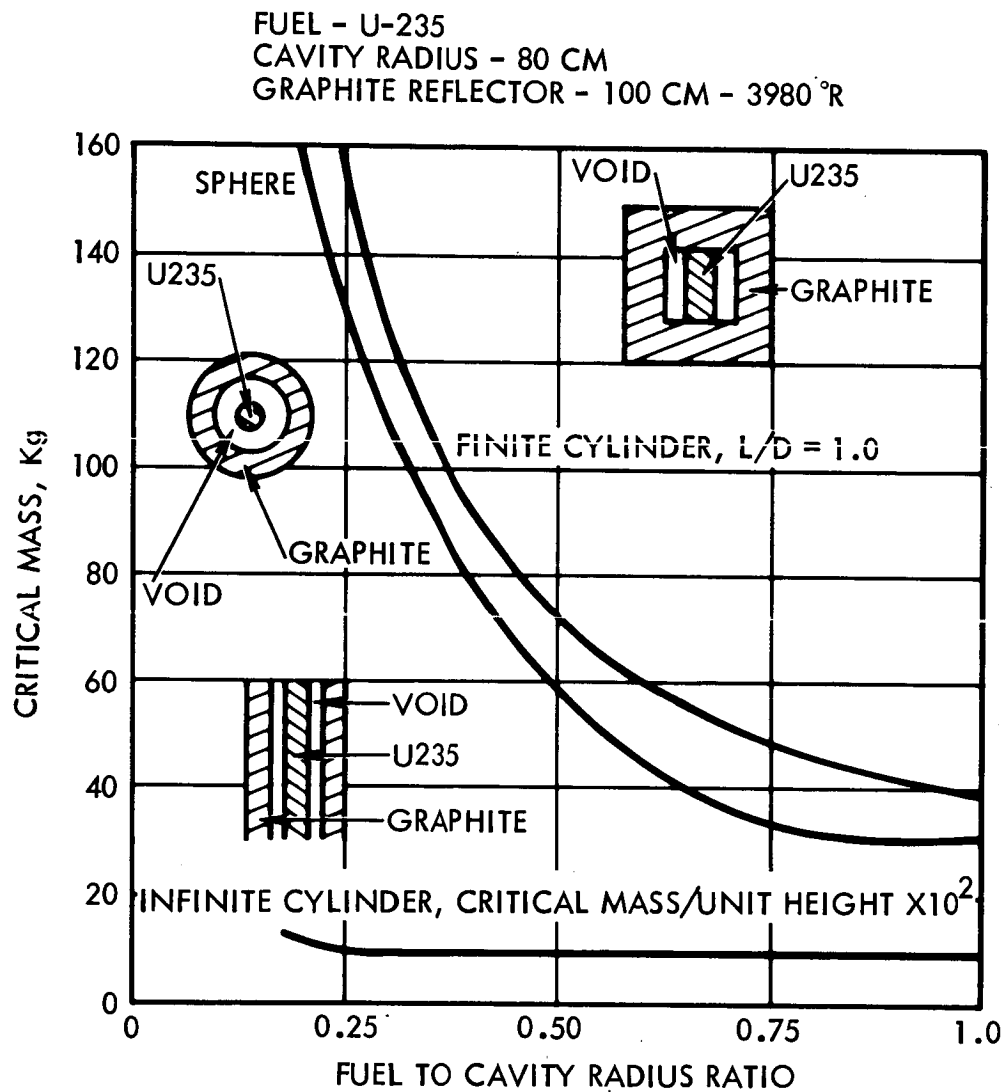


Figure 5-5 Critical Mass Variation with Fuel to Cavity Radius Ratio

Table 5-1 Gas Core Reactor Design Characteristics

<u>Reactor Geometry</u>	<u>Right Cylinder</u>		
Cavity Dimensions			
Diameter (ft)	5		
Length (ft)	10		
Length/Diameter	2		
Fuel Dimensions			
Fuel Radius/Cavity Radius	0.4	0.5	0.6
Fuel Diameter (ft)	2.0	2.5	3.0
Fuel Length (ft)	10	10	10
Critical Mass (kg)	76	60	50
Critical Density (lb/ft ³)	5.35	2.7	1.55
Reflector			
Inner Thickness (ft)	0.5 (Graphite at 5400°R)		
Outer Thickness (ft)	2.3 (Beryllium Oxide at 3600°R)		
Void	10% (both regions)		
Nozzle Throat Radius (ft)	0.5		

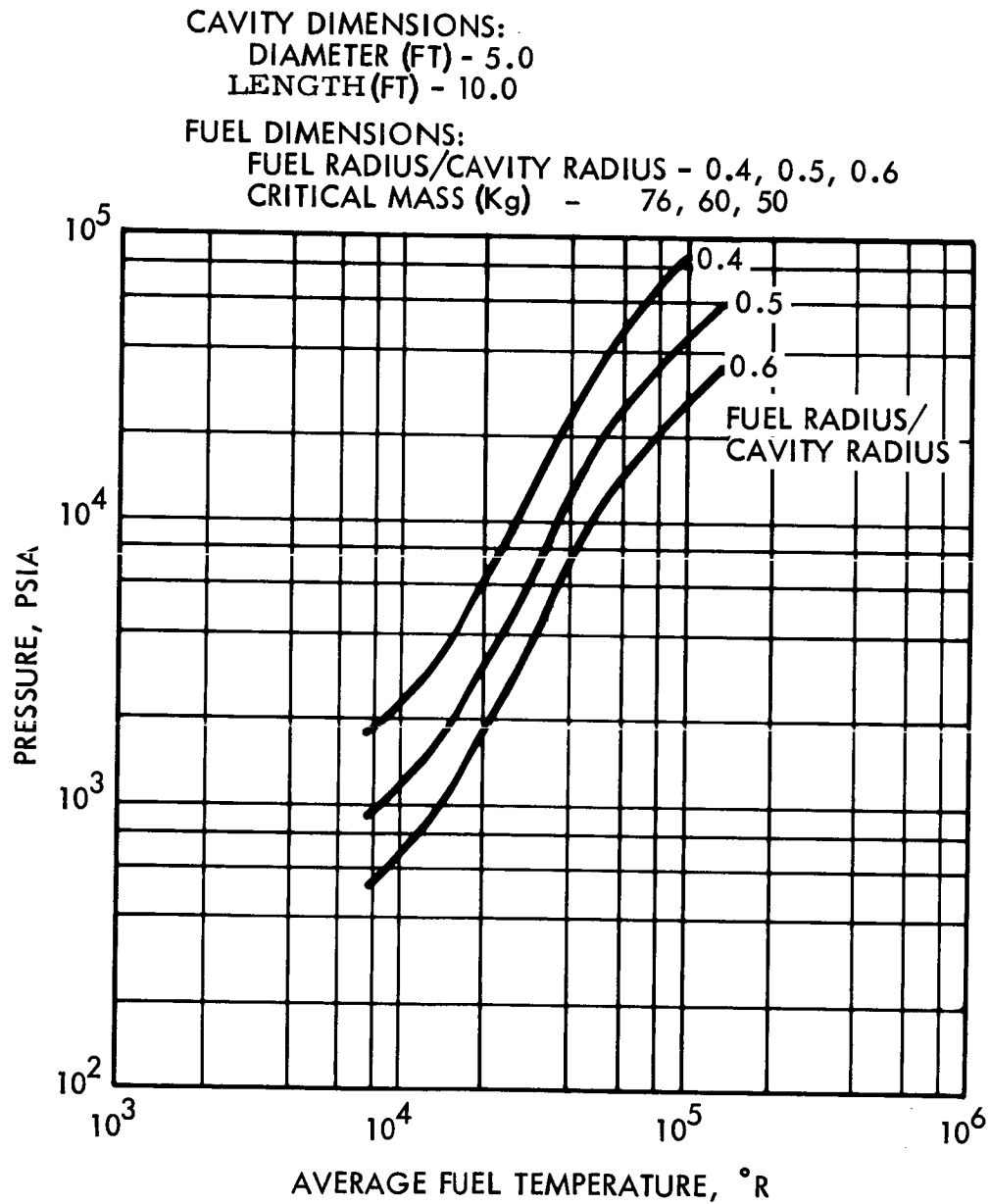


Figure 5-6 Fuel Temperature and Pressure Required for Criticality

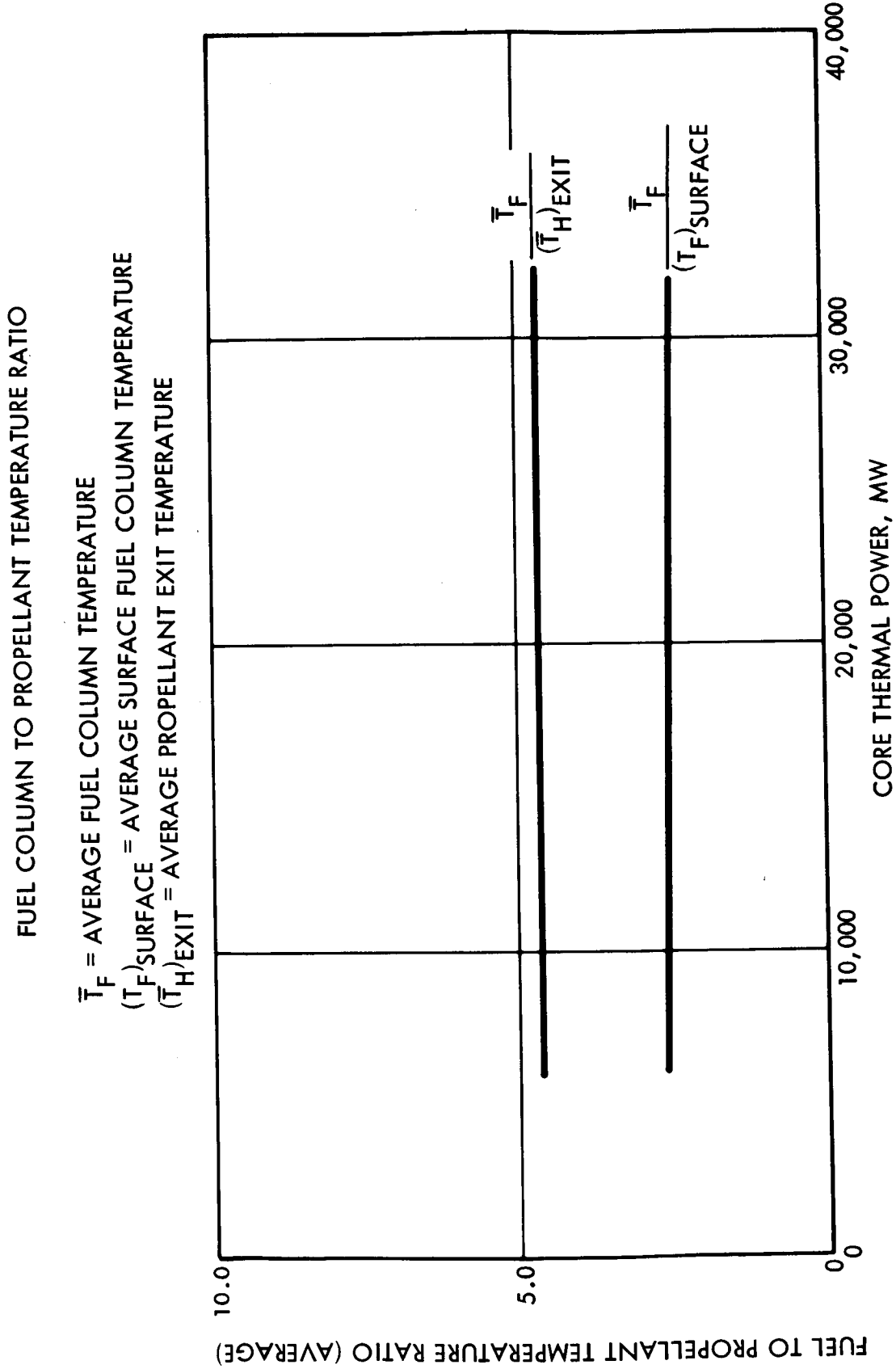


Figure 5-7 Fuel Column to Propellant Temperature Ratio

fuel temperatures greater than $50,000^{\circ}\text{R}$ must be generated. For the reference system, temperatures of this magnitude require pressures greater than 10,000 psi to achieve criticality. Pressures of this magnitude are beyond the present state of the art of turbomachinery and would make the feasibility of current gas core concepts marginal. Two major factors must be resolved before the feasibility of the gas core can be fully assessed. First, accurate estimates of the absorptivity of uranium must be made before a good estimate of the fuel column temperature to propellant temperature can be given. The best available data on the absorptivity of uranium were used in these heat transfer analyses; however, these data should be rechecked to insure their validity. Second, the criticality of gas core reactors should be thoroughly evaluated to determine if the critical mass of the system can be reduced significantly without sacrificing engineering feasibility. For example, one means of reducing the critical mass might be accomplished by using heavy water as the reflector material in place of beryllium or graphite. If means cannot be found to significantly reduce the critical mass required to achieve criticality or increase the propellant exit gas temperature in relation to the fuel temperature, then the present concepts of the gas core reactor may be technically infeasible at present or, if feasible, would not provide high enough performance to be superior over other advanced propulsion systems.

Initially, the engine performance analysis was intended to be done parametrically; however, the complexity of conducting a meaningful parametric analysis by hand was most tedious. Thus, only a limited number of parameters were investigated such as engine power. An equally important parameter is engine pressure which was impossible to vary parametrically due to time and funding limitations. For the purposes of this study, it was assumed that an operating pressure of 100 atm could be realized and the critical mass could be reduced sufficiently so that criticality could be achieved at this pressure. If pressures of 1000 atm are required, the engine weight would be extremely large and the feasibility of even producing these pressures is questionable.

5.1.2 Power Distribution

Since the vast majority of fissions in the gas core reactor are produced by thermal neutrons returning from the reflector, the power distributions would be expected to be closely approximated by the thermal flux distribution. A typical radial and axial power distribution for the gas core is shown in figure 5-8.

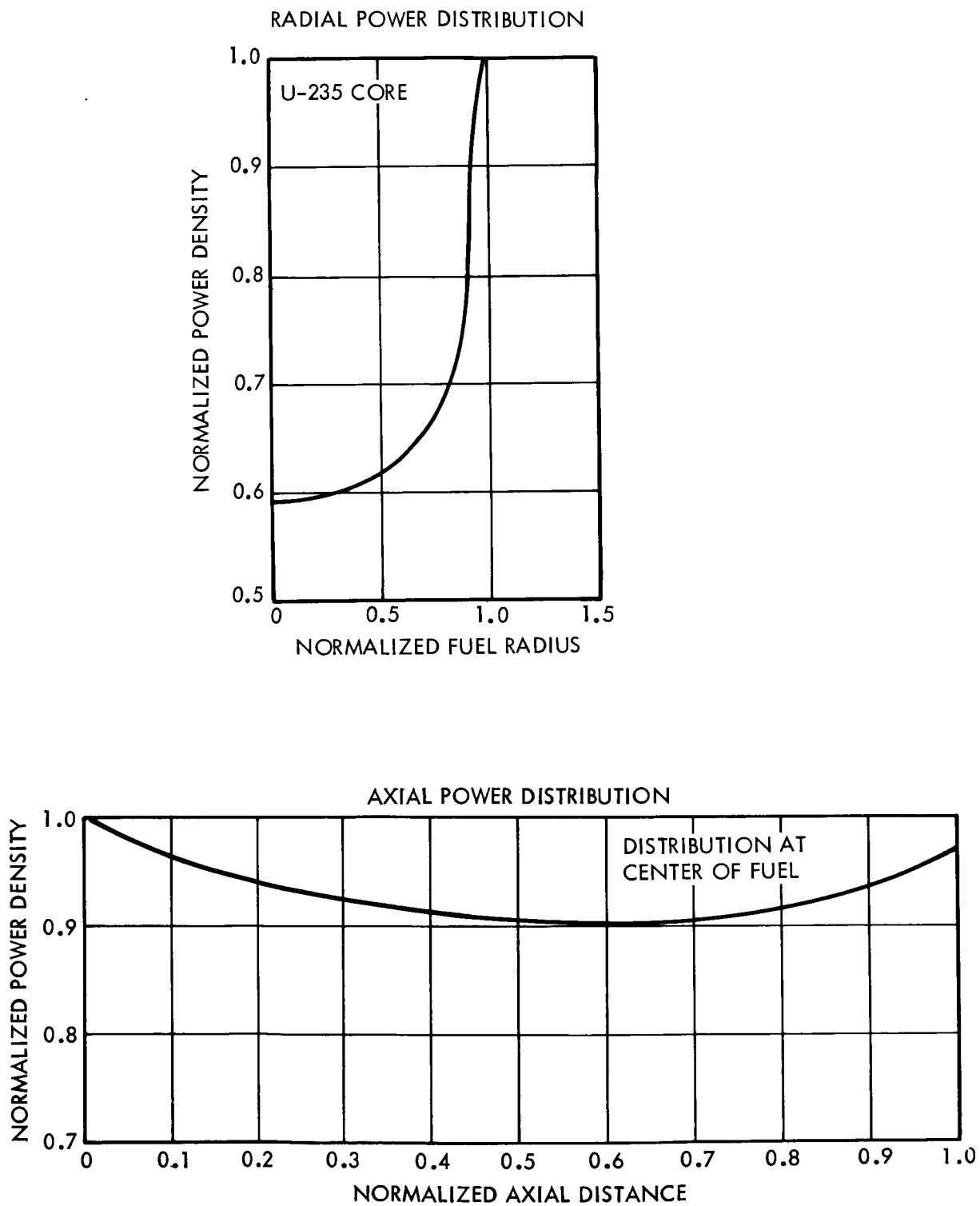


Figure 5-8 Radial and Axial Power Distribution for the Gas Core

5.2 ENGINE COOLING CONSIDERATIONS

To perform an engine preliminary design, it is necessary to determine the heat loads delivered to the engine components and the component and system cooling requirements. It is also necessary to determine the heat loads to the scoop, nozzle, and reflector. The radiative and convective heat loads to the scoop were analyzed in the scoop feasibility section of this report. The radiative heat loads to the nozzle convergent section and the reflector were discussed in the heat transfer section. The convective heat flux incident on the nozzle and the nuclear radiation heating of the reflector are investigated in this section. The cooling requirements for the nozzle and reflector are also considered in detail. The cooling of surfaces by means of transpiration cooling was discussed in considerable detail in the advanced cooling studies section. Cooling the nozzle and reflector by means of convective cooling techniques is also analyzed in this section. In addition, the uranium condensation cooling requirements as a function of core power are also discussed. The uranium condensation is a major factor in the feasibility of the particular gas core nuclear rocket engine concept under investigation. If the temperature of the fissioning uranium is too high, the amount of diffused hydrogen entering the scoop is too large, or the amount of available cool hydrogen to condense the uranium is too small, then the condensation of the uranium is impossible and the external separation of the uranium becomes infeasible.

5.2.1 Nozzle Convective Cooling

To adequately evaluate the feasibility of the gas core concept, the heat transfer and fluid flow characteristics of the nozzle must be investigated. The heat loads at the nozzle wall consist of a radiative heat input and a convective heat input from the hot gas flowing through the nozzle. The two primary methods of heat removal from the nozzle wall are transpiration cooling and regenerative heat removal by convective heat transfer. The purpose of this portion of the report is to discuss the nozzle hot side convective heat flux, the heat flux which may be regeneratively removed by the nozzle coolant, the coolant pressure drop and the coolant temperature rise.

5.2.1.1 Hot Side Heat Flux

Beginning with the basic Colburn heat transfer correlation and assuming isentropic expansion in the nozzle, the hot side convective heat flux equation was developed in reference 41 and is given below.

$$q/A = 0.0024 \left[M \alpha \left(\frac{2}{\alpha + 1} \right)^{\frac{\alpha + 1}{\alpha - 1}} \right]^{0.45} \left[\frac{P_c^{0.9} T_c^{0.35} \Phi_f}{\dot{m}^{0.1} \epsilon^{0.9}} \right] \left[\frac{\left\{ \frac{1 + (P_r)^{1/3} \left(\frac{\alpha - 1}{2} \right) M_a^2}{1 + \left(\frac{\alpha - 1}{2} \right) M_a^2} \right\} T_c - T_{wH}}{\left[1 + \left(\frac{\alpha - 1}{2} \right) M_a^2 \right]^{0.8}} \right]$$

where

q/A = heat flux, Btu/in²-sec

T_c = chamber temperature, °R

P_c = chamber pressure, psi

M = molecular weight evaluated at T_c and P_c

P_r = Prandtl number evaluated at T_c and P_c

α = specific heat ratio evaluated at T_c and P_c

ϵ = nozzle area ratio

M_a = mach number evaluated

\dot{m} = hot gas mass flow rate, lb/sec

T_{wH} = hot side wall temperature

Φ_f = heat transfer parameter evaluated at film temperature

$$\frac{k_f (Pr_f)^{0.4}}{T_f^{0.8} \mu_f^{0.8}}, \text{ Btu}/[(\text{ft-sec})^{0.2} (\text{lb})^{0.8} (\text{°R})^{1.8}]$$

K_f = gas conductivity evaluated at film conditions, Btu/ft-sec - °R

μ_f = fluid viscosity evaluated at film conditions, Btu/ft-sec - °R

Due to the presence of the uranium scoop in the gas core nozzle, the inside radius is given by:

$$R = \left[r_t^2 \epsilon + r_s^2 \right]^{1/2}$$

where

r_t = throat radius of conventional nozzle, in.

ϵ = nozzle expansion ratio

r_s = scoop radius = 18 in.

R = gas core nozzle inside radius, in.

Curves showing the gas core nozzle radius, R , as a function of mass flow rate for chamber temperatures of 10,000 °R and 15,000 °R and chamber pressures of 1,000, 5,000 and 10,000 psia, are shown in figures 5-9 and 5-10. Results are based upon a scoop radius of 18 inches.

Plots showing the convective heat flux as a function of nozzle expansion ratio for hydrogen mass flow rates of 100 and 500; chamber temperatures of 10,000 °R and 15,000 °R and chamber pressures of 1,000, 5,000, and 10,000 psi are shown in figures 5-11 through 5-14. For the results shown, the nozzle wall temperature was assumed to be maintained at a constant value of 3000 °R by transpiration cooling and the scoop radius was 18 inches.

Although the heat flux curves presented are based upon conventional nozzle geometry, corrections for the gas core nozzle geometry, which includes the uranium scoop, easily can be made. The only geometry dependent term which appears in the Colburn heat transfer correlation is the flow channel hydraulic diameter, D_c , which is raised to the 0.2 power. Thus, the correction is given by:

$$\frac{(q/A)_{gc}}{(q/A)} = \left(\frac{D_c}{D_{cgc}} \right)^{0.2} = \left[\frac{\left(\frac{4 A_f}{P} \right)}{\left(\frac{4 A_f}{P} \right)_{gc}} \right]^{0.2} = \left[\frac{P_{gc}}{P} \right]^{0.2} \approx \left[\frac{4 \pi R}{2 \pi r_t \sqrt{\epsilon}} \right]^{0.2}$$

$$\frac{(q/A)_{gc}}{(q/A)} = \left(\frac{2 R}{r_t \sqrt{\epsilon}} \right)^{0.2}$$

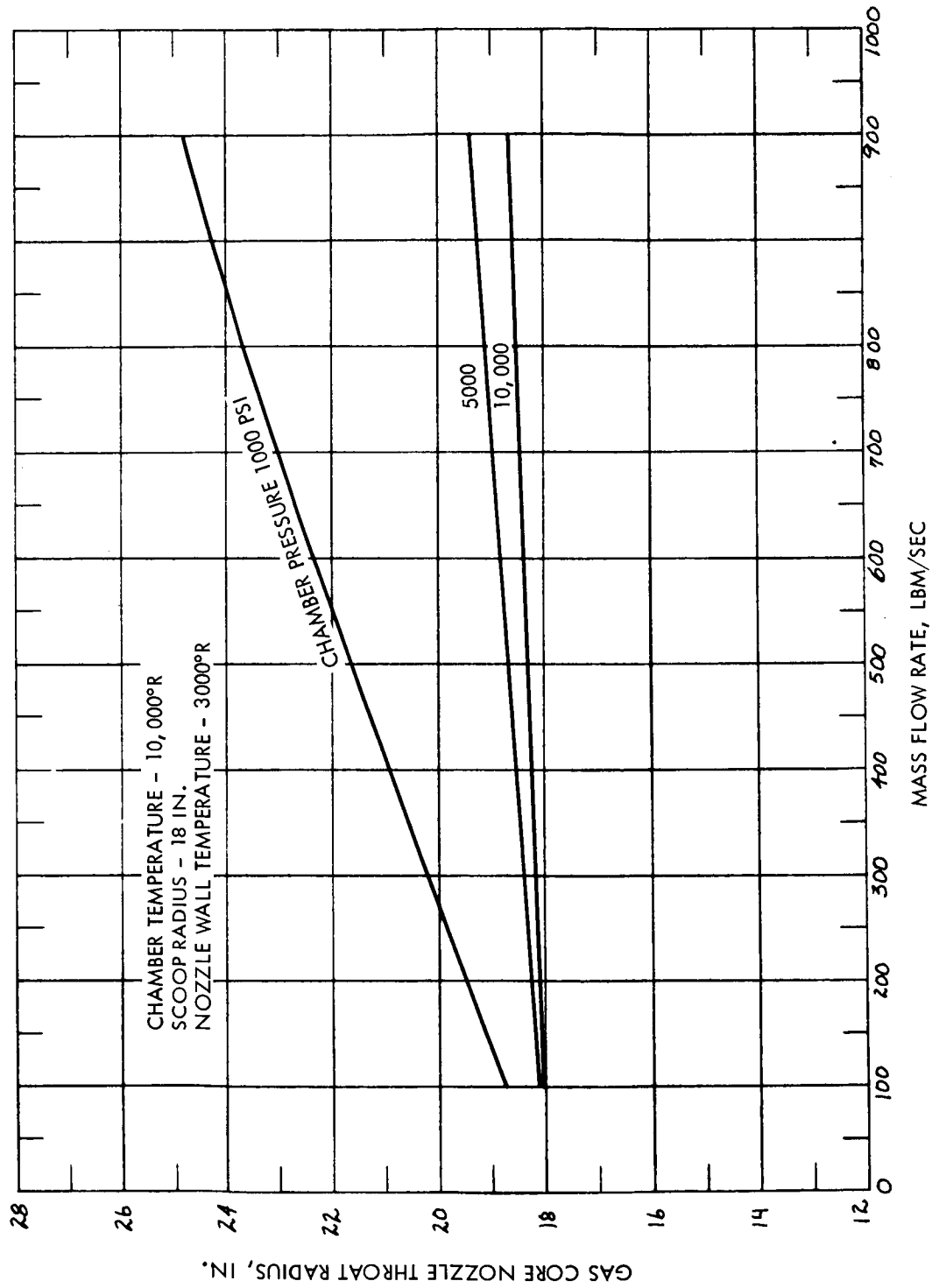


Figure 5-9 Gas Core Nozzle Throat Radius as a Function of Mass Flow Rate and Chamber Pressure

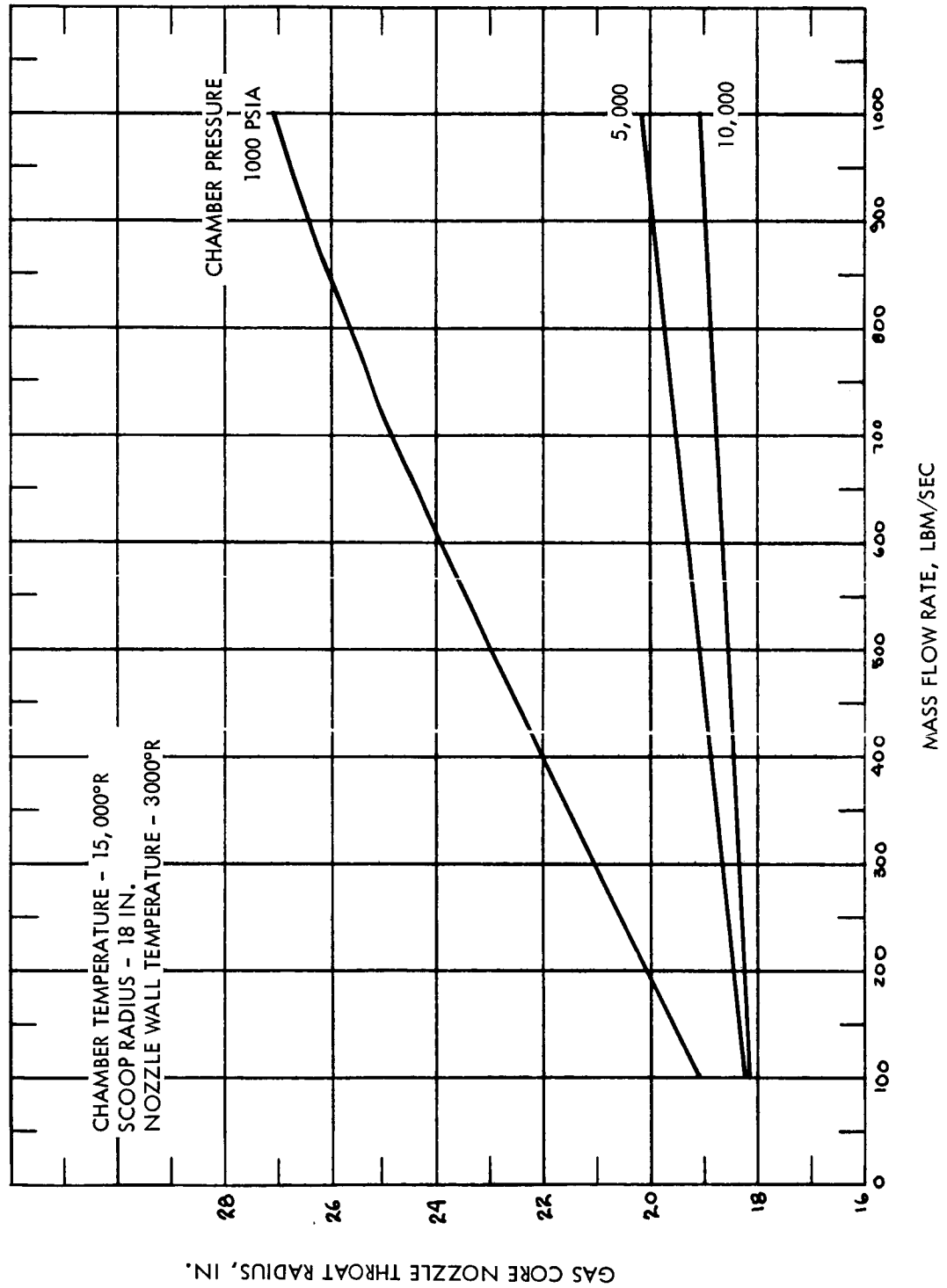


Figure 5-10 Gas Core Nozzle Throat Radius as a Function of Mass Flow Rate and Chamber Pressure

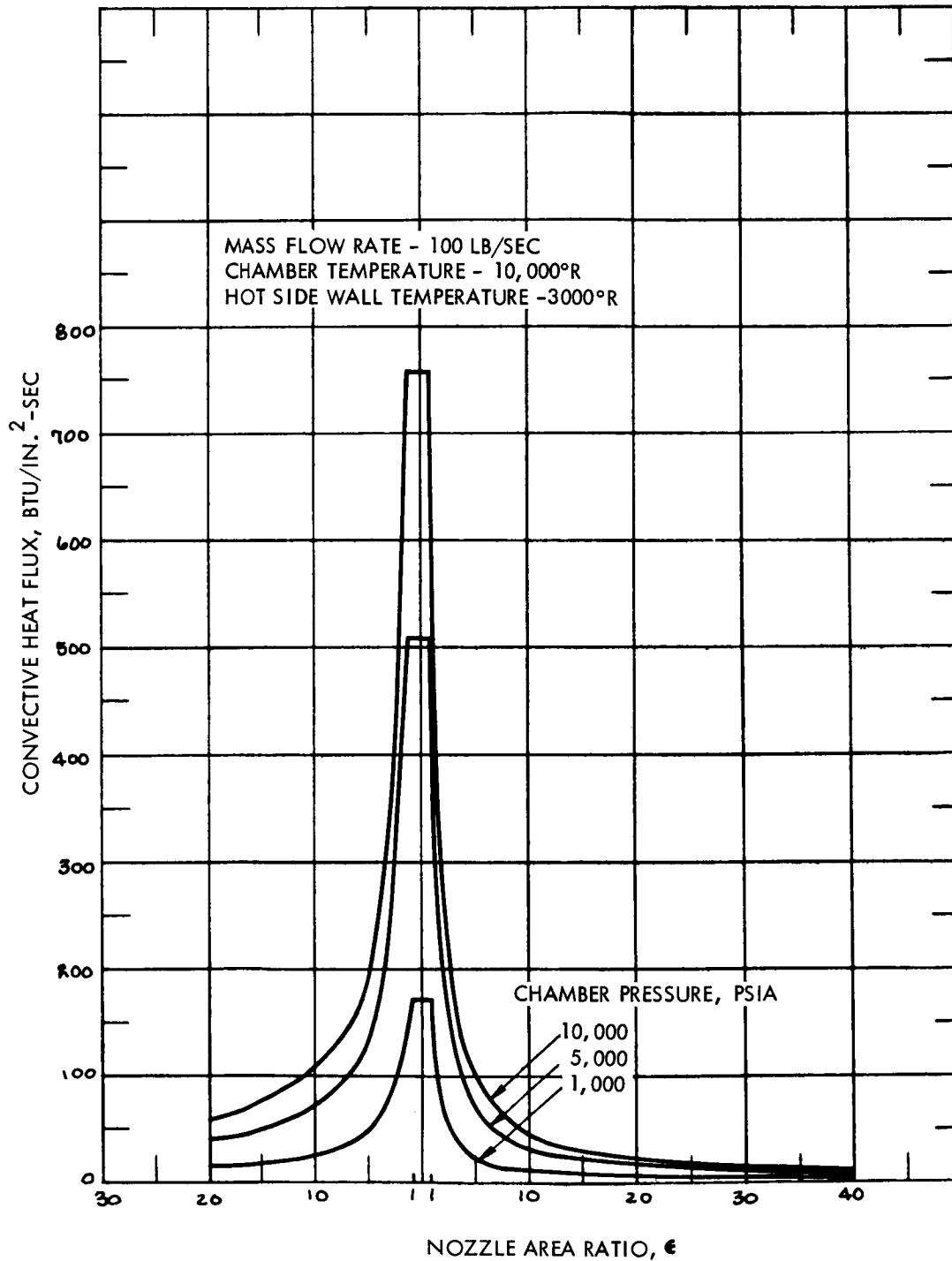


Figure 5-11 Nozzle Hot Side Convective Heat Flux
5-20

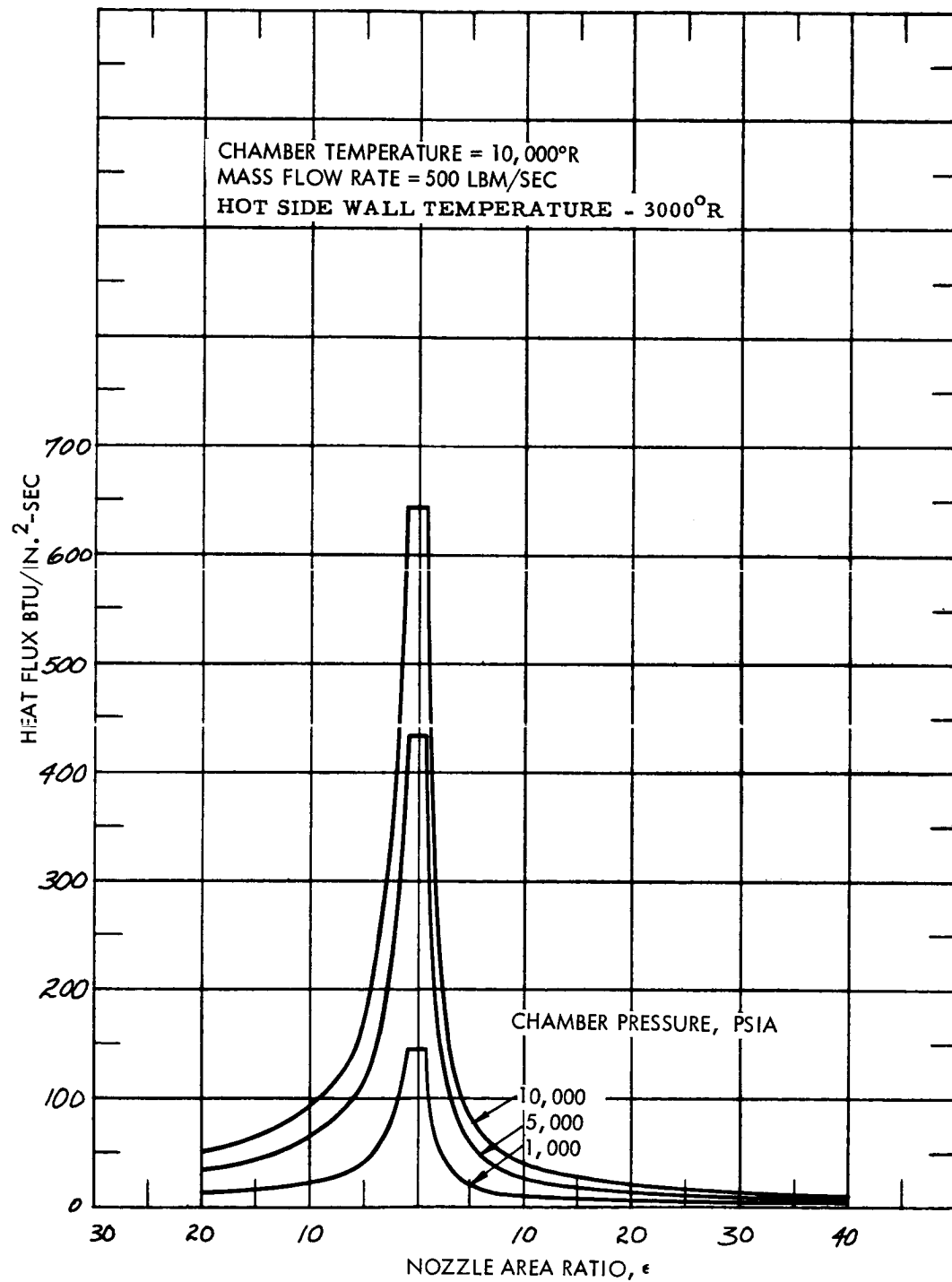


Figure 5-12 Nozzle Hot Side Convective Heat Flux
5-21

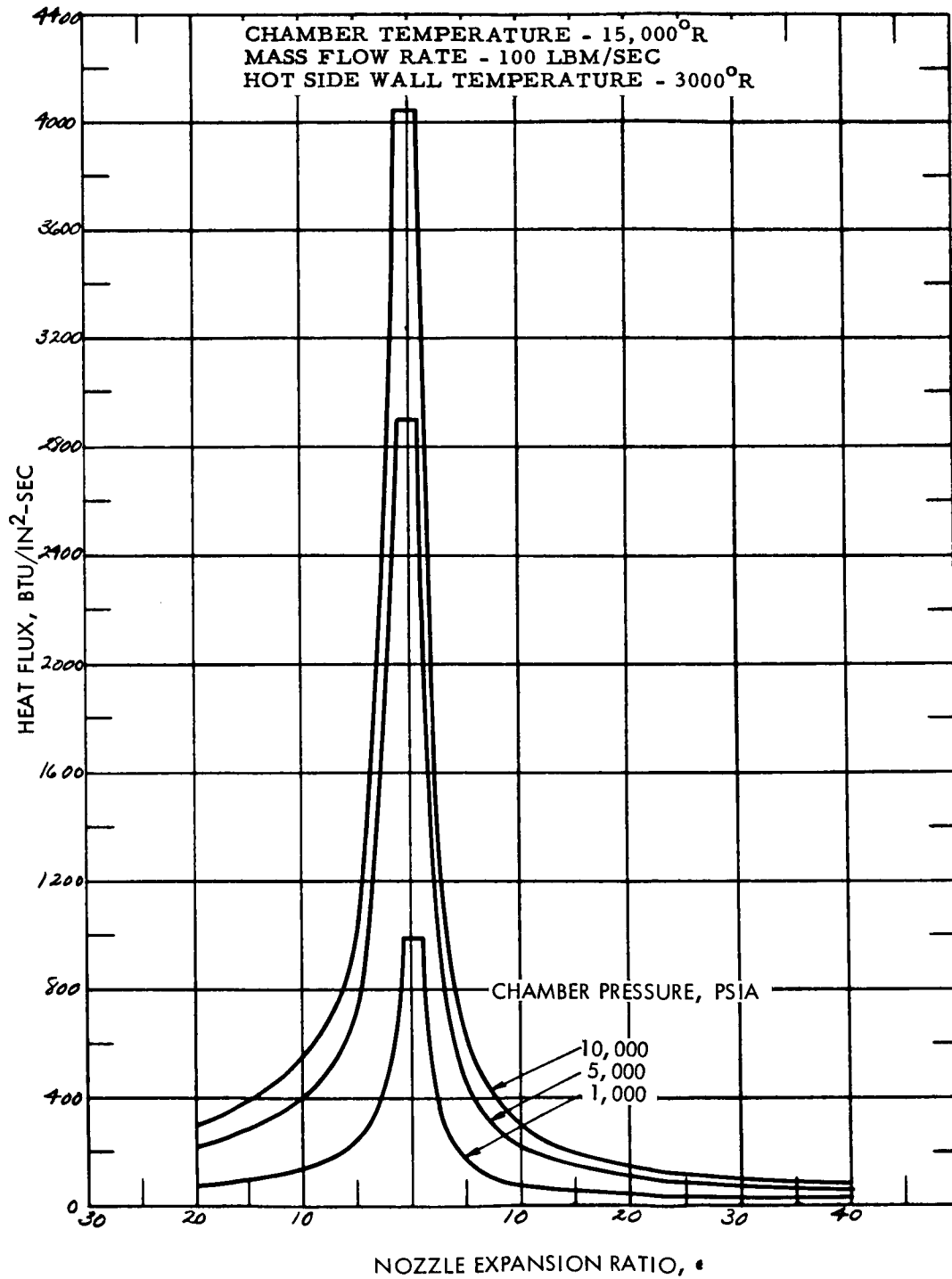


Figure 5-13 Nozzle Convective Heat Flux
5-22

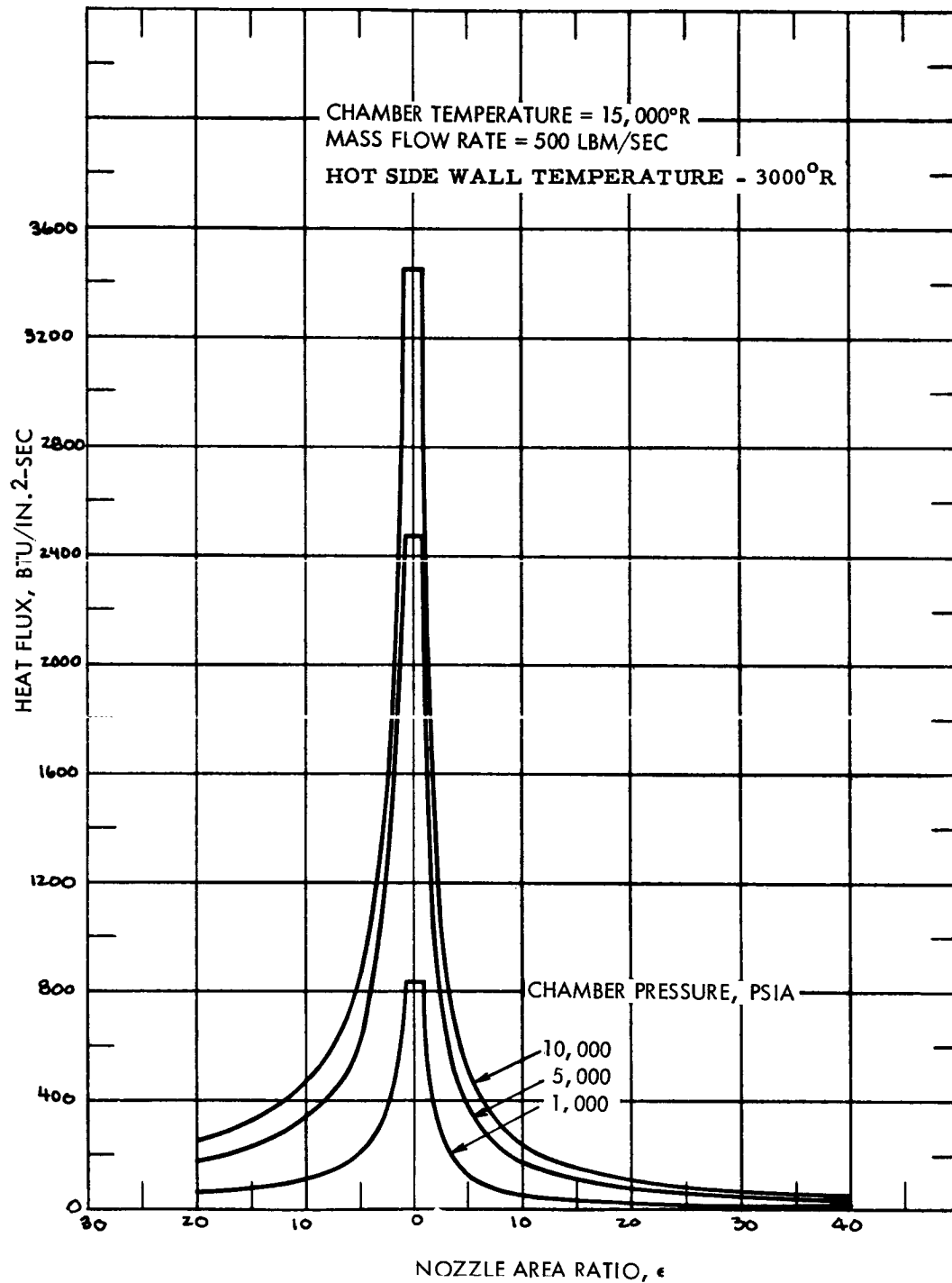


Figure 5-14 Nozzle Hot Side Convective Heat Flux

where

- q/A_{gc} = gas core nozzle convective heat flux, Btu/in²-sec
 q/A = conventional nozzle convective heat flux, Btu/in²-sec
 P_{gc} = wetted perimeter of gas core nozzle, in.
 P = wetted perimeter of conventional nozzle, in.

The gas core heat flux correction at the nozzle throat for a mass flow rate of 100 lbm/sec, a chamber temperature of 10,000 °R and a chamber pressure of 1000 psi is:

$$\frac{(q/A)_{gc}}{q/A} = \left[\frac{2(18.792)}{5.398} \right]^{0.2} = [6.97]^{0.2} = 1.47$$

For a mass flow rate of 1000 lbm/sec the correction is 1.113. Thus, the correction varies from about 50 to 11 percent depending on the mass flow rate.

The convective heat fluxes presented in the previous figures will be substantially reduced by the layer of coolant which results from the transpiration cooling of the nozzle walls. The blocking factors associated with various transpiration cooling mass flow rates are presented in another section of this report.

5.2.1.2 Coolant Side Convective Heat Flux and Pressure Drop

The above paragraphs have discussed the heat fluxes incident upon the hot side of the nozzle wall. The heat fluxes which may be removed by regenerative cooling and transpiration cooling remain to be determined. An equation describing the heat flux which may be regeneratively removed by cold hydrogen flowing on the coolant side of a nuclear rocket nozzle was developed in reference 41. The equation is based upon the Wolf-McCarthy heat transfer correlation and takes the following form:

$$q/A = 0.01521 \left[\frac{\dot{m}}{A} \right]^{0.8} \frac{\Phi_b}{D_c^{0.2}} \frac{T_b^{1.35}}{T_{wc}^{0.55}} (T_{wc} - T_b)$$

where

- q/A = heat flux, Btu/in²-sec
 $\frac{\dot{m}}{A}$ = coolant mass flow rate per unit area, lb/in²-sec

Φ_b = heat transfer parameter evaluated at bulk coolant temperature and pressure,

$$= \frac{k_b (Pr)^{0.4}}{T_b^{0.8} \mu_b^{0.8}}, \quad \frac{\text{Btu}}{(\text{ft-sec})^{0.2} (\text{lb})^{0.8} (^{\circ}\text{R})^{1.8}}$$

T_b = bulk coolant temperature, $^{\circ}\text{R}$

T_{wc} = coolant side wall temperature, $^{\circ}\text{R}$

D_c = coolant flow channel hydraulic diameter, in.

For these calculations, an annular coolant flow passage of width, t , around the periphery of the nozzle was assumed. For an annular flow passage, it can be shown that the hydraulic diameter is twice the annulus thickness, t , i.e., $D_c = 2t$. Also, assuming t is small with respect to the nozzle radius, R , the coolant flow area is given by:

$$A_c = 2\pi Rt = \pi D_c R$$

Substituting the above relationship for the coolant flow area in the coolant heat flux equation results in the following equation.

$$q/A = \frac{0.01521}{D_c} \left(\frac{\dot{m}}{\pi R} \right)^{0.8} \frac{\Phi_b T_b^{1.35}}{T_{wc}^{0.55}} (T_{wc} - T_b) \quad (26)$$

Equation 26 shows that the heat flux which may be removed regeneratively is inversely proportional to the hydraulic diameter of the flow channel. It is desirable from a heat removal standpoint, to construct a flow channel passage which has a very small hydraulic diameter. However, the coolant pressure drop is inversely proportional to approximately the square of the hydraulic diameter so the hydraulic diameter must be large enough to yield reasonable coolant pressure drops. Thus, the pressure drop as a function of hydraulic diameter was investigated and results are discussed in the following paragraphs.

A general integral form of the pressure drop equation can be obtained by solving the momentum equation, the continuity equation, and the equation of state simultaneously. These equations may be written in one dimension as follows:

Momentum:

$$dp = -\rho V dV - \frac{4 f_f}{D_c} \frac{1}{2} \rho V^2 dX$$

Continuity:

$$\dot{m} = \rho A_f V$$

Equation of State:

$$p = \frac{\rho R_u T Z}{M}$$

where

p = pressure

ρ = fluid density

V = fluid velocity

f_f = fanning friction factor = $0.046/(\text{Re})^{0.2}$

D_c = the hydraulic diameter = $4A_f/P$

A_f = fluid flow area

P = flow channel wetted perimeter

x = axial position

\dot{m} = mass flow rate

T = fluid temperature

R_u = universal gas constant = $1545 \frac{\text{ft} \cdot \text{lbf}}{\text{mole} \cdot ^\circ\text{R}}$

M = molecular weight of fluid, lbm/mole

Z = compressibility factor

Since hydrogen obeys the perfect gas law, i.e., the compressibility factor is unity, and the molecular weight on the coolant side of the nozzle is constant at 2.016 lbm/mole, the form of the pressure drop equation after integration over a variable range in which linear averages are valid becomes:

$$\begin{aligned}
p_2^2 = p_1^2 - \frac{23.8}{D_c^2} & \left\{ \left[\left(\frac{\dot{m}}{\pi R} \right)_1^2 T_1 + \left(\frac{\dot{m}}{\pi R} \right)_2^2 T_2 \right] \ln(p_1/p_2) \right. \\
& + \left[\left(\frac{\dot{m}}{\pi R} \right)_1^2 + \left(\frac{\dot{m}}{\pi R} \right)_2^2 \right] (T_2 - T_1) + (T_1 + T_2) \left[\left(\frac{\dot{m}}{\pi R} \right)_2^2 - \left(\frac{\dot{m}}{\pi R} \right)_1^2 \right] \\
& \left. + \frac{0.06688}{D_c} \left[\left(\frac{\dot{m}}{\pi R} \right)_1^{1.8} T_1^{\mu_1} + \left(\frac{\dot{m}}{\pi R} \right)_2^{1.8} T_2^{\mu_2} \right] (x_2 - x_1) \right\}
\end{aligned}$$

where

- p = pressure, psia
 D_c = hydraulic diameter, in.
 \dot{m} = coolant mass flow rate, lbm/sec
 R = nozzle inside radius, in.
 T = coolant temperature, $^{\circ}\text{R}$
 μ = coolant viscosity, lbm/(ft-sec)
 x = axial location, in.

It is desirable to solve for the hydraulic diameter for specified values of the inlet pressure, coolant mass flow rate, and the allowable nozzle coolant pressure drop. Assuming the $\ln p_1/p_2$ and $\left[(\dot{m}/\pi R_2)^2 - (\dot{m}/\pi R_1)^2 \right]$ terms are small, the above equation can be written as a cubic in D_c as shown below:

$$\begin{aligned}
D_c^3 - \frac{23.8 (T_2 - T_1)}{p_1^2 - p_2^2} & \left[\left(\frac{\dot{m}}{\pi R_1} \right)^2 + \left(\frac{\dot{m}}{\pi R_2} \right)^2 \right] D_c - \frac{1.592 (x_2 - x_1)}{p_1^2 - p_2^2} \\
& \left[\left(\frac{\dot{m}}{\pi R_1} \right)^{1.8} \mu_1^{0.2} T_1 + \left(\frac{\dot{m}}{\pi R_2} \right)^{1.8} \mu_2^{0.2} T_2 \right] = 0
\end{aligned} \tag{27}$$

Allowable pressure drops of 350 psi and 600 psi were selected and curves of hydraulic diameter, D_c , versus mass flow rate were constructed. Results are presented in figures 5-15 and 5-16 for chamber temperatures of 10,000 $^{\circ}\text{R}$ and 15,000 $^{\circ}\text{R}$ and chamber pressures of 1000 psi, 5000 psi and 10,000 psi. For the results shown in figures 5-15 and 5-16, an average value of the nozzle and internal radius, R , for a nozzle having an expansion ratio of 40:1, was substituted into Equation 27 along with a coolant inlet temperature of 45 $^{\circ}\text{R}$, a coolant temperature rise of 100 $^{\circ}\text{R}$, a viscosity evaluated at bulk coolant temperature of 100 $^{\circ}\text{R}$, and

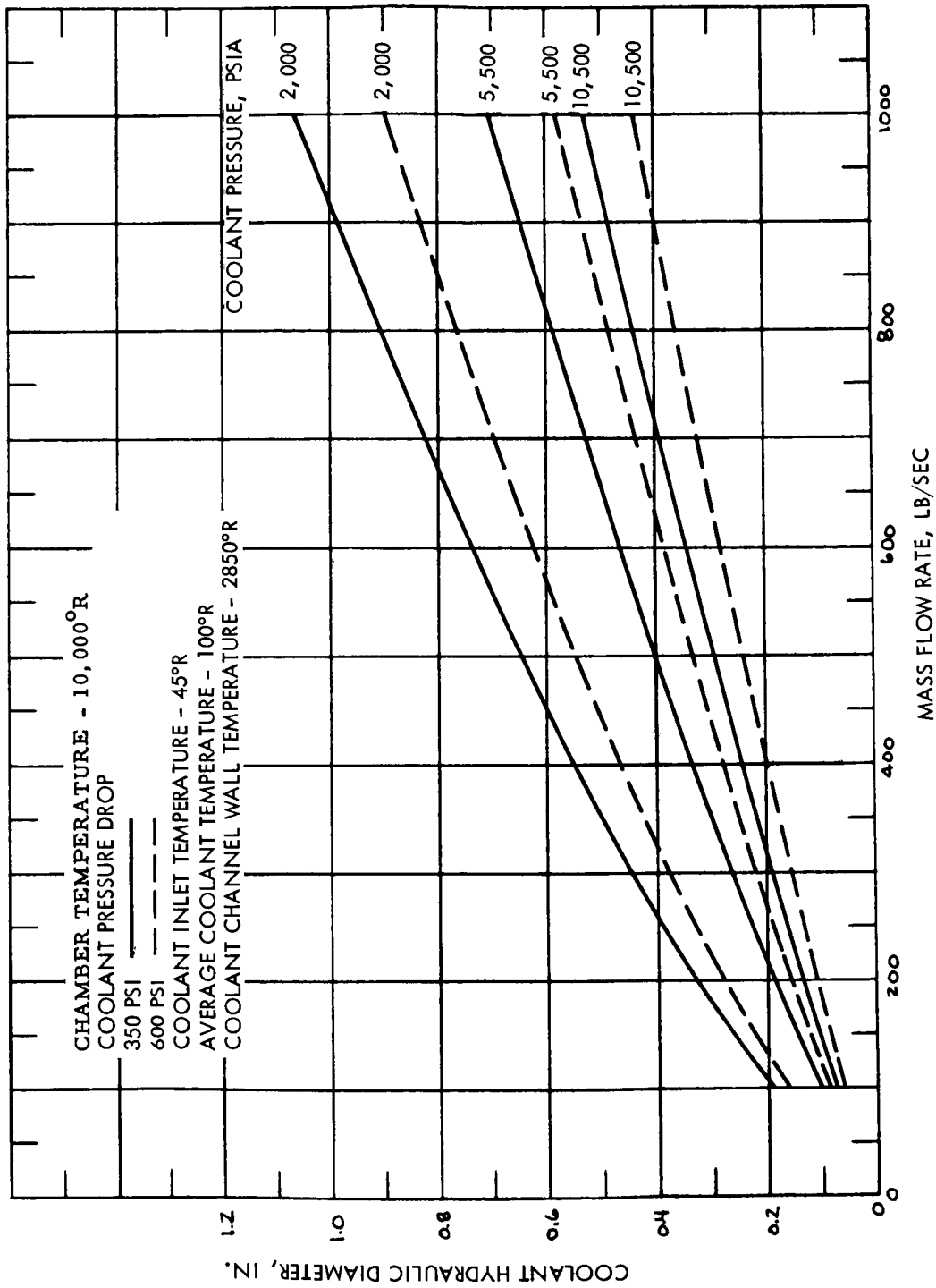


Figure 5-15 Nozzle Coolant Hydraulic Diameter

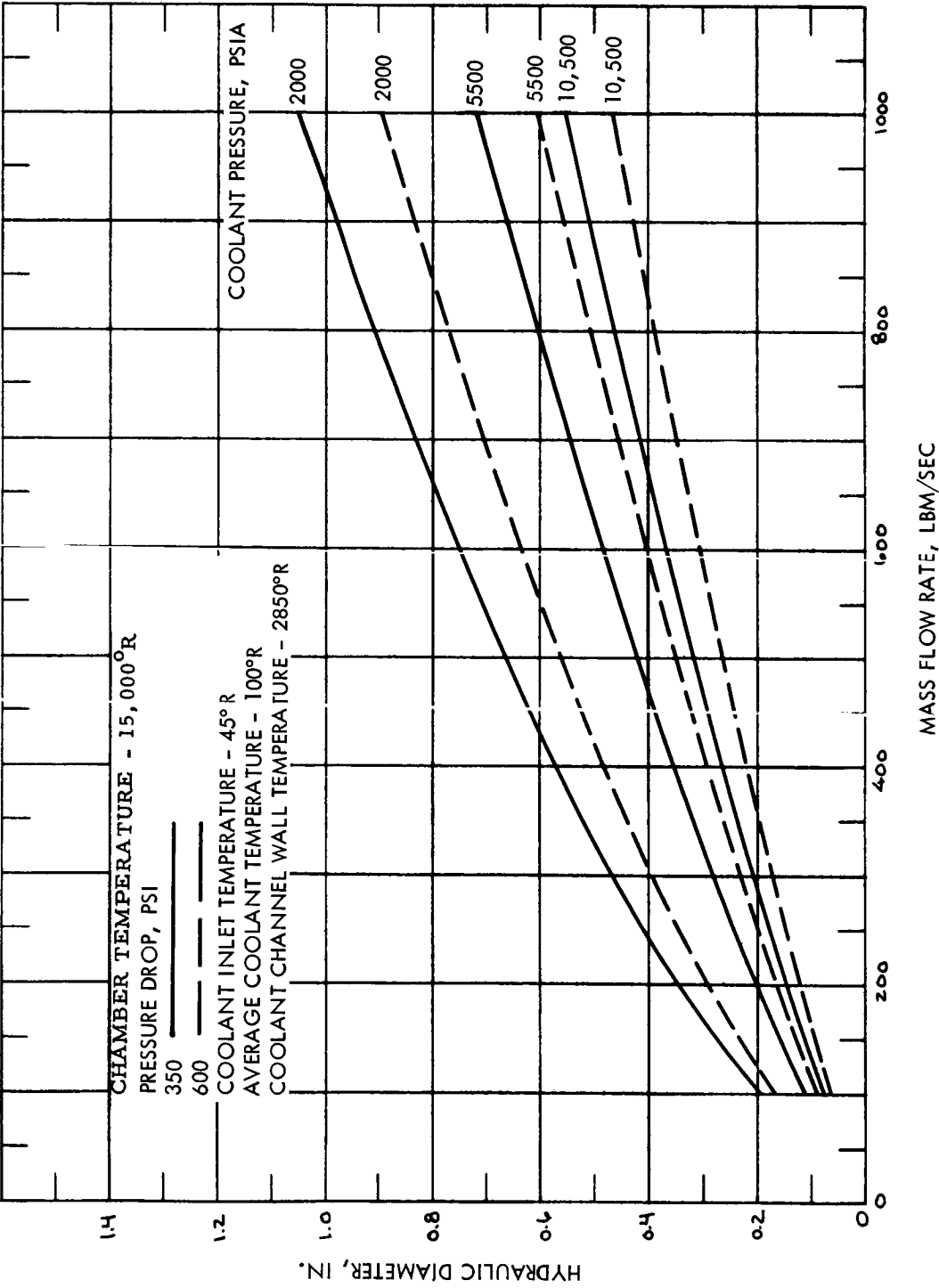


Figure 5-15 Nozzle Coolant Hydraulic Diameter

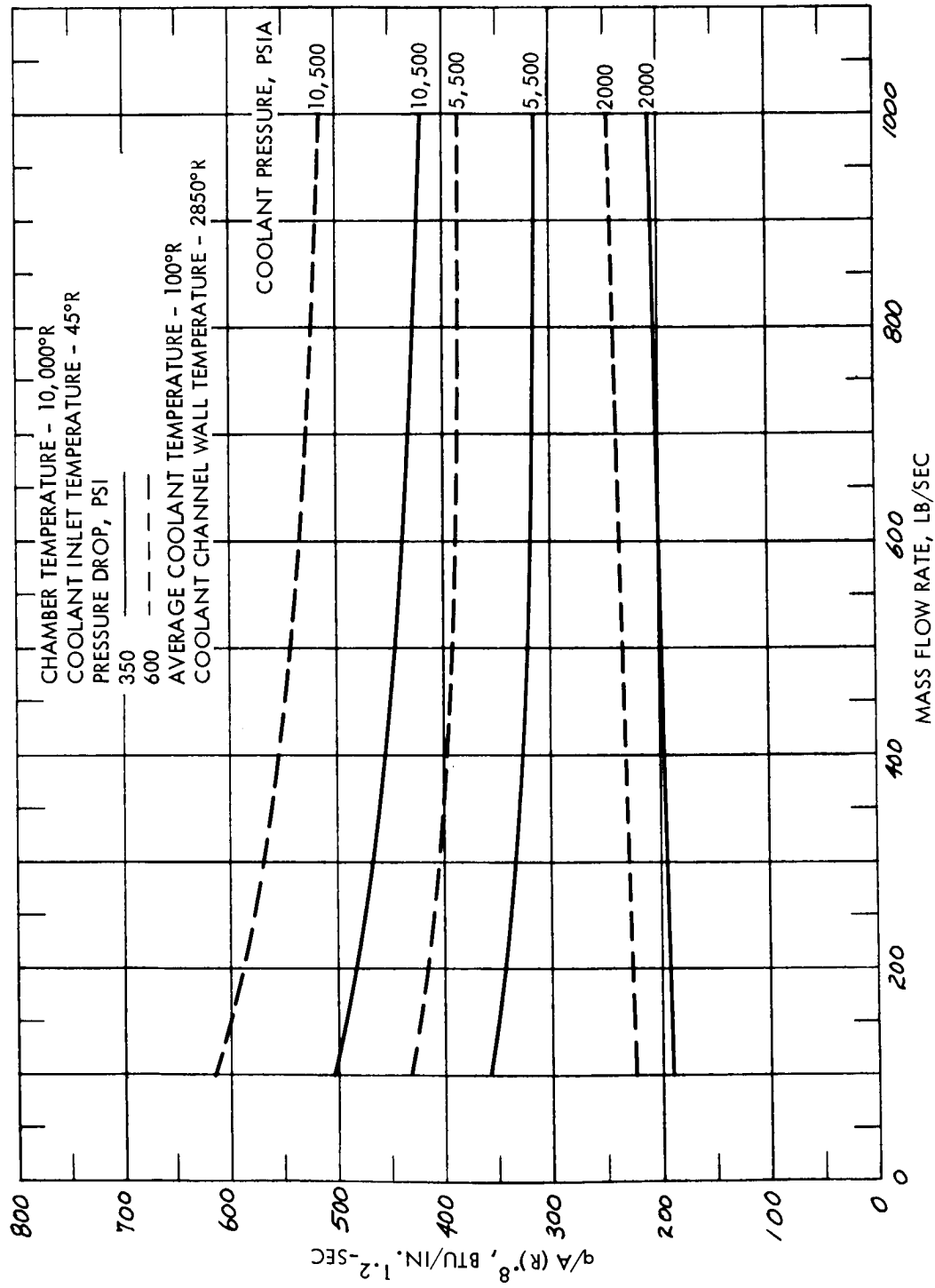


Figure 5-17 Nozzle Coolant Heat Flux Parameter

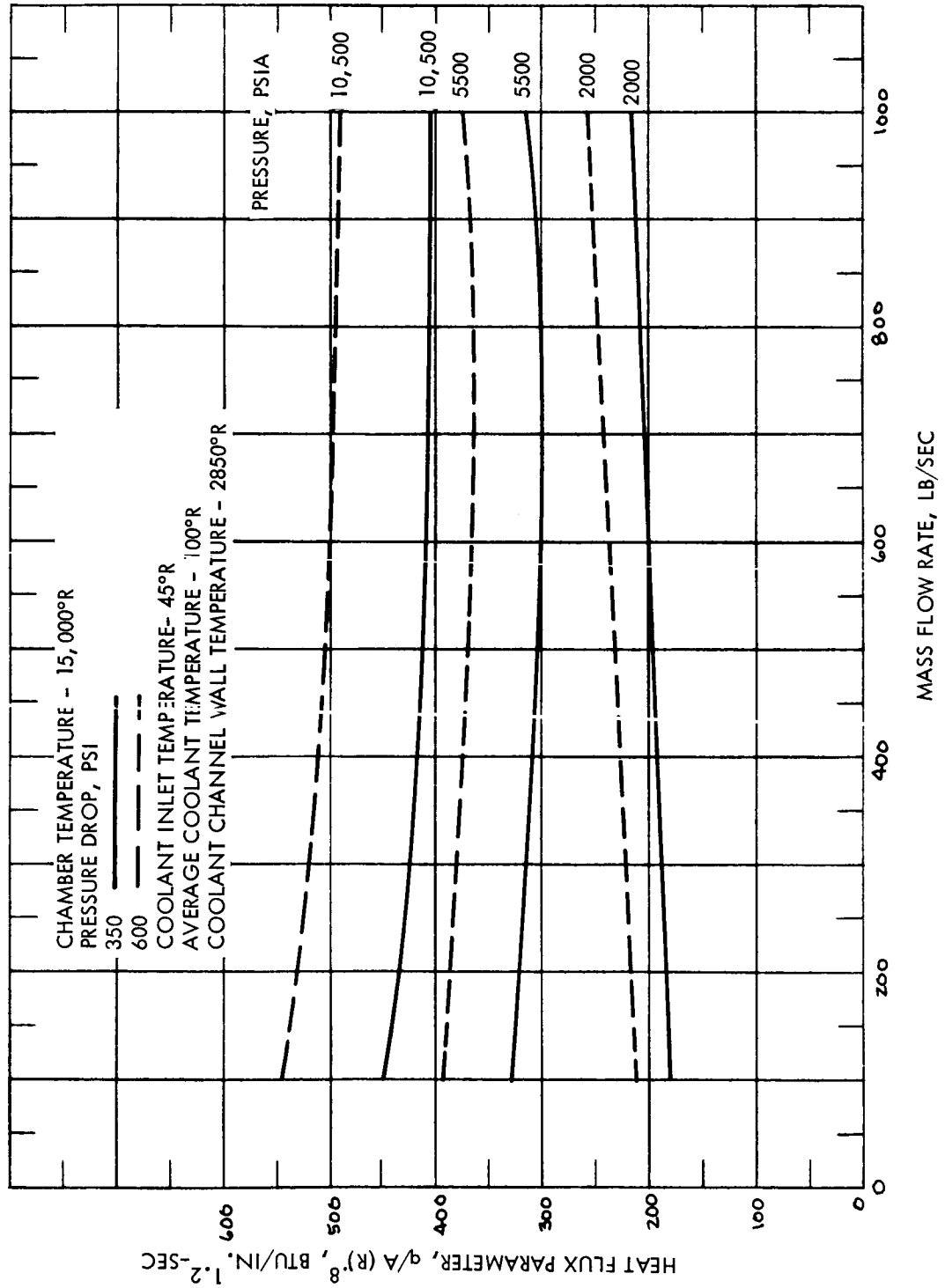


Figure 5-18 Nozzle Coolant Heat Flux Parameter

a nozzle coolant flow channel length, $x_2 - x_1$, based upon an expansion ratio of 40:1 and a cone half-angle of 17.5° . To account for the pressure drop from the coolant side of the nozzle to the chamber, the coolant bulk pressure at which the viscosity was evaluated was assumed to be 500 psi greater than the chamber pressure.

Utilizing this relationship between coolant pressure drop and the hydraulic diameter, the coolant side heat flux relationship, Equation 27 was evaluated function of coolant pressure drop. The product of the coolant side heat flux and $R^{0.8}$ is plotted as a function of mass flow rate in figures 5-17 and 5-18 for coolant pressure drops of 350 psi and 600 psi, chamber temperatures of $10,000^\circ\text{R}$, $15,000^\circ\text{R}$ and chamber pressures of 1000 psi, 5000 psi and 10,000 psi. Results were based upon a constant coolant side wall temperature, T_{wc} , of 2850°R and a coolant bulk temperature of 100°R . Although the results are shown only for the gas core nozzle which contains the uranium scoop, rough calculations indicate that the coolant in a conventional nozzle would remove heat fluxes which are 70% to 90% of those given in figures 5-17 and 5-18. That is, the gas core coolant would remove heat fluxes which are 10 to 30 percent greater than the heat fluxes which could be removed in a conventional nozzle with the same mass flow rate and pressure.

For a specific mass flow rate, coolant pressure drop and chamber conditions, a plot of the heat flux which can be regeneratively removed by the coolant may be obtained as a function of nozzle expansion ratio. This is accomplished first by using figure 5-8 to obtain the nozzle throat radius r_t as a function of mass flow rate and chamber conditions and then employing the relationship, $R = r_t^2 \epsilon + r_s^2$, to calculate R . For a typical case where $T_c = 10,000^\circ\text{R}$, $P_c = 1000$ psi, $\Delta P = 350$ psi and $\dot{m} = 100$ lbm/sec, the heat flux that can be regeneratively removed from the throat of the nozzle is about $18 \text{ Btu/in}^2\text{-sec}$. Plots showing the convective cooling capability at the nozzle throat are shown in figures 5-19 and 5-20.

In the nozzle hot side heat flux discussion section of this report, it was shown in figure 5-11 that for a case where $T_c = 10,000^\circ\text{R}$, $P_c = 1000$ psi, and $\dot{m} = 100$ lb/sec, the convective heat flux incident on the nozzle throat was about $170 \text{ Btu/in}^2\text{-sec}$. Since only about $18 \text{ Btu/in}^2\text{-sec}$ can be removed from the nozzle regeneratively, the remainder must be removed from the nozzle wall by transpiration cooling techniques. An additional advantage of transpiration

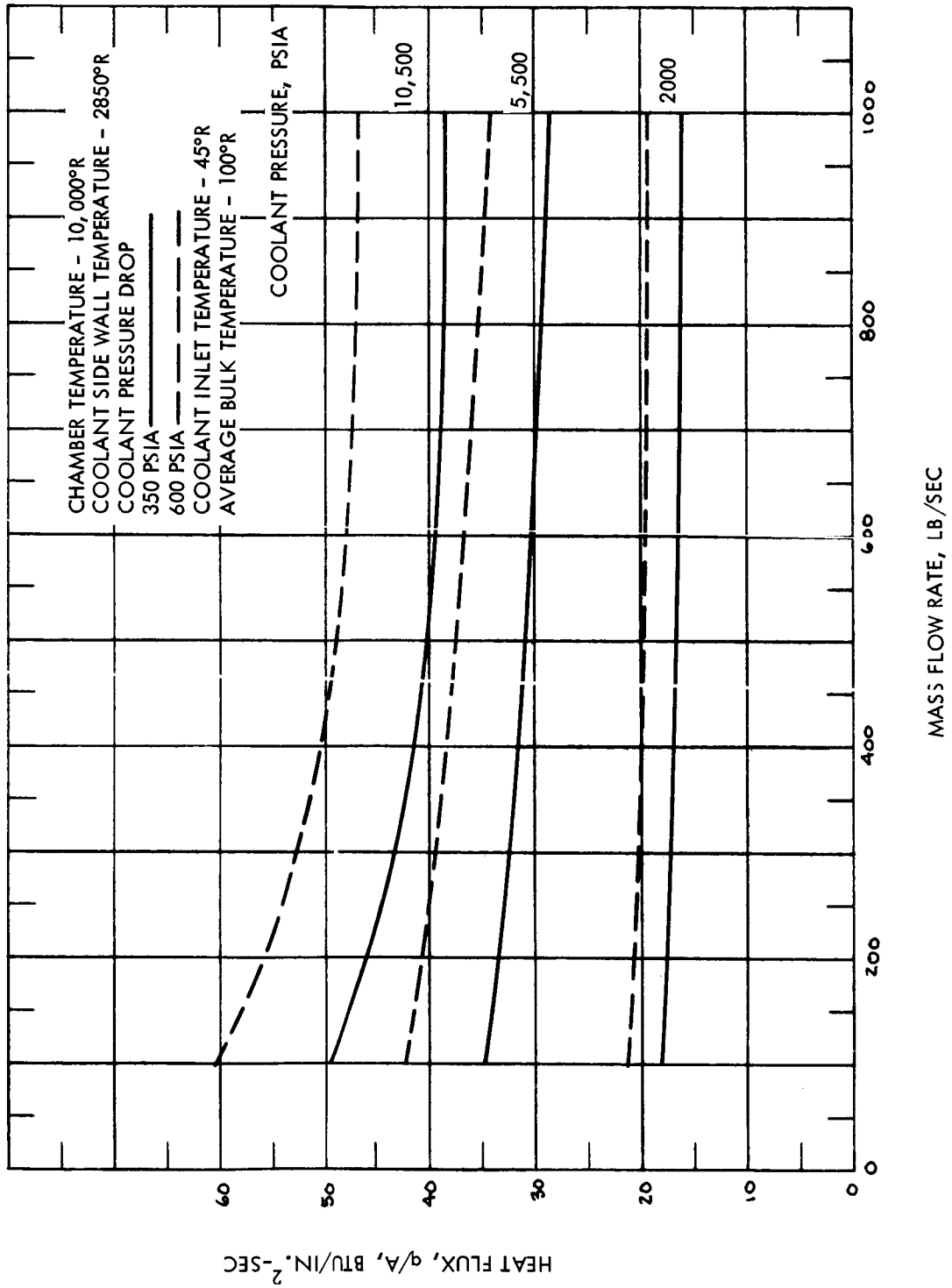


Figure 5-19 Nozzle Convective Cooling Capability at the Throat

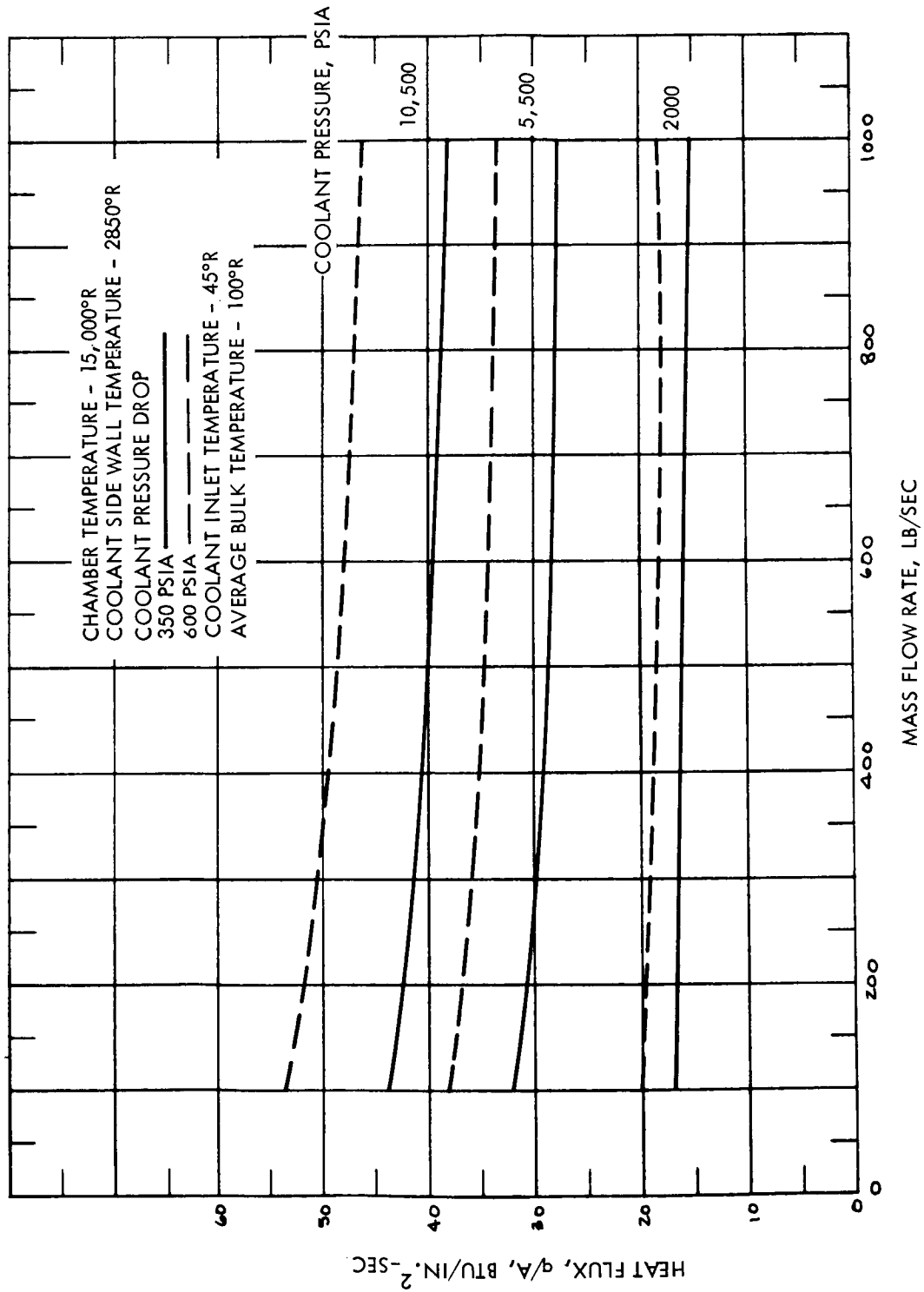


Figure 5-20 Nozzle Convective Cooling Capability at the Throat

cooling is the blocking effect on the convective heat flux resulting from the transpiration coolant which forms a boundary layer on the hot side of the nozzle wall. A discussion of the final nozzle cooling design will be presented in the Engine Preliminary Design section of this report and will include the convective blocking effects resulting from transpiration cooling.

5.2.1.3 Nozzle Coolant Temperature Rise

To complete the nozzle analysis, the temperature rise of the coolant as it passes through the nozzle must be evaluated. The basic coolant heat flux relationship, Equation (28), is multiplied by the heat transfer surface area to obtain the enthalpy rise of the coolant, thus:

$$\Delta H = \frac{0.01521}{D_c \dot{m}} \left(\frac{\dot{m}}{\pi \bar{R}_{fa}} \right)^{0.8} \frac{\Phi_b T_b^{1.35}}{T_{wc}^{0.55}} (T_{wc} - T_b) (2\pi \bar{R}_{ha} \Delta \ell) \quad (28)$$

where

\bar{R}_{fa} = the average value of the nozzle inside radius which yields the average coolant flow area, in.

\bar{R}_{ha} = the average value of the nozzle inside radius which yields the heat transfer area, in.

$\Delta \ell$ = length of nozzle wall surface, in.

ΔH = enthalpy rise of the coolant, Btu/lb

Substituting the following values in the above equation, $T_b = 100^\circ R$, $T_{wc} = 2850^\circ R$ and $\Phi_b = 0.0085$, the result is:

$$\Delta H = 5.70 \frac{\Delta \ell (\bar{R})^{0.2}}{D_c \dot{m}^{0.2}} \quad (29)$$

where

\bar{R} = the overall average R, in.

Average values for the nozzle radius, \bar{R} , were selected for a 40:1 nozzle expansion ratio and the various chamber conditions and mass flow rates of interest. The length of the nozzle coolant passage, $\Delta \ell$, was calculated assuming a nozzle expansion ratio of 40:1 and a nozzle divergent core half-angle of 17.5° . Values of the hydraulic diameter, D_c , were selected from figures 5-15 and 5-16. for coolant pressure drops of 350 psi and 600 psi. Using values for $\Delta \ell$, \bar{R} , and D_c obtained as outlined above, the coolant enthalpy rise was evaluated as a function of \dot{m} using equation (29). The enthalpy rise was converted to a temperature rise and results are plotted in figures 5-21 and 5-22.

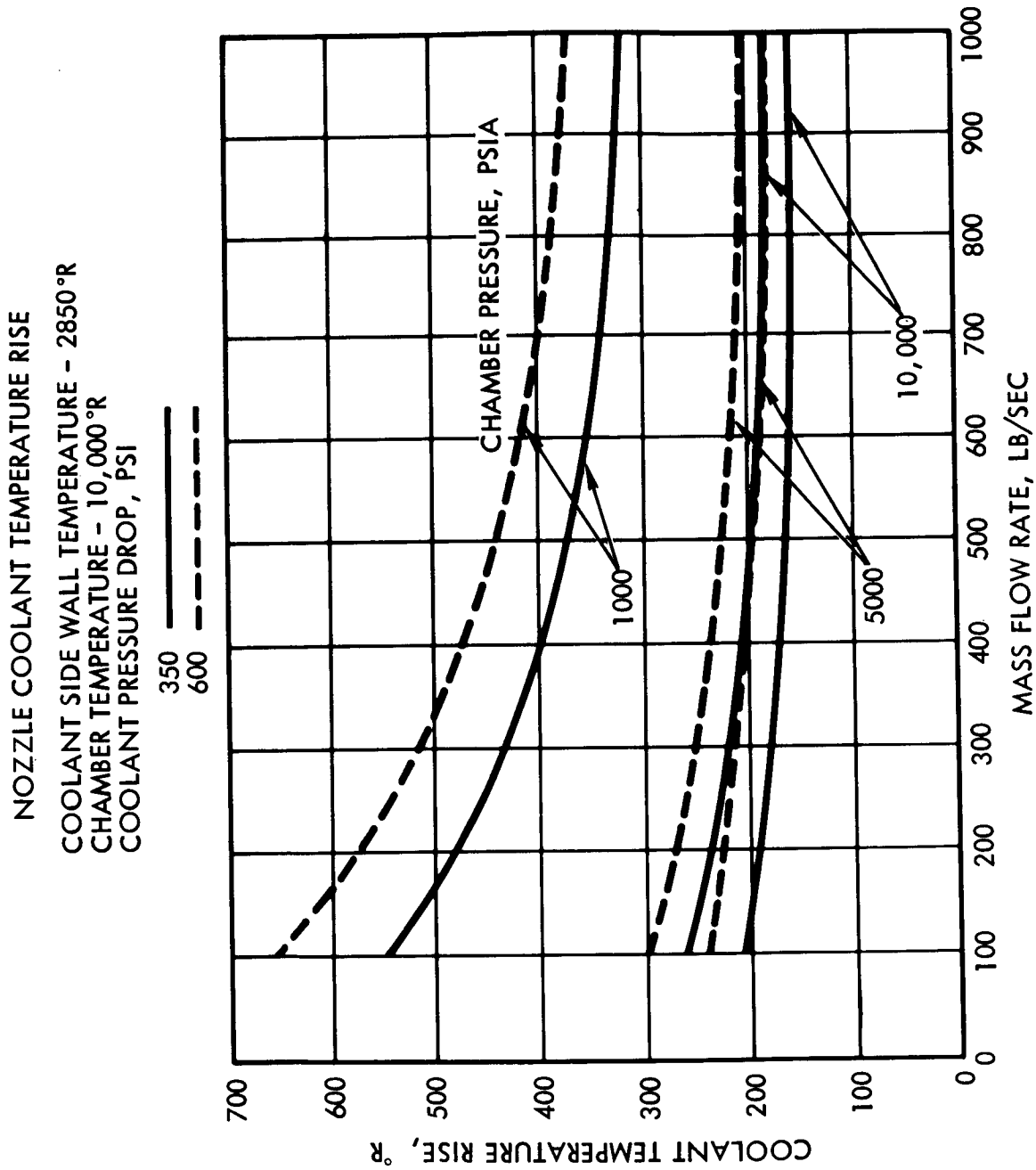


Figure 5-21 Nozzle Coolant Temperature Rise

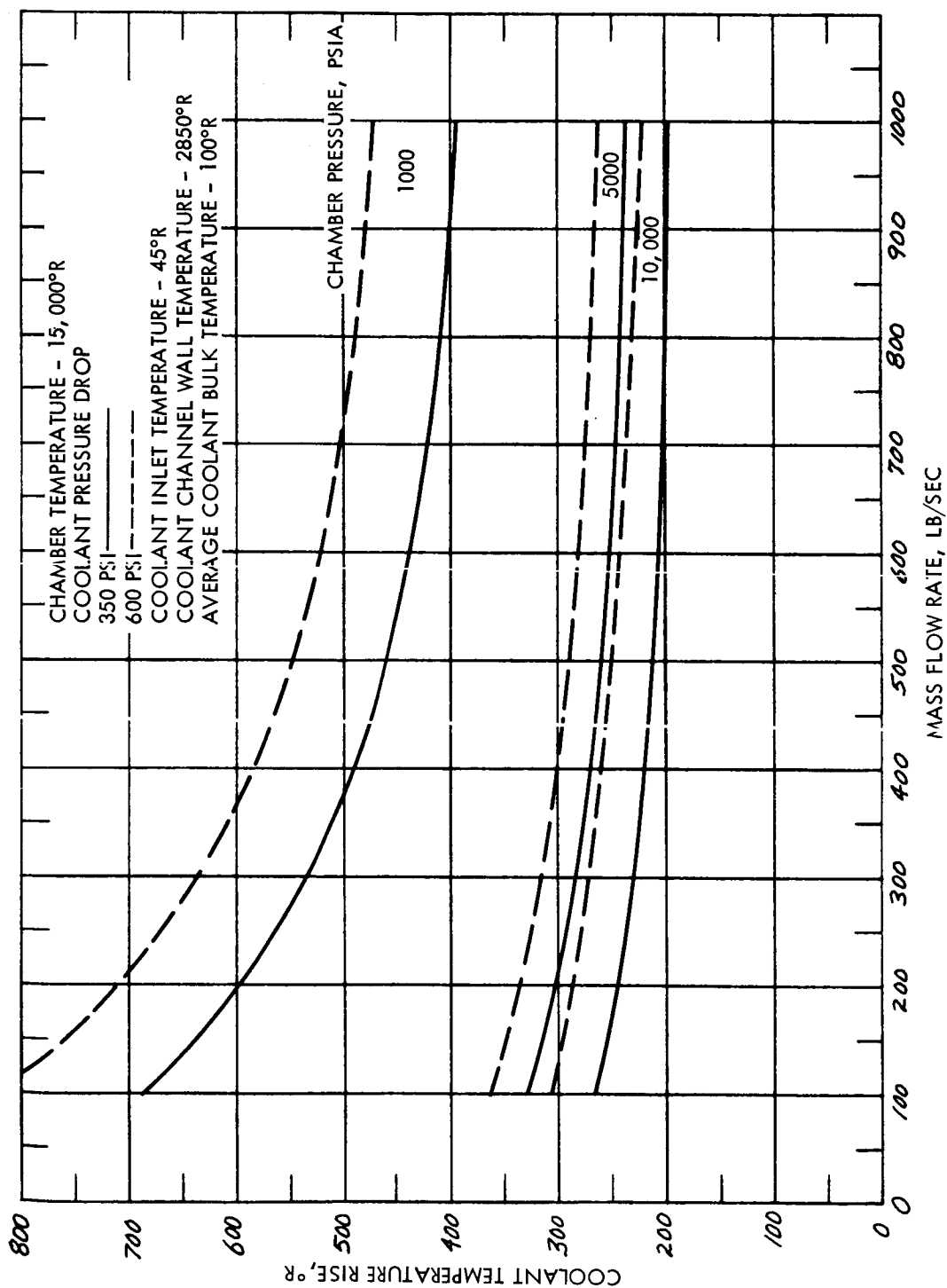


Figure 5-22 Nozzle Coolant Temperature Rise

It is important to emphasize that the results included in this section are preliminary. Simple annular flow channel geometry has been assumed and a lumped pressure drop-temperature rise analysis has been performed, wherein, fluid properties were averaged over the entire channel length. The results are probably most useful for the preliminary design analysis.

5.2.2 Reflector Cooling

The objectives of the reflector cooling analysis were to determine the heat inputs to the reflector and to estimate the coolant flow passage geometry and coolant pressure drop required to remove the heat. The thermal radiation heat input was determined as outlined in the Heat Generation portion of this report, and the nuclear radiation heating in the reflector will be estimated in this section. Knowing the total heat input to the reflector allows the specification of the coolant channel geometry and pressure drop necessary to remove the heat. Results are presented parametrically so that several reflector cooling designs may be analyzed.

5.2.2.1 Reflector Heat Inputs

The primary heat input to the reflector is thermal radiation from the fissioning uranium column. Figure 5-23 shows the total quantity of heat transferred to the reflector wall by thermal radiation as a function of core power for core operating pressures of 100 and 1000 atmospheres. Additional results which were obtained utilizing the computer codes discussed in the Heat Generation portion of this report are tabulated in Table 5-2. These results are required for the reflector cooling analysis.

The axial variation in the heat flux incident on the reflector is shown in figure 5-24 for a core power of 6340 mw and an operating pressure of 100 atm. The average heat flux to the reflector wall as a function of reactor power and pressure is shown in Table 5-3.

The total integrated heat input to the reflector as a percentage of the total power is given in figure 5-25 as a function of core power and operating pressure.

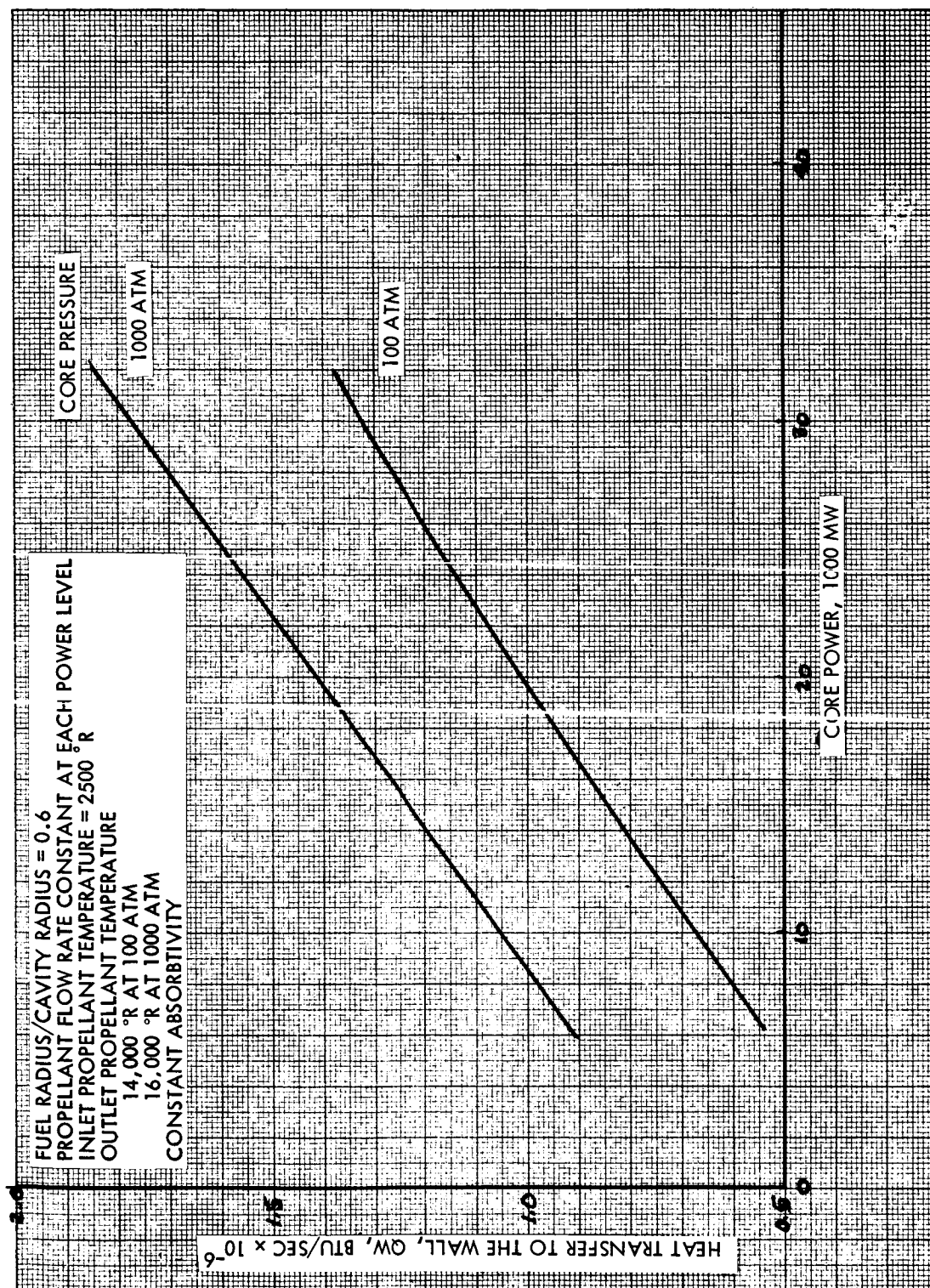


Figure 5-23 Heat Transferred to the Reactor Wall

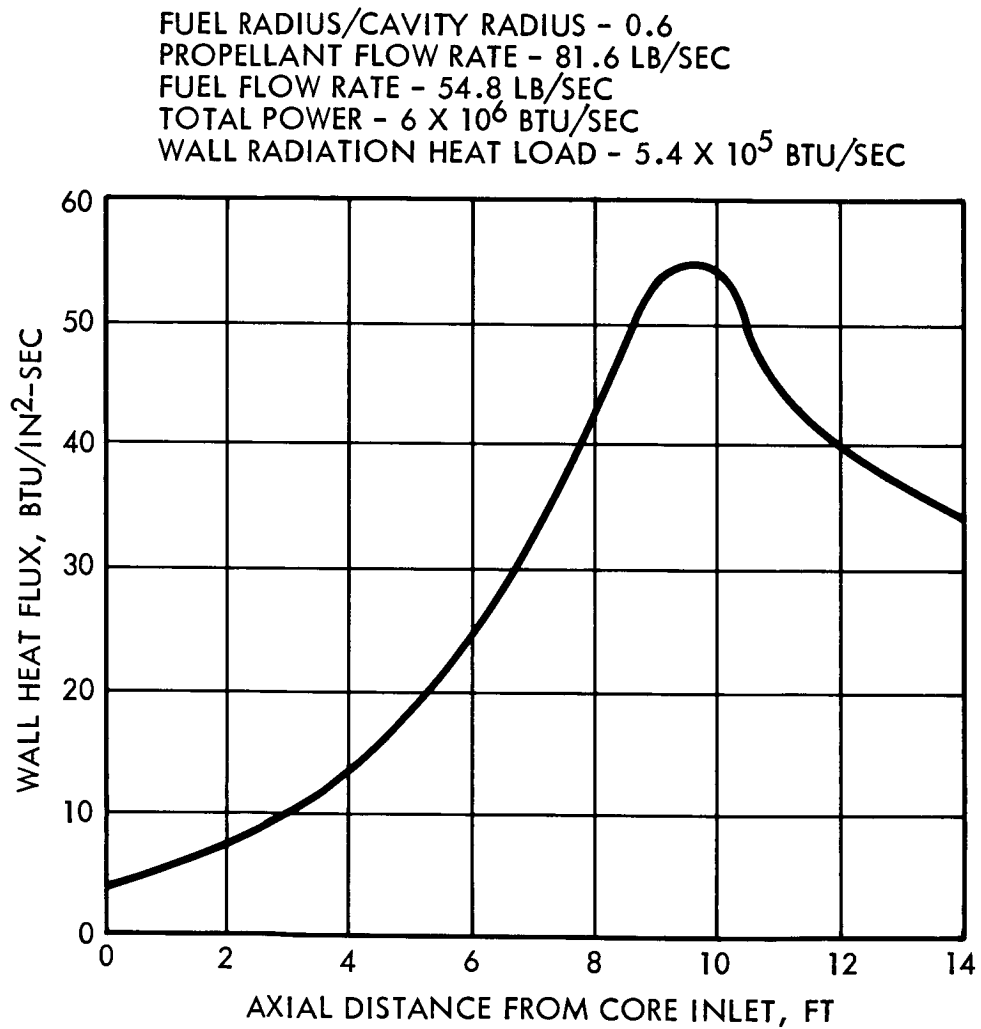


Figure 5-24 Reflector Wall Thermal Radiation Heat Flux

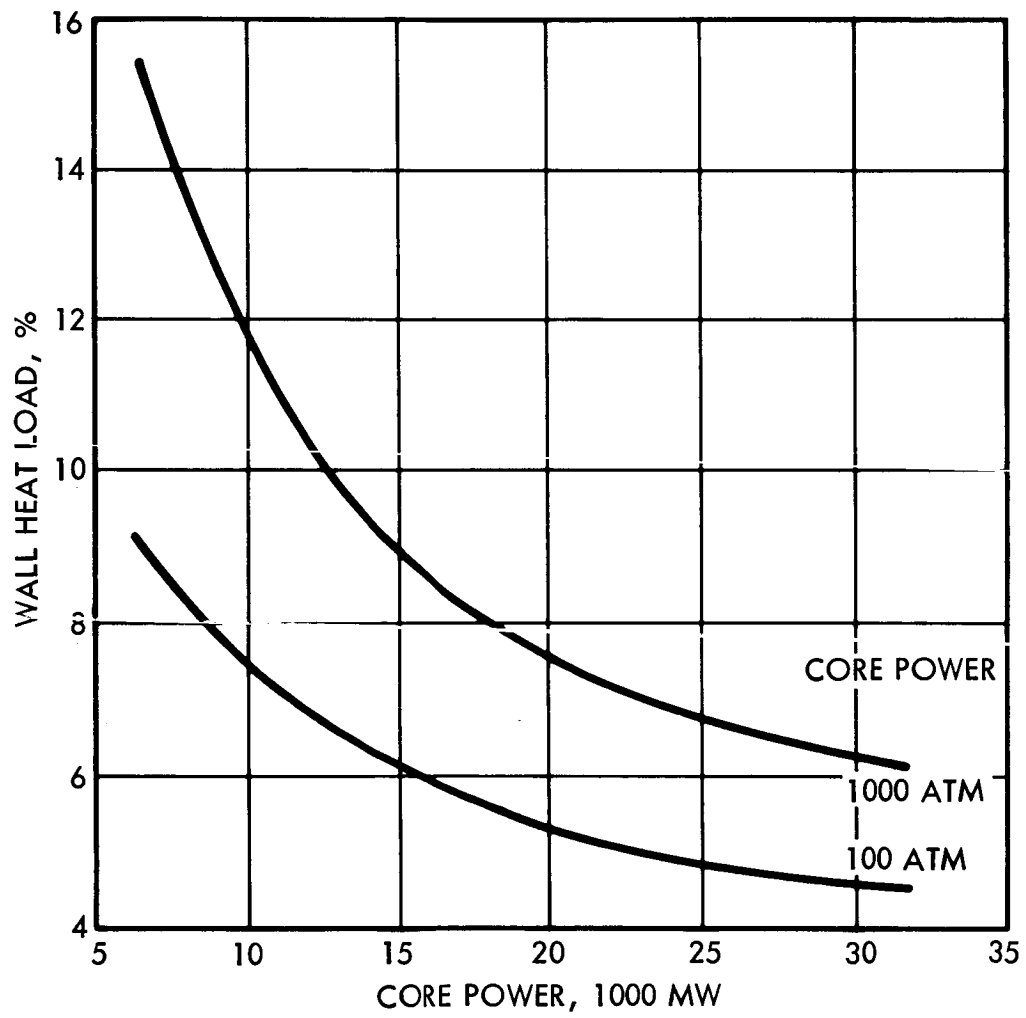


Figure 5-25 Reflector Wall Thermal Radiation Heat Load

Table 5-2 Gas Core Reactor Operating Characteristics

Core Power (megawatts)	H ₂ Mass Flow Rate (lbs/sec)	H ₂ Core Outlet Temperature		Heat Radiated to Wall			
				(Btu/secx10 ⁻⁶)		% of Core Power	
		100 atm	1000 atm	100 atm	1000 atm	100 atm	1000 atm
6,340	81.6	13,000	15,100	0.543	0.922	9.05	15.37
19,020	244.8	14,000	16,600	0.980	1.380	5.45	7.68
31,700	408	14,300	16,900	1.370	1,835	4.56	6.11

Table 5-3 Average Radiant Heat Flux to the Reflector

Core Power (mw)	Average Heat Flux (Btu/in ² -sec)	
	100 atm	1000 atm
6,340	24.1	40.8
10,020	43.4	61.1
31,700	60.6	81.3

Heat inputs to the reflector due to nuclear radiation are dependent upon the materials of which the reflector is made and the reactor power level. The reflector design considered here is similar to the design presented in reference 28. The reflector is composed of an inner graphite liner 15 cm thick surrounded by 70 cm of BeO. Graphite and beryllia were selected as the reflector materials because of their high temperature properties. A composite reflector design was required because heating rates near the core in a pure beryllia reflector would exceed the allowable values. The 15 cm graphite liner attenuates the radiation to levels which are tolerable for the BeO region.

Neutron and gamma heating rates obtained from reference 28 are presented in figure 5-26. The curves apply to a gas core system with an internal diameter of about five feet and values were calculated for locations at the core mid-plane. Neutron heating calculations included only the energy deposition due to elastic scattering and, thus, did not include the relatively small quantity of energy deposited by secondary radiations resulting from neutron capture. Gamma

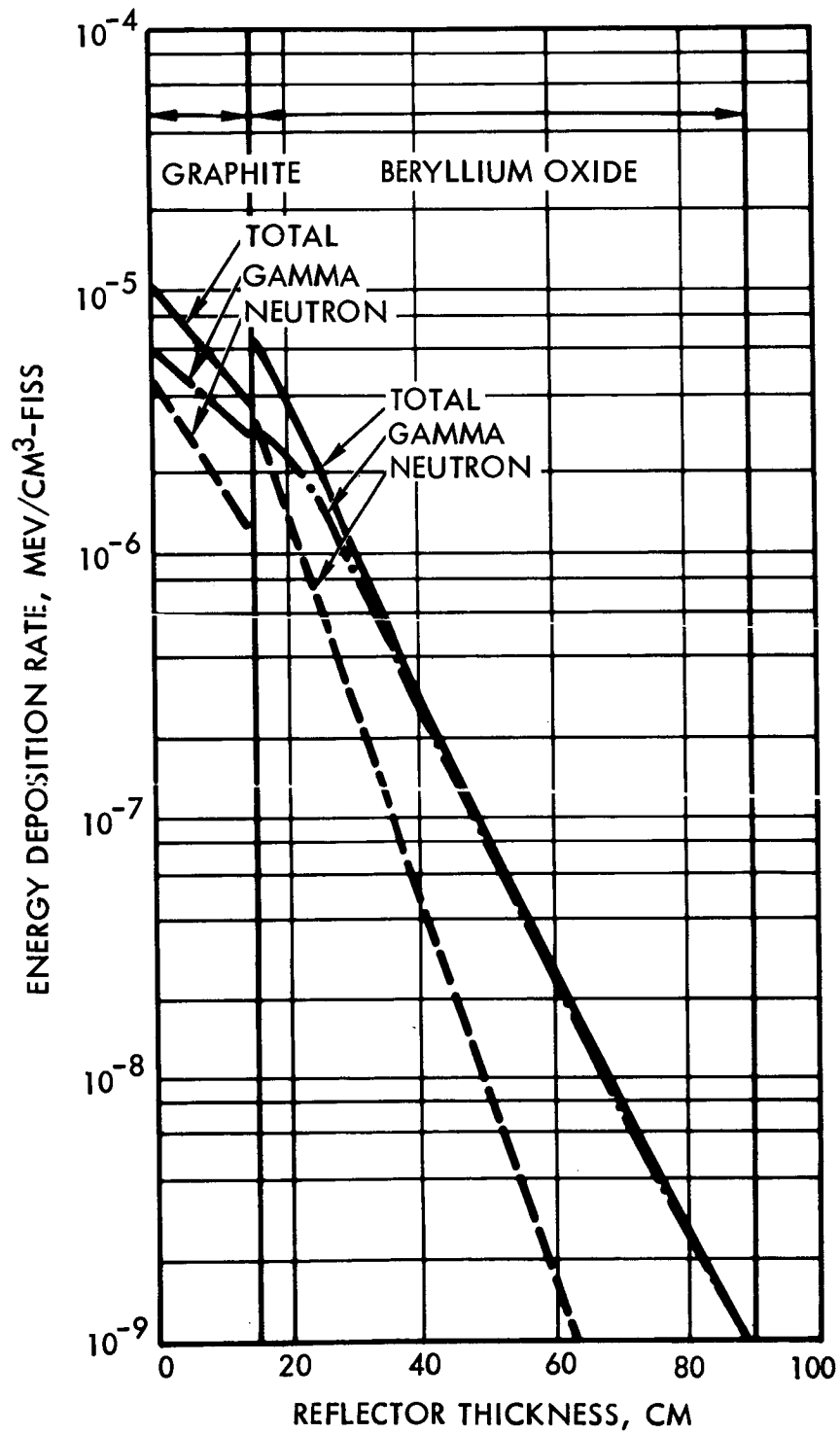


Figure 5-26 Reflector Wall Nuclear Heating Rates
5-43

heating calculations included the heating effects of both prompt and delayed gammas. Calculational methods outlined in the Reactor Shielding Design Manual, by T. Rockwell, were used for the gamma heating calculations. An independent check of the gamma heating results presented in reference 28 was made using a TRW Systems developed computer code, X-RAY. The results obtained from X-RAY compared well with results presented in reference 28. The results shown in figure 5-26 are based upon a single fission in the core and may be converted to Btu/sec-cm³ per megawatt of core power by multiplying by 5.26 (Btu-fiss)/(Mev-Mw-sec).

5.2.2.2 Reflector Heat Removal

The energy deposited with the reflector by nuclear radiation and the heat flux incident on the reflector must be removed by the hydrogen coolant. A discussion of the nuclear heat removal is followed by a discussion of the removal of the radiant heat flux incident on the reflector.

Average values for the heating rates in the reflector of 8×10^{-6} Mev/cm³-fiss for the 15 cm-thick graphite portion, 4×10^{-6} Mev/cm³-fiss for the first 15 cm of beryllia and 10^{-7} Mev/cm³-fiss for the remaining 55 cm of beryllia were obtained from figure 5-26. These heating rate values were multiplied by their respective volumes and the following relationship was obtained for the coolant mass flow rate required to remove the nuclear heat from the reflector.

$$\dot{m} = 168.0 \frac{P}{\Delta H} \quad (30)$$

where

\dot{m} = required coolant mass flow rate, lbm/sec

P = core power, Mw

ΔH = coolant enthalpy rise, Btu/lbm

Average heating rates from figure 5-26, on which the above equation is based, are average radial values for the core midplane and thus are peak axial heating rates. To take into consideration the axial heat generation rate profile, a peak-to-average heating rate ratio of 2 was assumed. This peak-to-average ratio yields about 9 percent of the core power deposited in the reflector. Incorporating the peak-to-average ratio into Equation 30, the relation becomes:

$$\dot{m} = 84.0 \frac{P}{\Delta H} \quad (31)$$

The mass flow rate required to remove the nuclear heat from the reflector obtained using the above equation is shown in figure 5-27 and 5-28. Results are given for inlet temperatures of 150°R and 500°R ; exit temperatures of 2500°R , 3000°R , 4000°R , and 5000°R ; and coolant pressures of 1500 psi and 10,000 psi.

To perform convective heat removal calculations at the reflector wall, it is necessary to assume a coolant channel geometry. The coolant channel geometry assumed for the calculations which follow is annular region of thickness, t_r . A schematic of the reflector showing the assumed coolant flow passage is shown in figure 5-29. The hydraulic diameter for an annular region as shown in figure 5-29 is twice the flow passage thickness, i.e., $D_c = 2 t_r$.

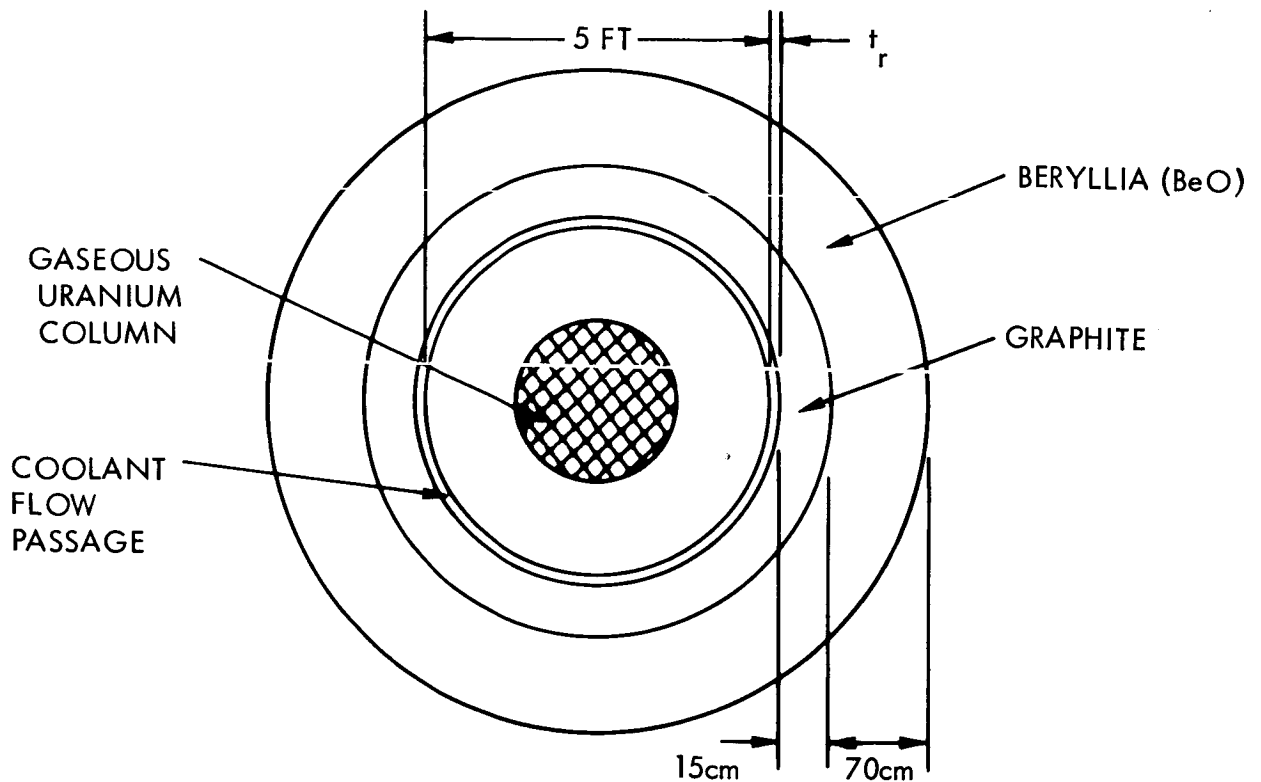


Figure 5-29 Reflector Schematic

The average heat flux removed from the reflector surface must be converted into a coolant enthalpy rise:

$$(q/A) \pi D_r L_r = \dot{m} \Delta H$$

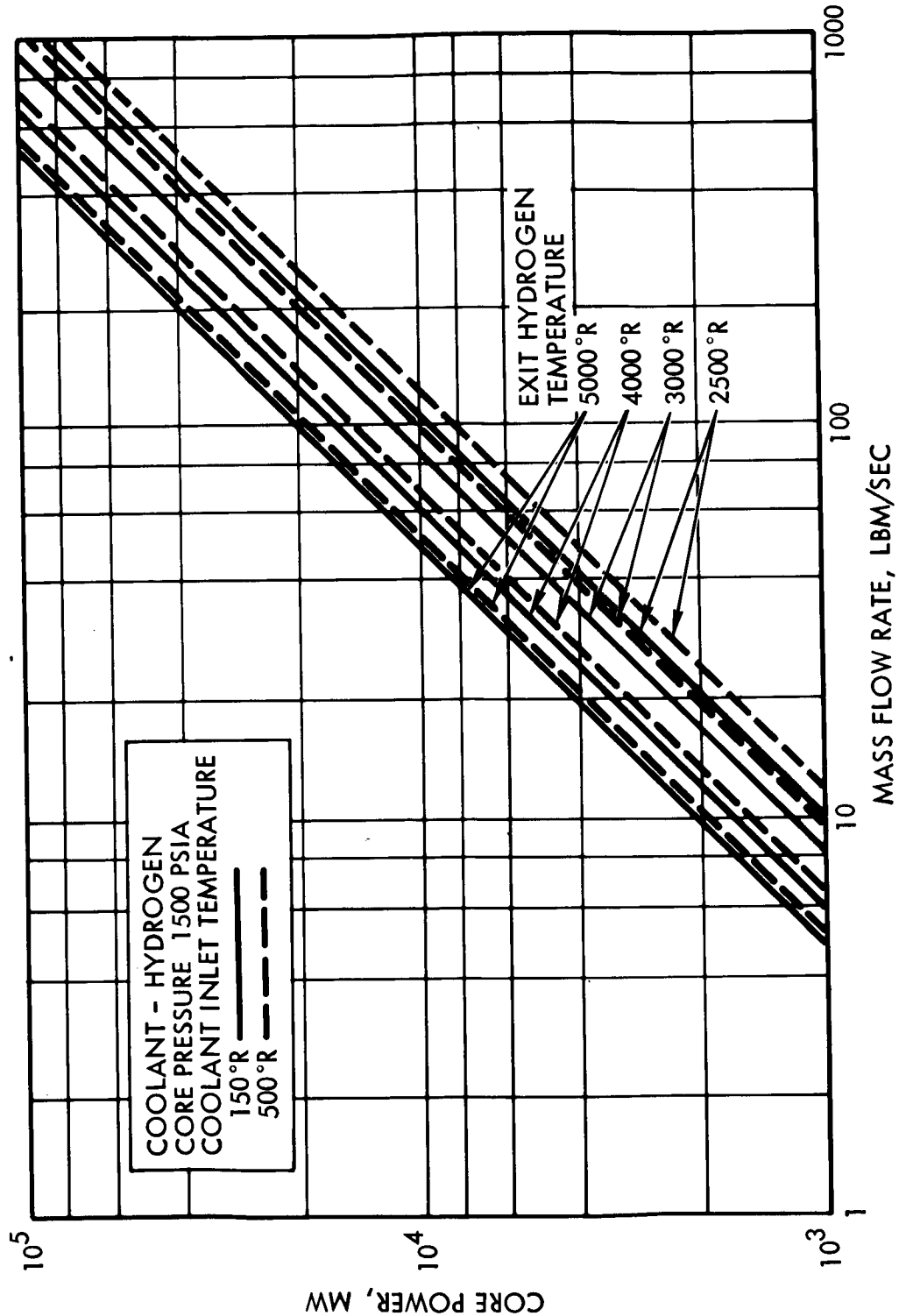


Figure 5-27 Reflector Nuclear Heating Coolant Requirement

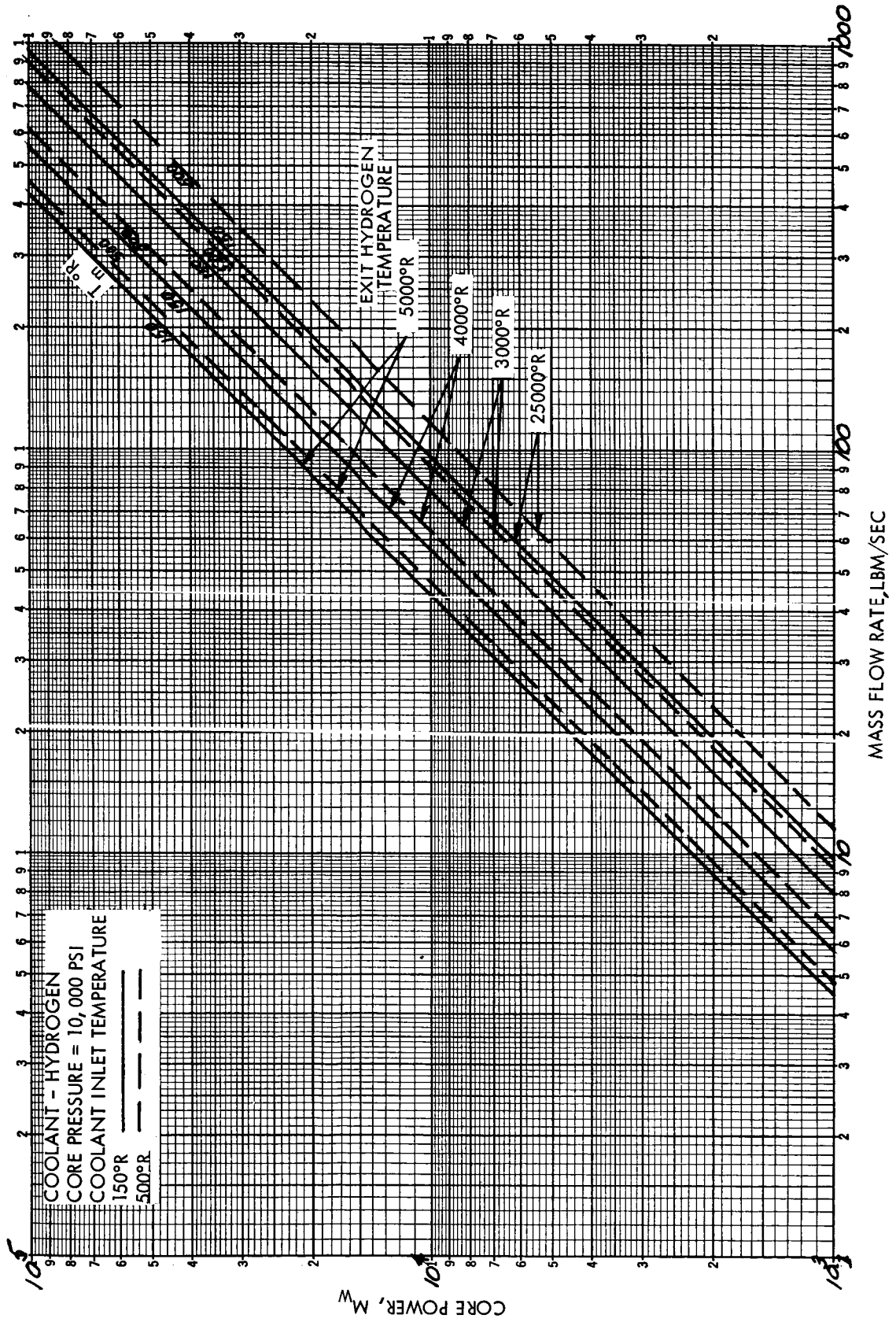


Figure 5-28 Reflector Nuclear Heating Coolant Requirement

where

q/A = heat flux removed from the reflector, Btu/(in²-sec)

D_r = reflector inside diameter = 60 in.

L_r = reflector length = 132 in.

\dot{m} = reflector coolant mass flow rate, lbm/sec

ΔH = coolant enthalpy rise, Btu/lbm

The heat flux which can be removed convectively is given by the following equation based on the Wolf-McCarthy heat transfer correlation for hydrogen:

$$q/A = 0.01521 \left[\frac{\dot{m}}{A} \right]^{0.8} \frac{\phi_b}{D_c^{0.2}} \frac{T_b^{1.35}}{T_w^{0.55}} (T_w - T_b)$$

where

q/A = coolant heat flux, Btu/in²-sec

\dot{m}/A = mass flow rate per unit of flow area, lbm/in²-sec

ϕ_b = heat transfer parameter evaluated at bulk coolant

$$\text{Conditions} = \frac{k_b (Pr)^{0.4}}{T_b^{0.8} \mu_b^{0.8}}$$

$$\text{Btu}/[(\text{ft-sec})^{0.2} (\text{lb})^{0.8} (^\circ\text{R})^{1.8}]$$

D_c = hydraulic diameter, in.

T_b = bulk coolant temperature, ^oR

T_w = coolant channel wall temperature, ^oR

k_b = conductivity of the bulk coolant, Btu/(ft-sec-^oR)

P_r = Pradtl Number

μ_b = bulk coolant viscosity, lbm/(ft-sec)

The coolant flow area is given by:

$$A_f = \pi D_r t_r = \pi D_r \frac{D_c}{2}$$

Substituting the flow area relationship into the heat flux equation, the result is:

$$q/A = 4.01 \times 10^{-4} \frac{\dot{m}^{0.8}}{D_c} \cdot \phi_b \frac{T_b^{1.35}}{T_w^{0.55}} (T_w - T_b) \quad (32)$$

The above heat flux relationship was substituted into the heat balance relationship, Equation 31 and the following equation for the hydraulic diameter was obtained:

$$D_c = \frac{10}{\dot{m}^{0.2}} \frac{\phi_b T_b^{1.35} (T_w - T_b)}{T_w^{0.55} \Delta H}$$

Hydraulic diameters were calculated for inlet hydrogen temperatures of 150°R and 500°R, exit hydrogen temperatures ranging from 2500°R to 5000°R and bulk coolant pressures of 1500 psi and 10,000 psi. The variation in the hydraulic diameter with exit gas temperature and bulk pressure was found to be less than 3 percent so that this variation could be neglected in the analysis. Results indicating the hydraulic diameter necessary to effect a heat balance are shown in figure 5-30 as a function of coolant mass flow rate and coolant inlet temperature. A constant wall temperature of 2500°R was assumed for the calculations in addition to a bulk fluid temperature given by the average of the inlet and exit bulk temperatures. The hydraulic diameters presented are the hydraulic diameters necessary to produce a specified enthalpy rise. If a hydraulic diameter less than the value given in figure 5-30 is used, then more heat can be transferred across the film in the assumed flow channel than can be removed by the given coolant mass flow rate. If a hydraulic diameter greater than the value given in figure 5-30 is used, it would be impossible to transfer enough heat across the film in the assumed flow channel to achieve the selected exit bulk temperature with the given mass flow rate. Thus, figure 5-30 may be used to specify the coolant flow channel width necessary to effect a heat balance in the reflector for coolant exit temperatures from 2500°R to 5000°R and coolant pressures from 1500 psi to 10,000 psi.

The average heat flux which may be removed from the reflector surface is given in figure 5-31 as a function of coolant mass flow rate and hydraulic diameter. Results were generated using Equation 32. A coolant channel wall temperature of 2500°R was assumed in addition to a bulk coolant temperature given by the average of the inlet and exit bulk temperatures.

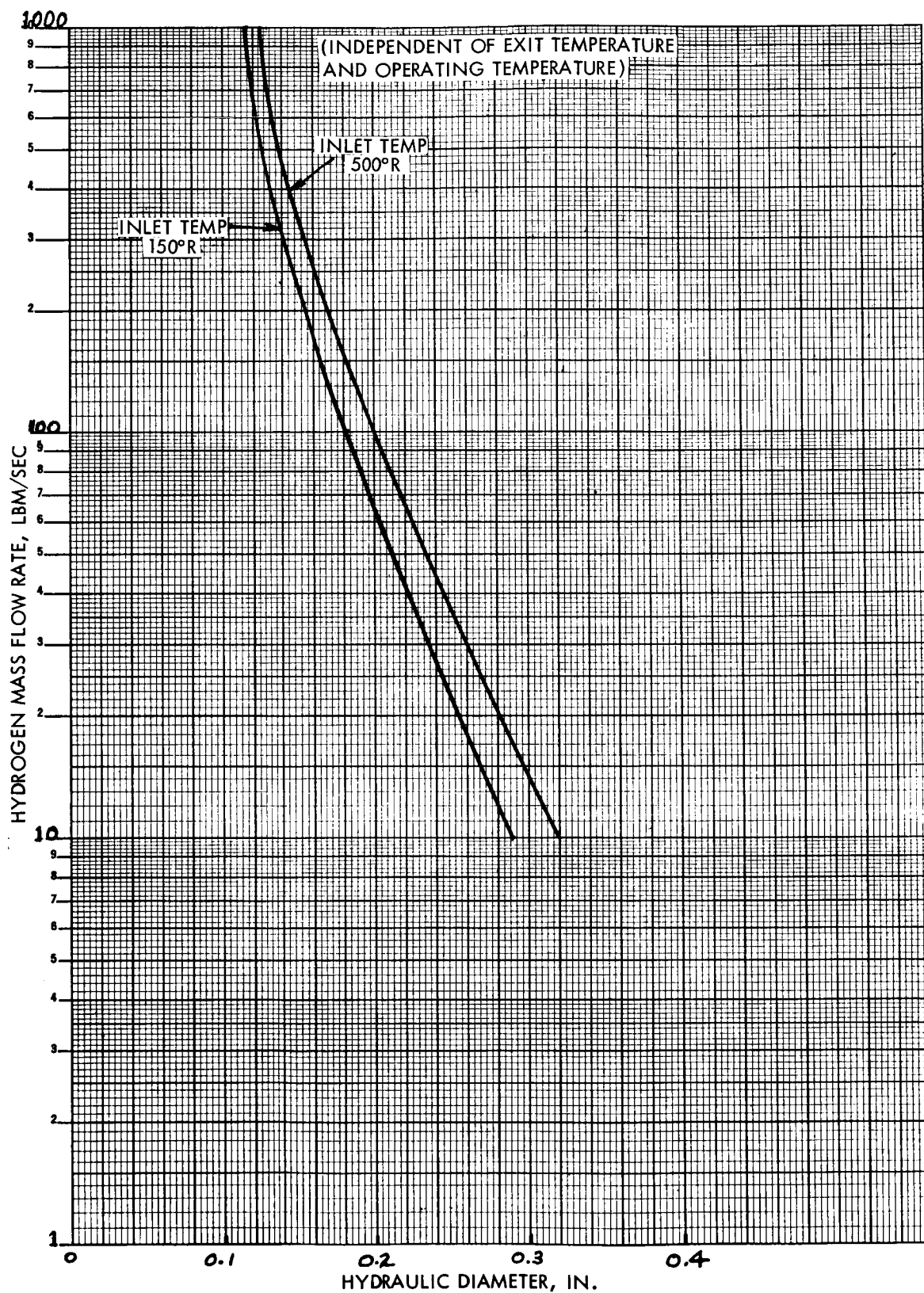


Figure 5-30 Hydraulic Diameter Required to Effect a Heat Balance in the Reflector
5-50

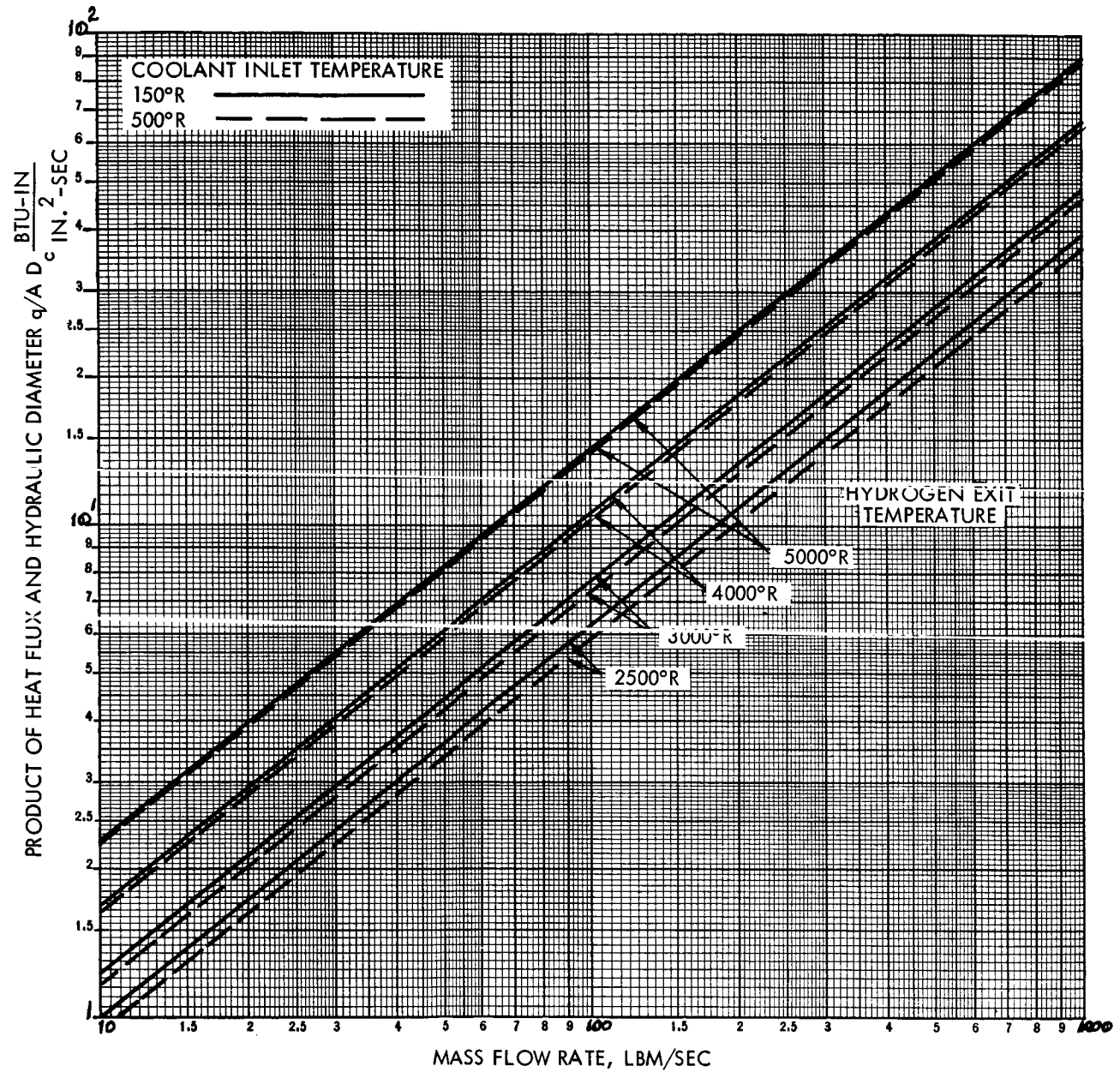


Figure 5-31 Heat Flux Which Can Be Regeneratively
Removed From The Reflector
5-51

5.2.2.3 Reflector Pressure Drop

An additional consideration in the reflector heat transfer-fluid flow analysis is the coolant pressure drop associated with a given channel width and given coolant conditions, i.e., coolant temperature rise, coolant bulk temperature, and coolant bulk pressure. The governing equation is given below:

$$p_1^2 = p_2^2 + 47.645 \left(\frac{\dot{m}}{A} \right)^2 \left\{ T_2 - T_1 + \frac{2 \bar{T}}{D_c} \bar{f}_f L + \bar{T} \ln \frac{p_2}{p_1} \right\} \quad (33)$$

where

p_1 = inlet pressure, psi

p_2 = exit pressure, psi

$\frac{\dot{m}}{A}$ = coolant mass flow rate per unit area, lbm/(in²-sec)

T_1 = inlet coolant temperature, °R

T_2 = exit coolant temperature, °R

L = channel length, in.

D_c = channel hydraulic diameter, in.

\bar{f}_f = average friction factor = $\frac{0.046}{(Re)^{0.2}}$

\bar{T} = average bulk temperature, °R

Re = average bulk Reynolds Number

After substituting a channel length of 132 inches into Equation (33) along with the expression for the Reynolds number and the channel flow area, the equation becomes:

$$p_1^2 = p_2^2 + 5.365 \times 10^{-3} \left\{ \frac{\dot{m}^2}{D_c^2} \left[(T_2 - T_1) + \bar{T} \ln \frac{p_1}{p_2} \right] + 21.9 \frac{\dot{m}^{1.8}}{D_c^3} \mu^{-0.2} \bar{T} \right\}$$

Values for hydraulic diameter were selected and the pressure drop was calculated for an inlet bulk temperature of 150°R and 5000°R. Results are shown in figures 5-32 and 5-33 for bulk coolant exit pressures of 1500 psi and 10,000 psi, respectively.

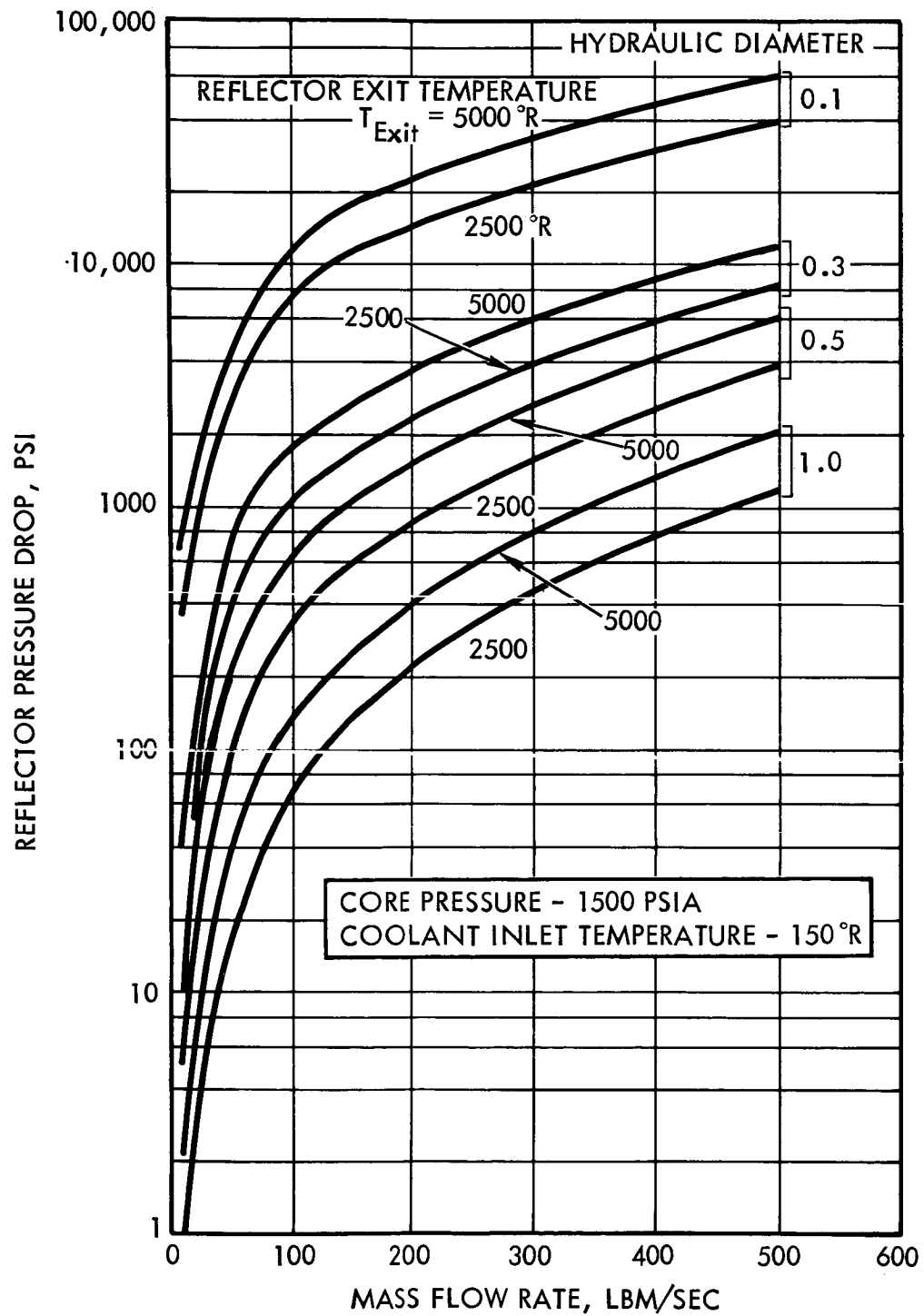


Figure 5-32 Reflector Pressure Drop

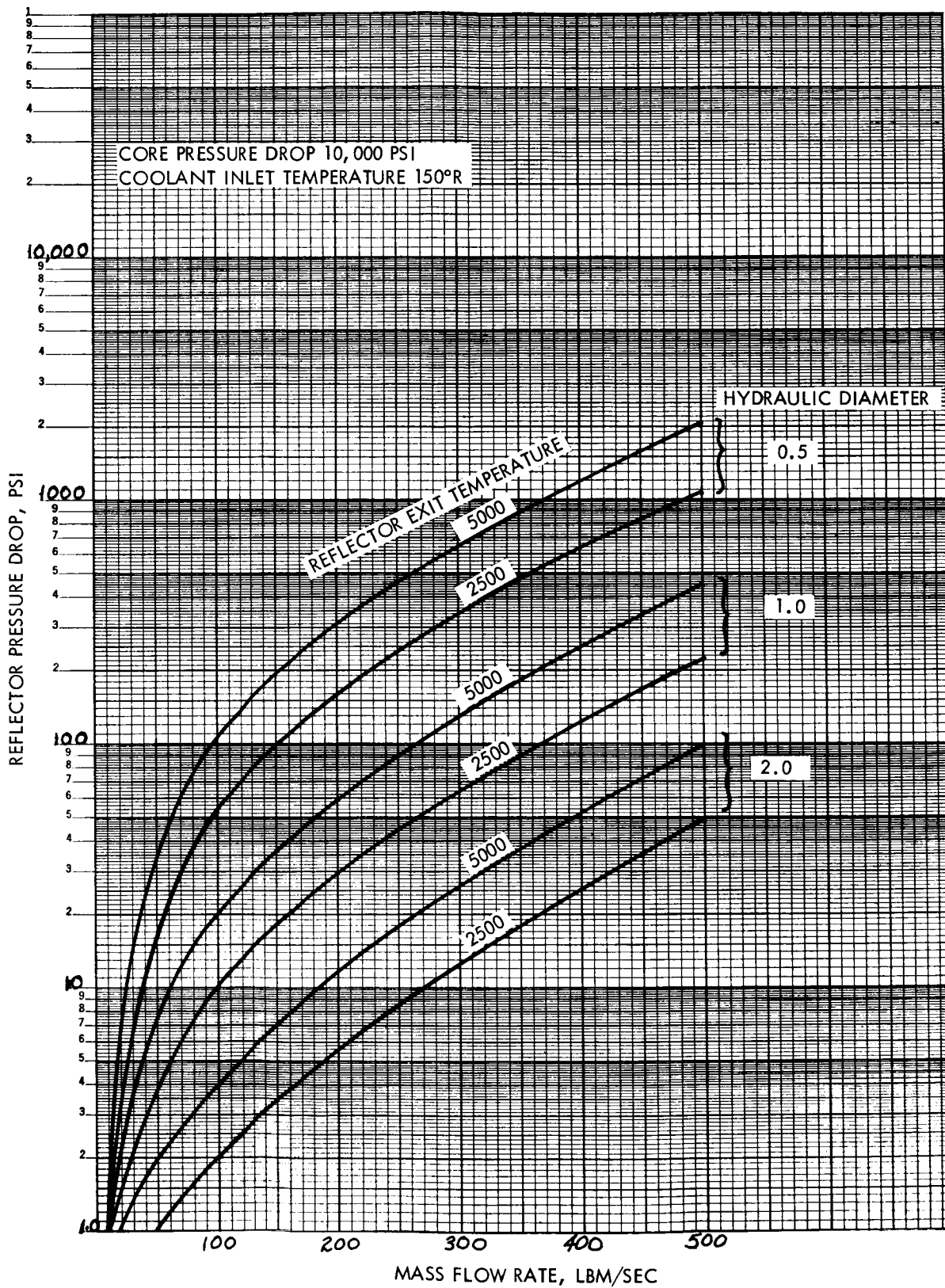


Figure 5-33 Reflector Pressure Drop
5-54

5.2.2.4 Conclusions

The curves shown provide an efficient means to determine reflector cooling requirements. For example, considering the reactor power of 6,340 Mw given in table 5-2, figure 5-21 shows that a coolant flow rate of 51 lbs/sec is required to remove the nuclear heat from the reflector for an inlet temperature of 150°R , an exit temperature of 3000°R , and a pressure of 1500 psi. If the total flow rate available is 81.6 lbm/sec as shown in table 5-2, the mass flow rate remaining to regeneratively cool the reflector is 30.6 lb/sec. Figure 5-30 shows that a hydraulic diameter of 0.235 is required to effect a heat balance in the reflector. Figure 5-31 shows that $12.5 \text{ Btu/in}^2\text{-sec}$ may be removed regeneratively from the reflector for a mass flow rate of 30.6 lb/sec, inlet temperature of 150°R , an exit temperature of 3000°R , and a hydraulic diameter of 0.235. The pressure drop for this particular design is shown in figure 5-32 to be about 350 psi.

Results included in this section are used to define the reflector temperature rise and pressure drop for several selected gas core rocket reactor configurations in subsequent sections of this study.

5.2.3 Uranium Condensation

The hot uranium trapped by the scoop is condensed by mixing the hot uranium with cool hydrogen. The amount of cool hydrogen required to condense the uranium is determined from the uranium temperature at the base of the scoop, the mass flow rate of the hot uranium, and the temperature of the hydrogen coolant. Figure 5-34 shows the heat flux from the uranium to the interior wall of the scoop as a function of scoop length. From figure 5-34 it is evident that the majority of the heat flux lost to the interior scoop wall occurs within the first three feet of scoop length. Thus, the major temperature decrease of the uranium in the scoop takes place within the first three feet of scoop length. Figure 5-36 shows the average uranium temperature in the scoop as a function of distance from the leading edge of the scoop. From figure 5-36 it is evident that the average temperature decreases from about $60,000^{\circ}\text{R}$ to $34,000^{\circ}\text{R}$ in the first three feet, but only decreases about another $4,000^{\circ}\text{R}$ in the next three feet. From the above discussion, it appears that a scoop length of three feet would be a desirable length for cooling the uranium while maintaining a reasonable scoop length.

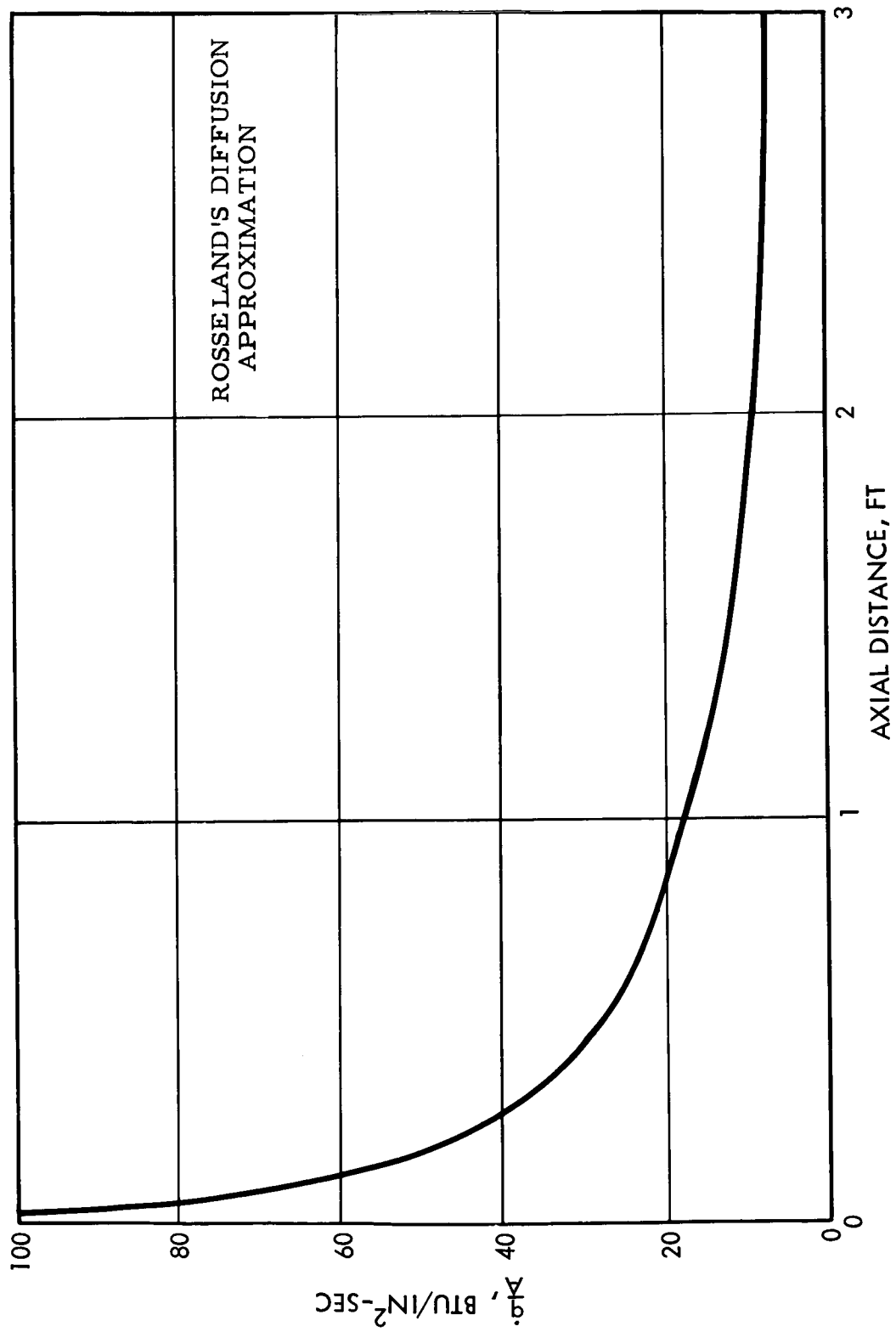


Figure 5-34 Heat Flux to the Interior Wall of the Scoop (from Uranium)

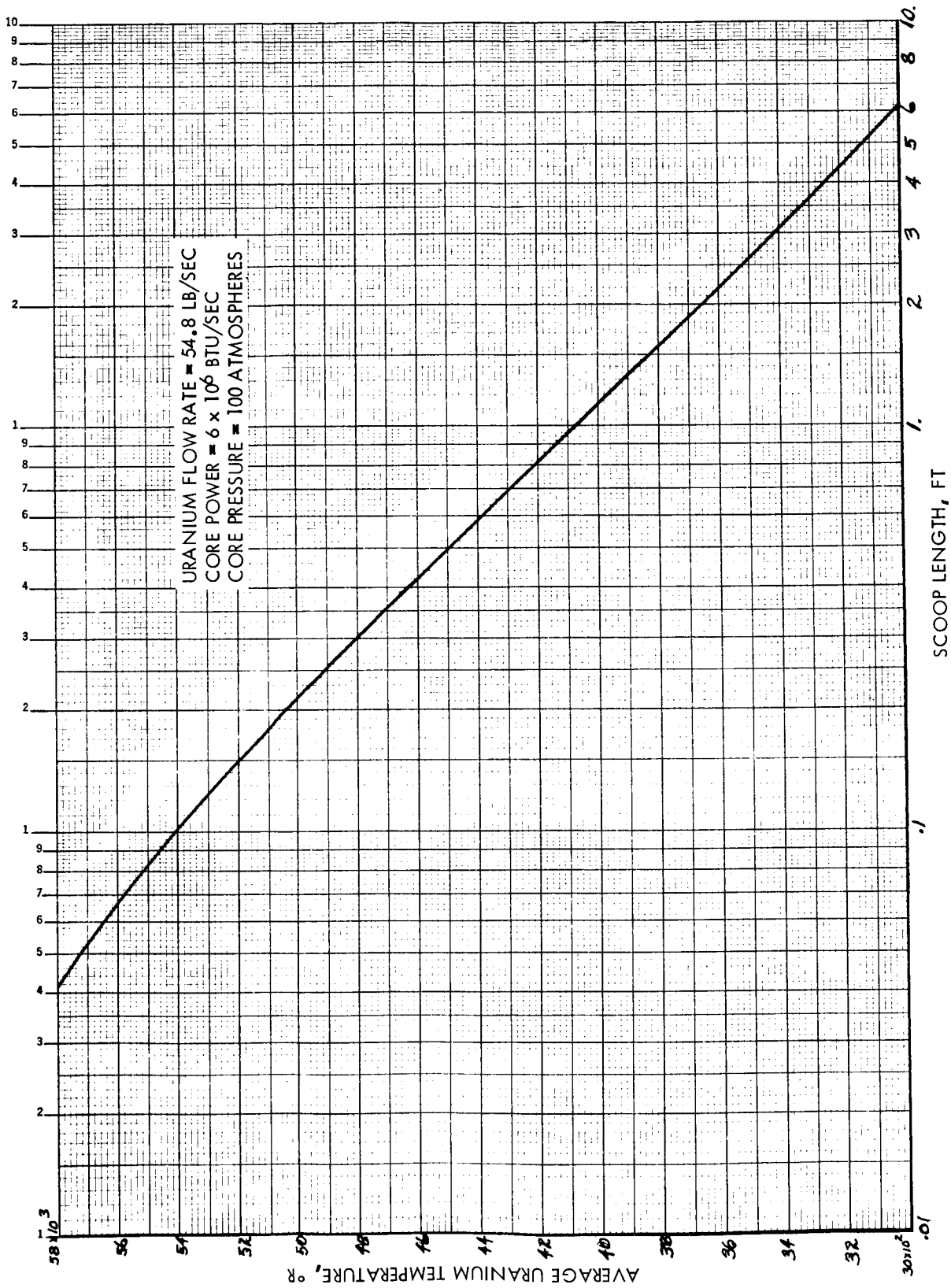


Figure 5-36 Average Uranium Temperature in Scoop

In addition to the hot uranium, the hot hydrogen propellant that diffuses into the uranium and is caught by the scoop must be cooled down by the cool hydrogen. The total amount of cool hydrogen required for the uranium condensation process is thus dependent upon the sum of the mass flow rate weighed enthalpy changes of the hot uranium and the hot hydrogen.

5.2.3.1 Uranium Enthalpy

The enthalpy of the uranium is calculated from the specific heat and ionization fraction of the uranium. Reference 29 states that for a monatomic gas, the translational contributions are the sole contributions to the thermodynamic properties. Thus on a per mole basis

$$C_p = (5/2)R$$

where

$$C_p = \text{specific heat of uranium, } \frac{\text{Btu}}{\text{mole} \cdot ^\circ\text{R}}$$

Thus, the specific heat for uranium on a per pound basis is:

$$C_p = \frac{5}{2} \left(1545 \frac{\text{ft} \cdot \text{lbf}}{\text{mole} \cdot ^\circ\text{R}} \right) \left(1.285 \times 10^{-3} \frac{\text{Btu}}{\text{ft} \cdot \text{lbf}} \right) \left(\frac{1}{235 \text{ lbm/mole}} \right)$$

$$C_p = 0.0211 \frac{\text{Btu}}{\text{lbm} \cdot ^\circ\text{R}}$$

To facilitate heat balance calculations, the quantity of energy necessary to singly, doubly, and triply ionize uranium must be considered. As shown in reference 29 there are two electrons in the outer (Q, 7, 0) shells and one in the (P, 6, 2) shell. References 29 and 30 indicate that the first level ionization potential is about 5.0 ev. The second level is conservatively 10 ev based on data for similar atoms (no data available for uranium). Thus, to singly ionize a uranium atom requires the removal of one of the two electrons in the outer shell and the expenditure of the following quantity of energy:

$$\Delta H_{\text{ioniz}}^{(1)} = \frac{0.6024 \times 10^{24} \left(\frac{\text{atoms}}{\text{gm-mole}} \right) 5 \text{ (ev/atom)} 1.5188 \times 10^{-22} \left(\frac{\text{Btu}}{\text{ev}} \right) 453.6 \left(\frac{\text{gm}}{\text{lbm}} \right)}{235 \left(\frac{\text{gm}}{\text{gm-mole}} \right)}$$

$$\Delta H_{\text{ioniz}}^{(1)} = 880 \frac{\text{Btu}}{\text{lbm}}$$

To doubly ionize a uranium atom requires the removal of both of the electrons in the outer shell or:

$$\Delta H_{\text{ioniz}}^{(2)} = 1760 \frac{\text{Btu}}{\text{lbm}}$$

To triply ionize a uranium atom necessitates the removal of both the electrons in the outer shell, plus the removal of the second level electron or:

$$\Delta H_{\text{ioniz}}^{(3)} = 3520 \frac{\text{Btu}}{\text{lbm}}$$

The fractions of singly, doubly, and triply ionized uranium from reference 32 are shown as a function of temperature for 100 atm and 1000 atm pressure in figure 5-37 and 5-38.

The enthalpy of uranium as a function of temperature is calculated as follows:

$$H_2 = H_1 + (C_p (T_2 - T_1) + (\alpha_2 - \alpha_1)^{(1)} 880 + (\alpha_2 - \alpha_1)^{(2)} 1760 + (\alpha_2 - \alpha_1)^{(3)} 3520$$

where

H = enthalpy of uranium, $\frac{\text{Btu}}{\text{lbm}}$

C_p = specific heat of uranium, $\frac{\text{Btu}}{\text{lbm} \cdot ^\circ\text{R}}$

T = temperature of interest, $^\circ\text{R}$

α = ionization fraction, unitless

subscript: 1 = base value at temperature T_1

2 = value at temperature of interest T_2

Assuming that the enthalpy H_1 at temperature $T_1 = 3000^\circ\text{R}$ is zero, the equation becomes,

$$H_2 = \Delta H_{\text{vap}} \text{ (for } T_2 > 6800^\circ\text{R)} + 0.0211 (T_2 - 3000) - \alpha_2^{(1)} 880 + \alpha_2^{(3)} 3520$$

Using a value of 775 Btu/lbm for the uranium vaporization enthalpy change, ΔH_{vap} the enthalpy of uranium at 100 and 1000 atm pressure is shown in figure 5-39 as a function of temperature.

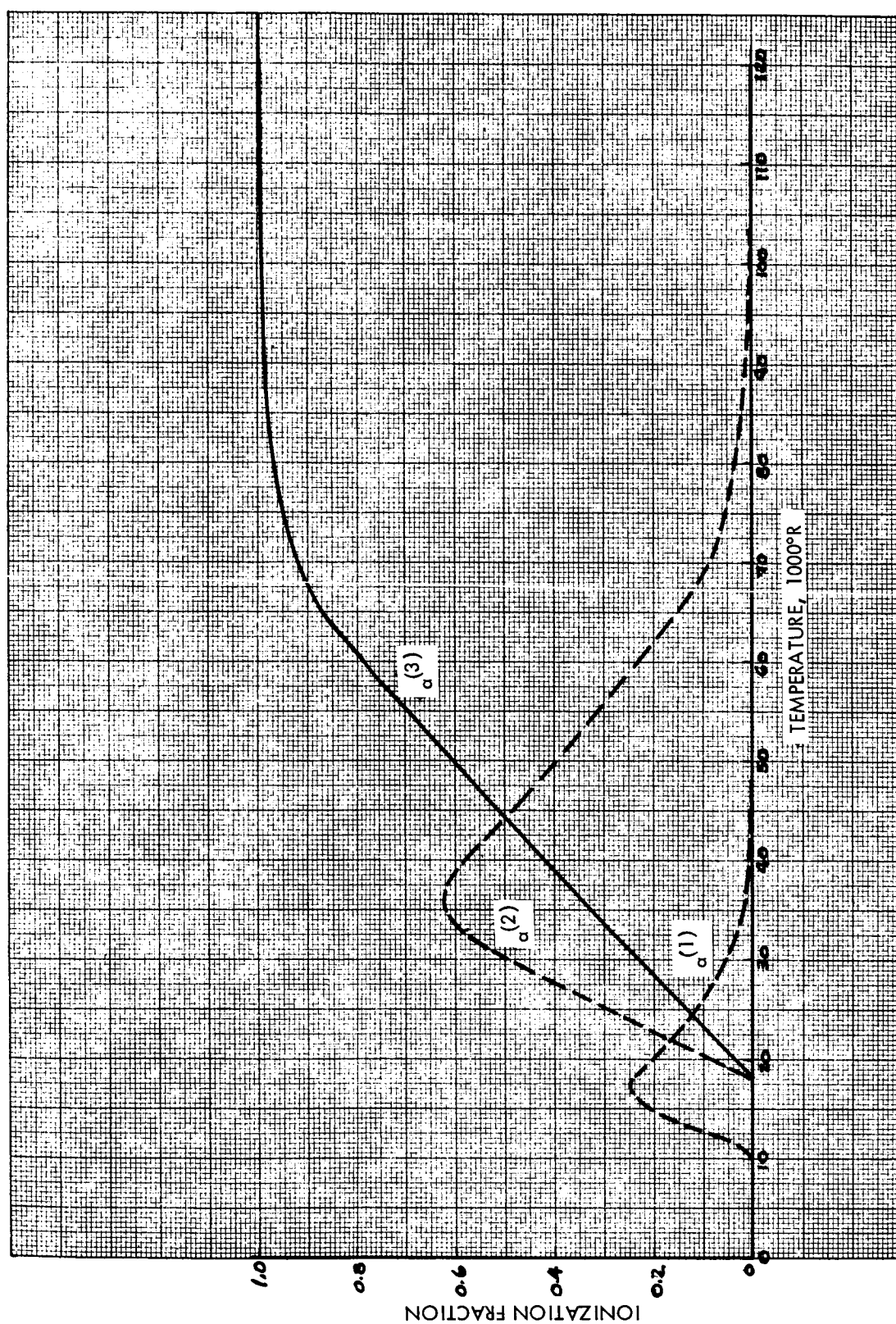


Figure 5-37 Ionization Fraction for Uranium at 100 Atm

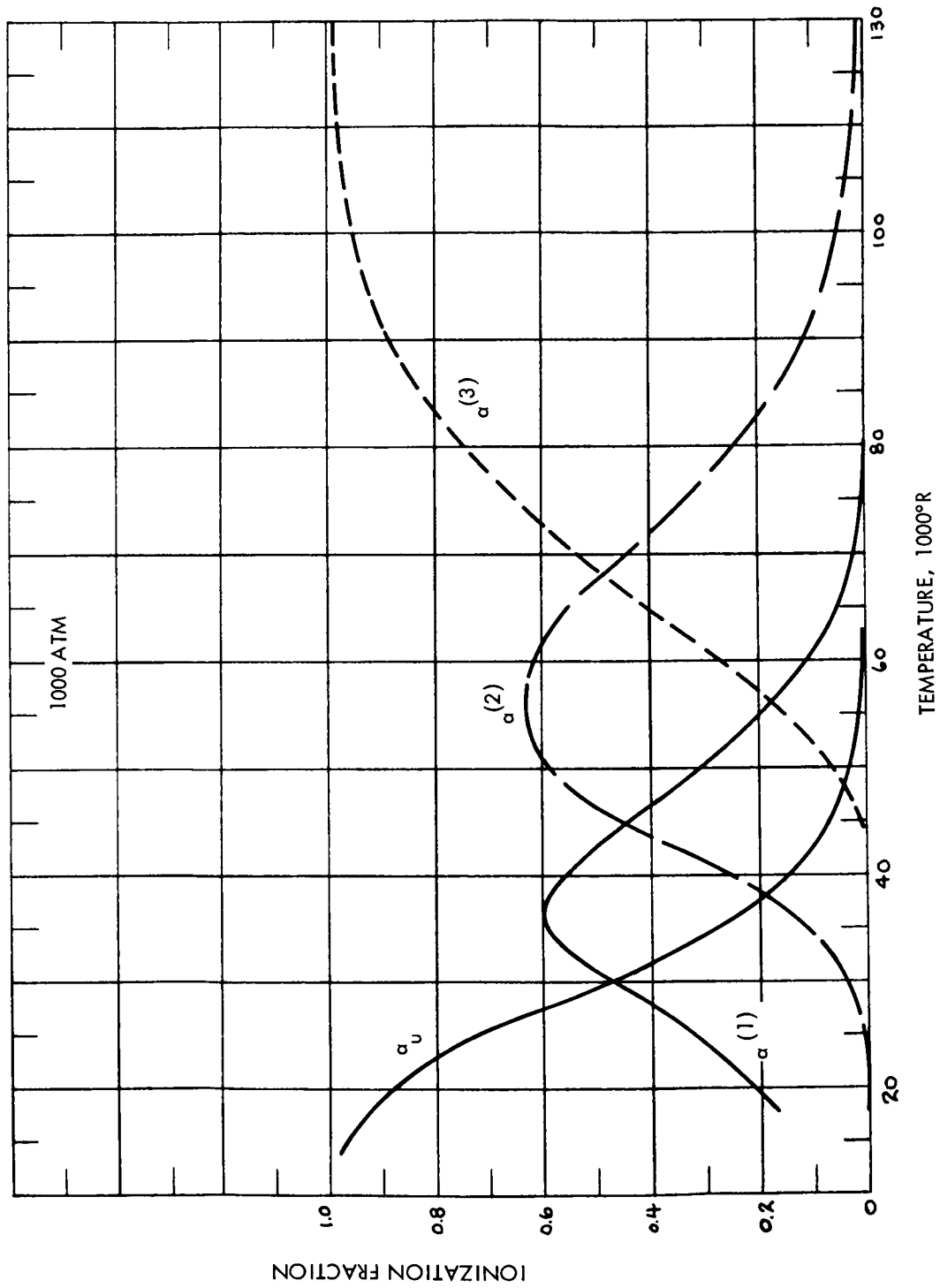


Figure 5-38 Ionization Fraction for Uranium

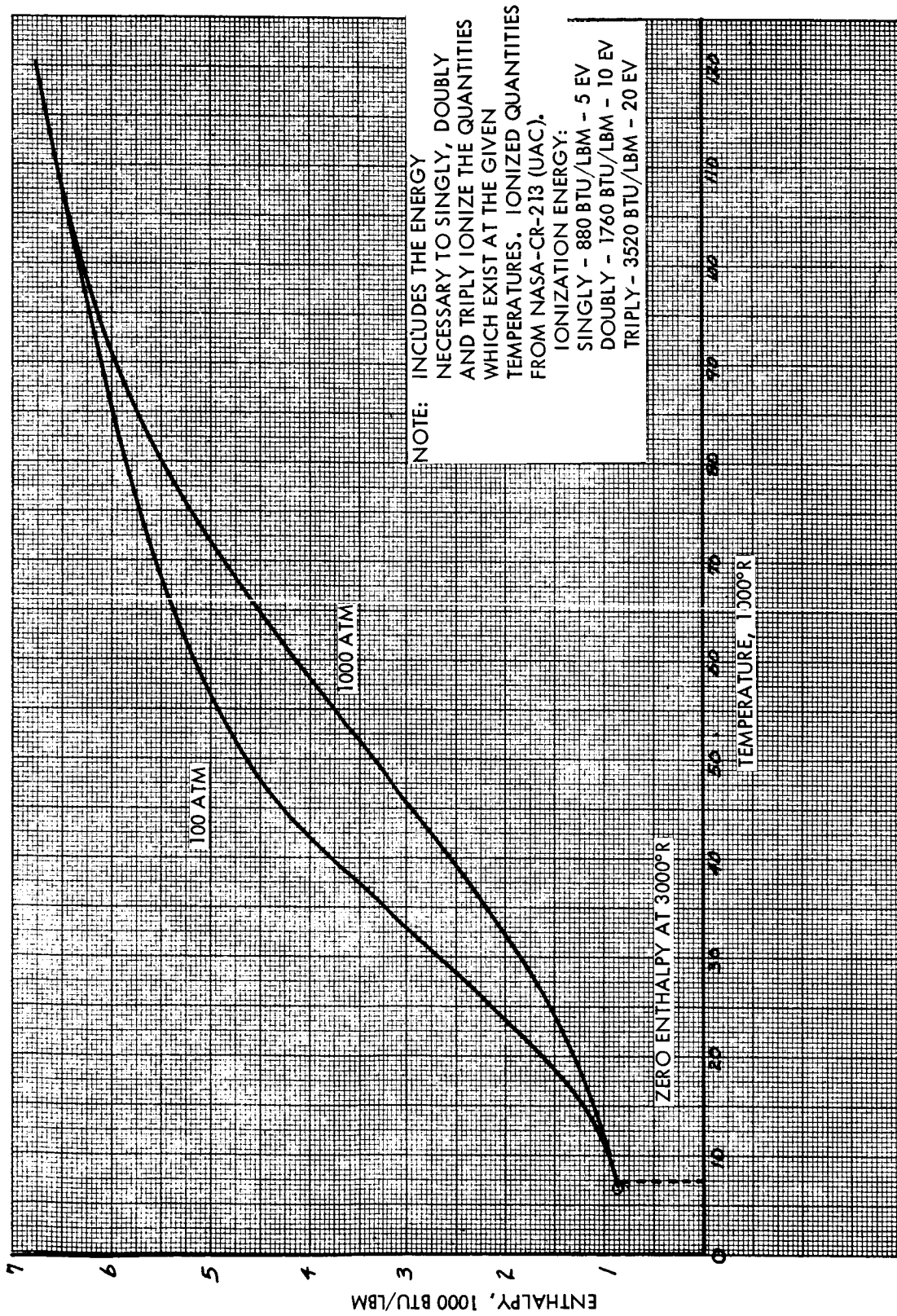


Figure 5-39 Enthalpy of Uranium

5.2.3.2 Hydrogen Enthalpy

The enthalpy of hydrogen as a function of temperature and pressure is given in tabular form in reference 33 . Since the uranium is condensed and cooled to a temperature of 3000°R , the hydrogen propellant that diffuses into the uranium and is caught by the scoop must also be cooled down to a temperature of 3000°R . . Figure 5-40 shows the curves for the hydrogen enthalpy change experienced in decreasing the hydrogen temperature from a specified temperature down to 3000°R .

5.2.3.3 Hydrogen Cooling Requirements

The quantity of cold hydrogen (500°R) required for the uranium condensation process is determined from the following energy balance:

$$\dot{m}_{\text{Hc}} \Delta H_{\text{Hc}} = \Delta H_{\text{u}} \dot{m}_{\text{u}} (f_{\text{u}}) + \Delta H_{\text{Hh}} \dot{m}_{\text{Hh}} (f_{\text{H}})$$

where

- \dot{m}_{Hc} = mass flow rate of cold (500°R) hydrogen, lbm/sec
- ΔH_{Hc} = enthalpy increase of cold hydrogen, Btu/lbm
- ΔH_{u} = enthalpy decrease of uranium, Btu/lbm
- \dot{m}_{u} = total mass flow rate of uranium entering the reactor, lbm/sec
- f_{u} = fraction of uranium caught in scoop, unitless
- ΔH_{Hh} = enthalpy decrease of hot hydrogen, Btu/lbm
- \dot{m}_{Hh} = total mass flow rate of hydrogen entering the reactor, lbm/sec
- f_{H} = fraction of hydrogen caught in scoop, unitless

The above equation can be written in the following form to obtain the total cold hydrogen mass flow rate per pound of hydrogen propellant entering the reactor cavity:

$$\frac{\dot{m}_{\text{Hc}}}{\dot{m}_{\text{Hh}}} = \frac{\Delta H_{\text{u}}}{\Delta H_{\text{Hc}}} \frac{\dot{m}_{\text{u}}}{\dot{m}_{\text{Hh}}} (f_{\text{u}}) + \frac{\Delta H_{\text{Hh}}}{\Delta H_{\text{Hc}}} (f_{\text{H}})$$

Obviously for the gas core reactor design to be feasible, the value of $\dot{m}_{\text{Hc}}/\dot{m}_{\text{Hh}}$ must be less than 1.0.

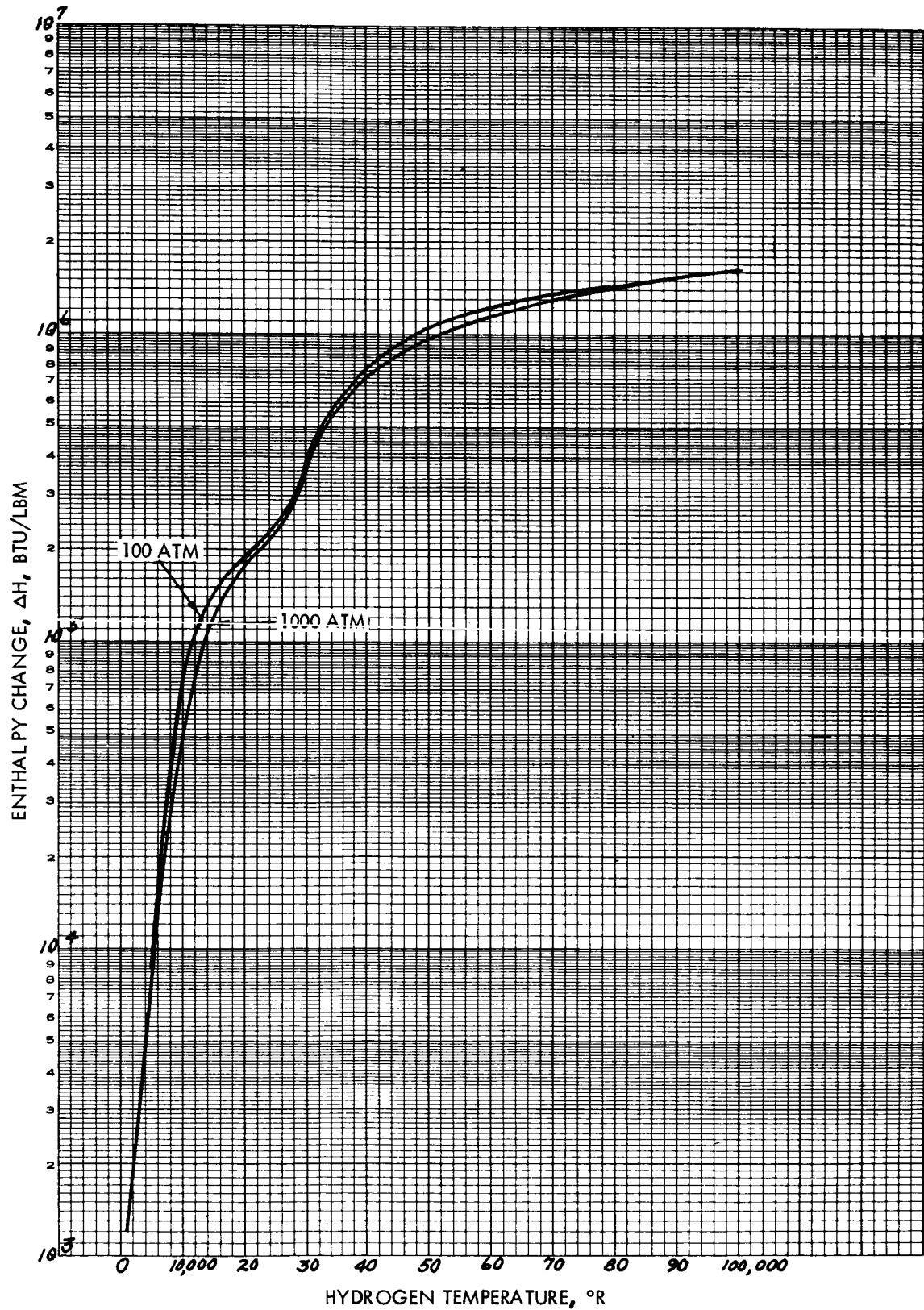


Figure 5-40 Enthalpy Change Required to Cool Hydrogen From
a Specified Temperature to 3000°R
5-65

Assuming that the hydrogen is initially at a temperature of 500°R , the enthalpy change required to increase the temperature to the equilibrium temperature of 3000°R is 9,125 Btu/lbm from reference 34. Figure 5-41 shows the ratio of $\Delta H_{\text{Hh}} / \Delta H_{\text{Hc}}$ as a function of the hot hydrogen temperature. The ratio of $\Delta H_{\text{Hh}} / \Delta H_{\text{Hc}}$ represents the pounds of cold hydrogen required to cool down one pound of hot hydrogen from a given temperature to 3000°R . The fraction of hot hydrogen entering the scoop, f_{H} , is shown in figure 5-42 as a function of scoop diameter.

The fraction of uranium that enters the scoop is shown in figure 5-43. For the purposes of the hydrogen cooling requirement calculations, f_{u} , may be taken to be 1.0. The ratio of $\dot{m}_{\text{u}} / \dot{m}_{\text{Hh}}$ affects the hydrogen exit temperature. From a series of computer runs on the Lewis Research Center Gas Core Computer Program, it was found that a ratio of $\dot{m}_{\text{u}} / \dot{m}_{\text{Hh}}$ equal to about 2/3 results in about the maximum hydrogen temperature at the core exit, with little hydrogen diffusion into the fissioning uranium column.

The hydrogen transpiration coolant entering the scoop can be neglected for this calculation since it is assumed that the transpiration hydrogen enters the scoop at 3000°R . Since the final temperature of the uranium-hydrogen mixture is at 3000°R , there is no net enthalpy change in the transpiration hydrogen after the transpiration coolant leaves the surface of the scoop wall.

Figure 5-44 gives the pounds of cold hydrogen per pound of hot hydrogen entering the reactor cavity and the total cold hydrogen mass flow rate that is required to condense and cool the uranium to a temperature of 3000°R as a function of scoop diameter. The curve in figure 5-44 is based upon the assumption that the diffused hydrogen is in equilibrium with the uranium near the interior surface of the scoop. For the purposes of the calculation, it was assumed that the average temperature of the diffused hydrogen could be represented by the uranium temperature at a radial distance of 1.490 feet. This results in an average diffused hydrogen temperature of $16,000^{\circ}\text{R}$. As discussed in more detail in the gas core pressure profile section of the report, the cold hydrogen is mixed with the hot gaseous uranium in the jet pump in order to provide a pressure increase in the uranium cycle.

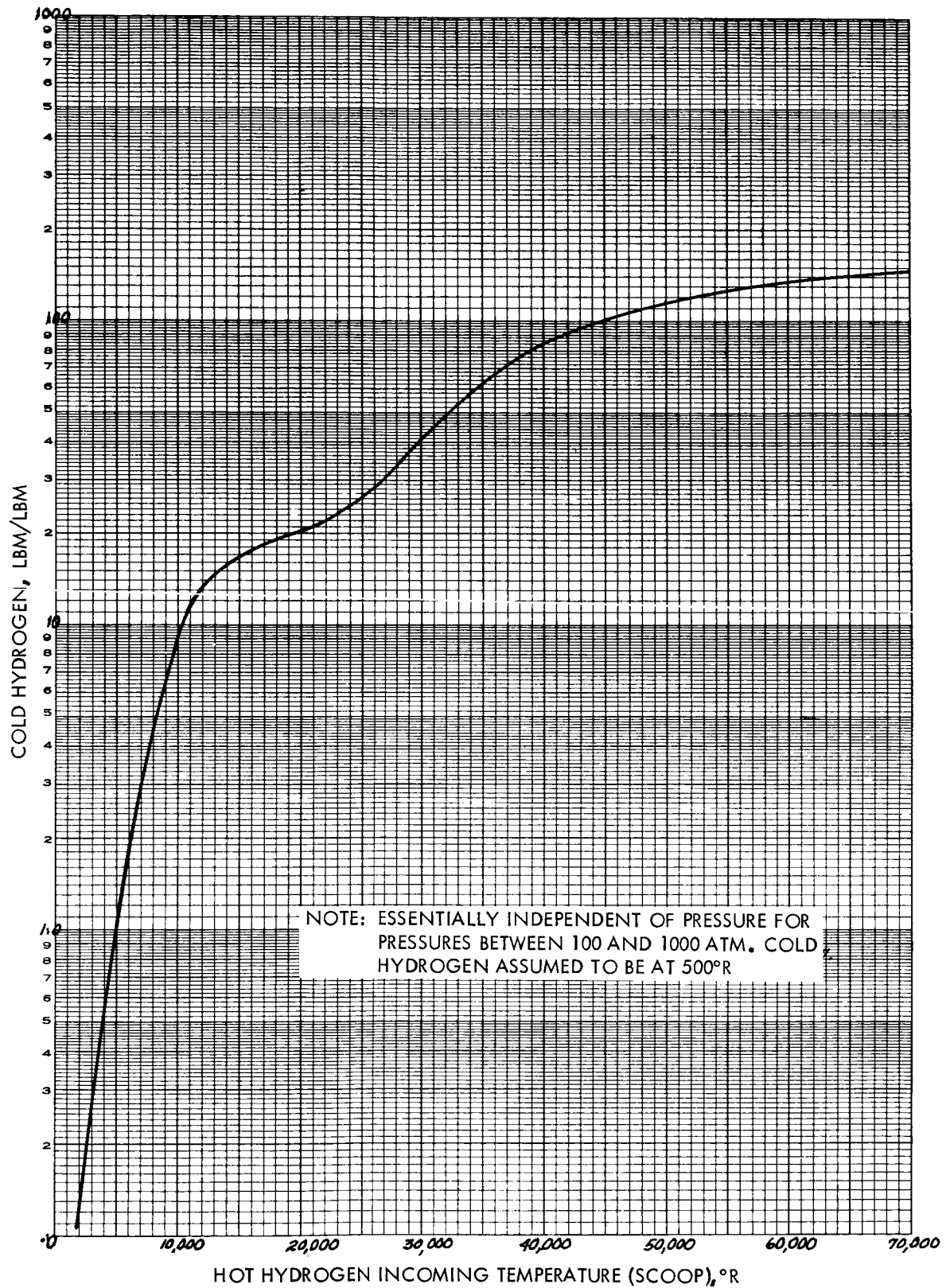


Figure 5-41 Cold Hydrogen Required to Hot Hydrogen From
a Specified Temperature Down to 3000°R
5-67

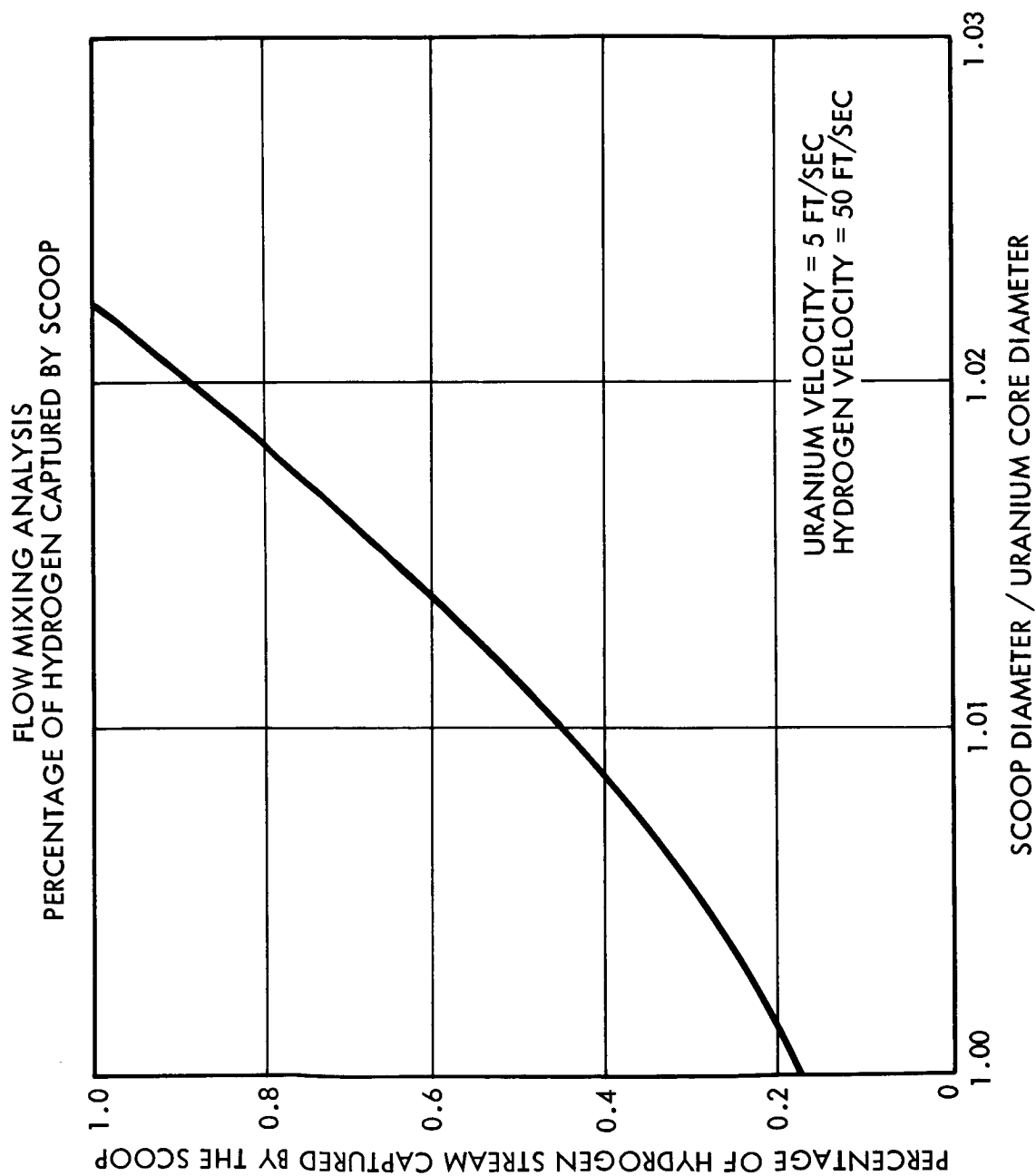


Figure 5-42 Hydrogen Diffusion Rate at the Scoop Entrance

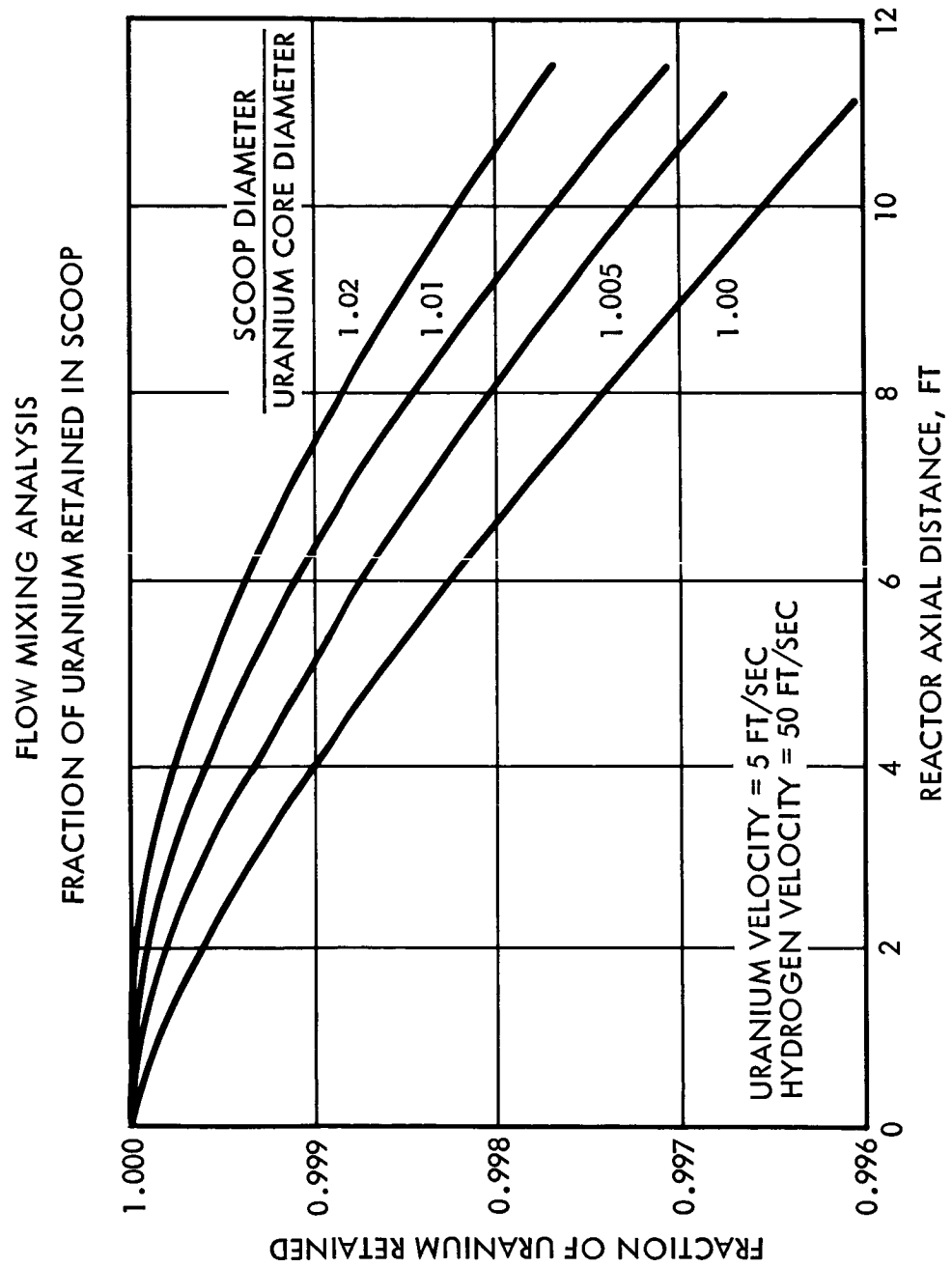


Figure 5-43 Uranium in the Scoop as a Function of Distance Between Scoop Leading Edge and Reactor Inlet

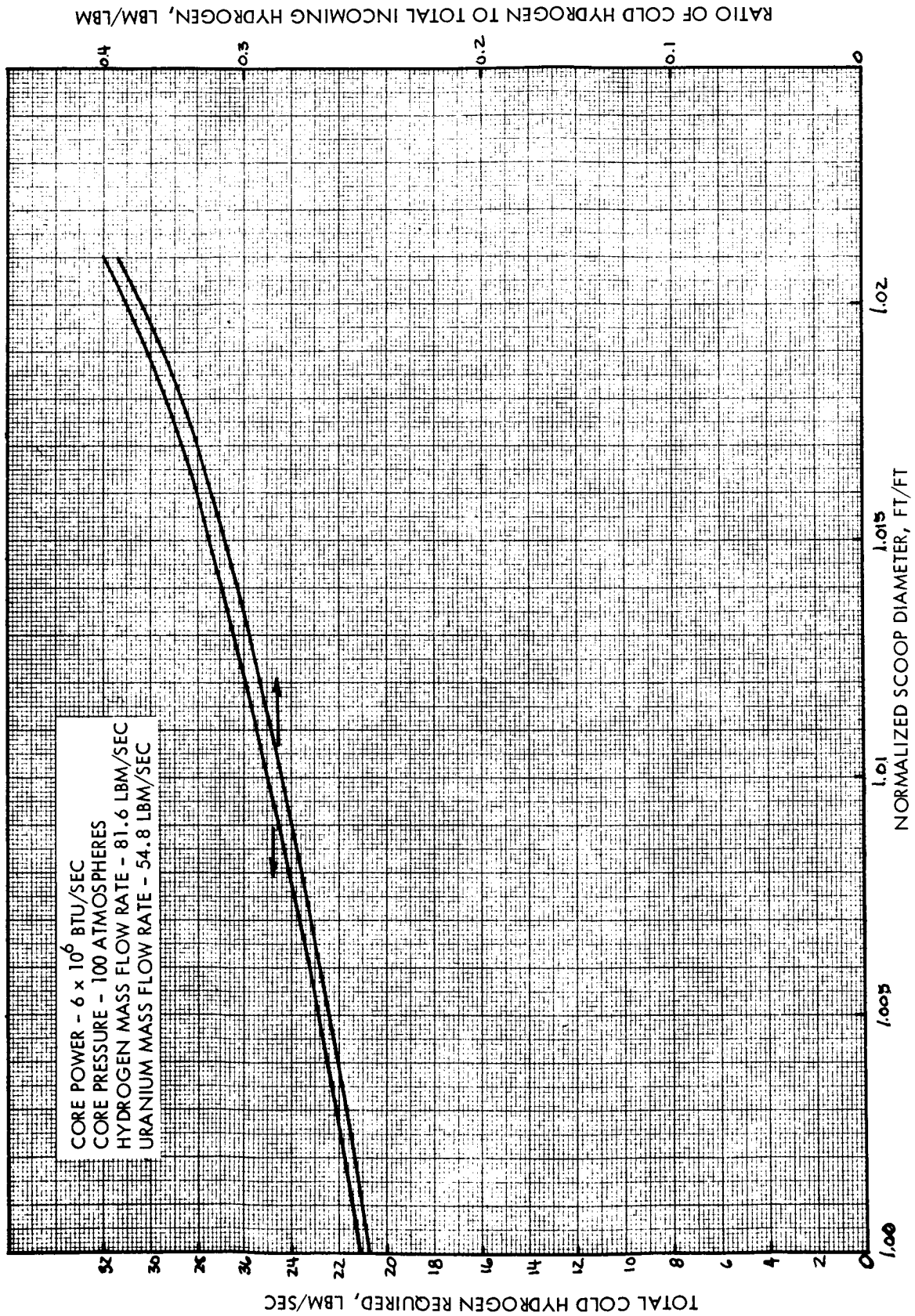


Figure 5-44 Gross Mixing Coolant Requirements

5.2.3.4 Uranium Condensation as a Function of Core Power

A preliminary investigation of the uranium condensation cooling requirements as a function of core thermal power can be obtained by assuming that the diffusion rates for the uranium and hydrogen remain constant as the core thermal power is varied. This assumption allows the utilization of figures 5-42 and 5-43 for the fractions of hydrogen and uranium, respectively, that are caught in the scoop.

The primary parameter that is affected by changes in core thermal power is the average temperature of the uranium at the scoop inlet. Figure 5-45 shows various uranium temperature distributions at the scoop inlet as a function of core thermal power. These uranium temperature distributions are for relatively low core thermal power levels resulting from some of the initial investigations in the gas core study. By extrapolating the mass flow rate weighed average uranium temperature, as obtained from figure 5-45, it is possible to obtain the average uranium temperature at the scoop inlet as a function of core thermal power. This curve of the average uranium temperature is shown in figure 5-46.

From figure 5-46 it is observed that the uranium average temperature at the end of the 3-ft scoop increases only slightly as the core thermal power is increased quite significantly. Thus, by utilizing figure 5-46 and table 5-2, it is possible to obtain the uranium condensation cooling requirements as a function of core thermal power. For the calculations, it is assumed that the average temperature of the hydrogen at the scoop exit is equal to the product of the hydrogen average temperature (for the base line case discussed in the previous section) and the ratio of uranium average temperatures at the scoop exit for the two power levels or,

$$T_H = T_{H_o} \left(\frac{T_u}{T_{u_o}} \right) = 16,000 \left(\frac{T_u}{34,200} \right) = 0.468 T_u$$

where

T_H = average diffused hydrogen temperature at scoop exit, °R

T_{H_o} = hydrogen temperature for the original calculation, °R

T_u = average uranium temperature at the scoop exit, °R

T_{u_o} = uranium temperature for the original

Utilizing the calculational methods employed in the previous section, the uranium condensation cooling requirements as a function of core thermal power are obtained and are presented in figure 5-47.

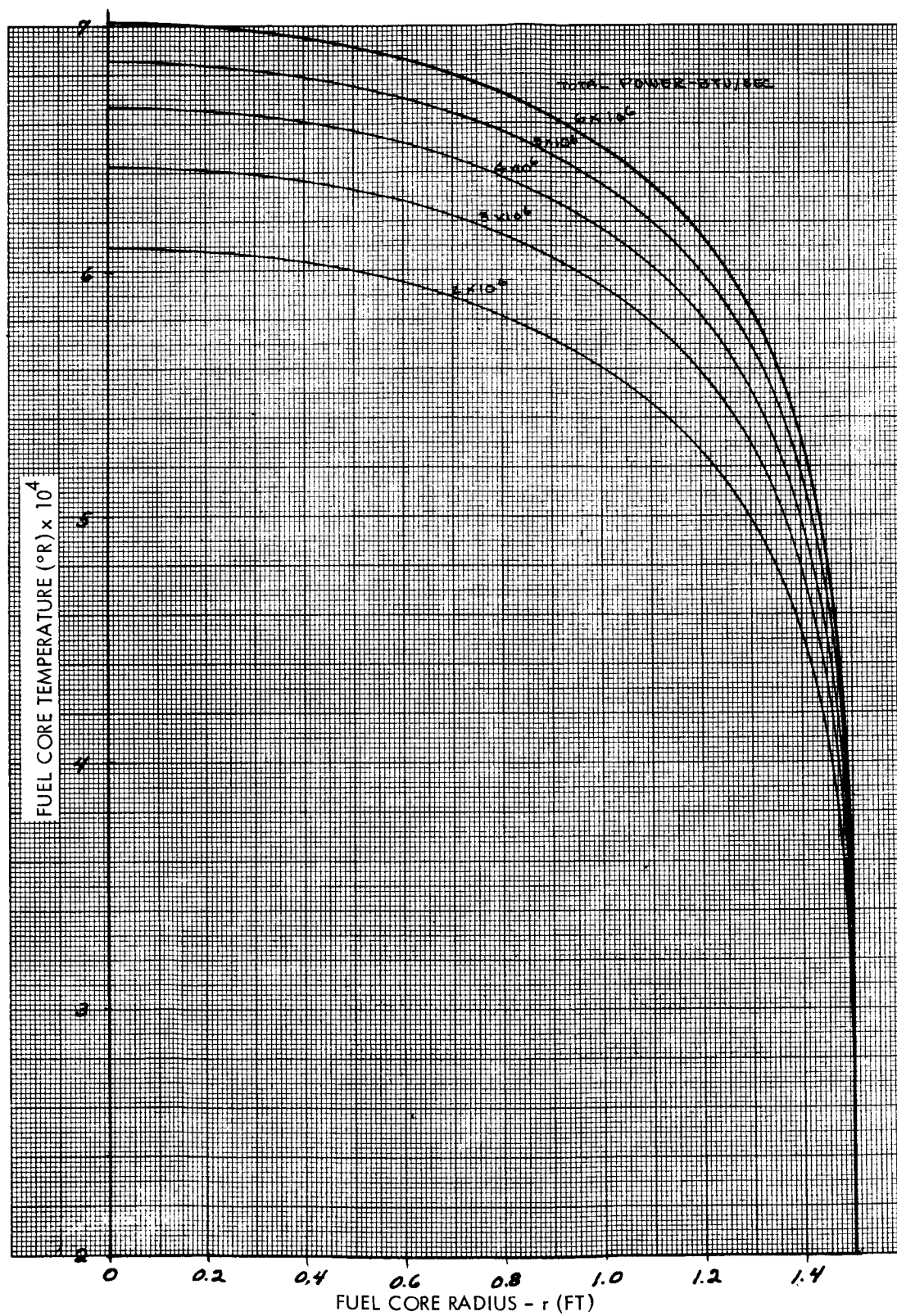


Figure 5-45 Uranium Core Steady-State Temperature Distributions
(for different heat sources)

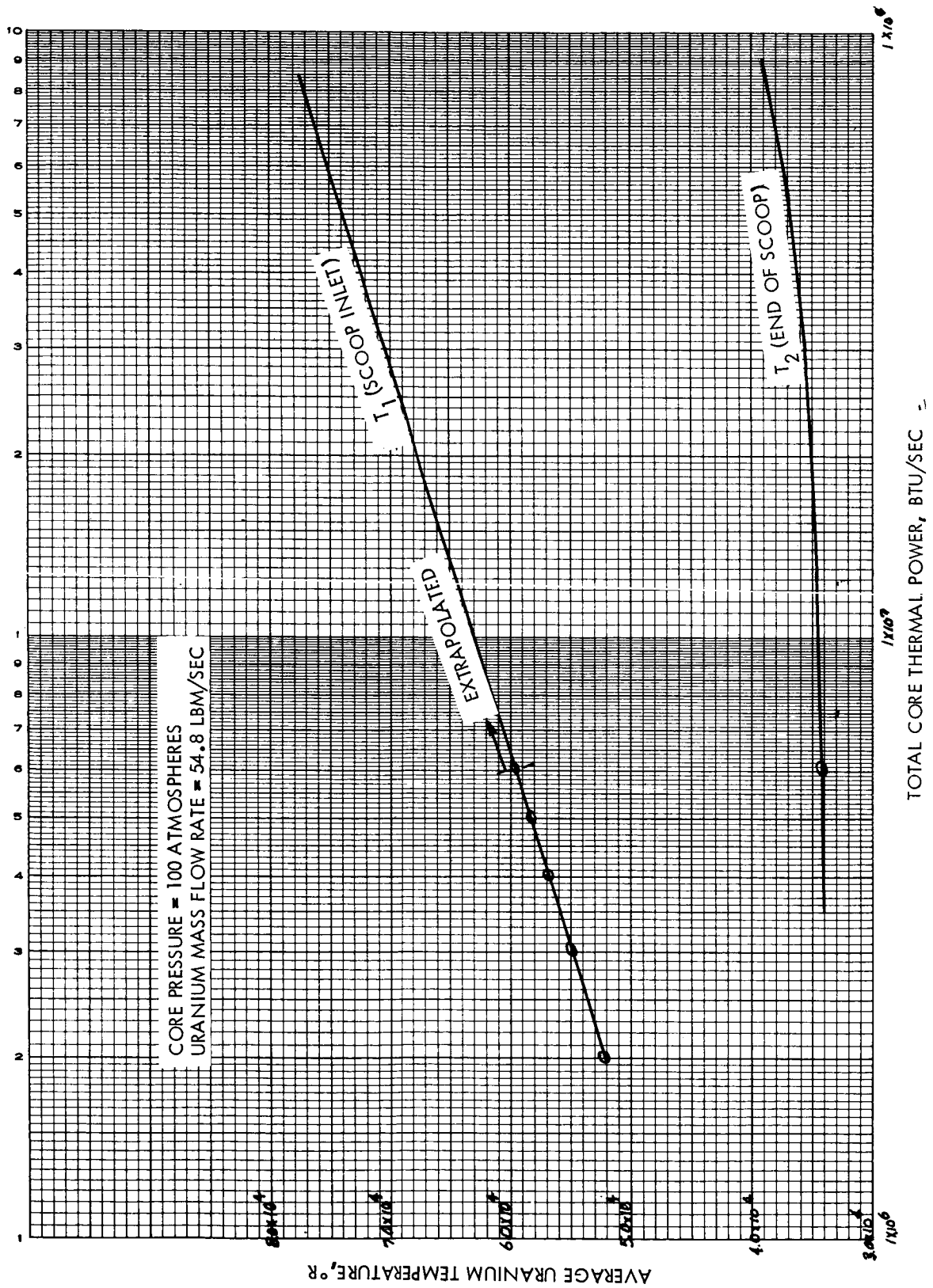


Figure 5-46 Average Uranium Temperature at Scoop Inlet and Exit as a Function of Core Thermal Power

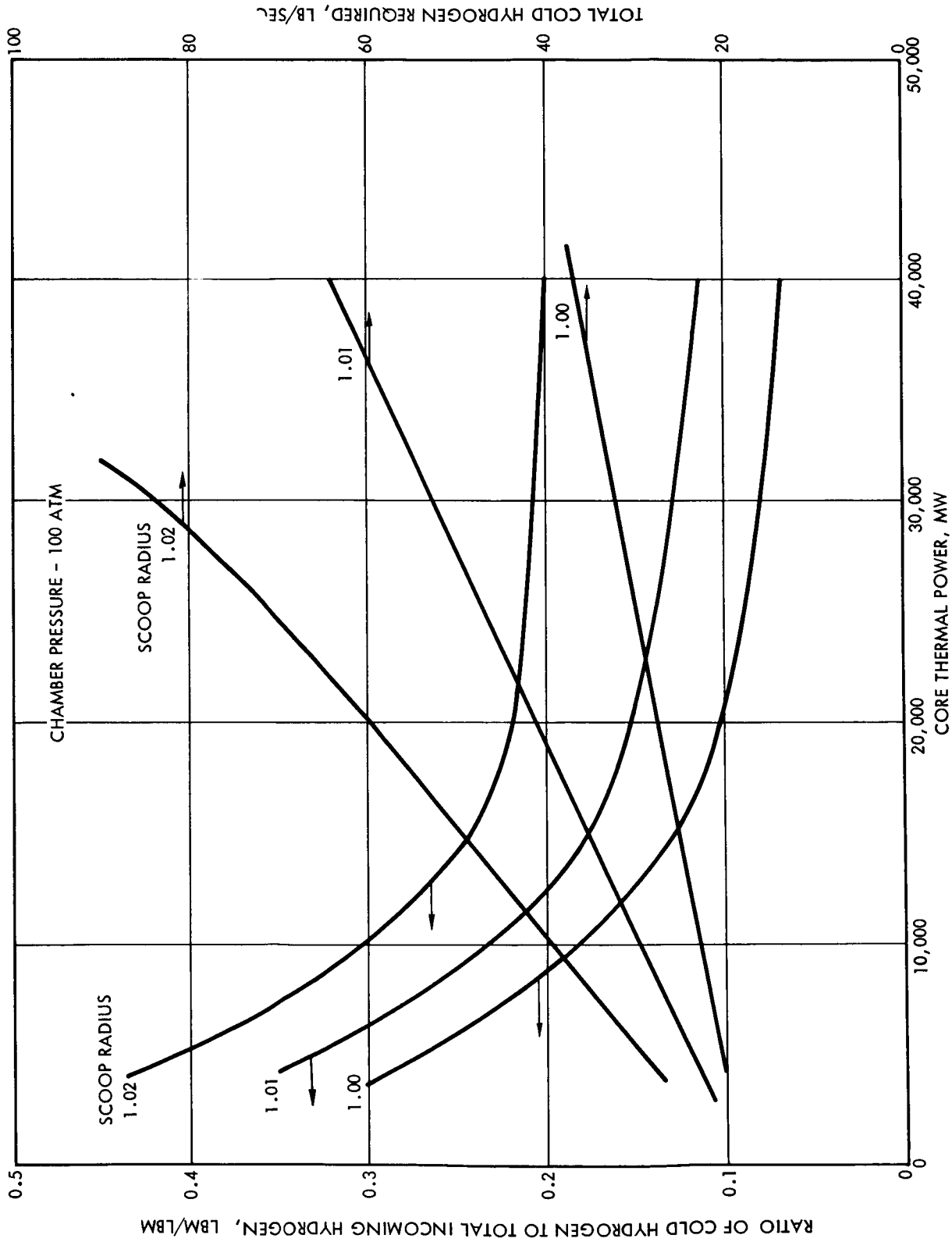


Figure 5-47 Hydrogen Coolant Requirement for Uranium Condensation in Scoop

5.3 ENGINE COMPONENT WEIGHTS

A preliminary parametric analysis of the various component weights is presented in this section. The weights of the components are obtained as functions of the component dimensions, local operating pressure, allowable material stress, material density, propellant mass flow rate, and core thermal power. The major components of a gaseous core nuclear rocket engine include the total uranium fuel inventory, graphite reflector, beryllium-oxide reflector, pressure vessel, radiation shield, nozzle, turbopump, propellant and uranium feed lines, thrust structure, scoop, hydrogen-uranium separator, tank valve assembly, diagnostic instrumentation system, pneumatic system, and control system. The techniques employed to evaluate the weight of each of these major engine components are discussed in the following paragraphs.

5.3.1 Total Uranium Inventory

The total uranium inventory for a gaseous core nuclear rocket engine is equal to the critical mass plus the uranium losses plus the uranium present in the external fuel cycle loop. Since the above quantities of uranium are not exactly known, an additional 20 percent is added to conservatively estimate the total uranium inventory. The total uranium inventory can be represented by the following expression (30 minute burn time assumed):

$$M_u = \left[M_{\text{crit}} + (\dot{m}_l) (1800) + M_{\text{ex}} \right]^{1.2}$$

where

M_u = total uranium inventory at launch, lbm

M_{crit} = critical mass of uranium, lbm

\dot{m}_l = mass flow rate loss of uranium, lbm/sec

M_{ex} = uranium present in the external loop, lbm

The critical mass is obtained from nucleonic considerations. The uranium mass loss per unit time is determined by the scoop diameter and the diffusion characteristics of the uranium. The uranium present in the external loop of the uranium cycle can be approximated by the product of the total flow volume of the external loop and the average density of the uranium in the external loop. The total flow volume is equal to the volume of the scoop, condensor-separator, and the uranium return line. Thus, the total uranium inventory can be approximated by utilizing the above procedure.

5.3.2 Reflector Weight

The reflector for the gaseous core reactor is composed of two regions. The inner region, nearest the gaseous core, is a graphite reflector. The outer reflector region, between the graphite reflector and the pressure vessel, is composed of beryllium-oxide. Figure 5-48 shows the relation of the two reflector regions and also the scaled schematic used to determine the weight of the reflector.

5.3.2.1 Graphite Region

As shown in figure 5-48, the graphite reflector region can be considered to be composed of a right circular cylinder with a circular disk at one end and a hollow cone at the other end. The weight of the graphite reflector region is simply:

$$W_{gr} = (V_{gr}) (\rho_{gr}) (1 - f_{gr})$$

where

W_{gr} = weight of the graphite reflector, lb.

V_{gr} = total volume of the graphite reflector, ft³

f_v = void fraction of the graphite reflector

ρ_{gr} = density of the graphite, lb/ft³

The total volume of the graphite reflector is given as the sum of the volume of the cylinder, disk and cone, or:

$$V_{gr} = V_{cy} + V_d + V_{co} = \pi L (t^2 + 2R_i t) + \pi (R_i + t)^2 t + \pi h t (t + r_{Bi} + r_{bi})$$

$$V_{gr} = \pi t \left[(t + 2R_i) L + (R_i + t)^2 + h (t + r_{Bi} + r_{bi}) \right]$$

where

t = thickness of graphite reflector, ft.

R_i = inside radius of the graphite reflector, ft.

L = length of the right circular cylinder, ft.

h = height of the nozzle converging cone, ft.

r_{Bi} = inside radius of the cone major base, ft.

r_{bi} = inside radius of the cone minor base, ft.

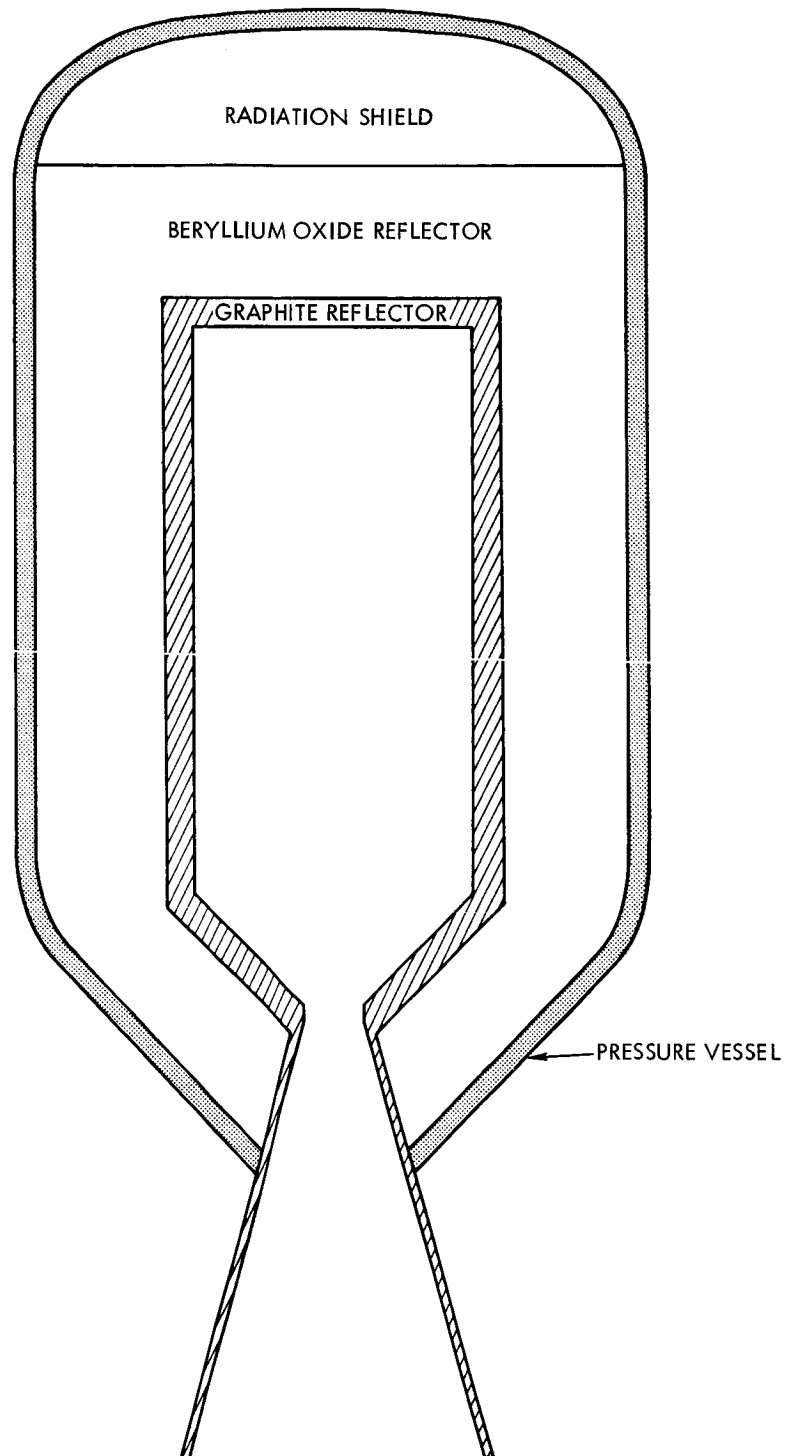


Figure 5-48 Model Used for Reflector Weight
5-77

From the dimensions of the graphite reflector, the volume is found to be 109.7 ft³. Figure 5-49 shows the graphite reflector weight as a function of the void fraction assuming a graphite density of 96.6 lb/ft³. The value of the void fraction is derived mainly from the reflector cooling requirements.

5.3.2.2 Beryllium-Oxide Region

The beryllium-oxide reflector has a configuration similar to the graphite reflector, i.e., composed of a right circular cylinder, a circular dish and a hollow cone. However, a portion of the diverging nozzle section passes through the beryllium-oxide reflector and necessitates subtracting off this conical void from the beryllium-oxide reflector volume. The conical section of the reflector can thus be considered to be composed of one hollow conical section, one solid conical section, and one void conical section. Figure 5-50 shows the three conical sections.

The weight of the beryllium-oxide reflector is given by the same expression used for the graphite reflector, i.e.,

$$W_{br} = (V_{br}) (\rho_{br}) (1 - f_{vbr})$$

The total volume of the reflector is thus:

$$V_{br} = V_{cy} + V_d + V_{co1} + V_{co2} - V_{co3}$$

$$V_{br} = \pi L (t^2 + 2R_i t) + \pi (R_i + t)^2 t + \pi h_1 t (t + r_{Bi} + r_{bi}) \\ + \frac{\pi h_2}{3} (r_{Bo}^2 + r_{bo}^2 + r_{Bo} r_{bo}) + \frac{\pi h_2}{3} (r_{bo}^2 + r_{bi}^2 + r_{bo} r_{bi})$$

where

subscript o = outside radius.

From the dimensions of the beryllium-oxide reflector, the volume is found to be 1096.6 ft³. Figure 5-49 shows the beryllium-oxide weight as a function of the reflector void fraction for an assumed BeO density of 156.3 lb/ft³.

The total reflector weight, composed of the total graphite weight plus the beryllium-oxide weight, is also shown in figure 5-49, as a function of void fraction.

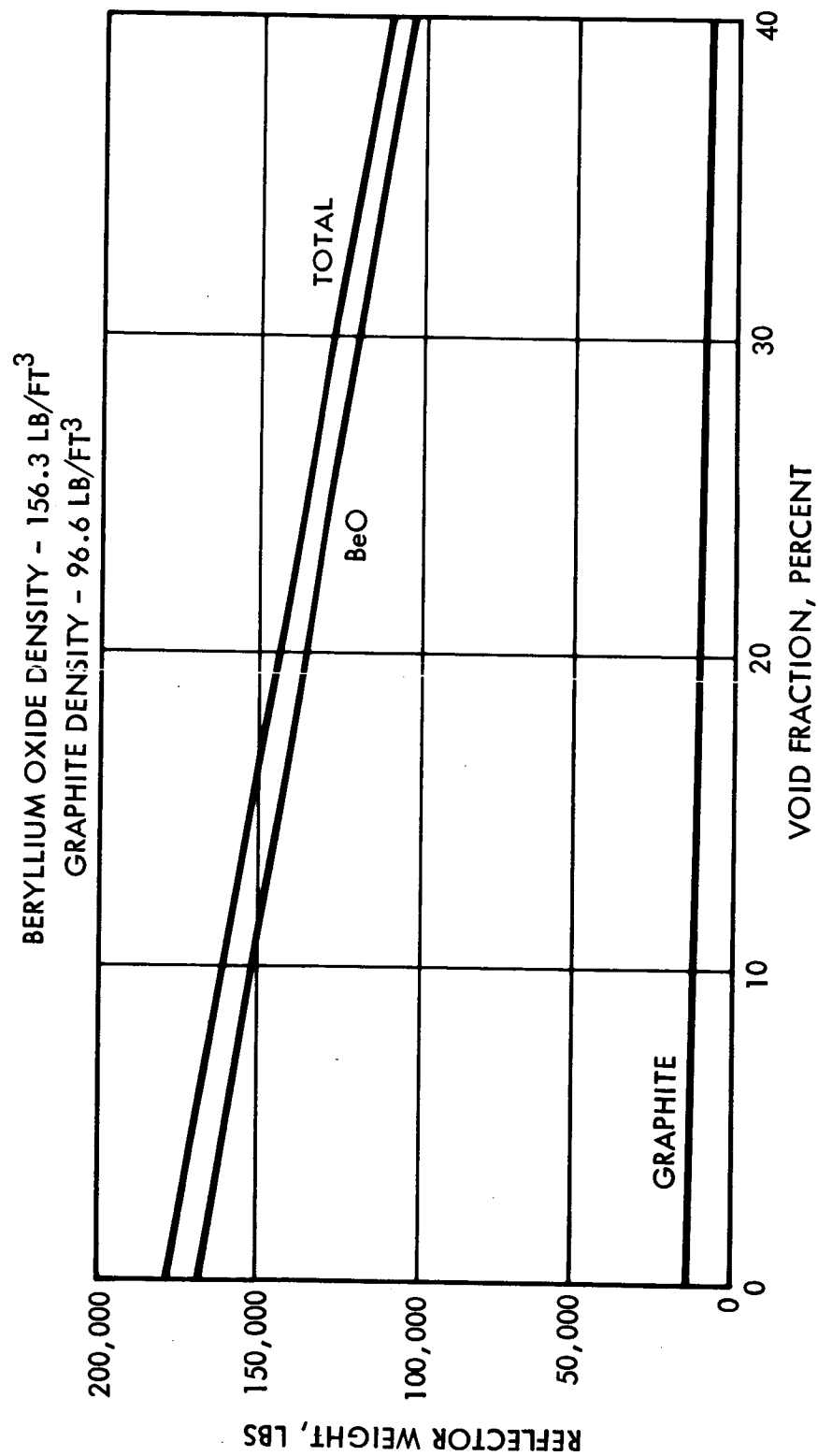


Figure 5-49 Reflector Weight

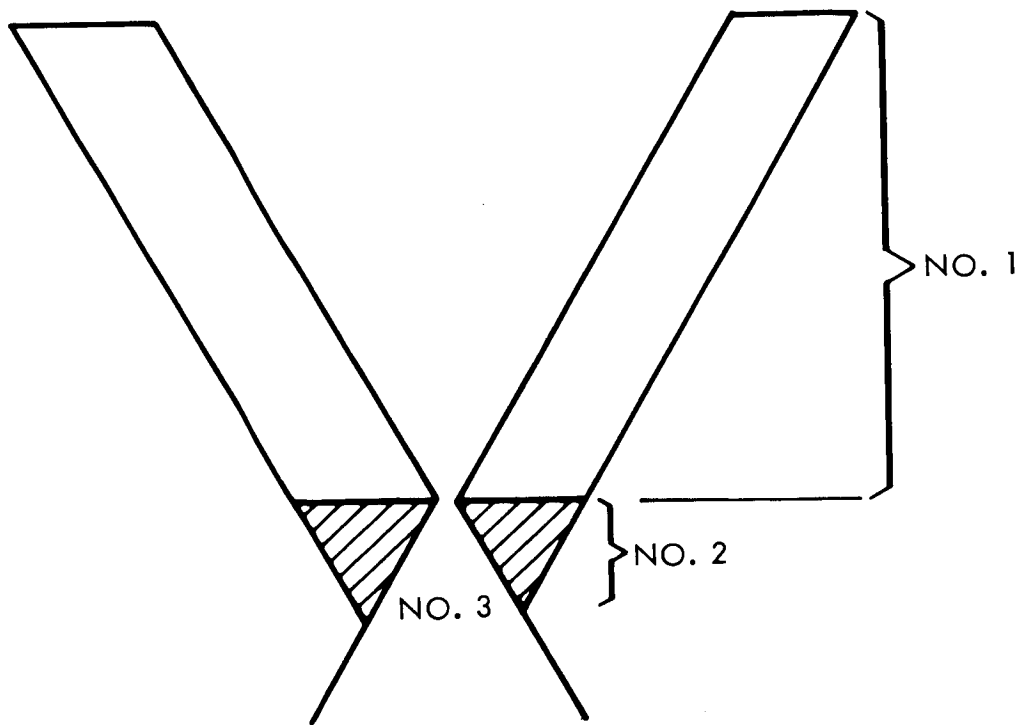


Figure 5-50 Beryllium Conical Section Geometry

5.3.3 Pressure Vessel

The model used for the determination of the pressure vessel weight is shown in figure 5-48. The pressure vessel can be considered to be composed of a right circular cylinder, a hollow 2:1 ellipsoidal dome, and a hollow right circular truncated cone.

Due to the high pressures anticipated in the gas core (100 to 1000 atmospheres) the pressure vessel design is based upon a thick, rather than a thin, pressure shell. The thickness of the pressure vessel is assumed to be the same for the cylindrical, dome, and conical sections. Since the cylinder requires the largest thickness for a specified internal pressure, the thickness of the pressure vessel is taken to be the minimum required thickness for the cylindrical section.

The maximum stress in a thick-walled cylinder due to an internal pressure is given by the following:

$$\sigma_{\max} = \frac{r_o^2 + r_i^2}{r_o^2 - r_i^2} P_i \quad (34)$$

where

$$\begin{aligned}\sigma_{\max} &= \text{maximum stress, psi} \\ r_o &= \text{outside radius of cylinder, ft.} \\ r_i &= \text{inside radius of cylinder, ft.} \\ P_i &= \text{internal pressure, psi}\end{aligned}$$

The outside radius is related to the inside radius and the thickness by:

$$r_o = r_i + t \quad (35)$$

where

$$t = \text{thickness of the cylinder, ft.}$$

Substituting Equation 35 into Equation 34 and solving for the required thickness yields the following equation:

$$t = \sqrt{\frac{2}{r_i} + 2r_i^2 / \left(\frac{\sigma}{P_i} - 1 \right)} - r_i$$

Figure 5-51 shows the pressure vessel thickness as a function of the internal pressure and the allowable tensile stress for the designed inside radius of 5.287 ft.

The weight of the pressure vessel is obtained from the following expression:

$$W_{pv} = (V_{\text{dome}} + V_{\text{cyl}} + V_{\text{cone}}) \rho_{pv} \quad (36)$$

where

$$\begin{aligned}V_i &= \text{volume of pressure vessel section } i, \text{ ft}^3 \\ \rho_{pv} &= \text{density of the pressure vessel material, lb/ft}^3\end{aligned}$$

The volume of the cylindrical section is given by,

$$V_{\text{cyl}} = \pi L(t^2 + 2R_i t) \quad (37)$$

where

$$R_i = \text{inside radius of the cylindrical cavity}$$

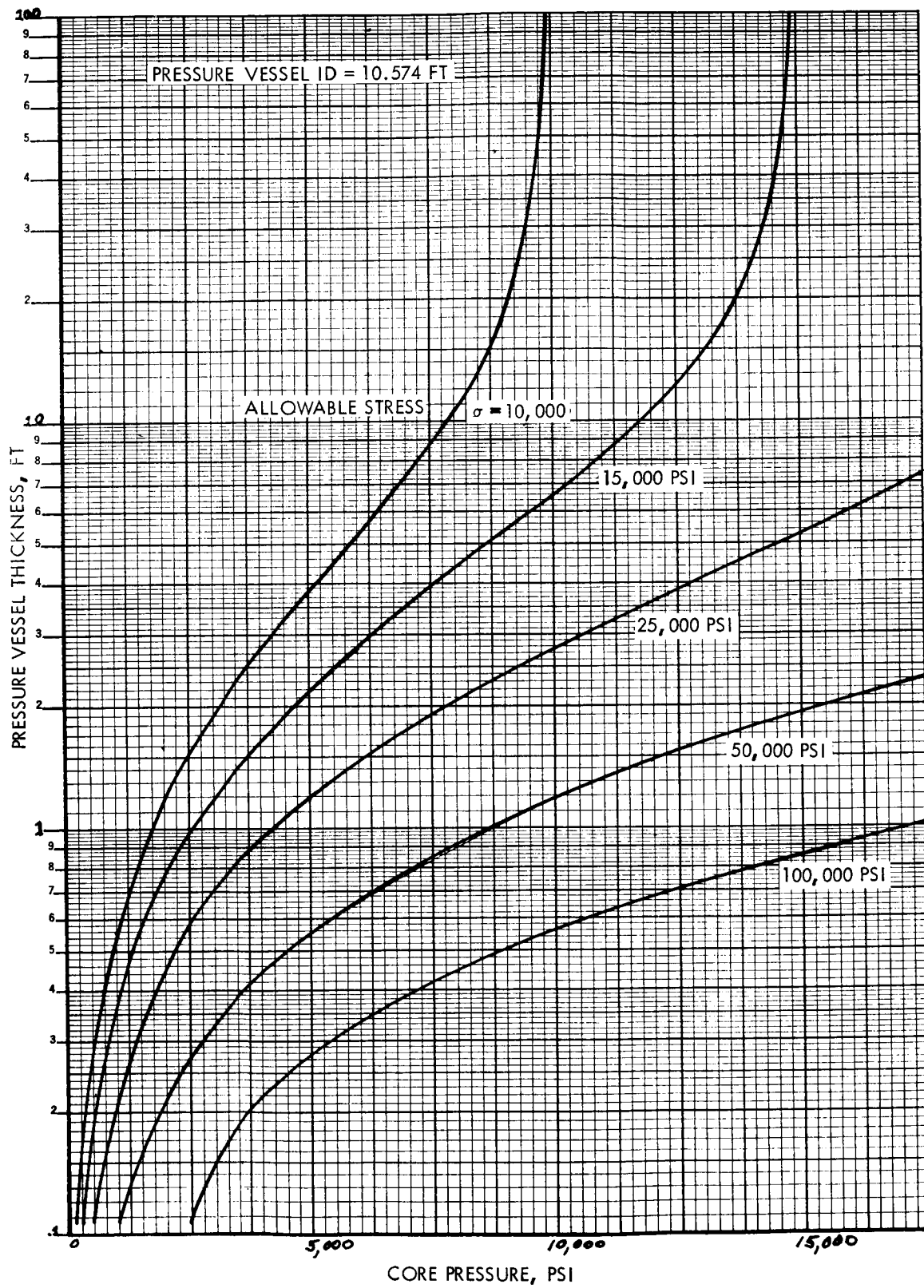


Figure 5-51 Pressure Vessel Thickness as a Function of
Core Pressure and Allowable Stress

The volume of the hollow oblate 2:1 ellipsoidal dome is given by,

$$V_{\text{dome}} = \frac{4}{3} \pi t \left(t^2 + \frac{5}{2} R_i t + 2R_i^2 \right) \quad (38)$$

The volume of the hollow cone is given by,

$$V_{\text{cone}} = \pi h t (t + r_{Bi} + r_{bi}) \quad (39)$$

Combining Equations 36 , 37 , 38 , and 39, the weight of the pressure vessel is given as the following:

$$W_{pv} = \pi t \rho_{pv} \left[(t + 2R_i) L + \frac{4}{3} \left(t^2 + \frac{5}{2} R_i t + 2R_i^2 \right) + h (t + r_{Bi} + r_{bi}) \right]$$

Figure 5-52 shows the ratio of the pressure vessel weight to density as a function of the internal pressure and allowable tensile strength.

5.3.4 Radiation Shield Weight

The radiation shield requirement is controlled by the allowable temperature rise in the propellant tank. The nuclear radiation impinging on the propellant tank and absorbed in the propellant increases the propellant temperature and causes an increase in the propellant boil-off rate. The allowable nuclear radiation heat flux out of the radiation shield is related to the allowable temperature rise in the propellant tank and the propellant exit mass flow rate by the following equation:

$$Q_{\text{tot}} = T_{\text{max}} \dot{m}_{\text{tot}} C_p \text{ Btu/ft}^2\text{-sec}$$

where

$$Q_{\text{tot}} = \text{total allowable nuclear radiation heat flux, Btu/ft}^2\text{-sec}$$

$$T_{\text{max}} = \text{propellant maximum allowable temperature rise, } ^\circ\text{R}$$

$$\dot{m}_{\text{tot}} = \text{total propellant exit mass flow rate, lb/sec}$$

$$C_p = \text{propellant heat capacity, } \frac{\text{Btu}}{\text{lb/ft}^2 \text{ } ^\circ\text{R}}$$

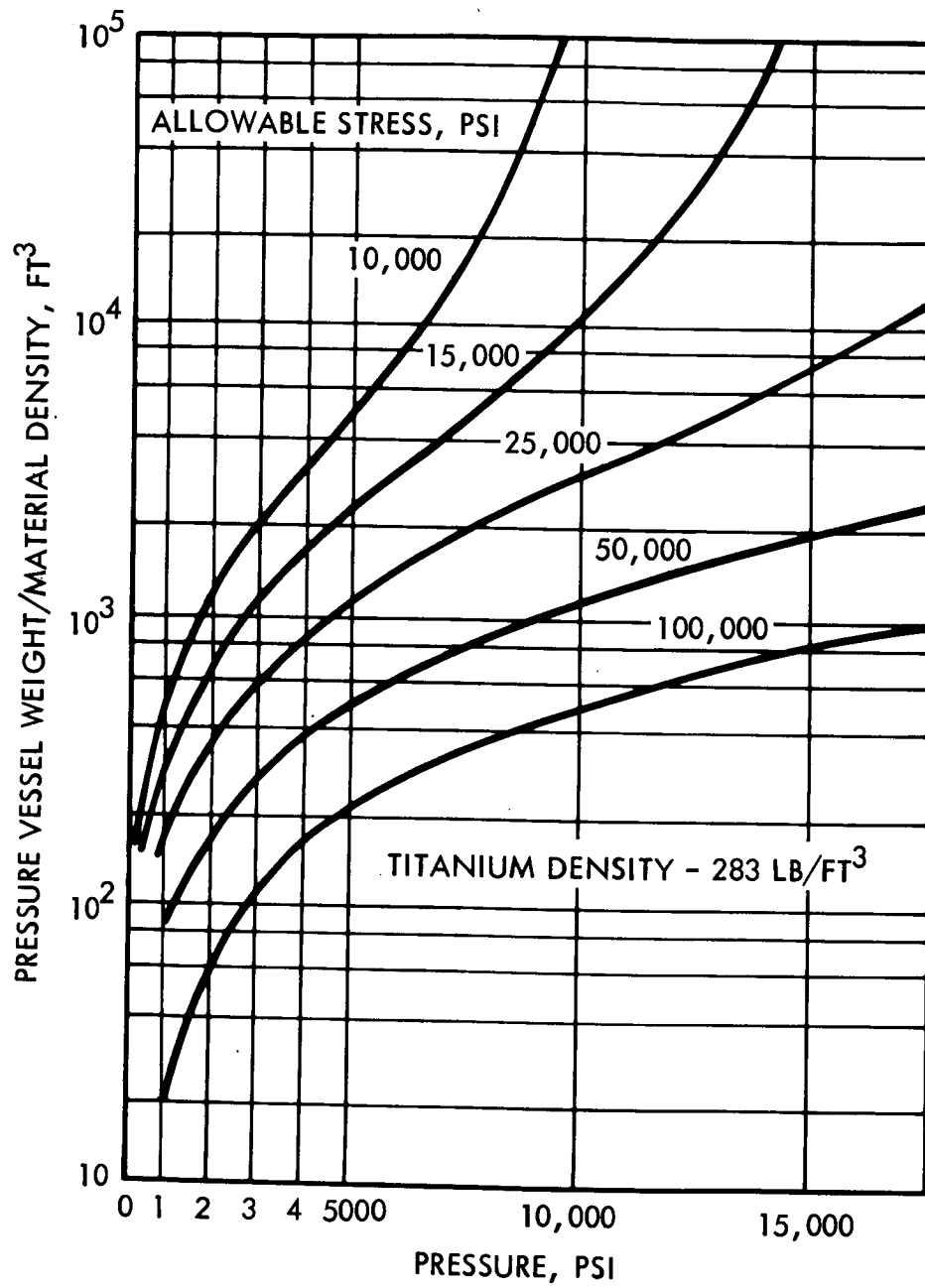


Figure 5-52 Pressure Vessel Weight
5-84

An estimation of the radiation shield thickness required for the gas core reactor can be determined by obtaining a correlation with the data used for the NERVA type solid core reactor. Volume IV of the TRW Systems report "Mission Oriented Advanced Nuclear Systems Parameter Study", (reference 41) contains the necessary data to obtain a corresponding radiation shield thickness for the gas core reactor.

Assuming that T_{\max} and C_p are the same for the NERVA and gas core stored hydrogen propellant, the allowable heat flux out of the gas core radiation shield is related to the heat flux out of the NERVA reactor by the ratio of the total mass flow rates; (subscript N = NERVA, G = Gas Core).

$$Q_{Go} = \frac{\dot{m}_G}{\dot{m}_N} Q_{No} \quad (40)$$

where

$$Q_o = \text{heat flux out of the radiation shield, } \frac{\text{Btu}}{\text{ft}^2\text{-sec}}$$

$$\dot{m} = \text{total exit mass flow rate, lb/sec.}$$

The radiation heat flux leaving the radiation shield is related to the radiation heat flux impinging on the radiation shield by the following expression:

$$Q_{Go} = Q_{GI} e^{-\mu T_G} \quad (41)$$

where

$$Q_I = \text{impinging heat flux, Btu/ft}^2\text{-sec}$$

$$\mu = \text{energy absorption cross-section, ft}^{-1}$$

$$T = \text{thickness of the radiation shield, ft}$$

From figure IV-4 of reference 41, μ is calculated to be approximately 3.36 ft^{-1} .

$$\mu = \frac{\ln(60/300)}{.36 - .84} = 3.36 \text{ ft}^{-1}$$

It is assumed that the flux impinging on the radiation shield is proportional to the core power, thus

$$Q_{GI} = Q_{NI} \frac{P_G}{P_N} \quad (42)$$

where

$$P = \text{reactor thermal power, MW}$$

A reasonable value of Q_{NI} for a power level of 100 MW is given by figure IV-4 of reference 41 to be approximately 500 Btu/ft²-sec (1680/3.36 = 500).

The thickness of the radiation shield, as a function of the gas core reactor power level, can be obtained by combining Equations 40, 41, and 42.

$$T_G = - \frac{1}{\mu} \ln \left(\frac{\dot{m}_G}{\dot{m}_N} \frac{Q_{No}}{Q_{NI}} \frac{P_N}{P_G} \right)$$

From figure IV-4 in reference 41, $Q_{No} = 30/3.36 = 9$ Btu/ft²-sec. The NERVA engine total mass flow rate is 67 lb/sec for a reactor thermal power of 1100 MW. Substituting in the numerical values for the known parameters, Equation 43 is simplified to the following expression:

$$T_G = - .298 \ln \left(.296 \frac{\dot{m}_G}{P_G} \right), \text{ ft.}$$

The weight of the radiation shield is given by,

$$W_{rs} = (T_G) (A) (\rho_{rs}), \text{ lb}$$

where

$$T_G = \text{thickness of the radiation shield, ft.}$$

$$A = \text{area of the radiation shield, ft}^2$$

$$\rho_{rs} = \text{density of the radiation shield material, lb/ft}^3$$

The radiation shield weight as a function of the total mass flow rate and the core thermal power is shown in figure 5-53. The radiation shield weights shown in figure 5-53 are calculated for a material density of 177.8 lb/ft³ and are determined assuming the shield is a circular dish with a 5.287 ft. radius.

5.3.5 Nozzle Weight

The nozzle is composed of three major components; the nozzle coolant annulus, the nozzle jacket, and the nozzle torus. An estimation of the total weight of the nozzle may be obtained by simply summing the weights attributed to each of the three major components. The weights of the nozzle components are calculated separately because the materials and, thus, the densities for each of the components are different, making it difficult to determine the total nozzle weight in a straight forward manner.

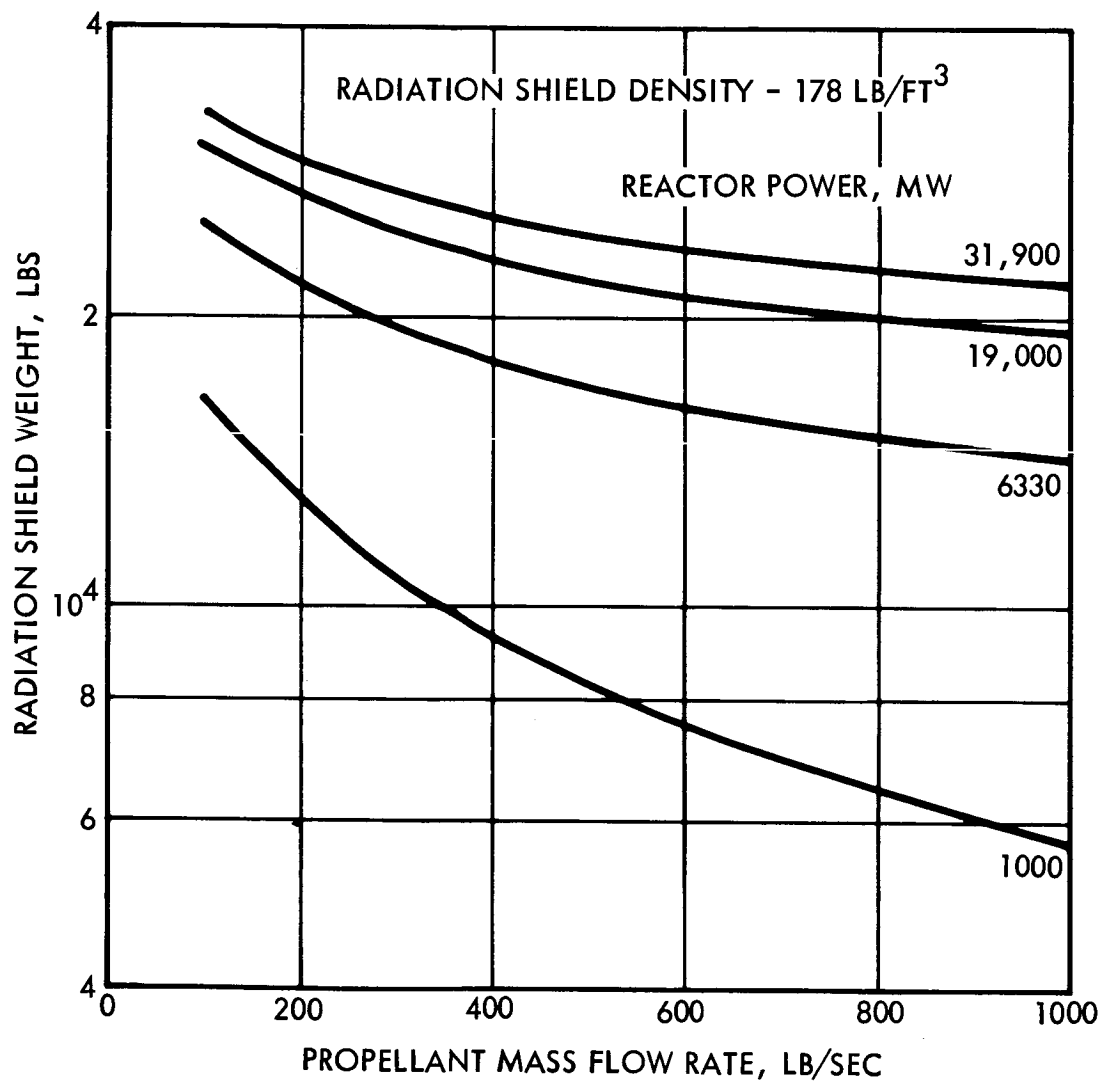


Figure 5-53 Radiation Shield Weight

5.3.5.1 Nozzle Coolant Annulus Weight

The function of the nozzle coolant annulus is to provide a path for transporting the cold hydrogen propellant through the entire nozzle structure so that the propellant can regeneratively cool and transpiration cool the nozzle structural material. The annulus wall material is necessarily thin to maximize the heat removal effectiveness of the hydrogen coolant. Figure 5-54 shows a schematic of the divergent section of the truncated nozzle cone used as a guide to calculate the weight of the nozzle annulus. The volume of the truncated hollow cone is given by the following equation:

$$V_{an} = \pi h t (t + r_B + r_t) \quad (44)$$

where

$$V_{an} = \text{volume of the annulus region of the cone, ft}^3$$

$$h = \text{axial length of the nozzle divergent section, ft.}$$

$$t = \text{radial thickness of the annulus wall material, ft.}$$

$$r_B = \text{inside radius at the base of the nozzle, ft.}$$

$$r_t = \text{inside radius of the nozzle throat, ft.}$$

The expansion ratio of the nozzle is defined as the ratio of the nozzle area at the point of interest to the nozzle throat radius. The overall expansion ratio of the nozzle is thus:

$$\epsilon = \frac{\pi r_B^2}{\pi r_t^2} = \frac{r_B^2}{r_t^2}$$

where

$$\epsilon = \text{the nozzle overall expansion ratio}$$

therefore

$$r_B = r_t \sqrt{\epsilon} \quad (45)$$

The axial length of the nozzle divergent section is related to the overall expansion ratio and the divergent cone half-angle by the following relation:

$$h = \frac{r_t (\sqrt{\epsilon} - 1)}{\tan \Theta}$$

where

$$\Theta = \text{the divergent cone half-angle, degrees}$$

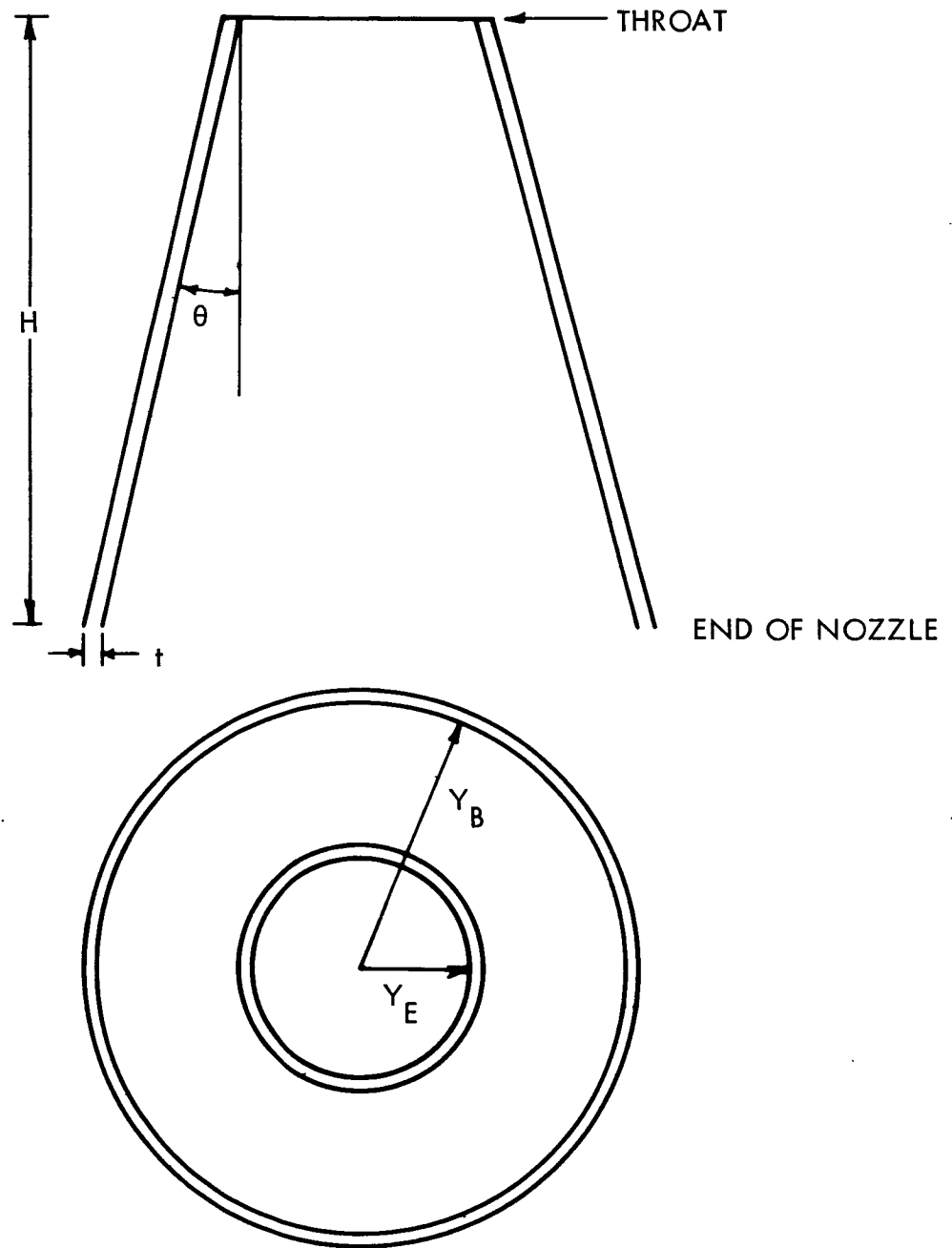


Figure 5-54 Nozzle Divergent Section Geometry

Substituting Equations 45 and 46 into Equation 44 , the expression for the volume of the annulus region becomes the following:

$$V_{an} = \frac{\pi r_t^2 (\sqrt{\epsilon} - 1) t}{\tan \Theta} (t + r_t + r_t \sqrt{\epsilon}) \quad (47)$$

Figure 5-55 shows the nozzle annular weight divided by the material density as a function of the nozzle throat radius. The curve shown in figure 5-55 calculated for $\epsilon = 100$, $t = 100$ mils, and $\Theta = 17.5^\circ$.

5.3.5.2 Nozzle Jacket Weight

The nozzle jacket is a structural support member surrounding the coolant flow path in the divergent section of the nozzle. For the purposes of the jacket weight analysis, it is assumed that the jacket thickness is constant and that the jacket thickness depends only on the hoop stress produced by the pressure in the nozzle chamber. The thickness of the jacket is thus given by the following equation:

$$t_j = \frac{P_c r_t}{\sigma_{jw}} \quad (48)$$

where

- t_j = jacket wall thickness, ft.
- r_t = nozzle throat radius, ft.
- P_c = nozzle chamber pressure, psia
- σ_{jw} = jacket wall allowable hoop stress, psi

The volume of the jacket wall is given by Equation 23 used for determining the volume of the nozzle coolant wall material. Substituting Equation 48 into Equation 47 yields the volume of the nozzle jacket wall in terms of the nozzle chamber pressure.

$$V = \frac{\pi r_t^3 (\sqrt{\epsilon} - 1) P_c}{\tan \Theta \sigma_{jw}} \left(\frac{P_c}{\sigma_{jw}} + \sqrt{\epsilon} + 1 \right) \quad (49)$$

The weight of the nozzle jacket is simply given as the produce of the nozzle jacket material density and the nozzle jacket wall volume.

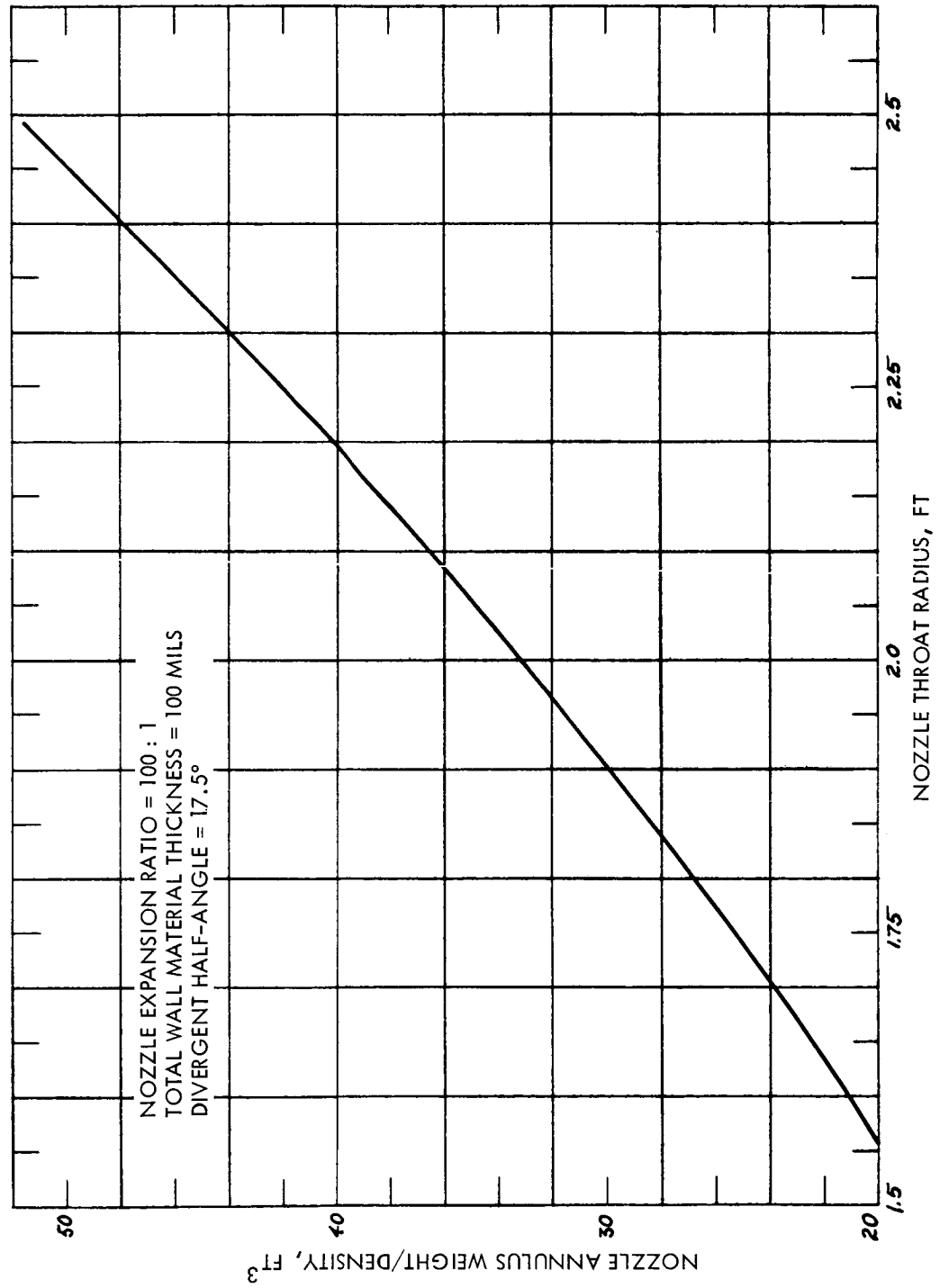


Figure 5-55 Nozzle Coolant Annulus Weight/Density

$$W_{jw} = \rho_{jw} V_{jw}$$

where

W_{jw} = weight of the nozzle jacket wall, lb.

ρ_{jw} = density of the jacket wall material, lb/ft³

V_{jw} = volume of the nozzle jacket wall, ft³

Figure 5-56 shows a plot of the nozzle jacket weight divided by the jacket material density as a function of the nozzle chamber pressure and the nozzle throat radius. The nozzle weights shown in figure 5-56 are based upon an expansion ratio ϵ of 40:1, a divergent cone half-angle of 17.5°, and an allowable jacket wall tensile stress of 30,000 psi.

5.3.5.3 Nozzle Torus Weight

The nozzle torus weight is obtained by means of a scaling relation involving the dependent nozzle cooling system parameters. The torus weight scaling relation is given by reference 41 to be the following expression:

$$W_{to} = C_1 r_t \sqrt{\epsilon_d} \dot{m}_c P_i$$

where

W_{to} = torus weight, lb.

C_1 = nozzle torus scaling constant = 6.38×10^{-4}

r_t = nozzle throat radius, ft.

ϵ_d = divergent section expansion ratio at torus location

\dot{m}_c = mass flow rate of coolant, lb/sec

P_i = nozzle coolant inlet pressure, psia

The nozzle torus material assumed in reference 41 was stainless steel with a density of 490 lb/ft³. Dividing through by the torus material density

$$\frac{W_{to}}{\rho_{to}} = C_2 r_t \sqrt{\epsilon_d} \dot{m}_c P_i$$

where

ρ_{to} = nozzle torus material density, lb/ft³

C_2 = nozzle torus scaling constant = 1.3×10^{-6}

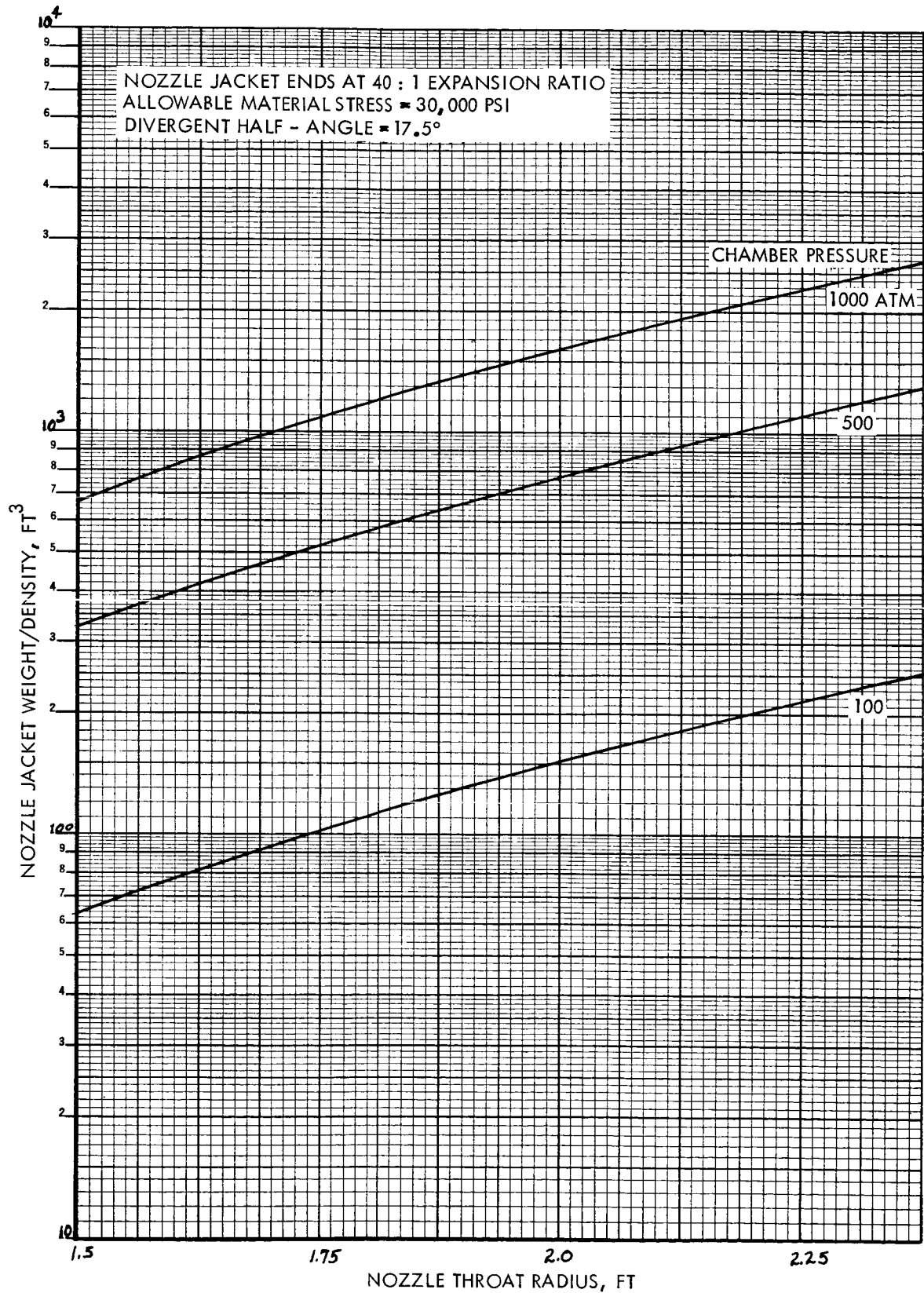


Figure 5-56 Nozzle Jacket Weight/Density
5-93

Figure 5-57 shows the ratio of the nozzle torus weight to density as a function of the nozzle throat radius, coolant flow rate, and inlet pressure for $\epsilon_d = 40$.

5.3.5.4 Total Nozzle Weight

The total nozzle weight is obtained by selecting the materials, and thus the densities, to be used for each of the major components of the nozzle. Selection of the materials yields the weight of the components as a function of the nozzle throat radius from figures 5-55, 5-56 and 5-57. The value of the nozzle throat radius is a function of the propellant chamber temperature, propellant mass flow rate, and the nozzle chamber pressure. Figure 5-58 gives the nozzle throat radius as a function of chamber pressure for two values of chamber temperature and three values of mass flow rate. The equation relating the nozzle throat radius to the chamber temperature, chamber pressure, and mass flow rate is presented in the nozzle thermal analysis section of this report.

5.3.6 Turbopump Weight

The turbopump weight is assumed to be a function of the propellant mass flow rate, the turbopump discharge pressure, the net positive suction head (NPSH) at the pump inlet, and the type of cycle employed to obtain the hydrogen used by the turbine (bleed cycle or topping cycle). The turbopump weight scaling law, as given by reference 41, is the following relation:

$$W_{tp} = \dot{m} \left[A_1 \frac{(A_2 - \text{NPSH})}{(\text{NPSH})^{a_1}} + A_3 \left(\frac{P_d}{A_4} \right)^{a_2} + A_5 \left(\frac{P_d}{A_6} \right)^{a_3} \right]$$

where

- W_{tp} = turbopump weight, lb.
- \dot{m} = propellant mass flow rate, lb/sec
- NPSH = net positive suction head at pump inlet, ft.
- P_d = pump discharge pressure, psi
- A_i, a_i = scaling constants

The scaling constants for the assumed topping cycle are:

$$\begin{array}{ll} A_1 = 0.0237 & a_1 = 2/3 \\ A_2 = 600. & a_2 = 0.2755 \\ A_3 = 2.625 & a_3 = 4.46 \end{array}$$

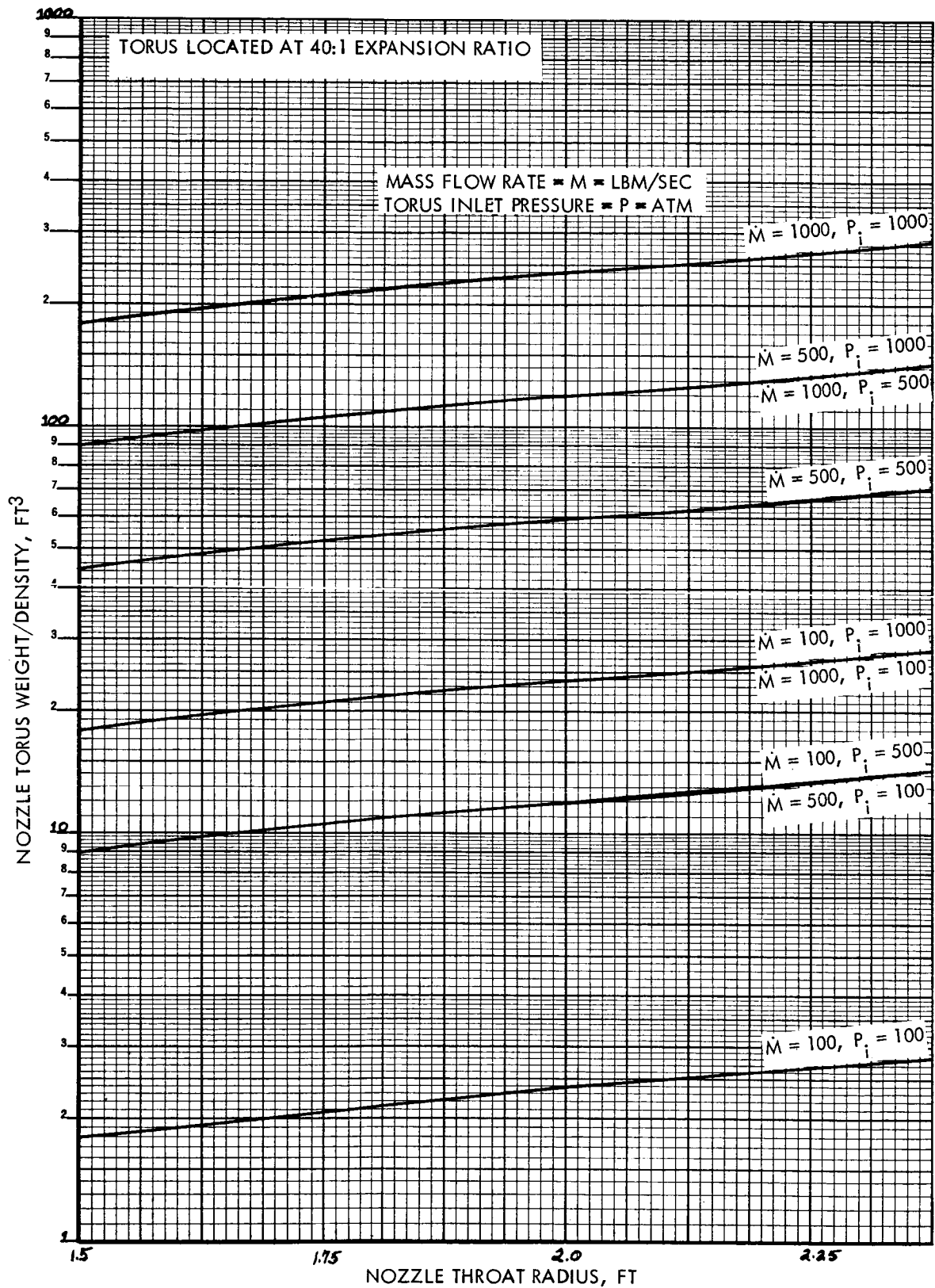


Figure 5-57 Nozzle Torus Weight/Density
5-95

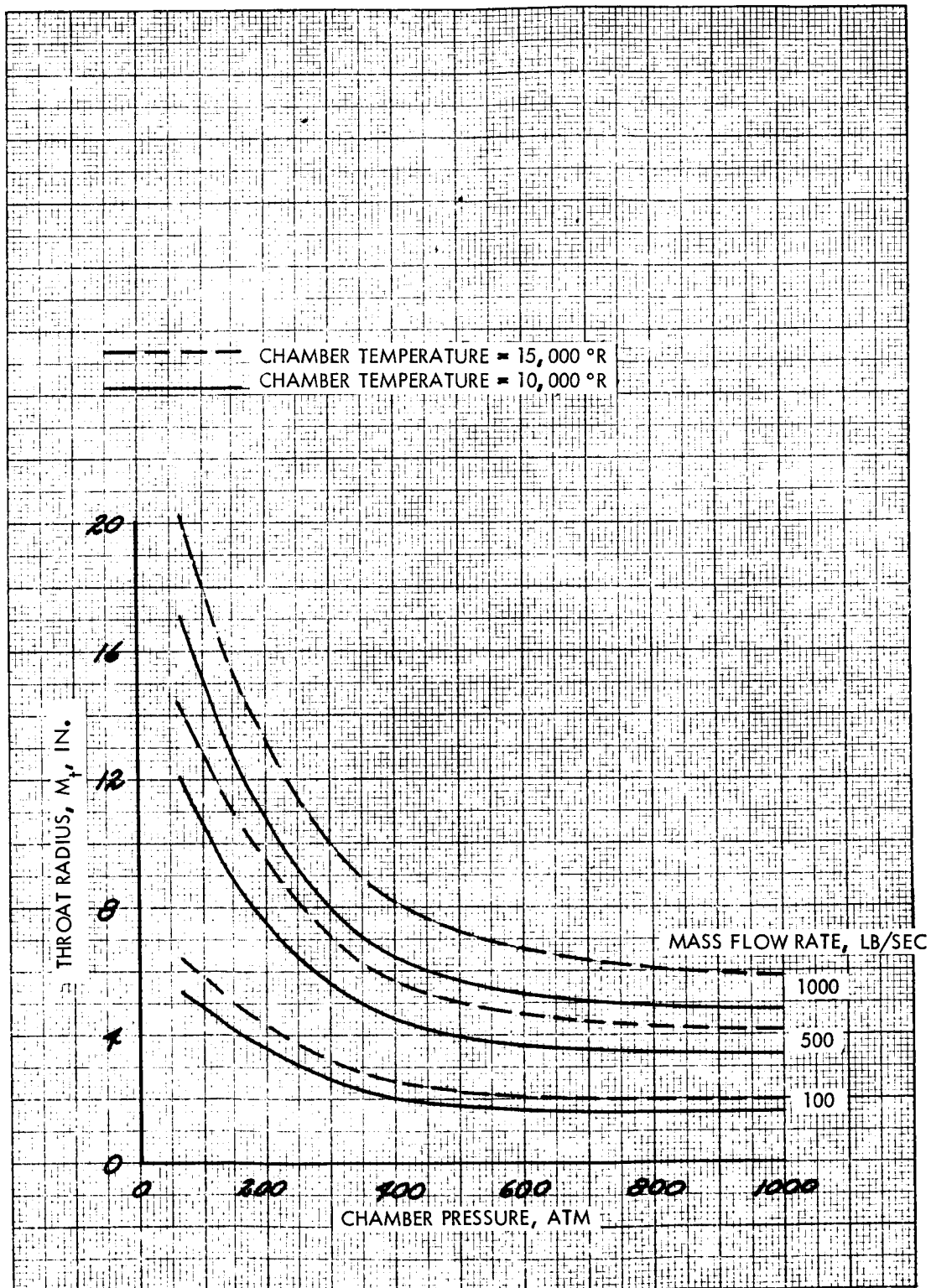


Figure 5-59 Conventional Nozzle Throat Radius as a Function of Chamber Temperature, Propellant Mass Flow Rate and Chamber Pressure
5-96

$$A_4 = 1000.$$

$$A_5 = 0.1808$$

$$A_6 = 2000.$$

The turbopump system consists of the low speed boost or booster pump, the high speed main pump directly driven by the turbine, and the turbine. The first term in the turbopump weight equation accounts for the weight contribution of the booster pump. The second and third terms in the equation are the two-term semiempirical relationships for the combined main pump and turbine weights. The terms in the turbopump weight equation are based upon the major dependent physical parameters.

When the turbopump is size scaled, the turbopump weight is a function of the mass flow rate to the 1.27 power. When the turbopump is unit scaled, the turbopump weight is a linear function of the mass flow rate. Thus, the lower weight turbopump system, for any given mass flow rate requirements, will result from unit scaling, rather than size scaling. Figure 5-59 shows the turbopump weight as a function of the mass flow rate and pump discharge pressure for a unit scaled system and the assumed topping cycle.

5.3.7 Propellant and Uranium Line Weights

5.3.7.1 Liquid Hydrogen Main Propellant Line

The main propellant line is the liquid hydrogen line that transports the propellant from the turbopump to the nozzle torus inlet. To determine the inside diameter and wall thickness of the main propellant line, the following three assumptions are made:

1. The line is sized for an inlet Mach number less than 0.2
2. The line is designed for a pressure drop less than 30 percent of the inlet pressure
3. The internal pipe surface is smooth, i.e., the absolute roughness of the pipe surface $e = 0.001$ foot.

Reference 41 gives the pressure drop for incompressible fluid flow to be the following:

$$P = \frac{K \dot{m}^2}{2 g_c \rho_{H_2} \pi^2 D^4 (144)}, \text{ psia}$$

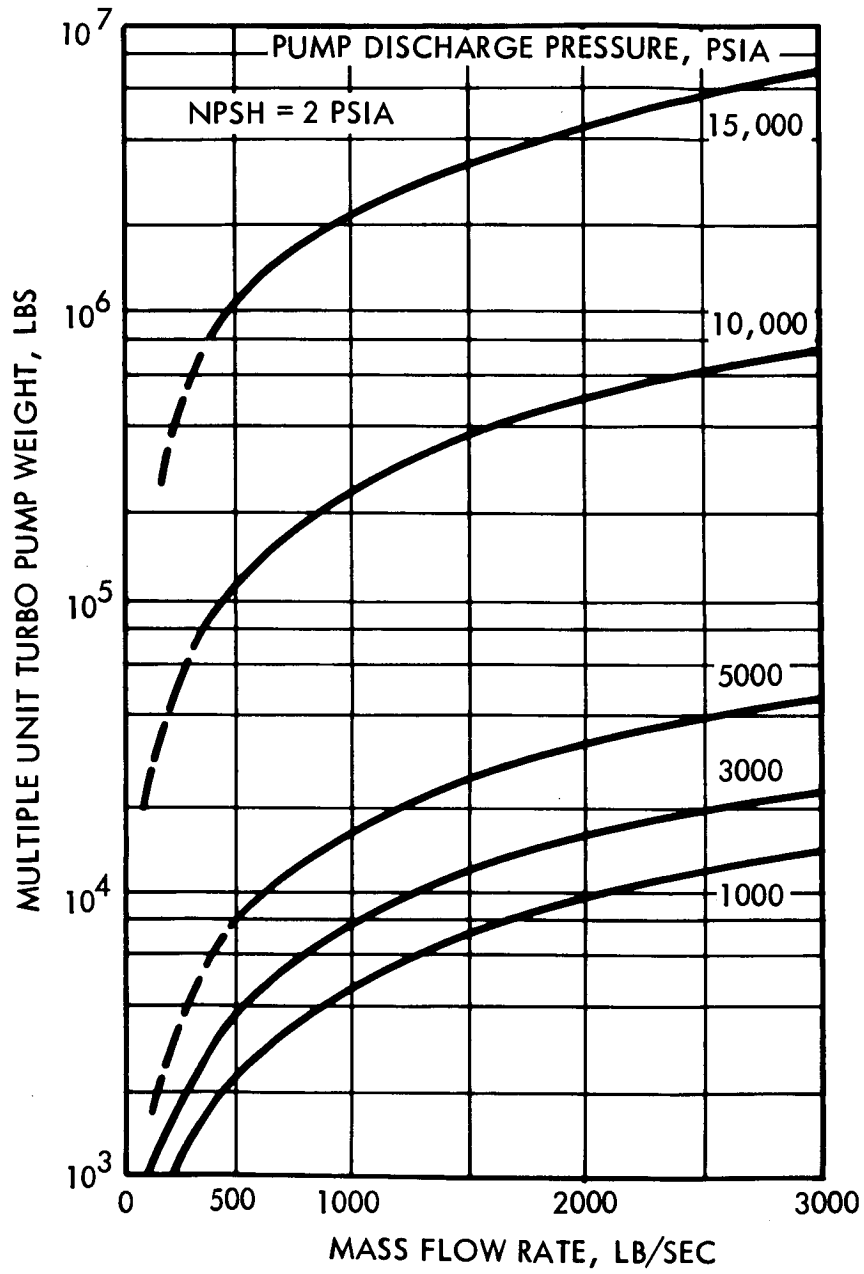


Figure 5-59 Multiple Unit Hydrogen Topping Cycle Turbopump
Weight
5-98

where

- P = pressure drop, lb/in^2
 \dot{m} = propellant mass flow rate, lb/sec
 g_c = gravitational acceleration, 32.17 ft/sec^2
 ρ_{H_2} = density of the hydrogen propellant, lb/ft^3
 D = propellant line inside diameter, ft.
 K = head loss coefficient

Assuming a line length of 30 ft., 4 bellows or elbows, a propellant line friction factor of 0.013; the head loss coefficient is reduced to:

$$K = (4.68/D + 1.2)$$

Figure 5-60 shows the pressure drop for the main propellant line as a function of the pipe diameter and mass flow rate for an assumed hydrogen density of 4.96 lb/ft^3 .

The weight of the propellant line is given simply by the pipe material volume times the material density.

$$W_{pl} = \pi D t L \rho_p$$

where

- W_{pl} = weight of the propellant line, lb.
 t = thickness of the pipe material, ft.
 L = length of the propellant line, ft.
 ρ_p = density of the pipe material, lb/ft^3

The thickness of the pipe material is determined from the allowable hoop stress:

$$t = \frac{PD}{2\sigma_a}$$

where

- P = internal pressure of the pipe, lb/in^2
 σ_a = allowable tensile stress of material, lb/in^2

The weight of the propellant line is thus:

$$W_{pl} = \rho_p \frac{\pi D^2 P L}{2 \sigma_a}$$

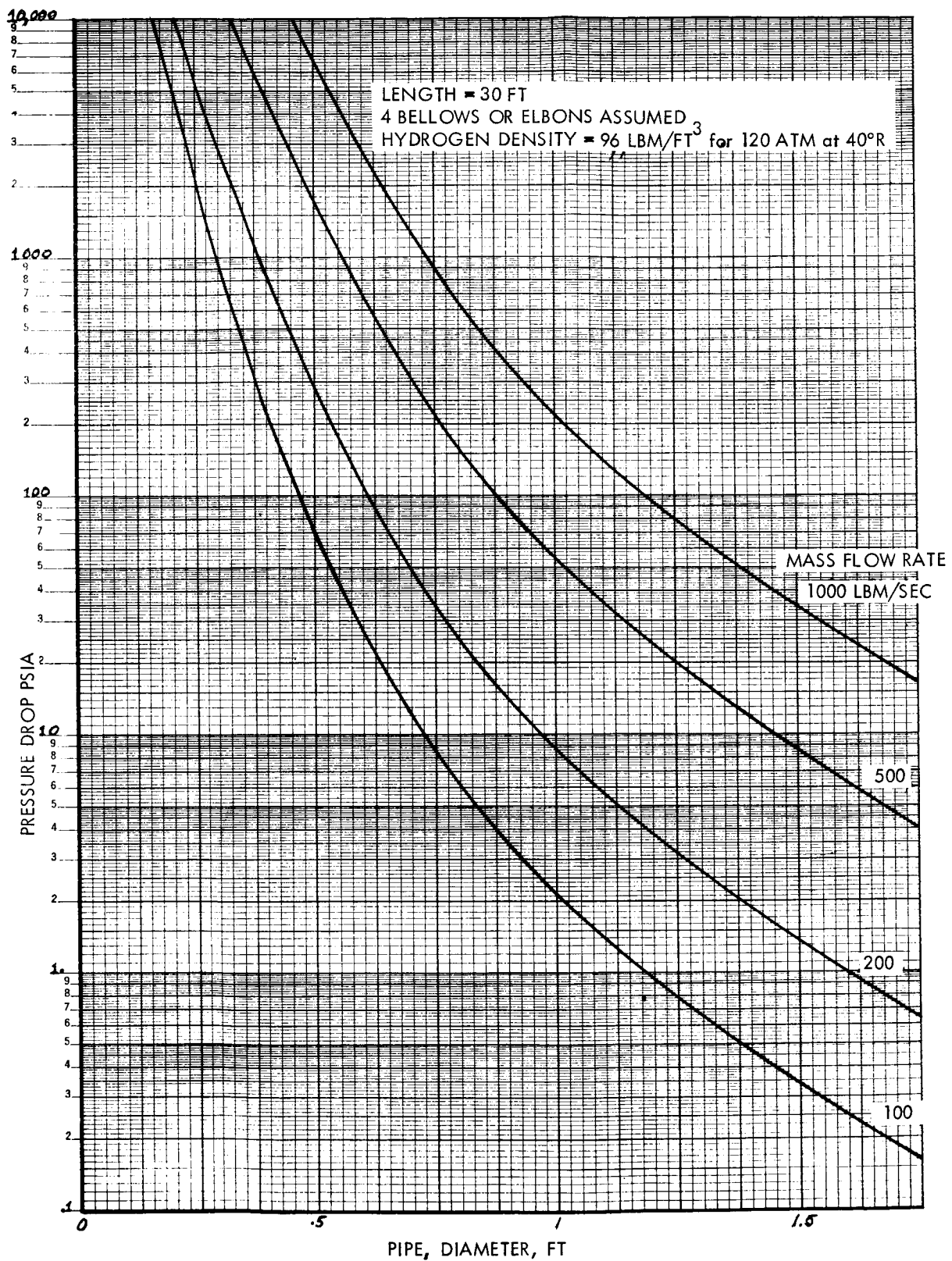


Figure 5-60 Pressure Drop in Main Propellant Line
5-100

Figure 5-61 shows the main propellant line weight per unit length as a function of the pipe diameter and propellant inlet pressure. The curves shown in figure 5-61 were obtained by assuming a propellant line material allowable tensile stress of 100,000 psia and material density of 491 lb/ft³.

5.3.7.2 Liquid Uranium Line Weight

The pressure drop per unit length can be approximated by the following equation from reference 35 .

$$dp = \rho V dV - \frac{4f}{D} \frac{1}{2} \rho V^2 dx$$

For the purposes of the weight analysis, the first term is considered to be equal to zero, thus

$$\frac{dp}{dx} = \frac{2f}{D} \rho V^2$$

where

$$f = \frac{0.50}{(R_e)^{0.2}}$$

From the definition of the Reynolds number and the continuity equation, the following two equations are obtained:

$$Re = \frac{\rho V D}{\mu} = \left(\frac{\dot{m}}{A} \right) \frac{D}{\mu}$$

$$\rho V = \frac{\dot{m}}{A}$$

Combining the above equations results in the following equation for the pressure drop per unit pipe length:

$$\frac{dp}{dx} = 2.78 \times 10^{-5} \frac{\left(\frac{\dot{m}}{A} \right)^{1.8} \mu^{0.2}}{D^{1.2} \bar{\rho}} \frac{\text{psi}}{\text{ft}}$$

For liquid uranium at 3000°R and 100 atm, the average density $\bar{\rho}$ is 1185 lbm/ft³ and the viscosity μ is 1.344×10^{-3} lbm/ft-sec. Figure 5-62 shows the liquid uranium line pressure drop per unit length as a function of pipe inside diameter and mass flow rate.

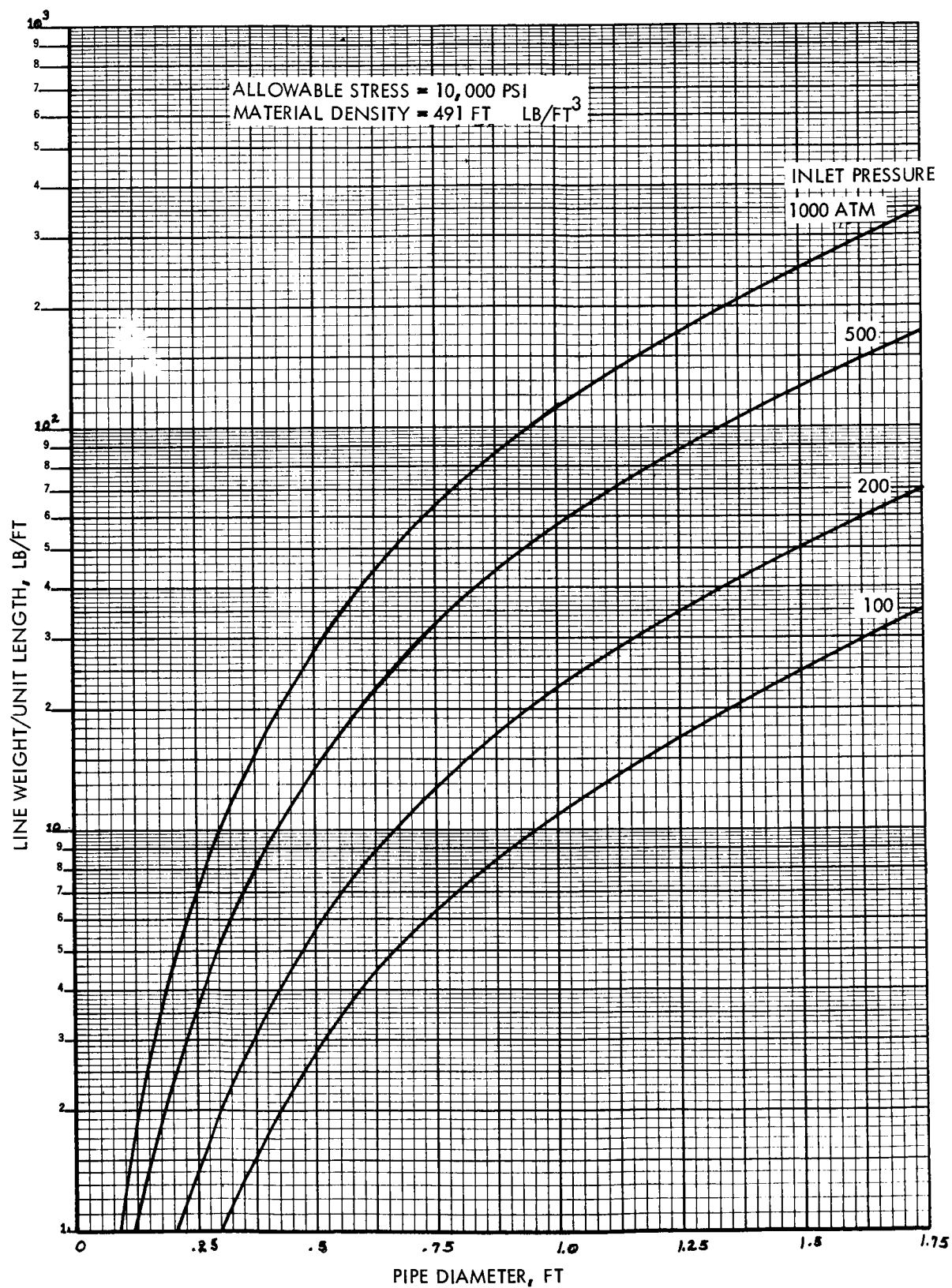


Figure 5-61 Propellant and Hydrogen Line Weights
5-102

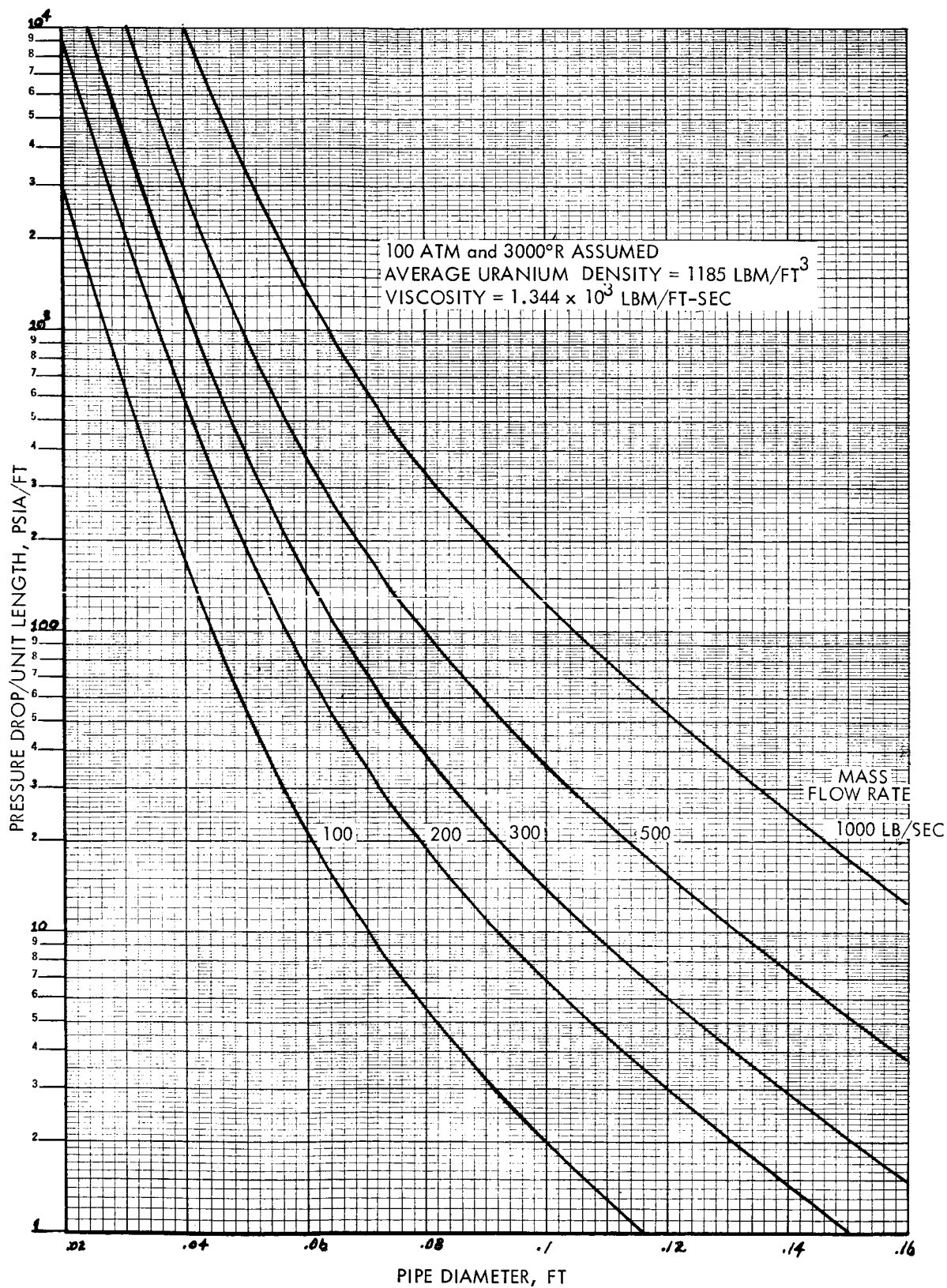


Figure 5-62 Liquid Uranium Line Pressure Drop
 5-103

The liquid uranium line weight per unit pipe length can be obtained from the product of the pipe material volume per unit length and the material density. From hoop stress considerations the thickness is given by

$$t = \frac{PD}{2\sigma_a}$$

The pipe volume per unit length is

$$\frac{\text{weight}}{\text{length}} = \frac{\text{Vol } \rho}{L} = \rho \frac{\pi}{4} (D_o^2 - D_i^2)$$

$$\text{But } D_o = D_i + t$$

Thus the weight/unit length is given by

$$\frac{\text{weight}}{\text{length}} = \frac{\pi}{4} \rho D_i^2 \left[\left(1 + \frac{P}{2\sigma_a} \right)^2 - 1 \right] \text{ lbm/ft}$$

Figure 5-63 shows the liquid uranium line weight per unit length as a function of pipe diameter and mass flow rate.

Hot Hydrogen Return Line

To a first approximation, the hot hydrogen return line pressure drop can be approximated by the pressure drop per unit length for the liquid uranium:

$$\frac{dp}{dx} = 2.98 \times 10^{-5} \frac{\left(\frac{\dot{m}}{A} \right)^{1.8} \mu^{0.2}}{d^{1.2} \bar{\rho}} \frac{\text{psi}}{\text{ft}}$$

Figure 5-64 shows the pressure drop per unit length for the hot hydrogen return line as a function of pipe diameter and hydrogen mass flow rate. The weight per unit length is given by the same expression developed for the main hydrogen propellant line and is given in figure 5-61.

5.3.8 Thrust Structure Weight

The weight of the thrust structure is directly proportional to the weight of the engine minus the weight of the thrust structure and the gravitational loadings subjected to the thrust structure. Therefore,

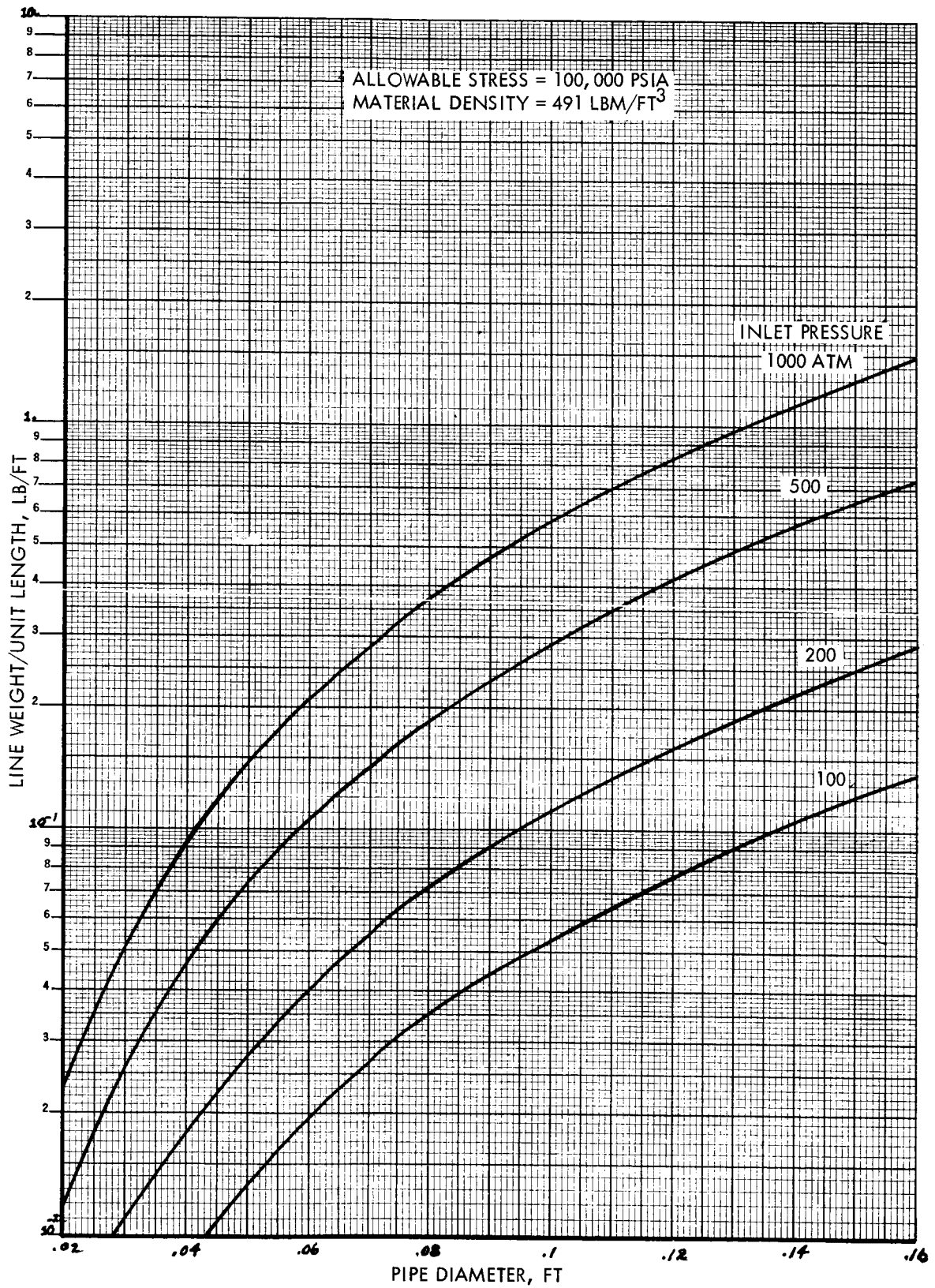


Figure 5-63 Liquid Uranium Line Weight
5-105

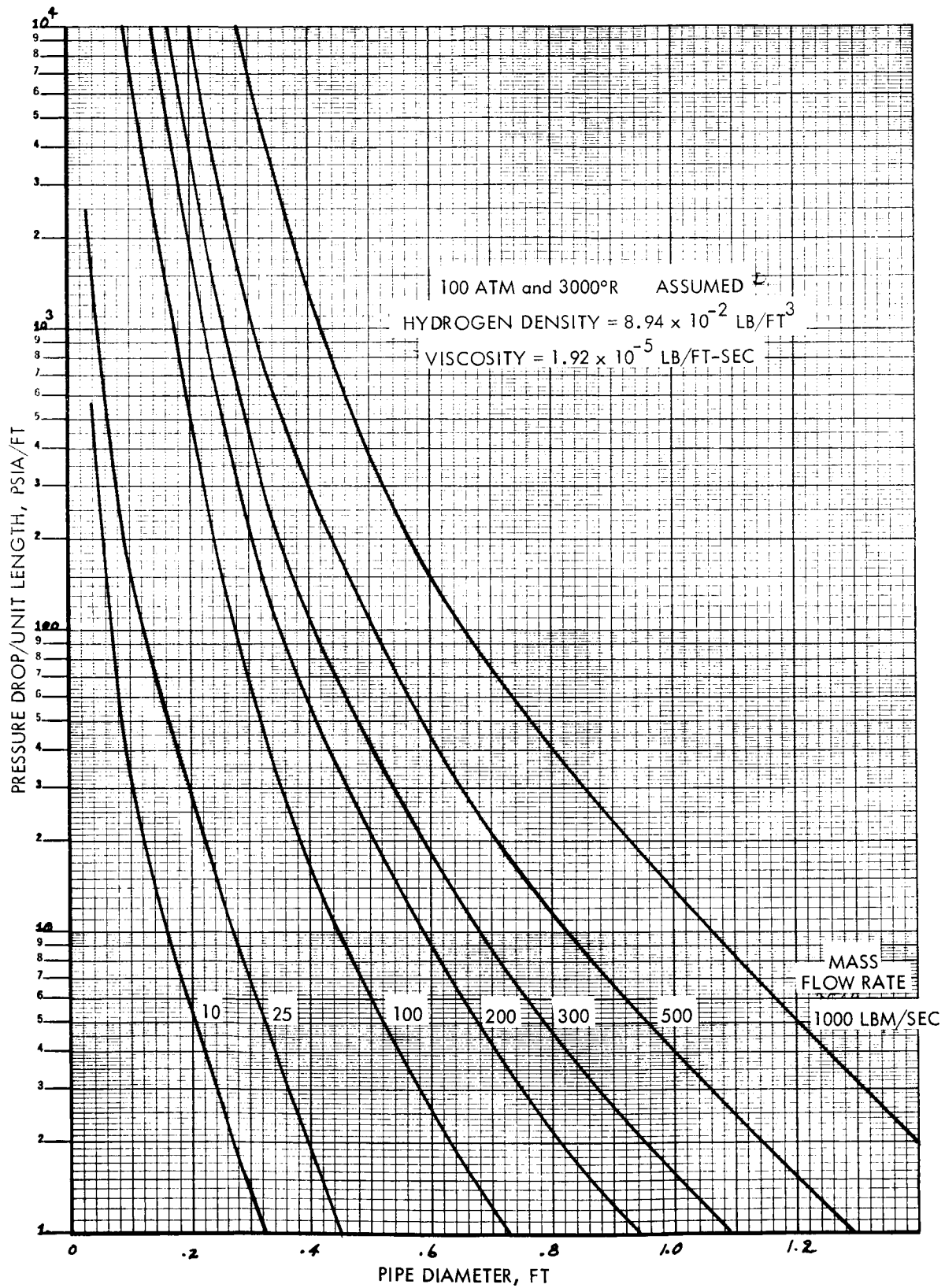


Figure 5-64 Hot Hydrogen Line Pressure Drop
5-106

$$W_{ts} = \frac{W_{tso} K_g (W_e - W_{ts})}{8 (W_{eo} - W_{tso})}$$

where

W_{ts} = weight of the thrust structure, lb.

W_{tso} = weight of the reference thrust structure, lbs.

K_g = gravitational loading, g's

W_e = weight of the engine, lbs.

W_{eo} = weight of the reference engine, lbs.

For the solid core NERVA type nuclear rocket engine, reference 41 indicates that the weight of the thrust structure is approximately 0.11 times the weight of the engine for a thrust structure designed to withstand a gravitational loading of 8 g's. For the gaseous core weight analysis, it is desirable to establish the relation for the thrust/structure in terms of the engine weight minus the thrust structure weight. If the thrust structure weight is 11 percent of the engine weight, then it follows that

$$W_{ts} = \frac{0.11}{0.89} (W_e - W_{ts}) = 0.1235 (W_e - W_{ts})$$

Figure 5-65 shows the weight of the thrust structure as a function of the engine weight minus the thrust structure weight.

5.3.9 Scoop Weight

The model employed for the scoop weight analysis is shown in figure 5-66. The scoop configuration consists of a 3-foot diameter cylinder of unspecified length. The main scoop structure is surrounded by coolant passages which supply the hydrogen used to regeneratively remove heat and transpiration cool the scoop surfaces which are exposed to the hot uranium on the scoop interior and exposed to the hot hydrogen on the scoop exterior. The model assumes that the pressure differential between the inside and outside of the scoop is primarily due to the pressure drop across the sonic nozzle. This assumption presupposes that the pressure inside the scoop is equal to the chamber pressure P_c .

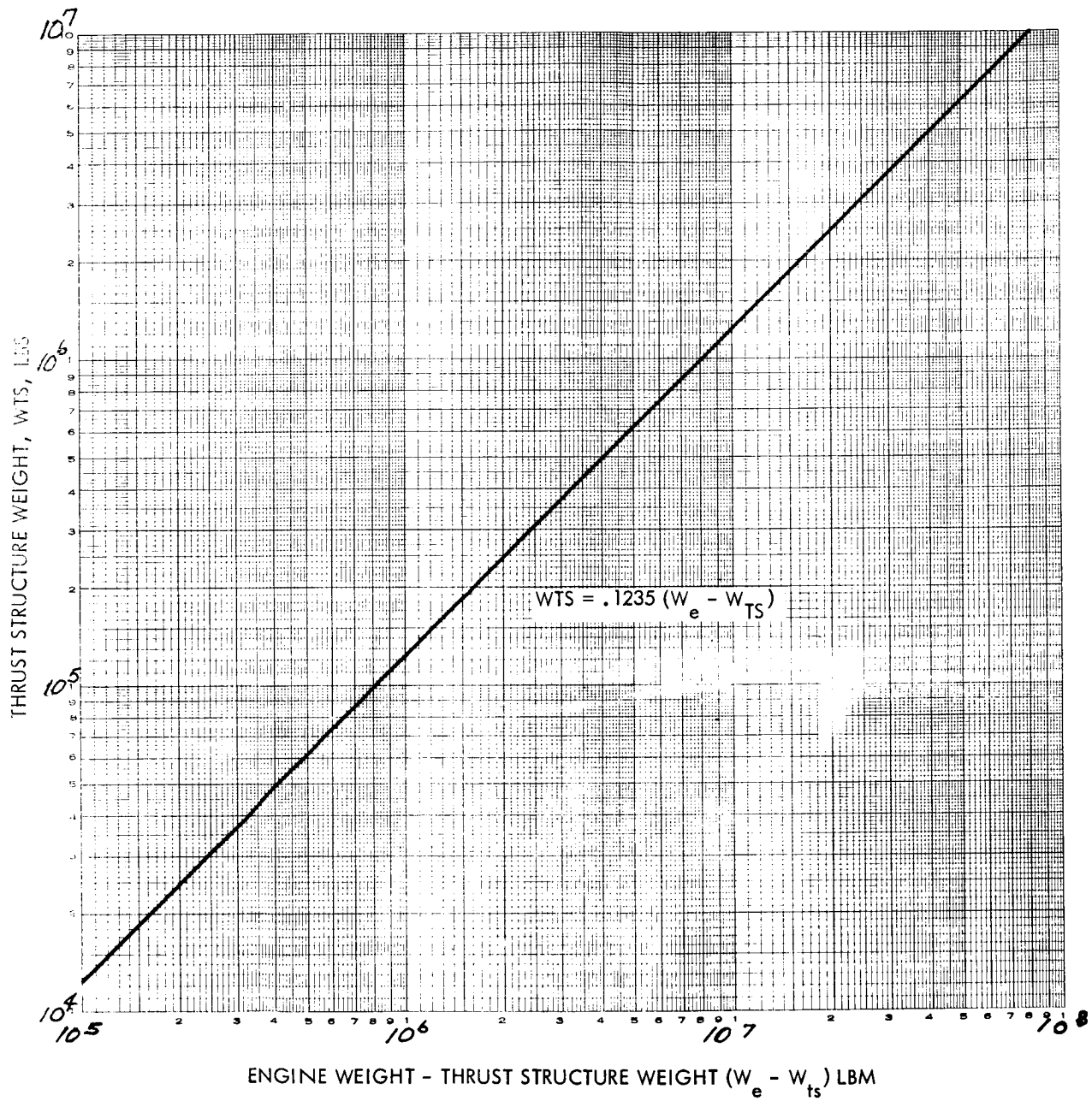


Figure 5-65 Thrust Structure Weight
5-108

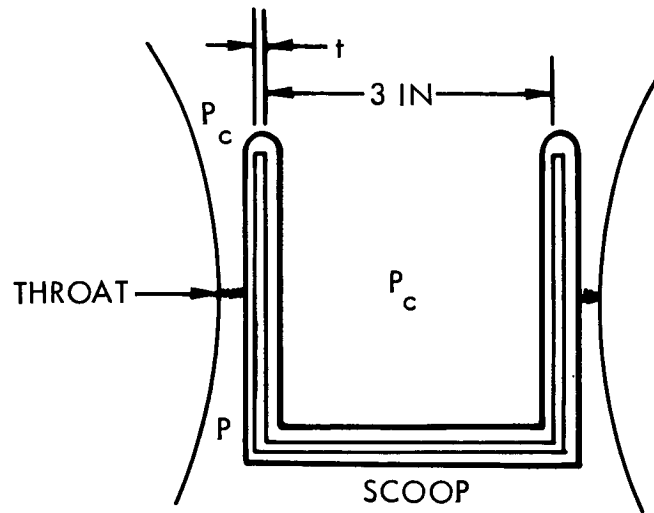


Figure 5-66

The relationship between the chamber pressure and pressure on the downstream side of the throat is the following:

$$\frac{P_c}{P} = \left[1 + \frac{\alpha - 1}{2} M^2 \right]^{\frac{\alpha}{\alpha - 1}}$$

where

P_c = chamber pressure, psia

P = downstream pressure, psia

α = ratio of propellant specific heats, unitless

M = mach number, unitless

For the sonic nozzle the mach number, M , is equal to unity. Also for hydrogen at 18,000°R and 100 atm, the ratio of the specific heats, α , is equal to 1.4. Therefore,

$$\frac{P_c}{P} = \left[1 + \frac{0.4}{2} \right]^{\frac{1.4}{.4}} = 1.892$$

$$\text{Thus, } \Delta P = P_c - P = P_c \left(1 - \frac{1}{1.892} \right) = 0.472 P_c$$

The above analysis shows that, for isentropic expansion through a sonic nozzle, the pressure drop is directly related to the chamber pressure.

The size, and thus the weight, of the scoop may be determined from hoop stress considerations. The required thickness of the scoop main structure is given by the following relationship:

$$t = \frac{P D_i}{2 \sigma_a} = \frac{0.472 P_c D_i}{2 \sigma_a}$$

where

D_i = inside diameter of the scoop, ft.

σ_a = tensile stress of the scoop material, psi.

The weight of the scoop can be approximated by the following equation:

$$W_{sc} = \rho_{sc} (V_c + V_d)$$

where

W_{sc} = weight of the scoop, lbm

ρ_{sc} = density of the scoop, lbm/ft³

V_c = volume of the hollow cylinder, ft³

V_d = volume of the end disc, ft³

Incorporating the expression for the scoop wall thickness from hoop stress considerations, the volume of the cylindrical section of the scoop is,

$$V_c = \frac{\pi}{4} D_i^2 L \left[\left(1 + \frac{0.472 P_c}{2 \sigma_a} \right)^2 - 1 \right]$$

where

D_i = inside diameter of scoop

L = scoop length

Assuming that the thickness of the disc is equal to the thickness of the cylindrical section wall, the volume of the end disc is,

$$V_d = \frac{\pi D_i^3 0.472 P_c}{8 \sigma_a}$$

The total scoop weight per unit material density can thus be reduced to the following relation:

$$W_{sc}/\rho_{sc} = \frac{\pi}{4} D_i^2 \left\{ L \left[\left(1 + \frac{0.472 P_c}{2 \sigma_a} \right)^2 - 1 \right] + \frac{0.472 D_i P_c}{2 \sigma_a} \right\}$$

Assuming an allowable tensile stress of 10,000 psi, and an inside scoop diameter of 3 ft., the equation for the total scoop weight per unit material density reduces to the following.

$$W_{sc}/\rho_{sc} = 7.07 \left\{ L \left[(1 + .236 \times 10^{-5} P_c)^2 - 1 \right] + 0.708 \times 10^{-5} P_c \right\}$$

Figure 5-67 shows the scoop weight per unit density of the scoop material as a function of the scoop length and chamber pressure.

5.3.10 Separator Weight

The function of the separator is to separate the liquid uranium droplets formed in the condensor from the hydrogen mixed with the uranium. The uranium droplets are separated from the hydrogen gas stream by Stokes' law flow of droplets in a swirling mixture of hydrogen and uranium. As described in reference 37, the mixture of hydrogen and uranium is swirled in a number of parallel pass tubes with centrifugal accelerations over 10^6 g's. A high tangential velocity is imparted to the stream by passing the mixture through a row of nozzles. The hydrogen swirl pattern adheres to radial equilibrium conditions and there is theoretically no radial component to its velocity. However, the dense uranium particles swirling approximately at the same speed as the hydrogen have an induced centrifugal force that exceeds the pressure gradient set up by the hydrogen tangential flow pattern. This causes these dense particles to migrate towards the outer periphery and producing the desired separation.

From preliminary analyses, it was found in reference 37 that 127 separator tubes are required. The dimensions of the separator tubes are the following: 1.2 inches in diameter and 5.3 inches in length. Assuming a 25 percent area fraction for structural material, the total cross-sectional area of the separator is determined by the following relation:

$$A_s = A_t + 0.25 A_s$$

or

$$A_s = A_t 0.75$$

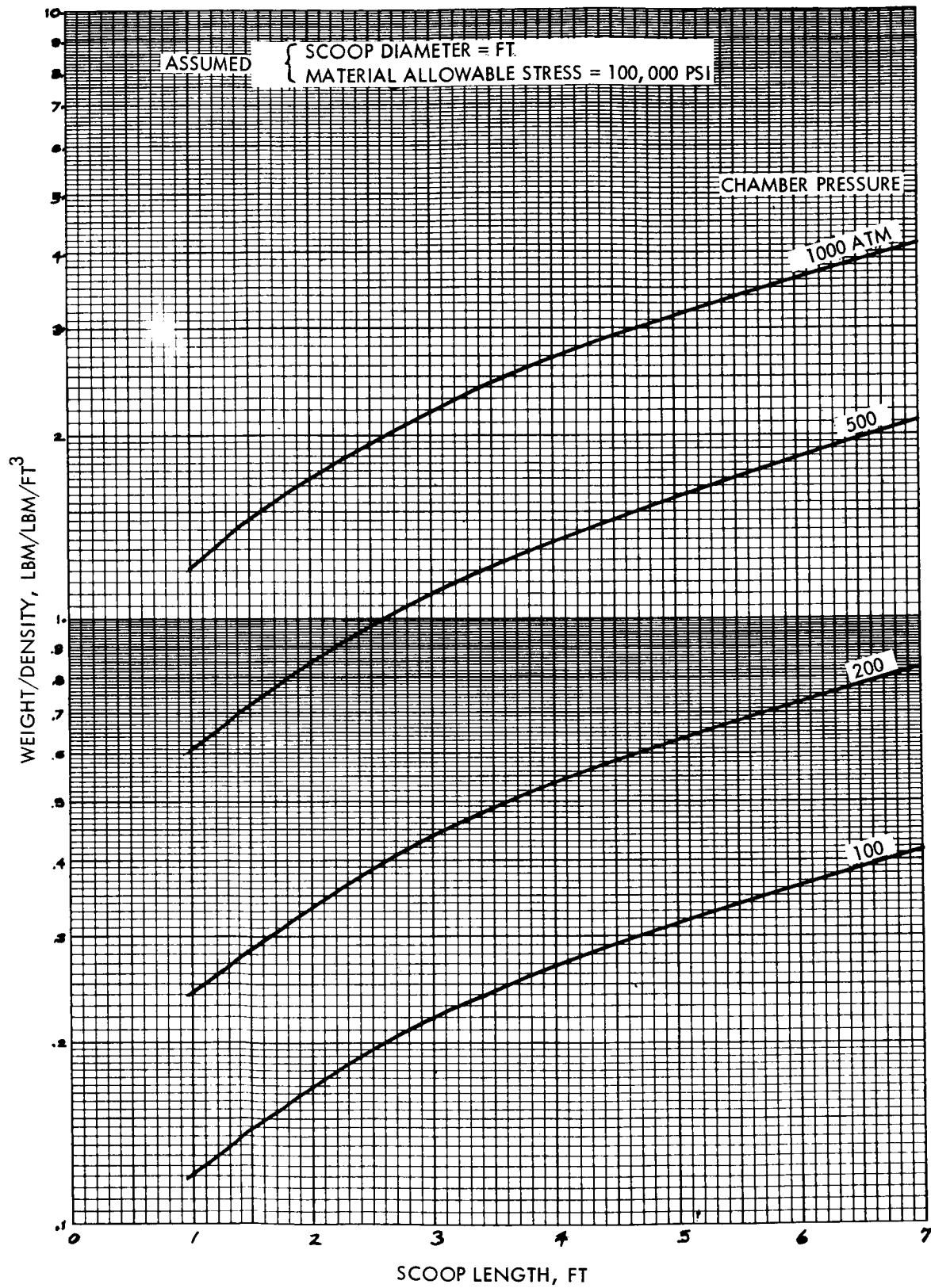


Figure 5-67 Scoop Weight/Density
5-112

where

A_s = cross sectional area of the separator, in^2

A_t = total cross sectional area of the 127 tubes, in^2

$$A_t = (127) \frac{\pi}{4} (1.2)^2 = 144 \text{ in}^2$$

Therefore, $A_s = 144/0.75 = 192 \text{ in}^2$ or 1.334 ft^2

The inside diameter of the separator required to contain the 127 tubes is thus:

$$D_s = \sqrt{\frac{4 A_s}{\pi}} = \sqrt{\frac{4(1.334)}{\pi}} = 1.304 \text{ ft}$$

The weight per unit length of the separator can be approximated by the relationship for the propellant line weight per unit length for an inside diameter of 1.304 ft. The additional structural material for the tubes and supporting structure is assumed to be approximately 25 percent of the total separator weight. Figure 5-68 shows the separator weight as a function of separator length for an assumed material tensile stress of 100,000 psi and material density of 491 lbm/ft^3 . For reasonable divergent and convergent sections of the separator, separator lengths on the order of 4 feet appear to be optimum.

5.3.11 Auxiliary Component Weights

The engine components classed as auxiliary components are as follows: diagnostic instrumentation system, pneumatic supply, control system, and tank valve assembly. The auxiliary component scaling relations for the solid core NERVA type nuclear rocket engine are given by reference 41 to be of the following form;

$$W_i = C_{1i}^1 + C_{2i}^1 P + C_{3i}^1 P^2$$

where

W_i = weight of the i^{th} auxiliary component of interest, lb.

P = engine power, MW

$C_{1i}^1, C_{2i}^1, C_{3i}^1$ = three scaling constants

The solid core power can be approximately represented in terms of the propellant mass flow rate through the core. For the NERVA type nuclear rocket engine, 1120 MW of power is equivalent to 75 lb/sec of hydrogen. Thus the auxiliary component weight equation can be rewritten in terms of the mass flow rate with new scaling constants:

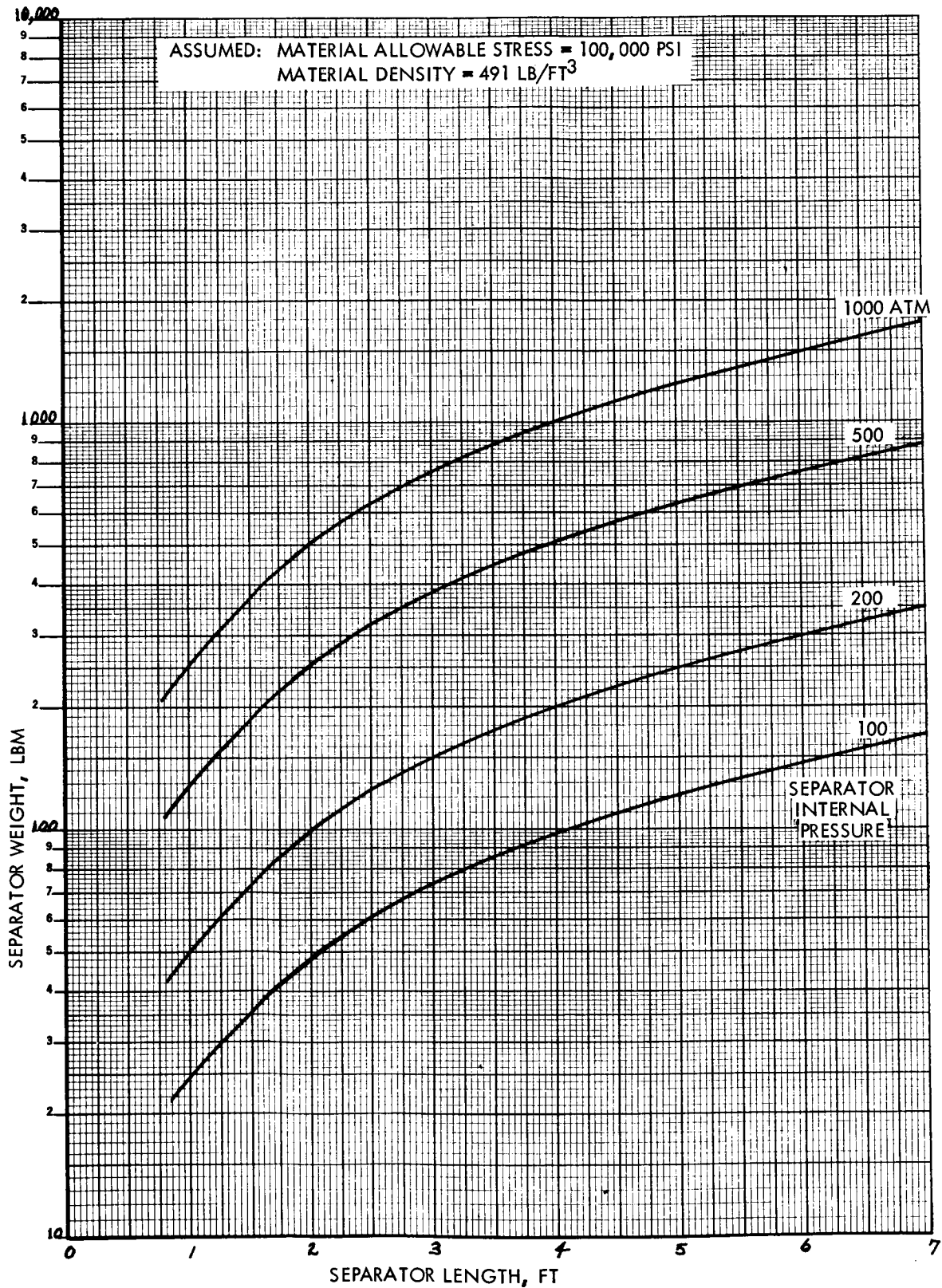


Figure 5-68 Separator Weight
5-114

$$W_i = C_{1i} + C_{2i} \dot{m} + C_{3i} \dot{m}^2$$

where

W_i = weight of the i^{th} auxiliary component of interest, lb.

\dot{m} = propellant mass flow rate, lb/sec

$$C_{1i} = C_{1i}^1$$

$$C_{2i} = 14.94 C_{2i}^1$$

$$C_{3i} = 223 C_{3i}^1$$

The values of the three power scaling constants for the NERVA type solid core nuclear rocket engine are given in reference 41 and the new mass flow rate scaling constants are given in table 5-4.

Table 5-4 Auxiliary Component Scaling Constants

i	Component	C_{1i}	C_{2i}	C_{3i}
1	Diagnostic Instrumentation System	166.9	0.111	-3.66×10^{-5}
2	Pneumatic Supply System	751.6	0.03105	5.24×10^{-5}
3	Control System	663.6	0.340	1.278×10^{-4}
4	Tank Valve Assembly	238.1	0.379	-1.79×10^{-4}

The auxiliary component weights are shown in figure 5-69 as a function of the total propellant mass flow rate.

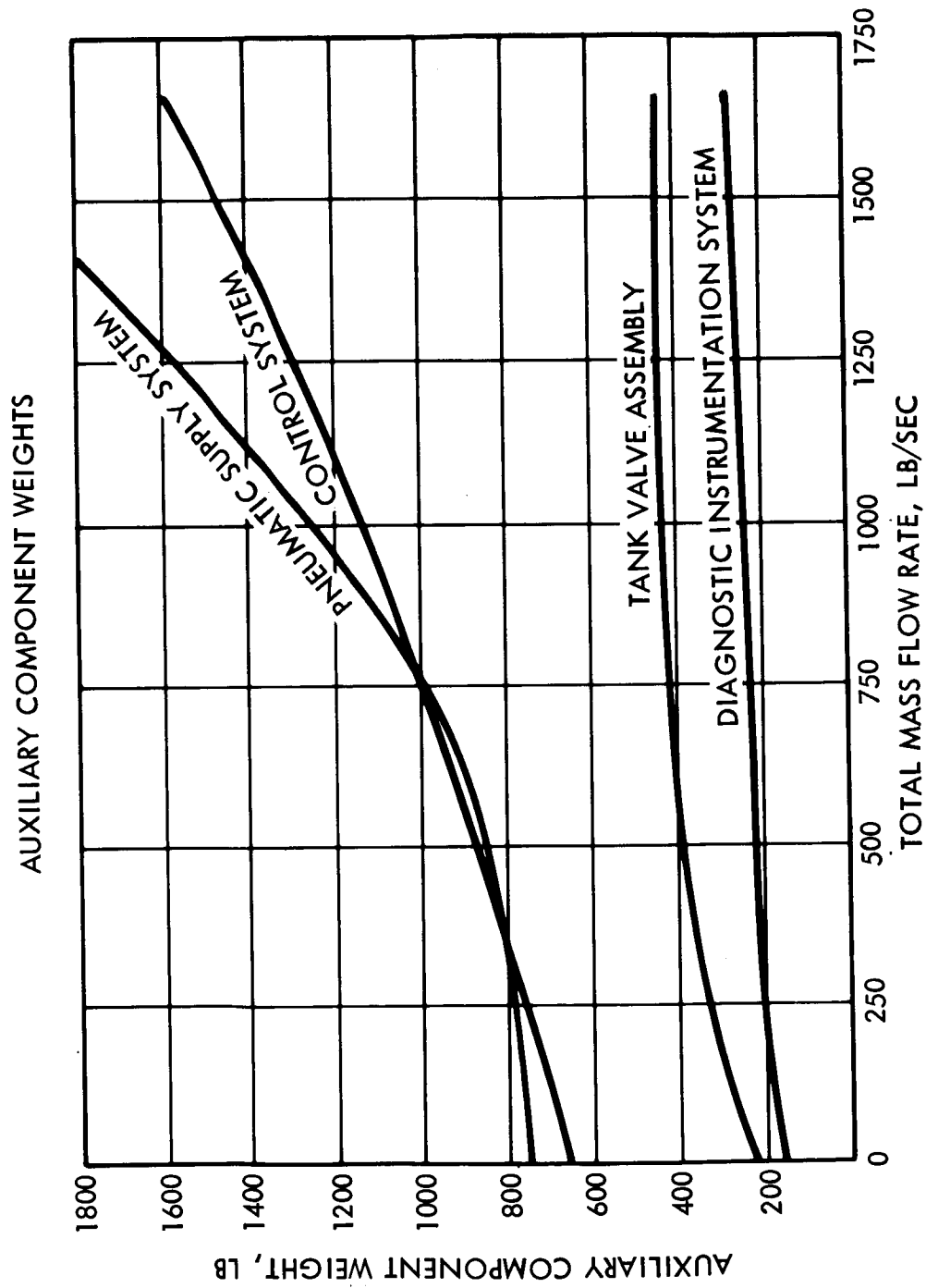


Figure 5-69 Auxiliary Component Weights

5.4 ENGINE TEMPERATURES, PRESSURE, AND MASS FLOW RATES

The engine temperature, pressure, and hydrogen mass flow rate distribution throughout the engine system is described in this section. As a result of the cycle analysis, the flow path dimensions and pressure drops through the various components are obtained. From the core operating pressure specified by the criticality analysis and the pressure drops throughout the system, it is possible to obtain the local operating pressures for the various components. From a knowledge of the operating pressures, the mass flow rates, and the flow path dimensions, an estimation of the component weights can be obtained.

To obtain the pressures and temperatures throughout the engine, it is first necessary to determine the flow paths required to supply the hydrogen coolant and propellant to the various parts of the engine. Figure 5-70 is a schematic of the hydrogen and uranium flow cycles for the gas core engine. It is necessary to establish the temperatures throughout the engine to obtain an indication of the possible material integrity problems. Since many of the component weights are dependent upon the local pressure, it is also necessary to determine the pressure at various locations throughout the engine. The pressure profile of the engine is determined by first establishing the fissioning core pressure from criticality considerations. Then, from pressure drop consideration, the pressures in the remaining components of the engine are determined by adding the pressure drops from the core to the turbopump exit.

From the above discussion, it is apparent that the pressures throughout the engine are dependent on the core operating pressure and selected pressure drops of the various engine components. The major components that are considered in determining the engine operating pressures are: the turbopump, main propellant line, nozzle, reflector, mixing chamber, turbine, core, scoop, jet pump, condensor-separator, uranium return line, and hot hydrogen return line.

5.4.1 Cycle Description

The direct flow, externally separated gas core reactor utilizes a parallel coaxial stream of propellant and fissioning fuel, with the hydrogen propellant

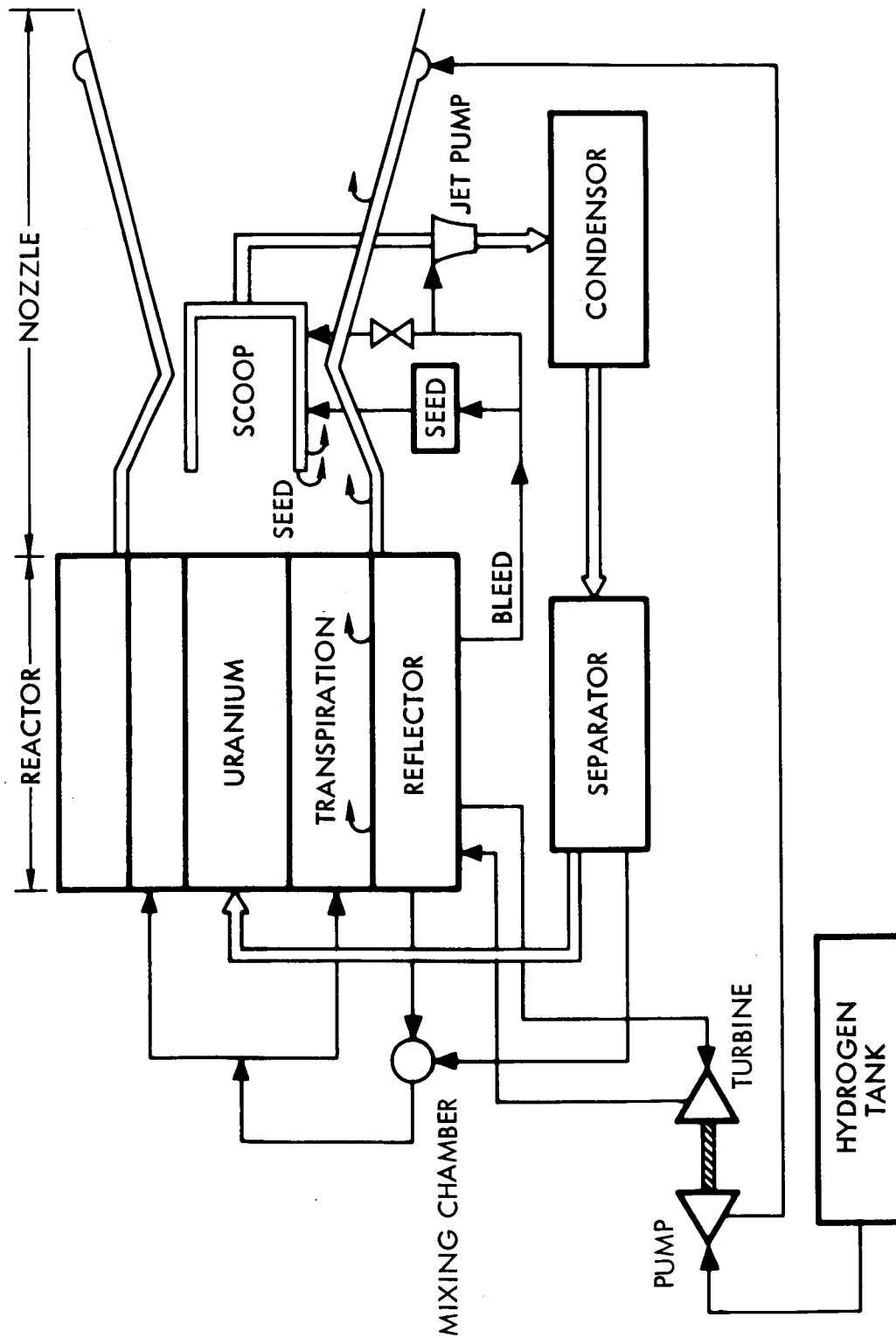


Figure 5-70 Cycle Schematic

surrounding the uranium fuel. At reactor discharge, the fuel is collected and cooled to a temperature below the boiling point of the uranium by mixing the fuel with incoming cold propellant. The resulting mixture is an aerosol of condensed uranium liquid droplets in a gas mixture. The mixture is then separated outside the reactor core, exploiting the liquid-gas phase difference to achieve nearly complete retention of fuel. Once separated, the uranium fuel is recycled through the reactor.

The propellant flows from the propellant tank to a turbopump and then follows three main flow paths. The first flow path is a regenerative path which absorbs the heat of the fissioning reactor that is deposited in the nozzle and reflector. The second flow path is bled from the nozzle and flows through the jet pump to provide a pressure increase in the uranium cycle and to condense the uranium fuel. The hydrogen used to condense the uranium is separated in the separator, mixed with the regenerative hydrogen, passed through the reactor cavity, and then passed out the nozzle to provide thrust. The third flow path is used to transpiration cool and to provide seeding coolant for the structural surfaces subjected to high heat loads. The major components which are transpiration cooled are the nozzle, scoop and reflector. For the engine configuration under consideration, only the exterior scoop surface is assumed to be protected by the carbon seeded hydrogen.

5.4.2 Pressure Drops

For the purposes of the analysis, the pressure at the mixing chamber exit is considered to be equal to the core inlet pressure. It is also assumed that the total pressure drop through the condensor and separator is of the order of 200 psia. To determine the pressure at the turbine inlet, it is assumed that the temperature and pressure rise in the reflector coolant is linear with axial distance through the reflector. Thus, for a turbine inlet temperature of 2400°R , reflector exit temperature of 4000°R , and reflector inlet temperature of 614°R , the pressure drop for the portion of the reflector up to the location where the hydrogen is channeled to the turbine is given by:

$$\Delta P_r^1 = \Delta P_r \frac{2400-614}{4000-614} = 0.528 \Delta P_r, \text{ psia}$$

where:

ΔP_r = the total pressure drop through the reflector, psia

ΔP_r^1 = the fractional pressure drop through the reflector, psia

The turbine inlet pressure is found from the following equation:

$$P_{ti} = P_{pe} - \Delta P_r(0.528) - \Delta P_n - \Delta P_{pl}$$

where:

P_{ti} = turbine inlet pressure, psia

P_{pe} = pump exit pressure, psia

ΔP_r = pressure drop through the reflector, psia

ΔP_n = pressure drop through the nozzle, psia

ΔP_l = pressure drop through the main propellant line, psia

The pressure drops through the hydrogen return line, jet pump, reflector, nozzle, and main propellant line are dependent on the hydrogen mass flow rates and the hydrogen flow path dimensions through the various components. The pressure and temperature profiles are thus dependent upon the core operating pressure and the hydrogen mass flow rate.

The hydrogen pressure at the separator exit is dependent on the uranium cycle pressures, since the separated hydrogen is in equilibrium with the uranium prior to entering the separator. As stated previously, the pressure drop through the condensor and separator is assumed to be 200 psia. In addition to this 200 psia drop, the uranium experiences an additional pressure drop through the uranium return line. The total uranium cycle pressure drop is compensated for by the uranium-hydrogen jet pump. The pressure at the separator outlet is thus:

$$P_{se} = P_{core} - \Delta P_{mc} - \Delta P_{ul}$$

where:

P_{se} = pressure at the separator exit, psia

P_{core} = core operating pressure, psia

ΔP_{mc} = hydrogen pressure drop through the mixing chamber, psia

ΔP_{ul} = uranium line pressure drop, psia

5.4.3 Jet Pump

The propellant-driver jet pump is used to develop the pressure rise required to offset the pressure losses incurred in the fuel loop. Typically, these losses would be of the order of one or two hundred pounds per square inch. The selection of the jet pump for circulation of the fuel is based on its simplicity and high reliability permitted by its lack of moving parts. The jet pump configuration is such that the hydrogen used to condense the uranium can also be utilized as the driving medium for the jet pump. Thus, the jet pump will be incorporated as part of the lower portion of the scoop to facilitate the simultaneous condensation and pressure increase of the uranium fuel.

5.4.4 Hydrogen Return Line

The total hot hydrogen mass flow rate in the hydrogen return line is equal to the sum of the diffused hydrogen caught in the scoop, the hydrogen transpiration coolant required for the interior scoop wall, and the cold hydrogen mixed in the jet pump to condense and cool the uranium to a temperature of 3000°R. From the uranium condensation section of this report, the quantities of diffused hydrogen and cold hydrogen were found to be 0.0139 and 21.1 lbm/sec, respectively, for a 3-ft scoop diameter. The quantity of transpiration hydrogen injected into the scoop was found to be 7.21 lbm/sec as determined from the scoop cooling evaluation section. Thus, the total mass flow rate combined with the uranium in the scoop is 28.31 lbm/sec. This quantity of hydrogen is also the amount of hydrogen that must be separated from the uranium in the separator and is the mass flow rate of hydrogen in the hydrogen return line. Thus, from Figure 5-62 an inside pipe diameter of 0.36 ft and a mass flow rate of 28.21 lbm/sec results in a pressure drop of 100 psi through the 25-ft hydrogen return line.

5.4.5 Pressure and Temperature Decrease through the Turbine

To obtain the turbine pressure drop, it is necessary to know the pumping requirements. The work per pound of liquid hydrogen required to pump the hydrogen isentropically from the propellant tank pressure to the required pump exit pressure is given by the following relation (assuming incompressible flow):

$$-W = \frac{c}{\eta_p} \int_{P_{ta}}^{P_{pe}} v \, dP$$

where:

- W = required pump work, Btu/lbm
- v = specific volume of hydrogen, ft^3/lbm
- P = pressure, lb_f/in^2
- P_{pe} = pump exit pressure, lb_f/in^2
- P_{ta} = tank pressure, lb_f/in^2
- c = $144/778$, $(\text{in}^2/\text{ft}^2)/(\text{ft-lb/Btu})$
- η_p = pump efficiency, unitless

Integrating the pump specific work equations yields (for constant v),

$$-W = \frac{144}{778} \frac{v}{\eta_p} (P_{pe} - P_{ta}), \text{ Btu/lbm}$$

The tank conditions are approximately 40°R and 30 psia. Assuming the specific volume remains constant, v is $0.237 \text{ ft}^3/\text{lbm}$ and thus the pump work equation reduces to the following pump power equation:

$$\text{Pump Power} = \frac{(144)(0.237)}{778\eta_p} (P_{pe} - 30) \dot{m}_p = \frac{0.0438}{\eta_p} (P_{pe} - 30) \dot{m}_p, \text{ Btu/sec}$$

where:

- \dot{m}_p = mass flow rate through pump, lbm/sec

This amount of power must be supplied by the turbine or,

$$\dot{m}_{tu} C_p \Delta T_{tu} = \frac{0.0438}{\eta} (P_{pe} - 30) \dot{m}_p$$

where:

\dot{m}_{tu} = mass flow rate through turbine, lbm/sec

C_p = heat capacity of hydrogen through the turbine, Btu/lbs $^{\circ}$ R

ΔT_{tu} = hydrogen temperature drop through the turbine, $^{\circ}$ R

η = combined efficiency of the turbine and pump, unitless

It will be assumed that the mixed mean temperature of the hydrogen from the reflector enters the turbine at 2400 $^{\circ}$ R and a pressure of P_{ti} . Assuming isentropic expansion through the turbine, the temperature ratio and pressure ratio across the turbine are related by the following expression:

$$\frac{T_{te}}{T_{ti}} = \left(\frac{P_{te}}{P_{ti}} \right)^{\frac{\gamma-1}{\gamma}}$$

where:

γ = the ratio of specific heats for hydrogen at the turbine average conditions

The expression relating the mass flow rate through the turbine and the pressure ratio across the turbine in terms of the pump exit pressure is the following:

$$\dot{m}_p \frac{(0.0438)}{\eta} (P_{pe} - 30) = \dot{m}_t T_{ti} c_p \left[1 - \left(\frac{P_{te}}{P_{ti}} \right)^{\frac{\gamma-1}{\gamma}} \right]$$

But from Figure 5-70, it is observed that the pressure at the turbine inlet, P_{ti} , is related to the pump exit pressure by the following:

$$P_{ti} = P_{pe} - \Delta P_{pl} - \Delta P_n - (0.528) \Delta P_r$$

Combining the previous two equations results in a single equation in terms of the pump exit pressure and the mass flow rate through the turbine,

$$P_{pe} = \frac{\eta \dot{m}_t C_p T_{ti}}{\dot{m}_p (0.0438)} \left[1 - \left(\frac{P_{te}}{P_{pe} - \Delta P_{pl} - \Delta P_n - (0.528) \Delta P_r} \right)^{\frac{\gamma-1}{\gamma}} \right]$$

For the topping cycle proposed, the mass flow rate through the turbine is taken to be the mass flow rate required to remove the nuclear radiation heating from the reflector. Thus, the above equation can be solved iteratively for the pump pressure.

In the previous equation, the factor outside the bracketed quantity has a large effect on the maximum turbine exit pressure, as well as the pump exit pressure. Figure 5-71 shows the maximum turbine exit pressure and maximum pump exit pressure as a function of this critical factor. From figure 5-71, it is observed that for a turbine inlet temperature of 2400°R, 100 percent turbopump efficiency, and turbine-to-pump mass flow rate ratio of 1.0. The maximum turbine exit pressure (or resulting core pressure) is 18,400 psia corresponding to a pump exit pressure of 51,200 psia, assuming no line losses. More realistically, with a turbopump efficiency of $(0.8)(0.7) = 0.56$, and a turbine-to-pump mass flow rate ratio of 81.6/149, the maximum turbine exit pressure is 5,500 psia with a corresponding pump exit pressure of 14,000 psia. Thus with line losses, it appears that an upper limit on the core pressure is of the order of 300 atmospheres.

5.4.6 Summary

Table 5-5 summarizes the flow path dimension through the various components. The flow path dimensions shown were selected on the basis that they appear to produce a reasonable compromise between the pressure drop through the component and the weight of the component. A dimension compromise is required since smaller component dimensions result in higher pressure drops which, in turn, result in a higher pump discharge pressure, and thus, a higher turbopump weight. The higher turbopump weight is, in turn, offset by the

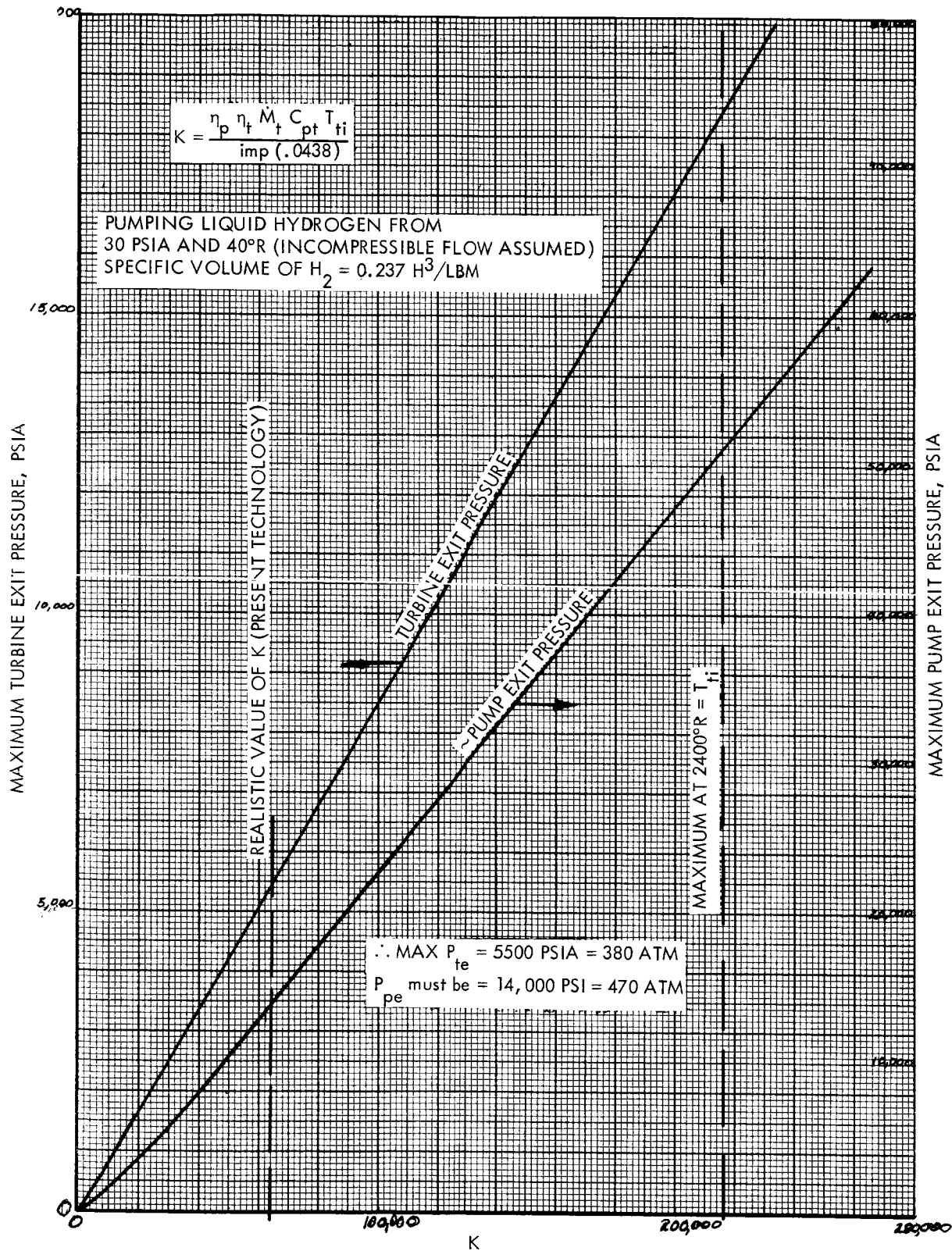


Figure 5-71. Maximum Turbine Exit Pressure and Maximum Pump Exit Pressure

Table 5-5

Component	Average m_H lbm/sec	Hydraulic Diameter	Length ft	Pressure Drop psia	Temperature Rise— $^{\circ}$ R
Main Propellant Line	148.62	0.5 ft	30	70	10° R
Nozzle	148.62	0.23 in	10.2	600	564° R
Reflector (Nuclear)	41.0	--	10	--	3500° R
Reflector (q/A)	28.74	0.262 in	10	454	3500° R
Separator	28.31 H_2 (54.8 U)	--	--	200	--
Hydrogen Return Line	28.31	0.36 ft	25	100	--
Uranium Return Line	54.8	0.07 ft	25	100	--

lower component weights resulting from the smaller component flow path dimensions. The pressures, temperatures, and mass flow rates for the uranium cycle, propellant cycle, and coolant cycle are summarized in figures 5-72, 5-73, and 5-74 for the engine core power level of 6×10^6 Btu/sec and core operating pressure of 100 atmospheres.

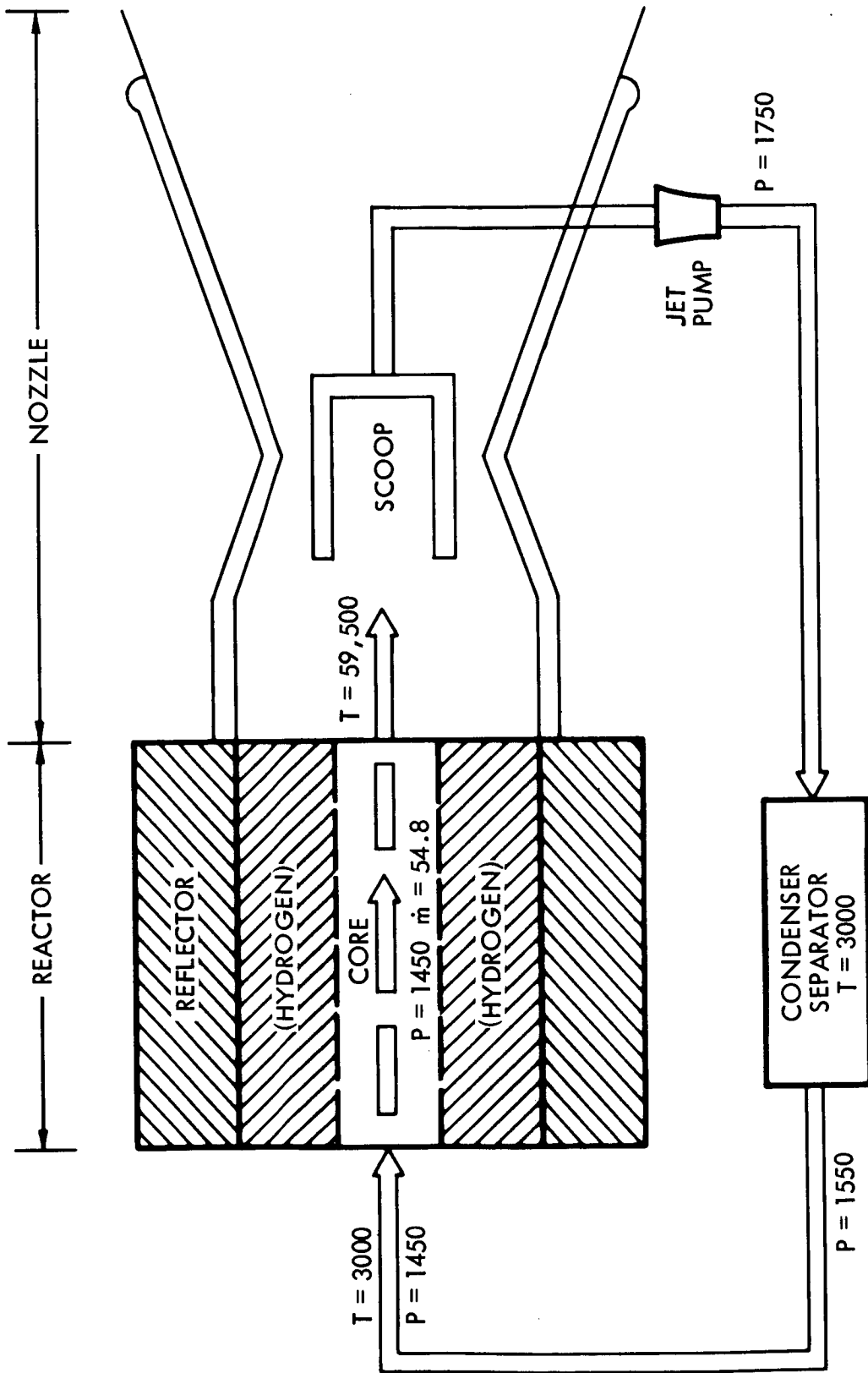
5.5 TOTAL ENGINE WEIGHT

The total engine weight is considered in this section. The engine weights for three different power levels and a core operating pressure of 100 atmospheres are obtained by summing the calculated engine component weights. From these three total engine weights, a curve of engine weight as a function of core power is constructed. This curve is important for assessing the weight penalties incurred in increasing the power level of a particular gas core nuclear rocket engine design.

5.5.1 Total Engine Weight

The total engine weight is determined by summing the weights of the individual engine components. The individual component weights are primarily a function of the hydrogen mass flow rate (or power) and the pressure at the component location. The results of the previous section, describing the relations governing the temperatures and pressures throughout the system along with the parametric analysis of the component weights, are used to obtain an estimate of the component weights for specified engine power and core operating pressure. Utilizing the flow path dimensions and the pressure drops through the major components that were given in the previous section, table 5-6 presents a summary of the component key dimensions, pressures, and weights for an engine operating at a power level of 6×10^6 Btu/sec. From table 5-6, the total engine weight is found to be of the order of 340,000 lbm. This weight value should be regarded as only a rough approximation. Based on the preliminary weight analysis, the weight may be incorrect by as much as -20% to +50%.

The total engine weights for the core thermal powers of 1.8×10^7 and 3.0×10^7 Btu/sec were obtained in a manner similar to the method employed to determine the total engine weight for the core thermal power level of 6.0×10^6



P, PRESSURE, PSIA
 T, TEMPERATURE, °R
 \dot{m} , MASS FLOW RATE, LB/SEC

Figure 5-72. Uranium Flow Schematic

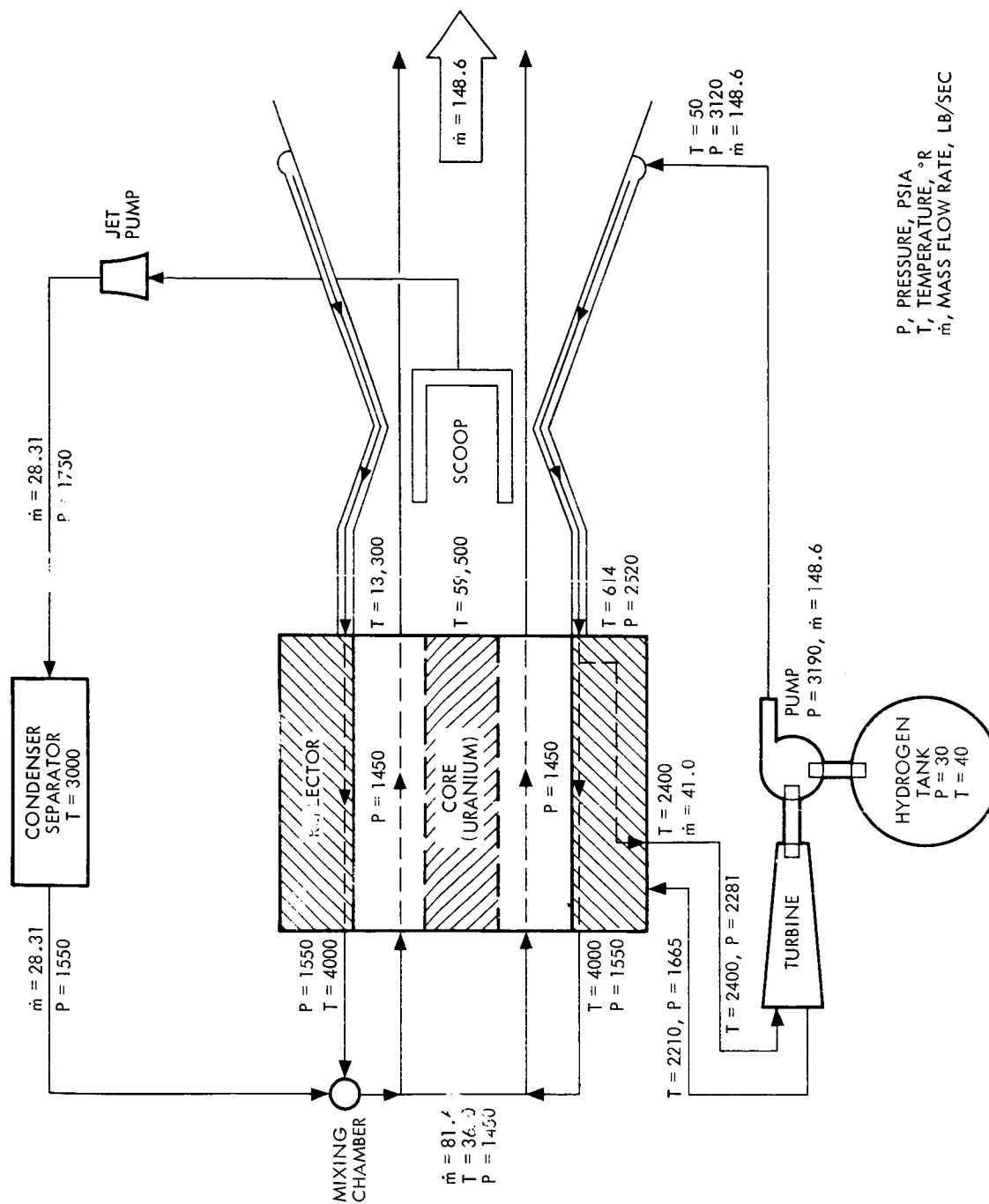


Figure 5-73. Propellant Flow Schematic

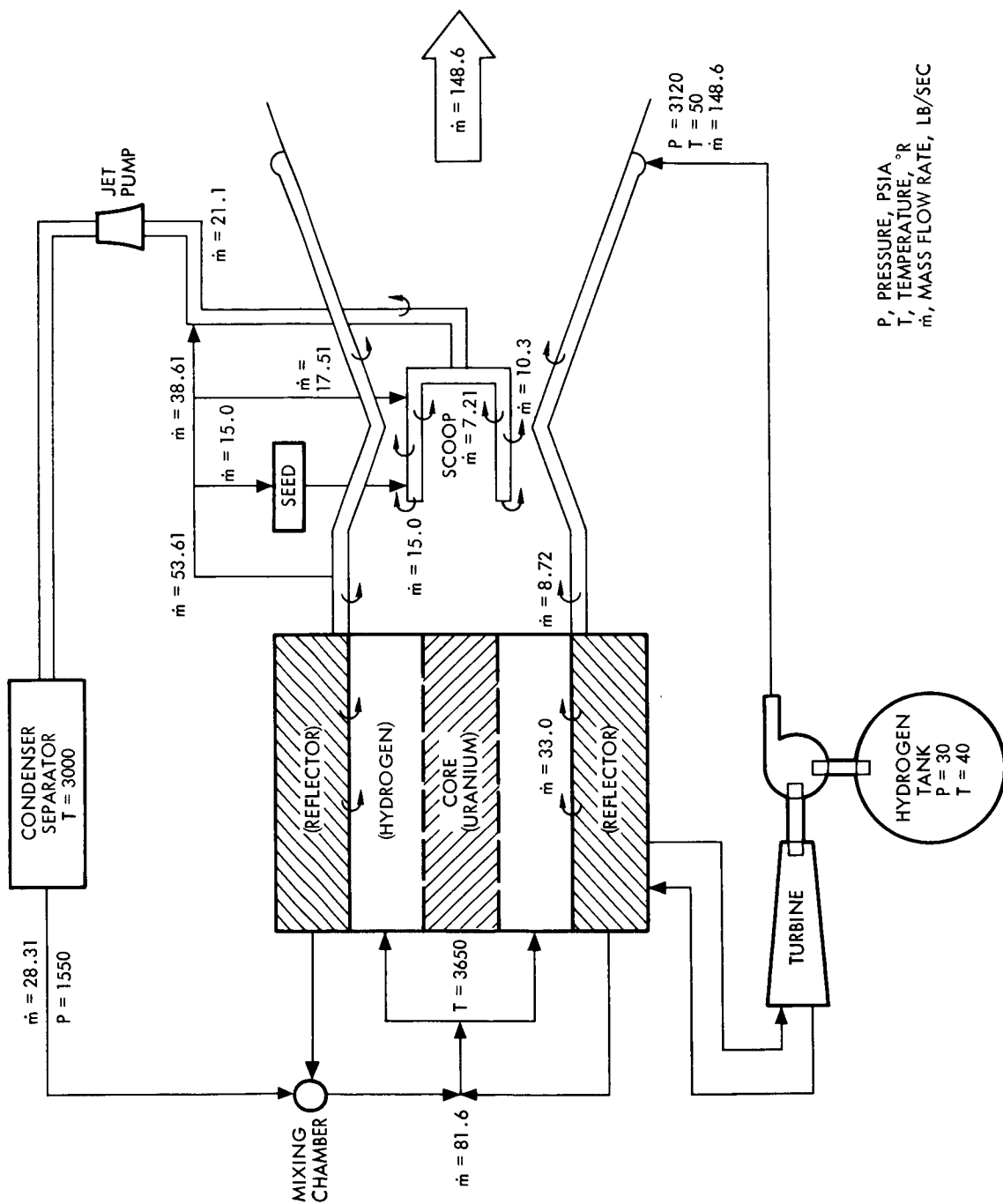


Figure 5-74. Coolant Flow Schematic

Table 5-6. Engine Weight Summary (Power = 6×10^6 Btu/sec, 6,340 MW)

Component	Local Pressure psia	Mass Flow Rate lbm/sec	Material Density lbm/ft ³	Allowable Stress (σ) psia	Weight
Uranium Fuel	--	54.8	--	--	1,000
Reflector (10% void)	--	--	--	--	162,000
Pressure vessel	1450	--	491	50,000	63,900
Radiation Shield	--	--	178	--	23,100
Nozzle	1450	149	491	30,000	49,000
Turbopump	3190	149	--	--	1,250
Main Propellant Line	3190	149	491	100,000	38
Uranium Line	1550	54.8	491	100,000	1
Thrust Structure	--	--	--	--	37,000
Scoop	1550	--	1200	100,000	265
Separator	1750	82.8	491	100,000	100
Auxiliary Components	--	81.6	--	--	2,035
TOTAL					<u>340,000</u>

Btu/sec. From an analysis of the temperature, pressure, and mass flow rate profiles, the component dimensions and pressure drops can be obtained for each power level. Table 5-7 summarizes the results from the cycle analysis for the two core power levels of interest. By knowing the pressure drops and mass flow rates through each of the components and specifying the core operating pressure, the local operating pressure and weight of each component can be obtained. Table 5-8 presents a summary of the component weights and the total weight for the two higher power levels of interest. The total engine weight as a function of power is shown in figure 5-75 for core power levels ranging from 0.5×10^7 to 3.0×10^7 Btu/sec.

Table 5-7

Component	Power Btu/sec	Average \dot{m}_H lbm/sec	Hydraulic Diameter ft	Length ft	Pressure Drop psia	Temp. Rise θ_R
Main Prop. Line	1.8×10^7	365.6	0.75 ft	30	100	10
Nozzle	1.8×10^7	365.6	0.447 in	10.2	600	520
Reflector (Nu)	1.8×10^7	173.2	--	10	--	--
Reflector (q/A)	1.8×10^7	35.0	0.252 in	10	500	3,000 exit
Separator	1.8×10^7	--	--	--	200	--
H ₂ Return Line	1.8×10^7	36.6	0.37 ft	25	100	--
U Return Line	1.8×10^7	54.8 (u)	0.07 ft	25	100	--
Main Prop. Line	3.0×10^7	574	0.95 ft	30	100	10
Nozzle	3.0×10^7	574	0.60 in	10.2	600	505
Reflector (Nu)	3.0×10^7	324.4	--	10	--	--
Reflector (q/A)	3.0×10^7	40	--	10	720	2,750 exit
Separator	3.0×10^7	--	--	--	200	--
H ₂ Return Line	3.0×10^7	43.6	6.39 ft	25	100	--
U Return Line	3.0×10^7	54.8(u)	0.07 ft	25	100	--

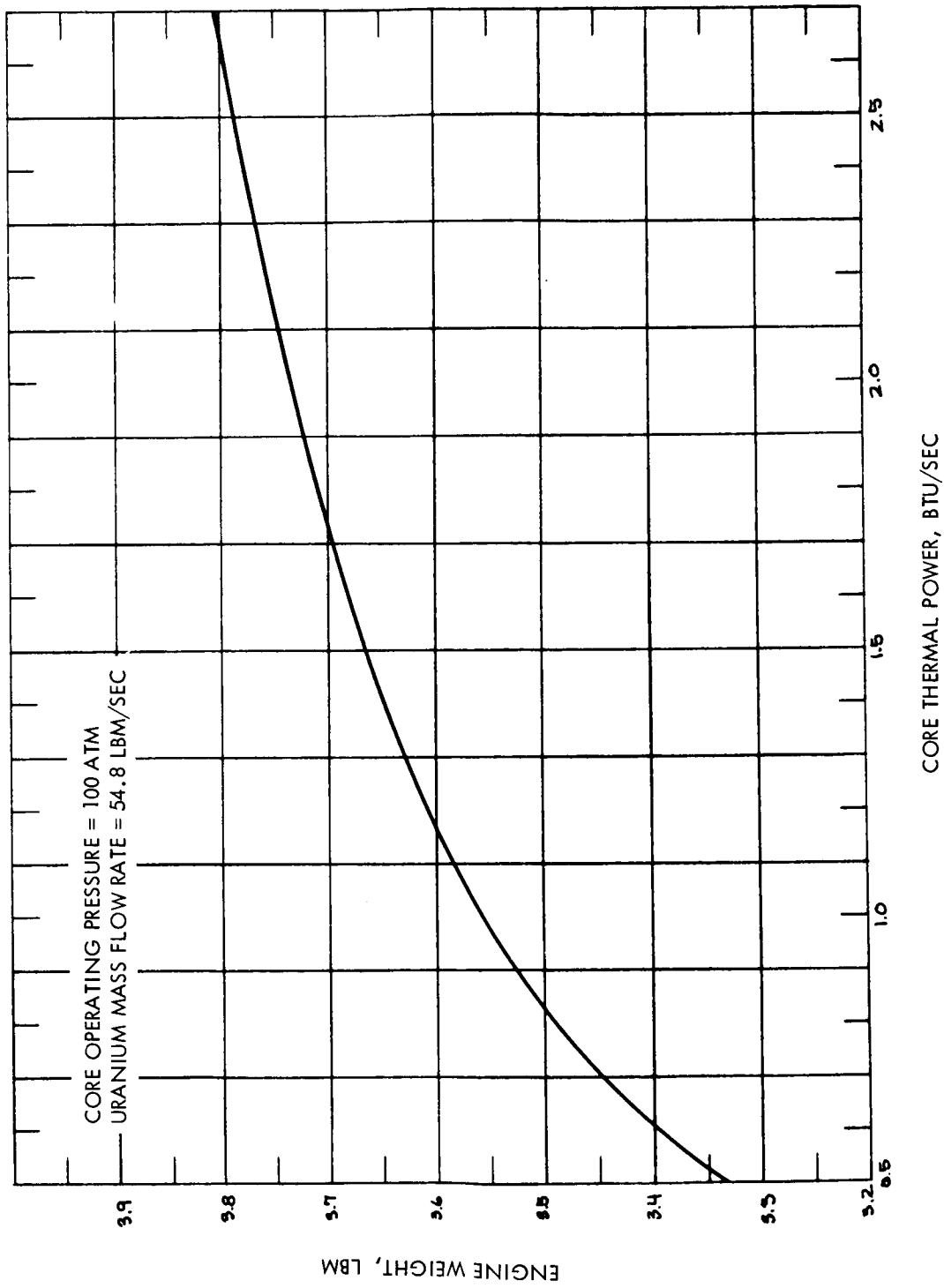


Figure 5-75. Engine Weight as a Function of Core Thermal Power

6. ENGINE PERFORMANCE ANALYSIS

The engine performance analysis is conducted for one of the reactor core flow schemes which appears to present the best engine performance. The configuration selected is the following: a fuel to cavity radius ratio of 0.6, uranium inlet velocity of 5 ft/sec, uranium mass flow rate of 54.8 lbm/sec, hydrogen inlet velocity of 50 ft/sec, hydrogen mass flow rate of 81.6 lbm/sec, average hydrogen temperature at the core exit of 13,300°R, total core thermal power of 6×10^6 Btu/sec, and the core operating pressure of 100 atmospheres.

The two best measures of the performance of an engine are the thrust-to-weight ratio and the specific impulse. The theoretical specific impulse of the gas core reactor engine is degraded in practice by the addition of relatively cool hydrogen from transpiration cooling, the hydrogen seeding coolant, the carbon seeding particles, and the addition of uranium from the core to the propellant stream. These means of specific impulse degradation are examined individually and are discussed in the following paragraphs.

6.1 URANIUM LOSSES

The uranium loss to the propellant stream is a function of the scoop diameter. Figure 5-43 shows the fraction of the total uranium entering the reactor core that is caught in the scoop. It is apparent that the uranium lost to the propellant stream is given by the following expression:

$$\dot{m}_{ul} = \dot{m}_u (1 - f_c), \text{ lbm/sec}$$

where:

\dot{m}_{ul} = mass flow rate of uranium lost to propellant stream, lbm/sec

\dot{m}_u = mass flow rate of uranium entering core, lbm/sec

f_c = fraction of uranium caught in the scoop.

For the purposes of the performance analysis, it is assumed that the temperature of the uranium in the propellant stream is equal to the average

temperature of the hydrogen propellant at an axial distance corresponding to the end of the scoop. Figure 2-10 shows the hydrogen propellant radial temperature profile as a function of distance from the leading edge of the scoop. For a scoop length of 3 ft, the mass flow rate weighted average hydrogen propellant temperature is found to be 12,040°R. The specific impulse of the uranium is estimated from the following equation:

$$I_{sp} = \sqrt{\frac{2\gamma}{\gamma-1} \frac{R_u}{Mg_c} T_c} \eta$$

where:

- I_{sp} = specific impulse, sec
- γ = ratio of specific heats, unitless
- R_u = universal gas constant, 1545 ft-lb_f/lb mole - °R
- M = molecular weight, lbm/lb mole
- g_c = constant, 32.17 lb_m - ft/lb_f - sec
- T_c = propellant temperature in the chamber, °R
- η = nozzle efficiency, unitless

For the gas core operating conditions presently under consideration, the specific impulse of uranium at 12,040°R and 100 atmospheres is 110.7 for $\gamma = 1.67$ and $\eta = 1$.

6.2 TRANSPIRATION COOL HYDROGEN ADDITION

The relatively cool hydrogen is added to the propellant stream as a by-product of the transpiration cooling process. This hydrogen enters the propellant stream at the same temperature as the hot side temperature of the transpiration-cooled wall. In the transpiration cooling analysis, it was assumed that the state-of-the-art at the time of the gas core nuclear rocket engine development would allow a hot side wall temperature of 3000°R. Since the specific impulse of the propellant is proportional to the square root of the absolute temperature, the addition of this 3000°R temperature hydrogen will result in a degradation of the overall specific impulse of the engine.

To determine the total quantity of cool hydrogen introduced to the propellant stream, it is necessary to first determine the heat flux to the walls adjacent to the propellant stream, then determine the quantity of hydrogen propellant per square foot required to flow through the walls to maintain a maximum wall temperature of 3000°R , and finally integrate the cooling requirement per square foot over the entire surface area exposed to the propellant stream. The total mass flow rate of the cool hydrogen entering the propellant stream is thus found from the following expression:

$$\dot{m}_H = \int_{\text{Area}} P \left(\frac{\dot{m}}{A_f} \right) dA_w, \quad \frac{\dot{m}}{A_f} = f(q/A_w)$$

where:

\dot{m}_H = total mass flow rate of cool hydrogen entering propellant, lbm/sec

P = porosity of wall material, unitless

\dot{m}/A_f = hydrogen mass flow rate per unit pore flow area, lbm/ft²-sec

q/A_w = heat flux incident on transpiration cooled wall, Btu/in²-sec

The heat flux to the walls adjacent to the propellant stream is obtained from the modified Lewis Research Center gas core computer program. The two transpiration cooled walls adjacent to the propellant stream are the reflector and convergent to the reactor wall, or the reflector and convergent nozzle section wall, as a function of the distance from the reactor cavity inlet. It is noted from figure 2-5 that the heat flux increases with distance from the reactor cavity inlet to a maximum of about 60 Btu/in²-sec at a location equivalent to the leading edge of the scoop and decreases to a value of 33 Btu/in²-sec at the end of the 3-ft scoop. Figure 2-11 shows the heat flux to the exterior surface of the scoop as a function of the distance from the scoop leading edge. It is noted that the heat flux decreases rapidly from a maximum of about 530 Btu/in²-sec at the scoop leading edge to a value of 136 Btu/in²-sec at the end of the 3-ft scoop.

The transpiration cooling requirement to maintain a maximum wall temperature of 3000°R in a heat flux environment as described in the preceding paragraph is described in the transpiration cooling section of this report. In the transpiration cooling section, figure 3-21 shows the hydrogen mass flow rate per unit pore flow area required to maintain a maximum wall temperature of 3000°R as a function of the incident heat flux and the pore diameter. For the purposes of the specific impulse degradation analysis, the average values of the heat flux are used to determine the transpiration coolant requirements. The actual heat flux that must be removed by transpiration cooling is equal to the difference between the total heat flux and the heat flux that can be removed regeneratively. From the convective cooling analysis section of this report, it is found that the highest average heat flux that can be realistically removed regeneratively from the reflector is $12.5 \text{ Btu/in}^2\text{-sec}$. For the nozzle convergent section, it appears that about $15 \text{ Btu/in}^2\text{-sec}$ is the upper limit for a realistic average heat flux that can be regeneratively removed. The average heat flux incident on the reflector wall is $24 \text{ Btu/in}^2\text{-sec}$ and incident on the nozzle convergent section is $42.9 \text{ Btu/in}^2\text{-sec}$. Thus, the net heat flux which must be removed from the walls by transpiration cooling is about $11.5 \text{ Btu/in}^2\text{-sec}$ and $28 \text{ Btu/in}^2\text{-sec}$ for the reflector and nozzle convergent section, respectively. From the scoop stress analysis, it was determined that the maximum heat flux that can be removed from the scoop is $20 \text{ Btu/in}^2\text{-sec}$.

The total quantity of transpiration coolant required for each of the three engine components (i. e. , the scoop exterior surface, the reflector wall, and the nozzle convergent section) is obtained from the following relation:

$$\dot{m}_{\text{Hc}} = \left(\frac{\dot{m}}{A_f} \right) P A_w$$

where:

\dot{m}_{Hc} = total mass flow rate of transpiration coolant for the particular engine component.

$\left(\frac{\dot{m}}{A_f} \right)$ = hydrogen mass flow rate per unit flow area required to remove the average heat flux

P = minimum porosity for the given \dot{m}/A_f to maintain a surface temperature of 3000°R

A_w total surface area of the component being transpiration cooled

The total surface area of the reflector adjacent to the propellant stream is 157 sq. ft. The convergent nozzle section surface area is 17.8 sq. ft., and the scoop exterior surface area is 28.3 sq. ft. The product of the transpiration coolant mass flow rate and the porosity are 0.21, 0.49, and 0.364 lbm/ft²-sec for the reflector, nozzle convergent section, and scoop exterior surface, respectively. Multiplying the mass flow rates per unit area by the total surface areas yields the total transpiration coolant mass flow rates for the three components. The transpiration coolant mass flow rates, average temperature, and specific impulse are summarized in table 6-1. The transpiration coolant for the reflector is assumed to be about $7,520^{\circ}\text{R}$ because the temperature of the transpiration coolant injected near the reactor inlet will increase to near the average propellant temperature ($12,040^{\circ}\text{R}$) while the temperature of the transpiration coolant near the core exit will only increase slightly. Thus the average temperature of the transpiration coolant for the reflector wall is approximately $7,520^{\circ}\text{R}$.

6.3 COOL HYDROGEN ADDITION WITH SEEDING

Seeded hydrogen (i. e., hydrogen seeded with 10^{-5} -cm diameter carbon particles) is utilized to partially block the thermal radiation from the hot propellant to the exterior surface of the scoop. The effect of the carbon, as well as the seeded hydrogen, on the specific impulse must be determined. From the scoop stress analysis, it was determined that the maximum heat flux that may be removed from the scoop exterior surface by transpiration cooling is 20 Btu/in²-sec. Since the heat flux incident on the scoop exterior surface at the leading edge is about 530 Btu/in²-sec, it is necessary to decrease the thermal radiation incident on the scoop exterior surface if the wall temperature is to remain at 3000°R . Figure 4-6 shows the hydrogen seeding coolant and carbon seeding requirements for the scoop exterior surface as a function reduction and the length of the scoop over which the seeding is to be effective.

Table 6-1*

Propellant Constituent	Mass Flow Rate lbm/sec	Temperature °R	Specific Impulse sec
Hot hydrogen	81.6	12,040	1868
Transpiration hydrogen**	19.02	3,000	683
Seeded hydrogen	15.0	6,500	1121
Transpiration hydrogen***	33.0	7,520	1311
Carbon seeding	0.713	6,500	360.6
Uranium	0.127	12,040	110.7

* Scoop diameter is 3.03 ft

** For the scoop exterior surface (10.3) and convergent nozzle section (8.72)

*** For the reflector wall

The equation for the average specific impulse of the engine is given by the following:

$$\bar{I}_{sp} = \frac{\sum_{i=1}^n I_{sp_i} \dot{m}_i}{\sum_{i=1}^n \dot{m}_i}$$

where:

\bar{I}_{sp} = average specific impulse of the engine, sec

I_{sp} = specific impulse of the i^{th} propellant constituent, sec

\dot{m} = mass flow rate of the i^{th} propellant constituent, lbm/sec

Subscripts:

$i = 1$, transpiration hydrogen (3000°R)(for nozzle and scoop)

$i = 2$, hydrogen propellant (12,040°R)

From figure 4-6 the hydrogen mass flow rate is 15 lbm/sec and the weight fraction of carbon is 0.0475 to produce an approximate radiation reduction of about 96 percent over the first foot of the scoop length. The one-foot length is valid for the purpose of the specific impulse calculation since it is assumed that the nozzle throat occurs at a distance of one foot from the leading edge of the scoop.

The specific impulse of the carbon is found from the same equation used for the uranium specific impulse given previously. The seeding analysis was performed by assuming that the carbon seeding was effective for controlling thermal radiation transmission for carbon temperatures up to 6500°R . Thus, it is assumed that, after passing the first foot length of the scoop, the carbon temperature is 6500°R . For a carbon temperature of 6500°R , ratio of specific heats of 1.667, and an assumed nozzle efficiency of 100 percent, the specific impulse of the carbon constituent of the propellant is 360.6 sec. The carbon mass flow rate is found to be 0.713 lbm/sec from the required carbon-to-hydrogen mass fraction of 0.0475 and the seeded hydrogen mass flow rate of 15 lbm/sec.

The seeded hydrogen is assumed to be in equilibrium with the carbon seeding at a temperature of 6500°R at the nozzle throat. From reference 34 the specific impulse of hydrogen at 6500°R and 100 atm is 1121 sec. The specific impulse data for the seeded hydrogen and carbon seeding are summarized in table 6-1.

6.4 SPECIFIC IMPULSE DEGRADATION

The average specific impulse of the engine for the combined propellant consisting of the hot hydrogen, transpiration hydrogen, seeded hydrogen, carbon seeding, and uranium is determined by weighting the specific impulse of each of the propellant constituents by the mass flow rate of such constituent. Table 6-1 summarizes the propellant composition:

i = 3, uranium (12,040°R)

i = 4, seeding hydrogen coolant (6,500°R)

i = 6, transpiration hydrogen (7,520°R)(for reflector)

From the above equation and the data presented in table 6-1, the average specific impulse of the engine for the specified conditions is 1506 sec.

6.5 TOTAL THRUST AND MASS FLOW RATE

The total thrust and propellant mass flow rate of the engine are calculated as follows:

$$F_t = \sum_{i=1}^n I_{sp_i} \dot{m}_i$$

$$\dot{m}_t = \sum_{i=1}^n \dot{m}_i$$

where:

F_t = total thrust, lb_f

\dot{m}_t = total propellant mass flow rate, lbm/sec

From table 6-1, the total thrust is 224,781 lb_f and the total mass flow rate of the propellant is 149.4 lbm/sec .

From the engine total weight section, the engine total weight was found to be approximately 340,000 lb. Thus, the engine thrust to weight ratio for the specified engine power of 6×10^6 Btu/sec (or 6320 MW) is equal to 0.667.

6.6 ENGINE PERFORMANCE AS A FUNCTION OF POWER

The performance of the gas core reactor nuclear rocket engine is very dependent on the core thermal power of the reactor. The major engine parameter that is affected by changes in core thermal power is the propellant mass flow rate required to obtain approximately the same propellant exit temperature. Table 6-2 is a summary of the results for three different core thermal power levels and two values of core operating pressure.

Table 6-2*

P atm	Q_t Btu/sec	U_u ft/sec	U_h ft/sec	\dot{m}_u lbm/sec	\dot{m}_h lbm/sec	T_{prop} T_R	Q_w/Q_t %	Q_w Btu/sec
100	6×10^6	5	50	54.8	81.6	1.33×10^4	9.05	5.4×10^5
100	1.8×10^7	5	150	54.8	244.8	1.40×10^4	5.45	9.80×10^5
100	3.0×10^7	5	250	54.8	408.0	1.43×10^4	4.56	1.37×10^6
1000	6×10^6	2.5	5	27.4	81.6	1.51×10^4	15.37	9.22×10^5
1000	1.8×10^7	2.5	15	27.4	244.8	1.66×10^4	7.68	1.38×10^6
1000	3.0×10^7	2.5	25	27.4	408.0	1.69×10^4	6.11	1.84×10^6

* All three power levels are for a hub-to-tip ratio of 0.6 and a thermal radiation coefficient of 3 ft^{-1}

In observing the values in table 6-2 it does not appear, at first glance, that there is a heat balance. However, the lower percentage heat flux delivered to the reactor wall for $Q_t = 1.8 \times 10^7$ and 3.0×10^7 Btu/sec is absorbed by the hydrogen and produces the higher propellant exit temperature. Another point which arises from the inspection of table 6.2 concerns the lower percentage heat flux to the reactor wall for the higher core power levels. The lower heat flux to the reactor wall at the higher core power levels may be explained as follows: the majority of the heat flux to the reactor wall is transferred by thermal radiation from the hot hydrogen propellant. Tripling the core power and the propellant mass flow rate (as in the second case in table 6-2) results in an average uranium temperature only slightly higher than that for the original core power level. The heat flux to the hydrogen mass flow rate is also tripled, the average temperature of the hydrogen remains approximately the same. With the same hydrogen temperature profile, the hydrogen propellant will transfer essentially the same heat flux to the reactor wall as in the case with the original core power level. Thus the fraction of

the total core power that is delivered to the reactor wall should be about 1/3 that for the original core power level. As observed from table 6-2, the percentage of the total heat transferred to the reactor wall is actually greater than 1/3 the previous case. The reason for the unexpected greater percentage core power delivered to the reactor wall is that some heat is transferred directly to the reactor wall from the hot uranium. The heat flux delivered to the reactor wall increases with increasing uranium temperature and, thus, the heat flux to the wall is proportionately higher since the uranium temperature is higher.

The exit temperature of the propellant is related to the specific impulse of the engine and thus affects the engine performance. As was shown previously in the engine performance section of this report, the temperature of the propellant, after leaving the core exit, is reduced while flowing past the scoop. Since the chamber temperature of the propellant is only known for the first case in table 6-2, it is necessary to develop a means of scaling the chamber temperature for other cases of interest. The temperature decrease of the propellant is due to the thermal radiation to the scoop and reactor walls. Thus the following relation must be satisfied:

$$\frac{q}{A_w} = \frac{\dot{m}_H}{A_w} C_p (T_1 - T_2) \simeq K^1 (\bar{T}^4 - T_w^4)$$

where:

- q/A_w = the heat flux transferred to exposed wall surface, $\frac{\text{Btu}}{\text{in}^2 \cdot \text{sec}}$
- \dot{m}_w = hydrogen propellant flow rate, lbm/sec
- A_w = total surface area of the exposed wall, in^2
- C_p = specific heat of the hydrogen, Btu/lbm- $^{\circ}\text{R}$
- T_1 = core exit temperature of hydrogen, $^{\circ}\text{R}$
- T_2 = chamber temperature, $^{\circ}\text{R}$
- K^1 = radiation constant = $f(\text{shape factor}, \epsilon, \sigma)$, Btu/in $^2 \cdot \text{sec} \cdot ^{\circ}\text{R}^4$

$$T = (T_1 + T_2)/2, \text{ } ^\circ\text{R}$$

$$T_w = \text{temperature of the exposed wall surface} = 3,000^\circ\text{R}$$

From the above equation, a new constant K can be obtained from the case with the known temperature decrease,

$$K = \frac{C_p}{A_w K^1} = \frac{(\bar{T}^4 - T_w^4)}{\dot{m}_H (T_1 - T_2)}$$

From the known values, K is found to be,

$$K = \frac{\left[\frac{13,300 + 12,040}{2} \right]^4 - (3,000)^4}{81.6(13,300 - 12,040)} = 2.69 \times 10^{11} \frac{\text{sec-}^\circ\text{R}^3}{\text{lbm}}$$

Using the values of \dot{m}_H and T_1 from table 6-2, it is possible to iteratively solve the following equation for T_2 .

$$2.69 \times 10^{11} = \frac{\frac{(T_1 + T_2)^4}{2} - T_w^4}{\dot{m}_H (T_1 - T_2)}$$

Figure 6-1 shows the hydrogen exit temperature from the core and the hydrogen chamber temperature as a function of the hydrogen mass flow rate for both the 100 atm and 1000 atm cases. The 1000 atm cases were calculated by assuming that the same value of K was valid for both the 100 and 1000 atm conditions. Since the specific impulse of the hydrogen propellant is a function of the chamber temperature and pressure, figure 6-1 relates the specific impulse, mass flow rate, and the thrust of the pure hot hydrogen propellant as a function of the core thermal power.

To determine the actual temperature of propellant due to the mixing of the transpiration hydrogen, seeded hydrogen, and carbon seeding with the propellant, it is necessary to determine the heat flux to the surfaces adjacent to the propellant stream as a function of core thermal power. An

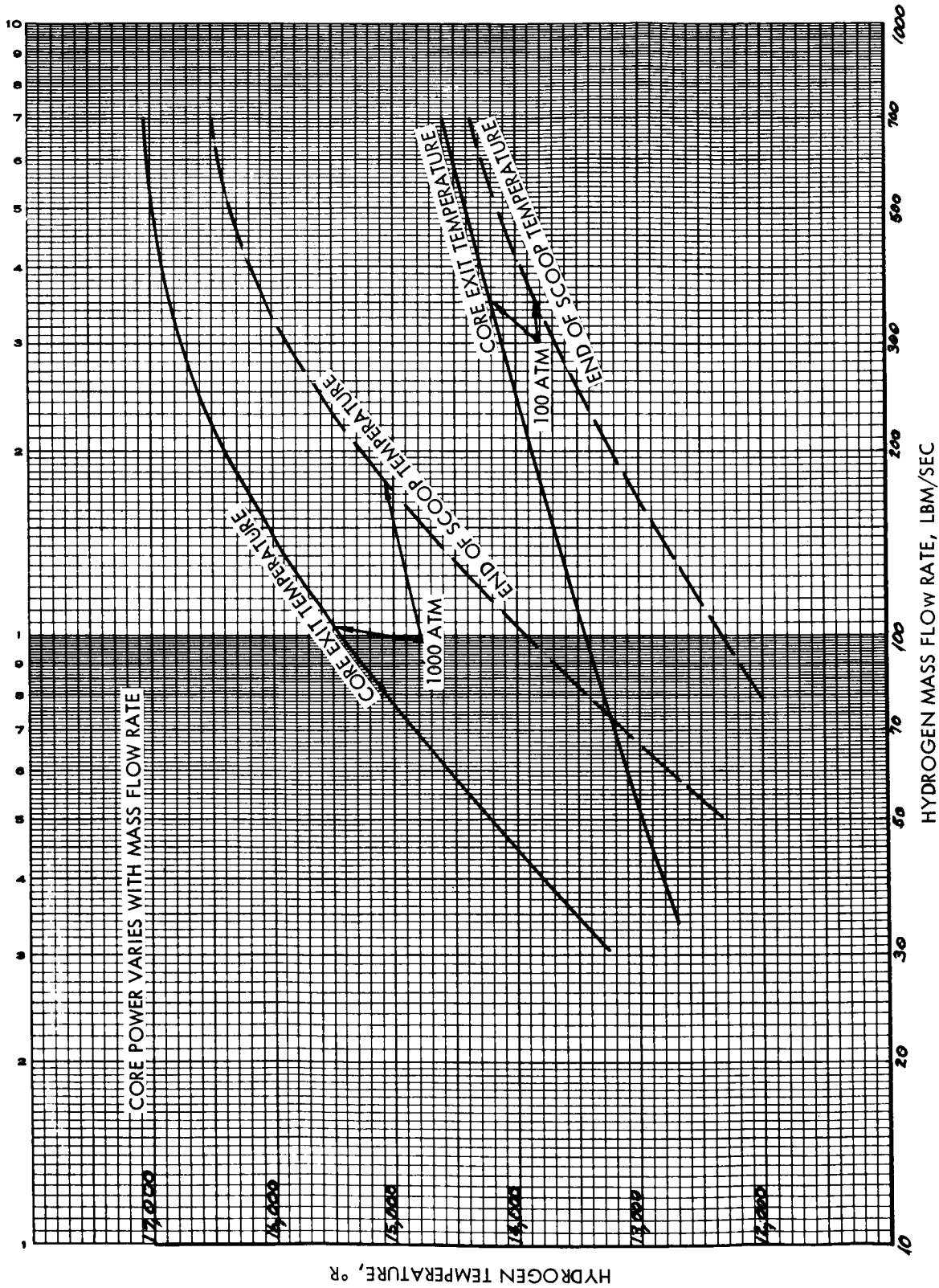


Figure 6-1. Hot Hydrogen Temperature at the Core Exit and at the End of the 3 Foot Scoop

estimation of the heat flux delivered to the surface of the nozzle convergent section and the surface of the scoop exterior is given by the following relation:

$$(q/A)_i = \left(\frac{q}{A} \right)_o \frac{\bar{T}_i^4}{\bar{T}_o^4}$$

where:

$$(q/A)_i = \text{heat flux at power } i, \text{ Btu/in}^2\text{-sec}$$

$$(q/A)_o = \text{heat flux at } 6 \times 10^6 \text{ Btu/sec, Btu/in}^2\text{-sec}$$

$$\bar{T}_i = \text{average hydrogen temperature at power } i, \text{ }^\circ\text{R}$$

$$\bar{T}_o = \text{average hydrogen temperature at } 6 \times 10^6 \text{ Btu/sec, }^\circ\text{R}$$

The total heat flux delivered to the reflector wall as a function of core power is given in table 6-2.

From the figure showing the heat flux to the reactor wall as a function of axial distance from the reactor inlet, figure 2-5, it is possible to obtain the average heat flux to the surface of the nozzle convergent section. The average heat flux to the nozzle convergent section is found to be 42.9 Btu/in²-sec. From figure 2-11, the maximum heat flux to the exterior surface flux to the nozzle convergent section and exterior scoop surfaces along with the average hydrogen temperature of 12,670^oR, the expressions for the heat flux become:

$$\text{Nozzle: } (q/A)_i^{\text{ave.}} = \frac{(42.9)}{(12,670)^4} \bar{T}_i^4 = (1.547 \times 10^{-15}) \bar{T}_i^4$$

$$\text{Scoop: } (q/A)_i^{\text{max.}} = \frac{530}{(12,670)^4} \bar{T}_i^4 = (1.910 \times 10^{-14}) \bar{T}_i^4$$

The average temperature \bar{T}_i as a function of hydrogen mass flow rate is obtained from figure 6-1. The average heat flux to the nozzle convergent section and the maximum heat flux to the exterior surface of the scoop are shown in figure 6-2 as a function of hydrogen mass flow rate.

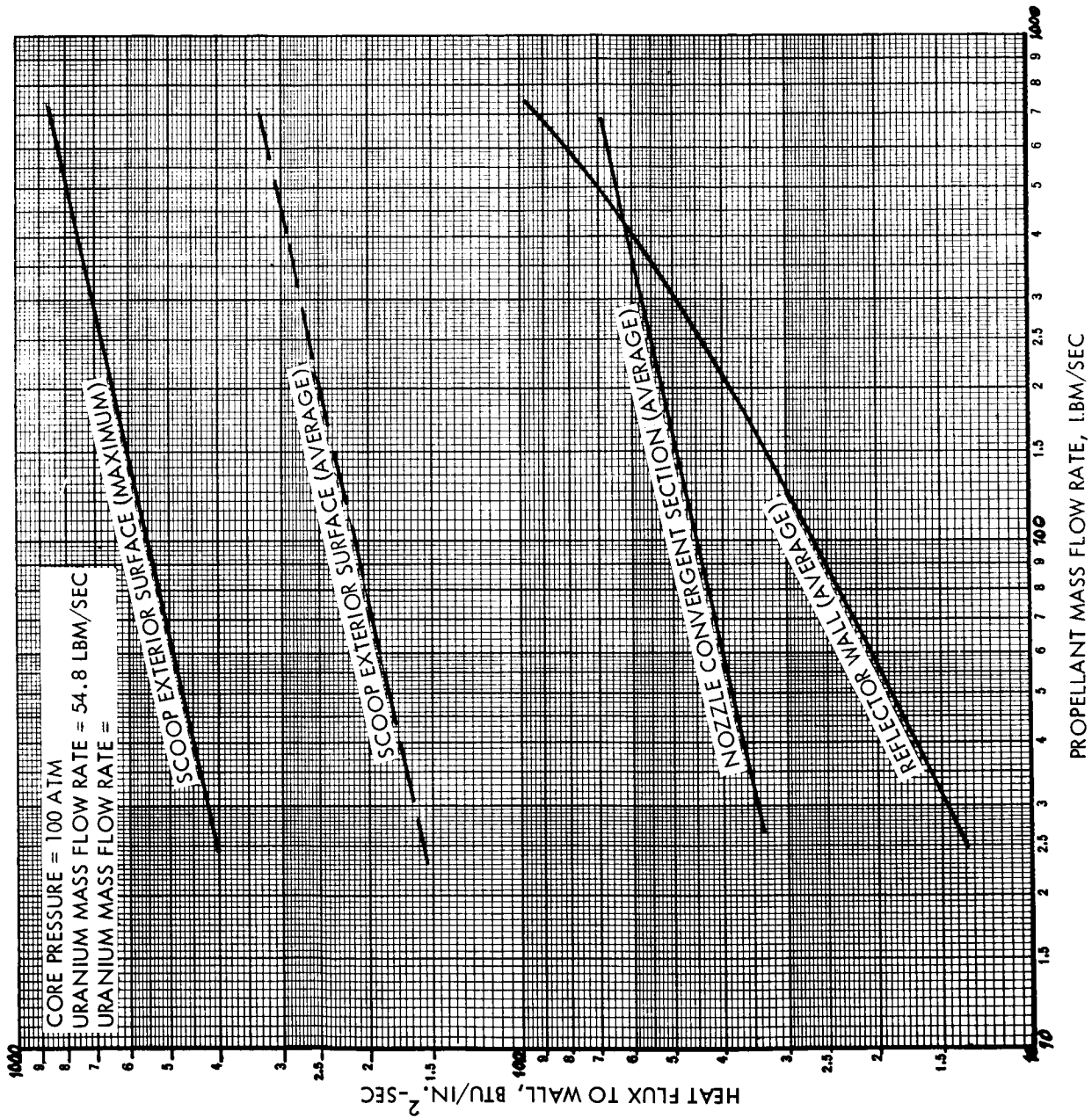


Figure 6-2. Heat Flux to the Exposed Surfaces Adjacent to the Propellant Stream

The actual transpiration hydrogen required for each of the three components is obtained by subtracting the quantity of heat that can be removed by either regeneratively cooling the components or blocking the thermal radiation transmitted to the components. To facilitate the calculation of the engine performance as a function of power, it is assumed that the amount of heat that can be regeneratively removed from the reflector and nozzle convergent section remains constant with power. Since the heat flux that can be removed from the scoop is limited by thermal and mechanical stress limitations, the maximum heat flux that can be removed by transpiration cooling remains constant at $20 \text{ Btu/in}^2\text{-sec}$. Figure 6-3 summarizes the heat fluxes and methods of heat removal for each of the three components as a function of core thermal power.

The mass flow rates required to cool the three components are obtained by utilizing the same approach used in the previous engine performance section. Figure 6-4 shows the mass flow rates required to transpiration cool the reflector and nozzle convergent section and to block the thermal radiation to the scoop interior surface by seeding. For the performance analysis, it is assumed that the transpiration hydrogen exits at a temperature of 3000°R for the scoop and the nozzle convergent section, the carbon and seeded hydrogen exit at a temperature of 6500°R , and the transpiration hydrogen for the reflector exits at a temperature equal to the average between 3000°R and the hot hydrogen average exit temperature shown in figure 6-1. In addition, the diffused uranium that flows out the nozzle is at a temperature equal to the hot hydrogen exit temperature. Employing the above assumptions and the mass flow rates shown in figure 6-4, the average specific impulse of the gas core engine as a function of power is obtained and is presented in figure 6-5. Also included in figure 6-5 are the total mass flow rate of the propellant and the total thrust of the engine as a function of power. The thrust to weight ratio as a function of core thermal power is shown in figure 6-6. Thus the gas core nuclear rocket engine performance is summarized in figure 6-5 and 6-6 for the core operating pressure of 100 atmospheres. For an operating pressure of 100 atm, the engine thrust to weight ratio varies between 0.6

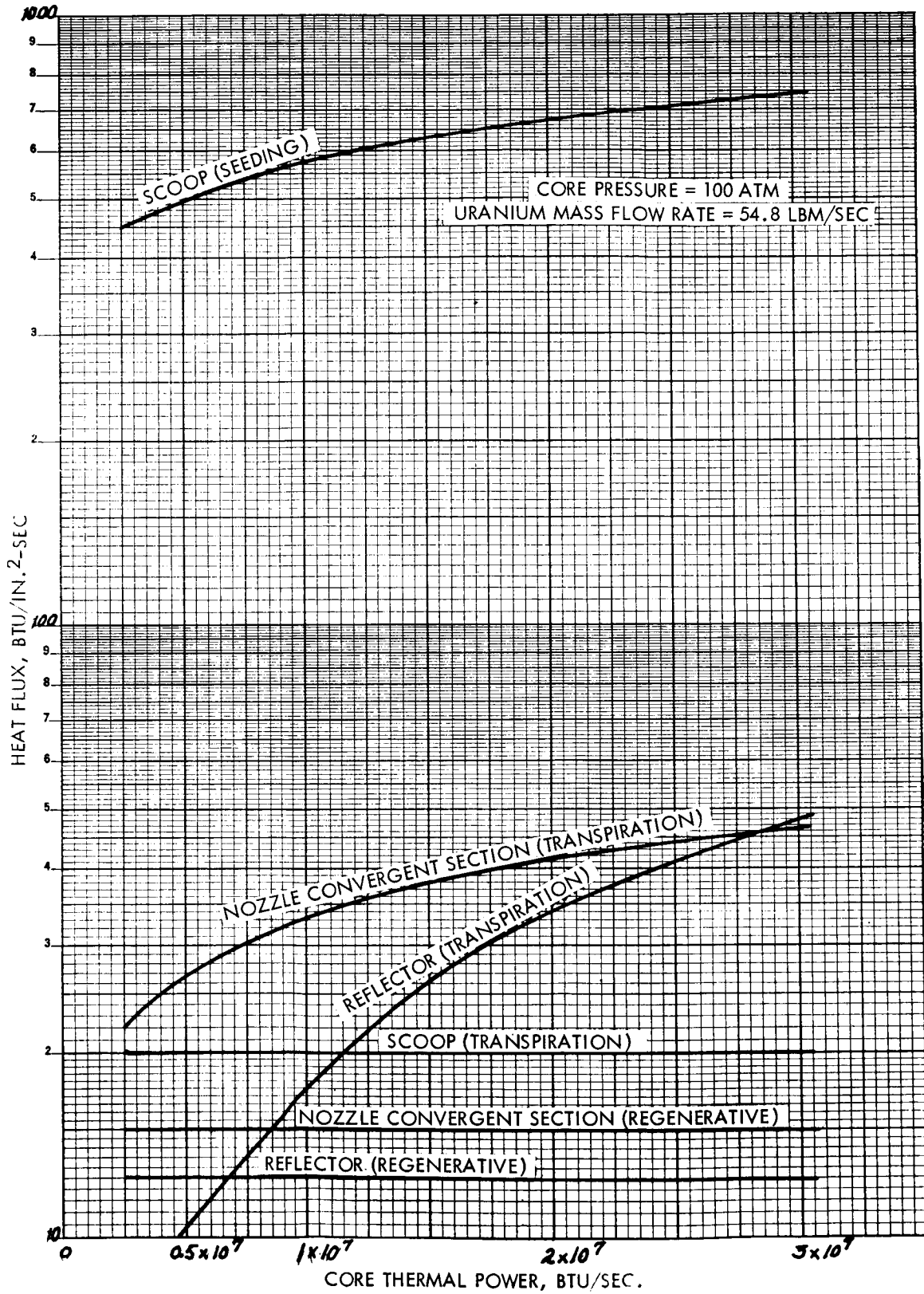


Figure 6-3. Required Heat Flux Removal for the Scoop, Nozzle, and Reflector

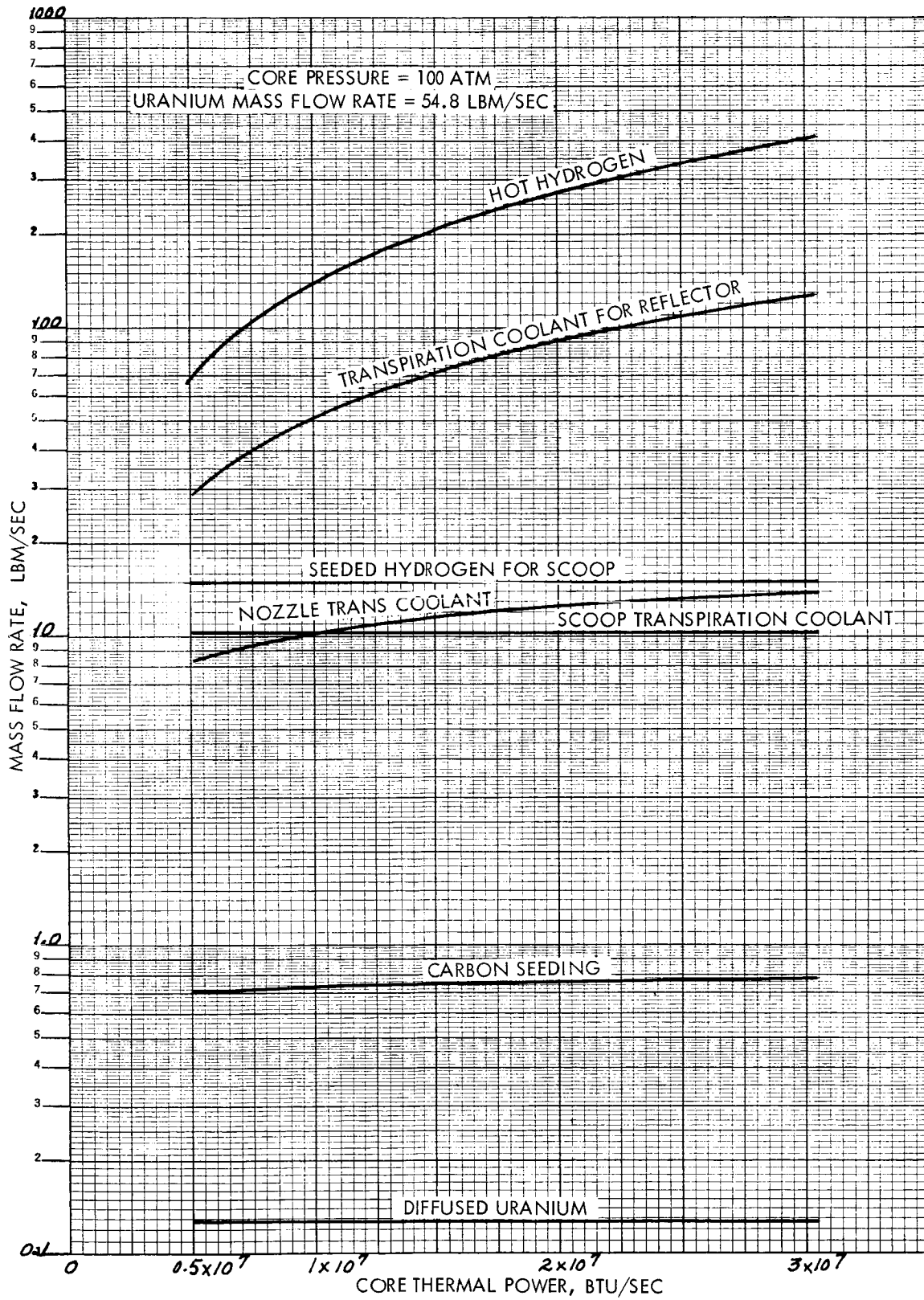


Figure 6-4. Mass Flow Rates of the Propellant Constituents

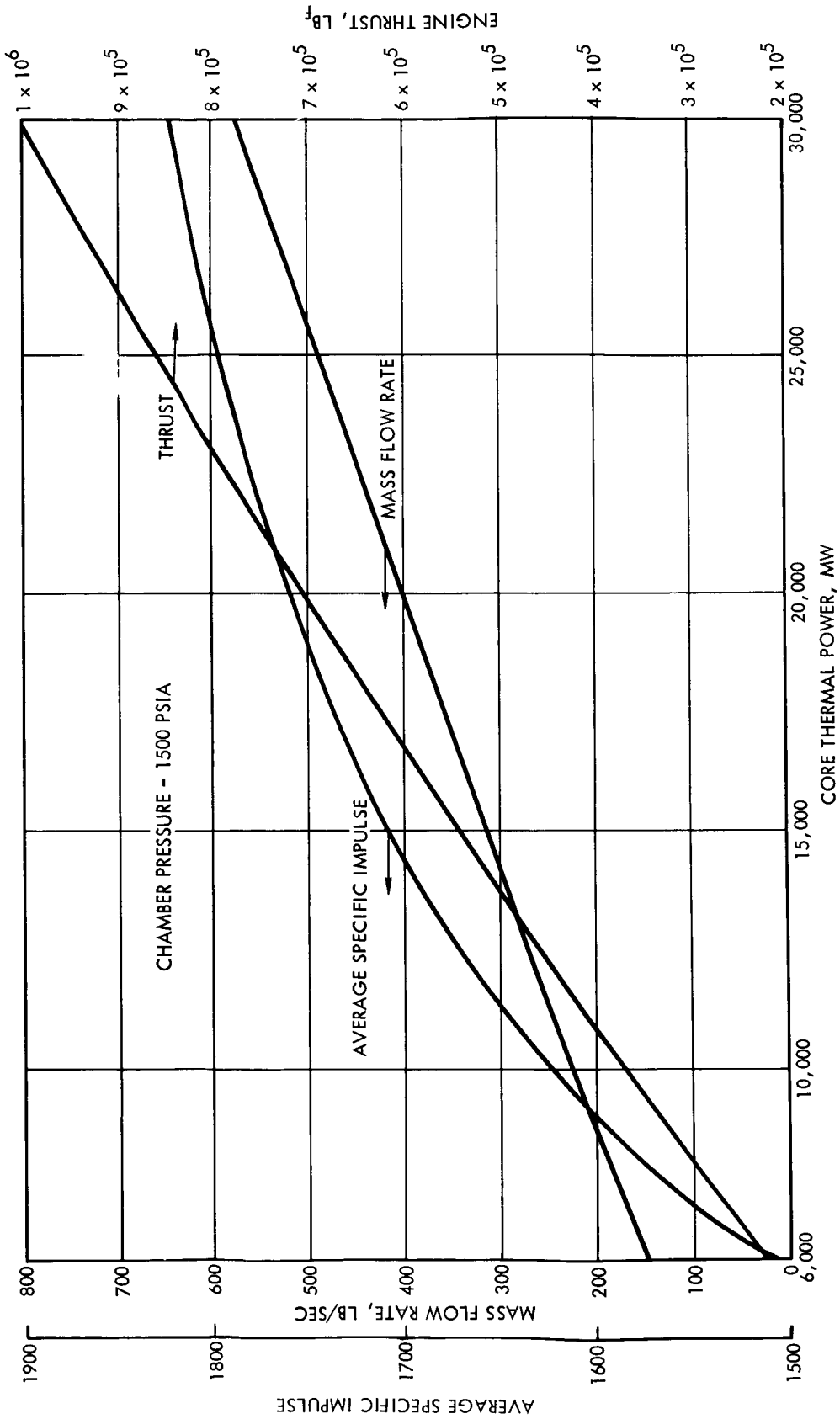


Figure 6-5. Engine Performance

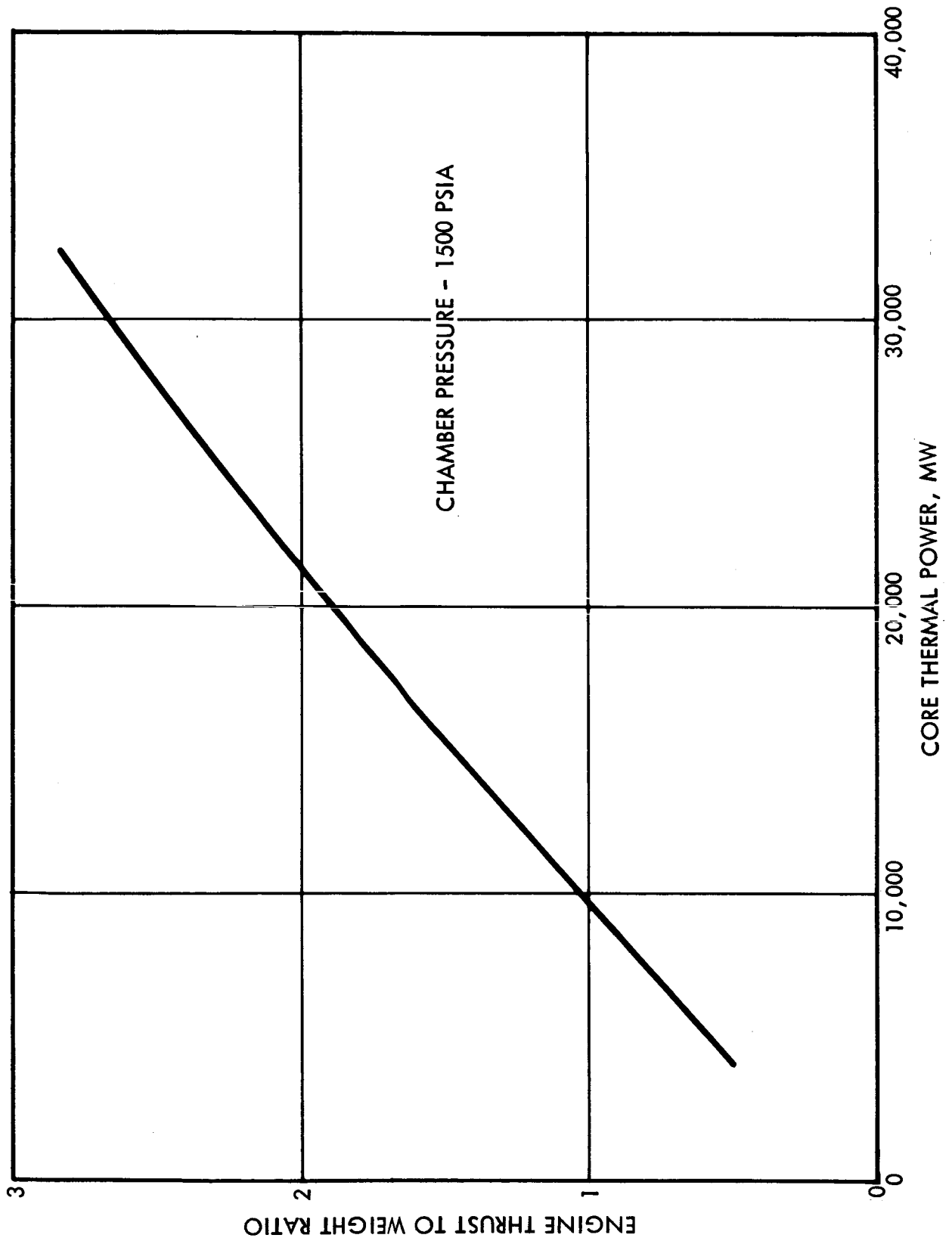


Figure 6-6. Engine Thrust to Weight Ratio

and 3.0. The results of this analysis show the desirability of operating at high power levels. The increase in thrust to weight ratio with power should level off due to thermal limitations. However to date no limitations as to the thermal blockage which can be obtained by seeded films or injected boundary layers have been determined. If the operating pressure increases significantly due to criticality considerations, then the thrust to weight ratio would be expected to decrease.

7. SUMMARY AND RECOMMENDATIONS

This study surveys in sufficient detail the potential of the gaseous core reactor proposed herein and delineates critical problem areas needing additional investigation. Primarily, the study confirms the feasibility of the scoop thermal design.

7.1 SCOOP EVALUATION

The principal task of this study was to examine the feasibility of the scoop under its extreme thermal environment. The NASA/Lewis heat transfer program, with suitable modifications, was used in predicting the unattenuated radiant heat flux and temperature distribution in the vicinity of the scoop. Radiation heat fluxes of 500 Btu/sec-in² at the leading edge of the scoop were predicted. Heat fluxes of this magnitude are extremely high, when judged by present standards. Recent work at NASA indicates that radiant heat fluxes can be attenuated more than two orders of magnitude by interposing a layer of material that is highly absorbing to thermal radiation between the incident radiation and the wall surface. In this study, a cool seeded layer of hydrogen enveloped the leading edge and downstream surfaces such that 96 to 99 percent of the radiant heat flux was blocked. Carbon or tungsten particles can be used as an effective seeding agent on the exterior surface and carbon or uranium particles in the interior of the scoop. In the case of uranium particles, additional investigation must be done to establish the advisability of this seeding material in the vicinity of an active fissioning environment. In any case, if carbon is used, the degradation in specific impulse due to the increased molecular weight of the propellant is negligible.

The heat flux incident on the wall and made up of the residual radiant heat and a small convective component can be made less than 20 Btu/sec-in² in the most severe location. The effectiveness of transpiration cooling techniques was examined in some detail and showed that pore sizes of 5 microns or less are necessary in a 30 percent porous wall to withstand heat fluxes of 150 Btu/sec-in². However, when practical considerations are given to the attendant pressure drops (500 psi), thermal stresses, and paucity of strength data on porous material properties, it was concluded that porous tubes may be used for transpiration cooling up to 20 Btu/sec-in². Reasonable advances in powder metallurgy techniques may be expected to increase the available porous material strength and make possible cooling of fluxes up to 100 Btu/sec-in².

The principal mechanism for reducing the heat fluxes to manageable values is due to the effectiveness of the seeded layer. Since this is crucial for the scoop, and in other advanced propulsion concepts, it is recommended that NASA continue with a rigorous analytical and experimental program on the effectiveness of seeding with the practical constraints of maintaining film stability under expected levels of turbulence. More emphasis should also be placed on advances in (and demonstrating) the capabilities of transpiration cooling technology including:

- 1) proving the unimpaired effectiveness of the transpiration cooling mode for long duty cycles under full load and
- 2) determining the actual high temperature strength and life expectancy of porous refractory materials.

Seeding has three major benefits to this proposed concept: First, seeding blocks the heat to the wall permitting conventional cooling techniques be utilized. Second, by selectively seeding the reactor cavity a much more favorable average propellant/uranium core surface temperatures can be obtained. This means a higher specific impulse can be achieved for the same scoop thermal environment. Third, the inherent limitation in specific impulse due to the regenerative cooling requirement can be minimized. Before heating, in the reactor, the hydrogen regeneratively cools the heat deposited in the structure and the heat remaining in the uranium column collected by the scoop. Therefore, the hydrogen temperature at reactor inlet is limited to temperatures compatible with structural cooling and the effective specific impulse is thus constrained by this relationship.

$$\text{Effective Isp}^2 \propto \text{Reactor inlet temp} / \frac{\text{Regenerative heat removed}}{\text{Total heat}}$$

This means that the regenerative heat load is detrimental to a high specific impulse. Seeding keeps the thermal radiation from reaching the walls and increases the regenerative heat load.

7.2 HEAT TRANSFER

Heat transfer is another important problem in the gas-core reactor. Heat must be transferred from the hot central uranium core to the surrounding stream of hydrogen without a significant portion reaching the reactor walls. The mechanism for heat transfer cannot be convective as this would lead to large mixing losses between the streams with the loss of unfissioned fuel making the system economically unsound. Heat transfer by radiation is the most desirable heat transfer agent, but there is no program presently available that provides a

complete solution to the heat transfer problem in the reactor. There are acceptable simplifications in the limits of optically transparent and opaque mediums. However, neither of these limiting conditions are really appropriate to the present problem.

A computerized solution by Einstein, made available from NASA/Lewis, was modified to provide the predictions of heat transfer in the reactor and in the vicinity of the scoop. The program is presently constrained to limited geometry, constant transport properties across the streams, and an optical path length of $\frac{1}{20}$. The program proved inadequate in the case of the optically dense uranium fuel column. Rosseland's approximation with a jump boundary temperature condition had to be employed to estimate the radial distribution of core temperature and heat flux distribution. A typical case shows the average propellant temperature at the reactor exit is 0.6 times the uranium core surface temperature. The hydrogen at high temperature ($>18,000^{\circ}\text{R}$) is relatively opaque to radiation and transparent to radiation at the colder temperatures ($<10,000^{\circ}\text{R}$). Therefore, the colder regions must be seeded with micron sized carbon or tungsten particles to increase the heat absorbed by the propellant and reduce the thermal energy incident on the wall. It was found that a hydrogen absorption coefficient of 2 to 3 ft^{-1} resulted in the maximum heating of the hydrogen and from 4 to 15 percent of the core power reached the surrounding reactor walls in the form of thermal radiation. This required 5×10^{-5} lb carbons per lb. of hydrogen in the reactor annulus, which had a negligible effect on degrading engine specific impulse.

7.3 COAXIAL MIXING OF THE STREAMS

The amount of turbulent coaxial mixing of the hydrogen and uranium streams, moving at unequal velocities, was predicted by Weinstein and Todd's computer program. The assumption of a constant value of density times velocity in a streamline is questionable and has led to unrealistic velocity profiles. However, the concentration profiles are not closely coupled with the velocity solution and may be more realistic. The major input assumption was the turbulent eddy diffusivity value of 10. This arbitrary value appears to be suitable for the low velocity cases examined in this study.

The mixing between the streams is also dependent on the ratio of scoop diameter/uranium column diameter. A realistic value of 1.01 was selected and the mixing rates are as follows:

$$\frac{\text{Uranium loss rate}}{\text{Total hydrogen flow rate}} = \frac{1}{1000}$$

$$\frac{\text{Hydrogen entrained in scoop}}{\text{Total hydrogen flow rate}} = \frac{2.5}{1000}$$

The uranium escaping into the outer hydrogen stream is lost through the nozzle, resulting in a loss of costly fuel and increased operating cost. However, the values attained in this study are low and very encouraging. The hot hydrogen entrained in the uranium stream can substantially increase the regenerative cooling load but, in this case, only accounts for 1 percent of the total fission heat. In summary, the mixing losses predicted by the NASA computer program are small and highly encouraging.

7.4 ENGINE PERFORMANCE

Propulsion is the major pacing item in future space travel. Current modes of propulsion allow only marginal or modest manned interplanetary flights. Chemical systems, although relatively simple and light, have a specific impulse potential of about 500 secs. Solid core nuclear systems have a specific impulse of 800 - 900 secs. The gaseous-core propulsion system performance examined in this study varied between 1500 - 2000 secs specific impulse and engine system weight/thrust between 1.5 to 0.35, with a minimum engine weight predicted to be 350,000 lbs. Obviously, the gaseous-core engine can only be considered for advanced space flights requiring extremely large payloads such as manned exploration of Mars and Jupiter. Other considerations are advanced manned missions to the outer planets where emphasis is placed on the reduction of trip time at the expense of large propulsion requirements. A simple comparison of the relative performance of typical chemical, solid core nuclear, and gaseous core nuclear reactor propulsion systems are shown in figure 7-1. The gaseous core reactor performance, even with a high weight/thrust ratio of 1.5 and specific impulse of 1600, has an appreciable performance margin over the chemical and solid core nuclear systems. The selection of a low thrust/overall stage weight ratio of 0.1 is necessary to balance the penalty of the engine weight required to achieve a pound of thrust.

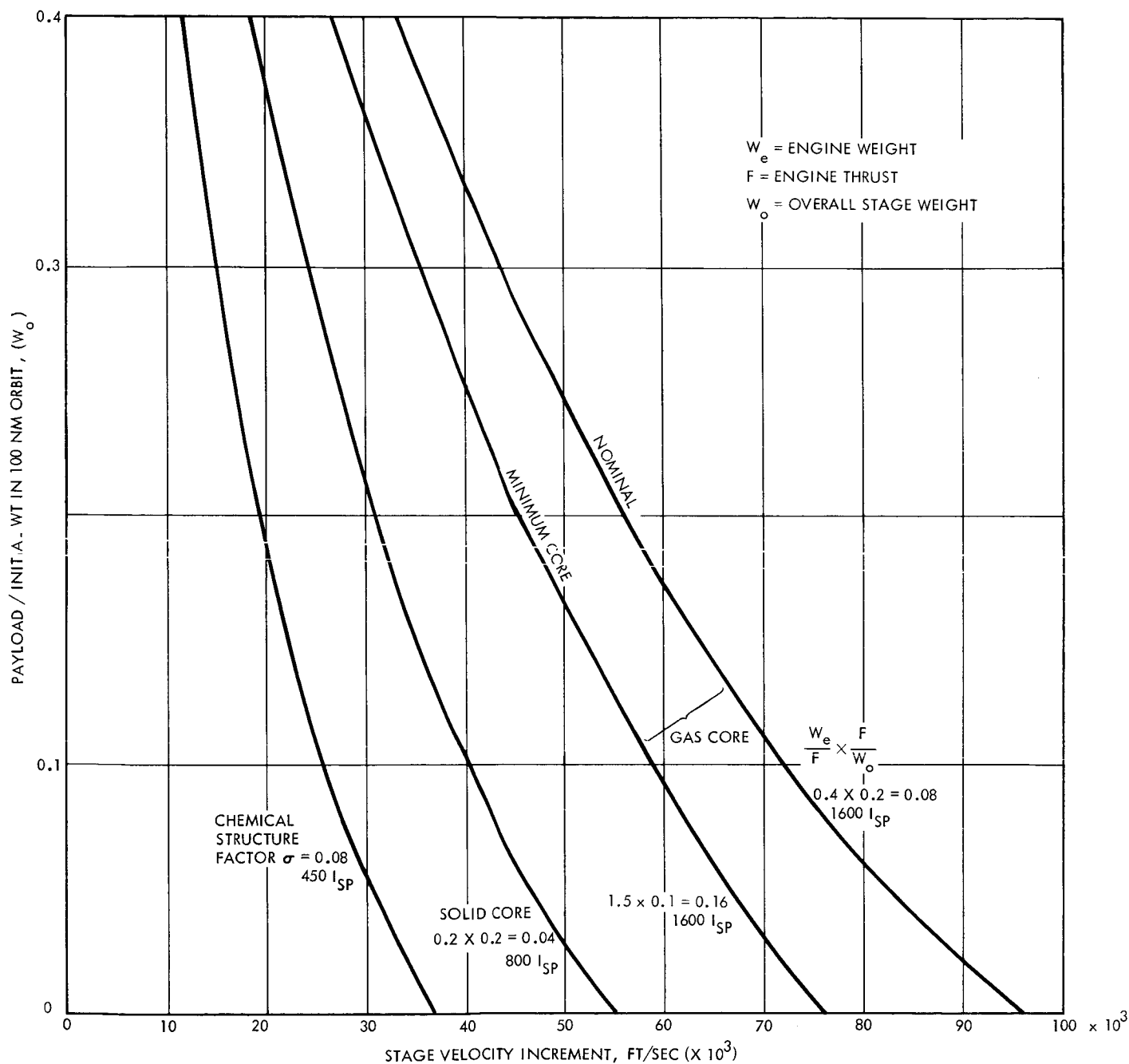


Figure 7-1 Performance Comparison of Gas Core, Solid Core and Chemical Propulsion Systems

The engine specific impulse and thrust were degraded to account for the heat reaching the wall structure, the coolant required to transpiration cool the nozzle, scoop and other pertinent structure, and carbon used in seeding the hydrogen. In a typical case, 80 lb/sec of hydrogen passes through the reactor (W_1) and as much as 70 lb/sec of coolant hydrogen (W_2) is dumped into the nozzle, downstream of the reactor exit. Fortunately, this excess hydrogen coolant has a small effect on engine specific impulse and the correction can be approximated as follows:

$$\text{Isp(effective)} = \frac{\text{Isp}_o \text{ (unattenuated)}}{\left(1 + \frac{W_2}{W_1}\right)^{1/2}}$$

A conservative weight estimate was made of the propulsion system including the reflector-moderator, shadow shield, pressure vessel, turbopump and the other major engine components. Funding and time constraints allowed only a limited performance appraisal. From the conditions examined, it cannot be concluded that optimum performance has been evaluated. However, the study was sufficient to establish reasonable design and performance conditions for evaluation of systems feasibility and uncovering critical problem areas.

The gaseous-core reactor propulsion system performance advantage, with attendant economics, must justify the enormous development and logistic risks this concept entails. A major cost item can be fuel loss but this concept has shown a high degree of fuel retention. Table 7-1 shows the substantial savings that can accrue in a typical advanced mission by achieving a fuel loss to propellant mass flow ratio of 10^{-4} , as opposed to 10^{-2} .

7.5 NUCLEONICS

The fundamental feasibility of the gas-core reactor depends on the ability to initiate and sustain a fissioning chain reaction in the central fuel core under operating conditions consistent with acceptable propulsive performance (weight/thrust and specific impulse). The results presented herein indicate that not less than about 15 kg of uranium is required for reactor criticality. For reasonable propulsive performance, hydrogen gas exit temperatures of 10,000°R or greater are required, corresponding to a temperature of at least 50,000°R in the fuel

Table 7-1 Comparison of Cost With Various Fuel Loss Rates

COST OF PROPELLANT IN ORBIT	= \$ 100/LB	
COST OF URANIUM	= \$7000/LB	
WEIGHT OF URANIUM LOSS/LB OF PROPELLANT	$\frac{1}{1000}$	$\frac{1}{100}$
COST OF URANIUM/LB OF PROPELLANT	\$ 7.0	\$ 70
TOTAL COST OF URANIUM PLUS PROPELLANT/LB OF PROPELLANT	\$107.00	\$170.00
TYPICAL WEIGHT OF PROPELLANT (400,000 LB ENGINE)	3×10^6	3×10^6
TOTAL COST OF (FUEL PLUS PROPELLANT)	320×10^6	510×10^6
SAVINGS/FLIGHT	$\$190 \times 10^6$	

core. Considering the problems of pumping hydrogen to high pressures, 300 atm appears to be a practical upper limit. At 300 atm pressure and 50,000°R temperature, less than 15 kg of uranium can be contained in the core. Thus, it can be concluded that methods for lowering the critical mass requirement of the reactor must be found.

The chief omissions, from the standpoint of nuclear heat distribution, were the fast and delayed fission contributions to the scoop inlet. Funding and study directives did not permit a preliminary nuclear analysis, although this was recognized as being important. However, a rough estimate shows that the power density due to fast fissions is about 10 percent of the total power density. Since the volume of the scoop could range from 10 to 30 percent of the volume of the fissioning fuel column, an additional 1 to 3 percent of the core power would be produced by fast fissions in the scoop. This amount of heat would require an additional amount of hydrogen to cool the uranium of from 30 to 100 percent more than that required to condense the uranium. The total amount of hydrogen necessary to remove the fast fission heat and to condense the uranium would still amount to only about half that flow through the reactor. This is not considering a feasibility limitation.

7.6 RECOMMENDED STUDIES

The performance potential of the proposed gaseous-core reactor propulsion system for future space exploration is vast, but the practicality of the concept is not presently known. Further work of a preliminary nature must be investigated before the valid appraisal of the system feasibility can be made. Some of the major areas requiring additional investigations are:

- Feasibility of reactor core inlet
- Analytical and experimental analysis of the effectiveness of the scoop's aerodynamic leading edge design
- Nuclear analysis and feasibility
- Condensation, separation, and jet pumping in the scoop
- Analytical and experimental program on transpiration cooling

APPENDIX A

CALCULATIONS OF MASS DIFFUSION

The rate of mass diffusion in a gaseous-core nuclear reactor can be determined by applying the laws of conservation of mass and mixtures of ideal gases. It is assumed that the molecular weights of both gases remain constant in the diffusion process and the velocities of both gases and their mixtures are exactly the same at a location in the reaction.

1. THE URANIUM DIFFUSION

The mass flow rate of uranium \dot{m}_1 passing through a circular cross section of radius r' at an axial distance z can be determined from the equation

$$\dot{m}_1 = 2\pi \int_0^{r'} r u_1 \zeta_1 dr \quad (1)$$

where u_1 and ζ_1 are functions of r only. u_1 can be obtained directly from the computer output and ζ_1 can be evaluated from

$$\zeta_1 = w_1 \zeta_m \quad (2)$$

where w_1 is related to the mole fraction c , a computer output, by

$$w_1 = \frac{m_1}{m_2} \left[\frac{c_1}{\beta c_1 + 1} \right] \quad (3)$$

and ζ_m is given by the perfect gas law

$$\zeta_m = \frac{p_m M}{RT_m} \quad (4)$$

In this equation, T_m is the local temperature of the mixture obtained from the computer output, p_m is known, R is the universal gas constant, and M is the molecular weight of the mixture, which can be evaluated by

$$M = \left[\frac{w_1}{m_1} + \frac{1-w_1}{m_2} \right]^{-1} \quad (5)$$

Thus, \dot{m}_1 at a specific z within r' can be determined with these expressions, and the other \dot{m}_1 's can be calculated in a similar manner. By normalizing these \dot{m}_1 's with the inlet uranium flow rate \dot{m}_{10} , it is possible, therefore, to determine the fraction of uranium that is retained in a certain size of scoop at an axial distance z .

2. THE HYDROGEN DIFFUSION

The diffusion of hydrogen into the uranium core can be determined in a very similar manner. The amount of hydrogen passing through a circular section of radius r' at an axial distance z can be calculated from the continuity equation

$$\dot{m}_2 = 2\pi \int_0^{r'} r u_2 \zeta_2 dr \quad (6)$$

Here,

$$u_2 = u_1 = u_m, \text{ and}$$

$$\zeta_2 = w_2 \zeta_m = (1 - w_1) \zeta_m \quad (7)$$

The magnitudes of w_1 and ζ_m are similarly evaluated by Equation (3) and (4). In this way, \dot{m}_2 is obtained, and the same is for the other \dot{m}_2 's. By dividing these \dot{m}_2 's by the initial hydrogen flow rate, \dot{m}_{20} , the portion of hydrogen which is diffused into a certain size of scoop at an axial distance z can then be determined.

APPENDIX B
NUMERICAL METHODS USED IN COMPUTING URANIUM
AND HYDROGEN TEMPERATURES

1. THE URANIUM TEMPERATURE

The temperature of the uranium inside the scoop is a function T of r , $0 < r < R$, and z , $z > 0$, satisfying the equation

$$\rho u c_p \frac{\partial T}{\partial z} = \frac{1}{r} \frac{\partial}{\partial r} \left(\frac{16}{3} r \sigma \ell T^3 \frac{\partial T}{\partial r} \right), \quad 0 < r < R, \quad z > 0 \quad (1)$$

with the conditions that

$$\frac{\partial T}{\partial r} = 0, \quad r = 0, \quad z > 0 \quad (2)$$

$$\frac{4}{3} \ell \frac{\partial T^4}{\partial r} = T_w^4 - T^4, \quad r = R, \quad z > 0 \quad (3)$$

and

$$T = T_o, \quad 0 < r < R, \quad z = 0 \quad (4)$$

where T_o is a function of r determined by the equations

$$\frac{1}{r} \frac{d}{dr} \left(\frac{16}{3} r \sigma \ell T_o^3 \frac{dT_o}{dr} \right) + w_i = 0 \quad (5)$$

$$\frac{dT_o}{dr} = 0, \quad r = 0 \quad (6)$$

and

$$T_o = T_{ow}, \quad r = R$$

In these equations ρ , u , σ , R , w_i , T_w and T_{ow} are assumed to be known positive constants, C_p and ℓ are assumed to be known positive functions of T . ρ , u , ℓ and C_p pertain specifically to uranium.

A first integral of equation (5) can be obtained analytically:

$$\frac{16}{3} r \sigma \ell T_o^3 \frac{dT_o}{dr} + \frac{1}{2} w_i r^2 = 0$$

This is a single first order ordinary differential equation for T_o . It may be written

$$\frac{dT_o}{dr} = - \frac{3}{32} \frac{w_i r}{\sigma \ell T_o^3} \quad (7)$$

(ℓ is here a given function of T_o). This equation was solved numerically, using a fourth order Runge-Kutta method. The solution was started at $r = R$, where T_o is known, and was computed at successively smaller values of r : $R - h$, $R - 2h$, ..., until the point $r = 0$ was reached. Several solutions were obtained corresponding to different values of the fixed step size h . The solution obtained for $h = 0.001$ was found to be in satisfactory agreement with solutions obtained for somewhat larger values of h .

Using the values of T at $Z = 0$ obtained in this way, equation (1) was solved by the Crank-Nicholson method. Equation (1) was approximated by a difference equation of the form

$$\begin{aligned} H_i(T_{i,j+1} - T_{i,j}) &= \lambda_j \left[P_{i+1/2}(T_{i+1,j} + T_{i+1,j+1}) \right] \\ &\quad - (P_{i+1/2} + P_{i-1/2})(T_{i,j} + T_{i,j+1}) \\ &\quad + P_{i-1/2}(T_{i-1,j} + T_{i-1,j+1}) \end{aligned} \quad (8)$$

where

$$\lambda_j = \frac{1}{2} (\Delta Z)_j / (\Delta r)^2$$

$$H_i = H \left(\frac{1}{2} (T_{ij} + T_{i+1,j}) \right)$$

$$P_{i+1/2} = 1 + \frac{1}{2i} K_{i+1/2}$$

$$K_{i+1/2} = 1/2 \left[K(1/2(T_{i,j} + T_{i,j+1})) + K(1/2(T_{i+1,j} + T_{i+1,j+1})) \right]$$

and H and K are functions of temperature:

$$H = \rho u C_p$$

$$K = \frac{16}{3} \sigma \ell T^3$$

The subscripts refer to discrete values of the independent variables

$$r_i = i \Delta r = \frac{iR}{n}, i = 0, \dots, n$$

$$n = \frac{R}{\Delta r} = 90$$

$$z_0 = 0$$

$$z_{j+1} = z_j + (\Delta z)_j, j = 0, 1, 2, \dots$$

Equation (2) was approximated by the equation

$$H_o(T_{o,j+1} - T_{o,j}) = 4\lambda_j K_{1/2}(T_{1,j} + T_{1,j+1} - T_{o,j} - T_{o,j+1}) \quad (9)$$

Equation (3) was approximated by the equation

$$\frac{4}{3} \frac{\ell_{n,j+1}}{\Delta r} (T_{n,j+1}^4 - T_{n-1,j+1}^4) = T_w^4 - T_{n,j+1}^4 \quad (10)$$

where

$$\ell_{n,j+1} = \ell(T_{n,j+1})$$

The method consists essentially of solving Equations (8), (9), and (10) for $j = 0$ to obtain temperature values at $z = z_1 = (\Delta z)_0$, then solving Equations (8), (9), and (10) for $j = 1$ to obtain temperature values at $z = z_2 = z_1 + (\Delta z)_1$, and so on for as many values of z as desired.

Equations (8), (9) and (10) were solved by an iterative process. At each stage of this process, the equations were linearized in such a way as to yield a tri-diagonal system of equations for the unknown quantities $T_{i,j+1}$, $i = 0, \dots, n$. Approximate values of the $T_{i,j+1}$ were used to compute the coefficients of this tri-diagonal system. The system was then solved to obtain new approximate values of the $T_{i,j+1}$. This procedure was iterated until successive approximate values of the $T_{i,j+1}$ agreed to within a relative error of 0.001.

A pre-selected dequence of step sizes $(\Delta z)_j$ was used, starting with $(\Delta z)_0 = 10^{-4}$ and increasing gradually to $\Delta z = 10^{-1}$.

Due to the extreme rapidity of the variation of the temperature T as a function of r near $r = R$, the temperatures in this region were recomputed using a finer mesh. The region $0.94R < r < R$ was divided into 90 intervals, and Equation (9) was replaced by the equation

$$T_{oj} = T(0.94 R, z_j) \quad (9')$$

The results of the first calculation were used to evaluate the right hand side of Equation (9'). The recalculation of T near $R = R$ then involved the iterative solution of Equations (8), (9'), and (10) with the subscript i now referring to values

$$r_i = 0.94 R + i \Delta r, \quad i = 0, \dots, 90$$

$$\Delta r = \frac{0.06R}{90}$$

for a new sequence of step sizes $(\Delta z)_j$. The step sizes started with $(\Delta z)_0 = 10^{-7}$ and increased gradually to $\Delta z = 10^{-1}$.

2. THE HYDROGEN TEMPERATURE

The temperature of the hydrogen in the annular region outside the scoop, $R \leq r \leq R'$, $z \geq 0$ is a function T satisfying the equation

$$\rho u C_p \frac{\partial T}{\partial z} = \frac{1}{r} \frac{\partial}{\partial r} \left(\frac{16}{3} r \sigma \ell T^3 \frac{\partial T}{\partial r} \right), \quad R \leq r \leq R', \quad z > 0 \quad (11)$$

with the conditions that

$$\frac{4}{3} \ell \frac{\partial T^4}{\partial r} = T^4 - T_w^4, \quad r = R, \quad z \geq 0 \quad (12)$$

$$\frac{4}{3} \ell \frac{\partial T^4}{\partial r} = T_w^4 - T^4, \quad r = R', \quad z \geq 0 \quad (13)$$

and $T = T_0$, $R \leq r \leq R'$, $z = 0$

where T_0 , in the interval $R \leq r \leq R'$, is a given function. ρ , u , and ℓ are assumed to be known positive constants and C_p is assumed to be a known positive function of T appropriate to the hydrogen gas. The distance $R' > R$ is also known. R and T_w have the same values as for the uranium temperature calculation. σ is a universal constant, (Stefan-Boltzmann constant).

The solution of Equations (11), (12) and (13) for hydrogen was very similar to solution of the corresponding equations (1), (2), and (3) for uranium. Equation (11) was again approximated by the difference equation (8) with the subscript i now referring to values of the independent variable.

$$r_i = R + i \Delta r, \quad i = 0, \dots, 90$$

$$\Delta r = (R' - R)/90$$

Equations (12) and (13) were approximated by the equations

$$\frac{4}{3} \frac{\ell}{\Delta r} (T_{1j+1}^4 - T_{0j+1}^4) = T_{0j+1}^4 - T_w^4 \quad (14)$$

and

$$\frac{r}{3} \frac{l}{\Delta r} (T_{nj+1}^4 - T_{n-1,j+1}^4) = T_w^4 - T_{nj+1}^4 \quad (15)$$

respectively. Again, $n = 90$. Equation (8), (14), and (15) were solved by the same iterative process as before, for a pre-selected sequence of step size ΔZ_j starting with $\Delta Z_0 = 10^{-2}$ and increasing to 10^{-1} .

REFERENCES

1. Einstein, Thomas H. , "Radiant Heat Transfer to Absorbing Gases Enclosed in a Circular Pipe with Conduction, Gas Flow, and Internal Heat Generation, " NASA TR R-156, 1963.
2. Krascella, N. L. , "Theoretical Investigation of Spectral Opacities of Hydrogen and Nuclear Fuel, ' RTD-TDR-63-1101, Research Laboratories, United Aircraft Corporation, November 1963.
3. Weinstein, Herbert, Todd, Carroll A. , "Analysis of Mixing of Coaxial Streams of Dissimilar Fluids Including Energy-Generation Terms, " NASA TN D-2123, March 1964.
4. Schneiderman, S. B. , "Theoretical Viscosities and Diffusivities in High-Temperature Mixtures of Hydrogen and Uranium, " NASA CR-213, April 1965.
5. Howell, John R. , Strite, Mary K. , and Renkel, Harold, "Analysis of Heat Transfer Effects in Rocket Nozzles Operating with Very High Temperature Hydrogen, " NASA TR R-220, February 1965.
6. Howell, John R. , and Strite, Mary K. , "Heat Transfer in Rocket Nozzles Using High Temperature Hydrogen Propellant with Real Property Variations, " Paper presented at AIAA Propulsion Specialists Conference, Colorado Springs, June 14 - 18, (1965).
7. Rosseland, S. , Astrophysik auf Atom-Theoretischer Grundlage; Springer-Verlag, Berlin, 1931, pp. 41-44.
8. Hammitt, A. G. , "Comments on Radiation Slip, " AIAA Journal, Vol. II, No. 5, p. 975.
9. Nickerson, G. R. , Peters, R. L. , Quan, V. , Starr, M. C. , "The Charring and Ablation Program, " Program No. AH54A, 9852.21-40, TRW Systems Group, July 1965.
10. Schlichting, H. , Boundary Layer Theory, McGraw-Hill, 4th Edition, 1960, p. 497.
11. Rubesin, M. W. , "An Analytical Estimation of the Effect of Transpiration Cooling on Heat-Transfer and Skin-Friction Characteristics of a Compressible Turbulent Boundary Layer, " NACA TN-3341, December 1954.
12. Rubesin, M. W. , Pappas, C. C. , "An Analysis of the Turbulent Boundary Layer Characteristics on a Flat Plate with Distributed Light-Gas Injection, " NACA TN-4149, February 1958.

13. Rubesin, M. W., Pappas, C. C., Okuno, A. F., "The Effect of Fluid Injection on the Compressible Turbulent Boundary Layer-Preliminary Tests of Transpiration Cooling of a Flat Plate at $M = 2.7$ with Air as the Injected Gas," NACA RM A55119, December 1955.
14. Leadon, B. M., Scott, C. J., "Transpiration Cooling Experiments in a Turbulent Boundary Layer at $M = 3$," JAS, Vol. 23, No. 8, pp. 798-9, August 1956.
15. Lanzo, C. D., Ragsdale, R. G. "Experimental Determination of Spectral and Total Transmissivities of Clouds of Small Particles," NASA TN D-1405, September 1962.
16. Green, L., "Gas Cooling of a Porous Heat Source," J. of Appl. Mechanics, p. 178, 1952.
17. Green, L., Jr. and P. Durvez, "Fluid Flow Through Porous Metals," J. Appl. Mechanics, Vol. 18, p. 39, 1951 (ASME).
18. Hill, J. A. F., "The permeability of Porous Walls," Internal Memo, MTP-TM-4, Naval Supersonic Laboratory, Cambridge, Mass., September 1956.
19. Bernicker, R. P., "An Investigation of Porous Wall Cooling," Technical Report 393, AFOSR-TN-59-873, Naval Supersonic Laboratory, Cambridge, Mass., June 1959.
20. Weinbaum, S., and Wheeler, H. L., "Heat transfer in Sweat-Cooled Porous Metals," J. Appl. Physics, Vol. 20, January 1949.
21. Schmidt, F. F. and H. R. Ogden, "The Engineering Properties of Tungsten and Tungsten Alloys," Defense Metals Information Center Report DMIC 191, Sept. 1963.
22. Kirkpatrick, M. E. and R. A. Mendelson, "Final Report on the Development of High Performance Porous Tungsten Ionizers," TRW Systems Report AFML-TR-65-215, July 1965.
23. "Feasibility Demonstration of a Transpiration Cooled Nozzle System, First Interim Report," TAPCO (a division of Thompson-Ramo Woodridge) Report ER-5209-11, 1963.
24. Odquist, F. K. G. and J. Hult, "Kriechfestigkeit Metallischer Werkstoffe (Creep Strength of Metals)," Springer-Verlag, Berlin, 1962.
25. Personal Communication for E. Poulos, TRW, Cleveland, Dec. 29, 1965.
26. Hall, R. J. and Plunkett, "Nuclear Analysis of Gaseous Core Reactors, Rpt. No. SM-44041, Missile and Space System Division, Douglas Aircraft Company, 23 May 1963.

27. Hyland, R. E., Ragsdale, R. G., and Gunn, E. J., "Two-Dimensional Criticality Calculations of Gaseous-Core Cylindrical-Cavity Reactors," NASA TN D-1575, Lewis Research Center, March 1963.
28. Holl, R. J., "Reflector Heating in Gaseous Core Reactors," Douglas Report SM-44878, 15 Nov., 1963.
29. Hirschfelder, J. O., Molecular Theory of Gases and Liquids, John Wiley and Sons, 1954.
30. Semat, H. and White, H. E., Atomic Age Physics, Rinehart and Co., Inc., New York.
31. Samsonov, C. V., High Temperature Materials, Plenum Press, 1964.
32. Schneiderman, S. B., "Theoretical Viscosities and Diffusivities in High-Temperature Mixtures of Hydrogen and Uranium," NASA-CR-213, April, 1965.
33. Krascella, N. L., "Tables of the Composition, Opacity, and Thermodynamic Properties of Hydrogen at High Temperature," NASA SP-3005, 1963.
34. King, C. R., "Compilation of the Thermodynamic Properties, Transport Properties, and Theoretical Rocket Performance of Gaseous Hydrogen," NASA-D-275, April 1960.
35. Bussard, R. W., and DeLauer, R. D., Nuclear Rocket Propulsion, McGraw-Hill Book Company, Inc., 1958.
36. Rosser, R. C., Memo Subject: Thrust Structure Contribution for STL Contract for Mission Oriented Advanced Nuclear Systems Parametric Study, REON, 14 August 1964. (C)
37. "Direct Flow Externally Separated Gas-Core Reactor Propulsion System," 9990-6599-PC-000, TRW Systems, January 1964. (C)
38. Grier, N. T., Transport Properties of Hydrogen, NASA TN D-1406, October 1962
39. Rohsenow, W. M., Choi, H. Y., Heat, Mass and Momentum Transfer Prentice Hall, 1961
40. Stewart, J. D., Transpiration Cooling, G.E. Document No. R59SD338, 1959.
41. "Mission Oriented Advanced Nuclear System Parameters Study" Final Report Volume IV: Detailed Technical Report Nuclear Rocket Engine Analysis, TRW 8423-6008-RL000, March 1965 (CRD)